

AN ANALYTICAL METHOD FOR PREDICTING PERMANENT
DEFORMATION OF FOUNDATIONS
UNDER CYCLIC LOADS

by

GEORGE BOUCKOVALAS

Dipl. National Technical University, Athens, Greece
(1978)

S.M., Massachusetts Institute of Technology
(1981)

SUBMITTED TO THE DEPARTMENT OF
CIVIL ENGINEERING IN PARTIAL
FULFILLMENT OF THE
REQUIREMENTS FOR THE
DEGREE OF

DOCTOR OF SCIENCE

at the

MASSACHUSETTS INSTITUTE OF TECHNOLOGY

June 1982

c Massachusetts Institute of Technology 1982

Signature of Author Signature redacted
Department of Civil Engineering
June, 1982

Certified by Signature redacted
Robert V. Whitman
Thesis Co-Supervisor

Signature redacted
Allen W. Marr
Thesis Co-Supervisor

Accepted by Signature redacted
Archives
Francois Morel
Chairman, Department Committee

MASSACHUSETTS INSTITUTE
OF TECHNOLOGY

NOV 19 1982

LIBRARIES



77 Massachusetts Avenue
Cambridge, MA 02139
<http://libraries.mit.edu/ask>

DISCLAIMER NOTICE

The pagination in this thesis reflects how it was delivered to the Institute Archives and Special Collections.

Missing page 288

AN ANALYTICAL METHOD FOR PREDICTING PERMANENT
DEFORMATION OF FOUNDATIONS
UNDER CYCLIC LOADS

by

GEORGE BOUCKOVALAS

Submitted to the Department of Civil Engineering
on June 29, 1982 in partial fulfillment of the
requirements for the Degree of Doctor of Science in
Civil Engineering

ABSTRACT

An analytical model has been developed to predict permanent stresses and strains in sands under general loading and boundary conditions. Static triaxial tests and drained cyclic triaxial tests are required to define the model parameters. Model predictions have been compared with experimental results from cyclic oedometer tests and cyclic undrained triaxial tests under various initial stresses. Good correlation was found to exist between the predicted and measured response.

A non linear finite element model was developed to predict permanent displacement of foundations subjected to repeated loads. The model was used to predict the permanent displacement of the Oosterschelde barrier under combined tidal and wave loading. The results were compared with the displacement patterns observed during one field test, as well as, with results from previous analyses, yielding a good correlation. The effect of stress redistribution and drainage conditions on permanent displacements is evaluated.

Thesis Co-Supervisor: Pr. Robert V. Whitman

Title: Professor of Civil Engineering

Thesis Co-Supervisor: Dr. Allen W. Marr

Title: Research Associate

ACKNOWLEDGMENTS

I wish to express sincere appreciation to the following individuals and organizations:

To my advisors Professor Robert Whitman and Doctor Allen Marr for their guidance and support throughout my graduate studies at M.I.T.

To Professor Edwardo Kausel and Doctor John Christian for their invaluable help as members of the thesis supervising committee.

To the Civil Engineering Department of M.I.T. and the Instituto Tecnológico Venezolano del Petróleo for supporting financially parts of this study.

To my wife Maria for her typing of the mathematical equations and the text, but mainly for her spiritual support and the sacrifices she had to make throughout the course of my studies at M.I.T.

Last but not least to Doctor Vassilios Papazoglou for his friendship and his encouragement during the latest and most difficult part of this thesis.

TO MARIA

TABLE OF CONTENTS

	<u>Page</u>
TITLE PAGE	1
ABSTRACT	2
ACKNOWLEDGEMENTS	3
TABLE OF CONTENTS	5
LIST OF TABLES	9
LIST OF FIGURES	11
LIST OF NOTATIONS	17
CHAPTER 1 INTRODUCTION	
1.1 Problem Description	21
1.2 Prediction Methods	22
1.3 Objective of Research	25
1.4 Thesis Organization	27
1.4.1 Part I	28
1.4.2 Part II	30
CHAPTER 2 CONTRACTION AND DILATION IN CYCLIC LOADING	
2.1 Introduction	33
2.2 The "Characteristic Threshold" Model	34
2.2.1 The "Characteristic Threshold" - Definition	34
2.2.2 Drained Loading	35
2.2.3 Undrained Loading	36
2.3 Cyclic Behavior of Sand A	37
2.3.1 The Characteristic Threshold for Sand A	37
2.3.2 Undrained Loading	38

	<u>Page</u>
2.3.3 Drained Loading	40
2.4 Evaluation of the Characteristic Threshold Model	40
2.5 Summary	43
CHAPTER 3 PERMANENT STRAIN IN DRAINED CYCLIC TRIAXIAL TESTS	
3.1 Introduction	56
3.2 Permanent Volumetric Strain	57
3.3 Permanent Vertical Strain	60
3.4 Limits on Permanent Strain Accumulation	61
3.4.1 Volumetric Strain	61
3.4.2 Vertical Strain	63
3.5 Cyclic Shear Strain in Triaxial Tests	64
3.5.1 Peak to Peak Cyclic Shear Strain	65
3.5.2 The Hyperbolic Model	67
3.5.3 Suggested Model for Cyclic Shear Strain	72
3.6 Summary	75
CHAPTER 4 A CONSTITUTIVE MODEL FOR CYCLIC LOADING OF SAND	
4.1 Introduction	106
4.2 Cyclic Loading versus Creep	108
4.3 Determination of Viscosity Functions	110
4.4 Determination of Soil Moduli	113
4.4.1 Shear Modulus	115
4.4.2 Bulk Modulus	116
4.5 Evaluation of Model Parameters	118
4.6 Summary	120

	<u>Page</u>	
CHAPTER 5	EVALUATION OF MODEL PREDICTIONS	
5.1	Introduction	123
5.2	Cyclic Oedometer Tests	123
5.2.1	Test Results	124
5.2.2	Model Prediction	126
5.2.3	Summary	129
5.3	Undrained Cyclic Triaxial Tests	130
5.3.1	Model Prediction	130
5.3.2	Predicted versus Measured Response	133
5.3.3	Summary	137
5.4	Conclusion	138
CHAPTER 6	FINITE ELEMENT MODELING OF CYCLIC LOADING OF FOUNDATION	
6.1	Introduction	165
6.2	Principle of Virtual Work	166
6.2.1	Definition	166
6.2.2	Volume Incompressibility	167
6.3	Finite Element Implementation	169
6.4	A Computer Program for Finite Element Analysis	172
6.5	Checking the Finite Element Program	176
6.6	Summary	178
CHAPTER 7	CASE STUDY: THE OOSTERSCHELDE BARRIER	
7.1	Introduction	183
7.2	Caisson Test at Neeltje Jans, the Netherlands	185
7.3	Predicted Response of Oosterschelde Barrier	186
7.4	Stress Redistribution due to Cyclic Loading	189

	<u>Page</u>
7.5 Comparison with Previous Analyses	192
7.6 Undrained Cyclic Loading	194
7.7 Summary	199
CHAPTER 8 SUMMARY AND CONCLUSIONS	
8.1 Summary	227
8.2 Conclusions	230
8.3 Future Research	230
LIST OF REFERENCES	234
APPENDIX A DESCRIPTION OF SAND A	240
APPENDIX B STRENGTH PROPERTIES OF SAND A	245
APPENDIX C FINITE ELEMENT MATRICES	251
APPENDIX D ANALYTICAL SOLUTION FOR CYCLIC LOADING UNDER PLANE STRAIN CONDITIONS	254
APPENDIX E LISTING OF FINITE ELEMENT PROGRAM FEAP-CYC	261

LIST OF TABLES

<u>Table</u>	<u>Page</u>
2.1 Summary of Static Undrained Triaxial Tests used to determine ϕ_{CT} for Sand A	44
2.2 Summary of Static Drained Triaxial Tests used to determine ϕ_{CT} for Sand A	45
2.3 Summary of Cyclic Undrained Triaxial Tests used to determine ϕ_{CT} for Sand A	46
2.4 Summary of Cyclic Drained Triaxial Test Conditions-Sand A	47
3.1 Ratio of Vertical to Volumetric Permanent Strain in Drained Cyclic Triaxial Tests on Sand A	77
3.2 Summary of the Basic Parameters Required to Define the ESP during Undrained Cyclic Loading	78
3.3 Predicted γ_{cyc} along the Estimated and Measured ESPs	79
3.4 Computational steps required for the Prediction of γ_{cyc}	80
4.1 Definitions of Stress and Strain Quantities used with the Proposed Model	121
5.1 Summary of Cyclic Oedometer Test Conditions on Sand A	140
5.2 Summary of Test Conditions for Undrained Cyclic Triaxial Tests on Sand A	141
7.1 Static Head Loss and Cyclic Wave Load Combinations	202
7.2 Material Properties of Oosterschelde Soils and Oosterschelde Closure	203
7.3 Effect of Stress Redistribution on Predicted Settlement	204
7.4 Effect of Stress Redistribution on Predicted Horizontal Displacement	204
7.5 Effect of Stress Redistribution on Predicted Differential Settlement	205
7.6 Effect of Drainage on Predicted Permanent Movement of the Pier	206
A.1 Summary of Basic Characteristics of Sand A	243

TablePage

B.1 Summary of Undrained Triaxial Tests on
Sand A

247

LIST OF FIGURES

<u>Figure</u>		<u>Page</u>
1.1	Observed and Predicted Movement of Model Test in Neeltje Jans	32
2.1	Determination of the Characteristic Threshold C.T. during an Undrained Test	48
2.2	Determination of the Characteristic Threshold C.T. during a Drained Test	48
2.3	Characteristic Criterion Bounding the Contractancy Domain of Granular Materials	49
2.4	Diverse Cyclic Behavior of Sand Observed during Drained Shearing under Constant Confinement Condition	49
2.5	Undrained Cyclic Shearing in the Subcharacteristic Domain	50
2.6	Prolonged Cyclic Shearing	50
2.7	Maximum Friction Angle (ϕ_{max}) and Characteristic Threshold Angle (ϕ_{CT}) of Sand A	51
2.8	ϕ_{CT} Determined by Static and Cyclic Tests on Sand A	52
2.9	Cumulative Vertical Strain in Undrained Cyclic Triaxial Tests on Sand A	53
2.10	Cumulative Volumetric Strain in Drained Cyclic Triaxial Tests on Sand A	54
2.11	Cumulative Vertical Strain in Drained Cyclic Triaxial Tests on Sand A .	55
3.1	Permanent Volumetric Strain versus γ_{cyc}	81
3.2	Permanent Volumetric Strain versus Cycle Number	82
3.3	Effect of Initial Density on Permanent Volumetric Strain	83
3.4	Effect of Initial Porosity on Vertical Permanent Strain	84
3.5	Effect of γ_{cyc} on Vertical Permanent Strain	84

<u>Figure</u>		<u>Page</u>
3.6	Effect of Stress Ratio on Vertical Permanent Strain	85
3.7	Definition of Normalized Distance away from the Limit State	86
3.8	Effect of Limit State	86
3.9	Typical Effective Stress Path and Cyclic Shear Strain for Drained Cyclic Triaxial Tests	87
3.10	Typical Effective Stress Path and Cyclic Shear Strain for Undrained Cyclic Triaxial Tests	88
3.11	Comparison of Hodge's Empirical Relationship with data from Drained Cyclic Triaxial Tests	89
3.12	Comparison of Hodge's Empirical Equation with Data from Undrained Cyclic Compression Tests	90
3.13	Comparison of Hodge's Empirical Equation with Data from Undrained Cyclic Isotropic Tests	91
3.14	Comparison of Hodge's Empirical Equation with Data from Undrained Cyclic Extension Tests	92
3.15	Hyperbolic Stress-Strain Relation: (a) Equation 3.12, (b) Equation 3.13	93
3.16	Definition of Δq_{\max} for the Hyperbolic Stress-Strain Relationship	94
3.17	Comparison of Hyperbolic Model with Data from Drained Cyclic Triaxial Tests	95
3.18	Undrained Test on a Loose Sand Cycled with Varying Amplitude of Stress Ratio	96
3.19	Undrained ESP for Sand A: (a) Static Loading (b) Cyclic Loading	97
3.20	Estimation of ESP for Undrained Cyclic Loading	98
3.21	Predicted and Measured ESP for Undrained Cyclic Loading of Sand A	99
3.22	Comparison of the Hyperbolic Model with Data from Undrained Cyclic Compression Tests	100
3.23	Comparison of the Hyperbolic Model with Data from Undrained Cyclic Isotropic Tests	101

<u>Figure</u>	<u>Page</u>
3.24 Comparison of the Hyperbolic Model with Data from Undrained Cyclic Extension Tests	102
3.25 Prediction of γ_{cyc} for Undrained Cyclic Compression Tests by Hodge's ^{cyc} Model and by the Hyperbolic Model	103
3.26 Prediction of γ_{cyc} for Undrained Cyclic Isotropic Tests by Hodge's ^{cyc} Model and by the Hyperbolic Model	104
3.27 Prediction of γ_{cyc} for Undrained Cyclic Extension Tests by Hodge's ^{cyc} Model and by the Hyperbolic Model	105
4.1 Comparison between G_{50} for Sand A and G_{max}	122
5.1 Typical Results from Cyclic Oedometer Tests	142
5.2 Comparison of Strain Accumulation in Cyclic Oedometer and Drained Triaxial Tests	143
5.3 Change in Horizontal stress during Cyclic Oedometer Tests	144
5.4 Comparison between Cyclic Oedometer and Drained Cyclic Triaxial Test Results	145
5.5 Change in Stress Volume during Cyclic Oedometer Test on Normally Consolidated Sand	146
5.6 Bulk Modulus Variation for 1-D Unloading	147
5.7 Typical Model Prediction for Cyclic Oedometer Tests	148
5.8 Comparison between Predicted and Measured Cyclic Response for Oedometer Tests on Sand A	149
5.9 Comparison between Measured and Predicted Cyclic Response in Oedometer Tests-Reduced Bulk Modulus	150
5.10 Prediction of Cyclic Response in Oedometer Tests under Free Horizontal Strain and under No Horizontal Strain	151
5.11 Bulk Modulus for Cyclic Undrained Triaxial Tests	152
5.12 Estimation of the Parameter "l" for the Effect of Limit State	153
5.13 Typical Cyclic Response in Undrained Cyclic Compression Tests	154
5.14 Typical Model Prediction for Undrained Cyclic Triaxial Compression Tests	155

<u>Figure</u>	<u>Page</u>
5.15 Comparison between Predicted and Measured Cyclic Response in Undrained Triaxial Compression Tests	156
5.16 Typical Cyclic Response in Undrained Cyclic Isotropic Tests	157
5.17 Typical Model Predictions for Undrained Cyclic Isotropic Tests	158
5.18 Comparison between Predicted and Measured Response in Cyclic Undrained Triaxial Tests	159
5.19 Typical Cyclic Response in Undrained Cyclic Extension Tests	160
5.20 Typical Model Prediction of Cyclic Response for Extension Tests	161
5.21 Comparison between Predicted and Measured Cyclic Response in Undrained Extension Triaxial Tests	162
5.22 Comparison between Predicted and Measured Cyclic Response in Undrained Extension Tests - INCREASED BULK MODULUS	163
5.23 Comparison between Predicted and Measured Cyclic Response in Undrained Extension Tests - REDUCED VOLUMETRIC VISCOSITY	164
6.1 Major Events in the Life of a Foundation	180
6.2 Summary of Simple Static Problems Solved with FEAP-CYC	181
6.3 Summary of Simple Cyclic Problems Solved with FEAP-CYC	182
7.1 Oosterschelde Pier	207
7.2 (a) Plant of Test Caisson (b) Section of Test Caisson	208
7.3 Loading Schedule - TEST 1A	209
7.4 Permanent Movement - TEST 1A	209
7.5 Finite Element Mesh for Oosterschelde Barrier	210
7.6 Predicted Permanent Movement of Oosterschelde Barrier	211
7.7 Effect of Soil Densification on Predicted Permanent Movement	212

<u>Figure</u>		<u>Page</u>
7.8	Effect of Stress Redistribution on Predicted Permanent Movement	213
7.9	Stresses Applied 4 m Below the Base of the Pier - CASE A	214
7.10	Typical Stress Paths Below the Base of the Pier - CASE A	215
7.11	Contours of Change in Octahedral Stress due to Stress Redistribution - CASE A	216
7.12	Contours of Change in Maximum Shear Stress due to Stress Redistribution - CASE A	217
7.13	Stress Paths due to Stress Redistribution - CASE A	218
7.14	Predicted Settlement of the Center of the Pier's Base	219
7.15	Predicted Horizontal Displacement of the Center of the Pier's Base	220
7.16	Predicted Differential Settlement of the Pier's Base	221
7.17	Permanent Movement of the Pier due to Undrained Cyclic Loading	222
7.18	Permanent Settlement of the Center of the Pier's Base -Effect of Drainage	223
7.19	Permanent Horizontal Displacement of the Center of the Pier's Base - Effect of Drainage	224
7.20	Permanent Differential Settlement of the Pier's Base - Effect of Drainage	225
7.21	Stress Paths 4 m Below the Heel of the Pier During Undrained Cyclic Loading - CASE A	226
7.22	Excess Pore Pressure Contours due to Cyclic Loading - CASE A	226
7.23	Excess Pore Pressure Contours due to Cyclic Loading -Simplified Approach -CASE A	226
B.1	Maximum Static Friction Angle versus Porosity - Sand A	248

<u>Figure</u>		<u>Page</u>
B.2	Mean Effective Stress at Failure versus Porosity - Sand A	249
B.3	Undrained Shear Strength versus Porosity - Sand A	250

LIST OF NOTATIONS

B	bulk modulus coefficient
C_u	coefficient of uniformity, $= d_{60}/d_{10}$
D	differential operator
d_{10}	grain size for which 10% of sample is finer
d_{50}	mean grain size
d_{60}	grain size for which 60% of sample is finer
d_{90}	grain size for which 90% of sample is finer
Dr	relative density
ESP	effective stress path
E	Young's modulus
e_{ij}	deviatoric strain component
e	void ratio
f	distributed force vector
F	concentrated force vector
G	shear modulus
G_{max}	shear modulus at small strain
G_s	specific gravity
\tilde{G}	pore pressure component of cyclic stiffness matrix
\tilde{H}	coupling component of cyclic stiffness matrix
\tilde{I}	unit vector
k	ratio of horizontal to vertical effective stress
k_1	limiting k in cyclic oedometer tests
K	bulk modulus
\tilde{K}	displacement component of cyclic stiffness matrix

KO	cyclic oedometer test with lateral stress measurements
LC	Lambe cyclic tests
m	bulk modulus exponent
N	number of cycles
N	shape function matrix for displacements
\tilde{N}^*	shape function matrix for pore pressure
n	porosity
O	zero vector
OCR	overconsolidation ratio
p	total average mean normal stress, $= \frac{\sigma_1 + \sigma_3}{2}$
\bar{p}	effective average mean normal stress
q	average shear stress, $= \frac{\sigma_1 - \sigma_3}{2}$
Δq	cyclic shear stress, (maximum - average)
R	load vector
S_u	undrained shear strength
S_{ij}	deviatoric stress component
TSP	total stress path
u	pore pressure
U	displacement vector
V	volumetric viscosity function
R	deviatoric viscosity function

Greek Letters

γ	shear strain, $= \epsilon_1 - \epsilon_3$
γ_{cyc}	cyclic shear strain, (maximum - minimum)
δ	virtual quantity

δ_{ij}	Kronecker delta
ϵ	strain
ϵ_1	major principal strain
ϵ_3	minor principal strain
ν	Poisson ratio
σ	average total stress
$\bar{\sigma}$	average effective stress
$\Delta\sigma$	cyclic stress, (maximum - average)
ϕ_{\max}	maximum static friction angle
ϕ_{CT}	friction angle on the CT-line

Subscripts

v	vertical
h	horizontal
vol	volumetric
oct	octahedral
o	initial
1, 2, 3	principal directions
x, y, z	directions parallel to Cartesian coordinates
r, θ , z	directions parallel to cylindrical coordinates
max	maximum
min	minimum

Abbreviated Units

o	degrees
cm	centimeter
in	inch
kg	kilogram

ksc kilograms per square centimeter

m meter

mm millimeter

N newton

Pa pascal

psi pounds per square inch

t tonnes

t/m^2 tonnes per meter square

CHAPTER 1

INTRODUCTION1.1 PROBLEM DESCRIPTION

Cyclic loading of structures is not an unusual situation: a winter storm in the sea subjects offshore structures to cyclic loads that may last several days; ground waves produced by earthquakes are another cause of repetitive loading. Existing offshore and earthquake experience indicates that cyclic loading results in long term accumulation of movement of the foundation, which can be as important as short term generation of excess pore pressure.

During October and December, 1975 the Dutch Government sponsored in situ static and cyclic tests on a caisson at Neeltje Jans; figure 1.1 shows some aspects of the performance of the caisson [1]. To evaluate the Engineer's ability to predict such a performance in advance of the test, coastal experts around the world were asked to predict the caisson's movements. Eight different methods were used including simple empirical formulations, rigorous plasticity models, centrifuge tests, and small scale laboratory tests. Figure 1.1b shows the comparison between predicted and measured response as reported by

Lambe et al (1978) [4], who stated:

"Studying Figure VIII-2 (same as Figure 1.2b of this thesis) enables one to draw a most important conclusion, namely: The geotechnical engineer has difficulty in predicting with great accuracy the deformation of a caisson subjected to a cyclic load."

Foundation displacements may distort the supported structure in an unpredictable way and thus endanger its safety. In addition to safety problems, large unexpected deformations may force temporary or permanent disruption of the facility operation and may damage the environment by rupturing critical connections. Large movement of an offshore platform for oil production for example could spill tonnes of oil into the sea, while in the case of a nuclear power plant radioactive wastes would be released and harm the population and the environment.

1.2 PREDICTION METHODS

It is helpful to consider two groups of prediction methods: The first group performs an incremental analysis in which the entire cyclic load history is applied. This approach uses a hysteretic stress-strain relationship, like those developed in the anisotropic theory of plasticity ([8], [9], [10] etc.), to predict the soil

response within each cycle of loading. The main advantage from the use of this procedure is generality. Cyclic loading is treated as consecutive static loadings and unloadings, requiring for its description a few new parameters in addition to those describing static behavior. With plasticity models formulated in terms of effective stresses, solutions can be obtained under different drainage conditions: fully drained, undrained, or partially drained.

Despite generality of the procedure, serious disadvantages have so far limited its application to cyclic loading of soils. Hysteretic constitutive laws are commonly expressed by a system of linear equations in the respective increments of stress and strain. Solutions with such models, therefore, would have to proceed by small steps through each cycle of loading of a parcel that might contain several hundreds of cycles. The solution would involve enormous computational effort.

A second serious limitation is the strong dependence of incremental stiffness on effective stress, direction of increments and previous strain history. Although this dependence has been fairly well understood for the virgin loading of soils, very little is known when considerable preshearing has been applied, as is the case with cyclic loading. Application of incremental hysteretic models thus implies an accumulation of errors from incomplete knowledge that become important within a few cycles. Van Eekelen [12] identifies this disadvantage of the anisotropic theory of plasticity and states that it can only reproduce some of the characteristic behavior associated with cyclic loading. As an example he cites results

presented by Mroz et al [10] in which the calculated pore pressure generated by undrained cyclic loading is too small for initially normally consolidated clays and has the wrong sign for heavily overconsolidated clays.

Thus hysteretic models are, as yet, outside of the range of applicability for sustained cyclic loading. Several authors ([6], [7], [13], [14], [15], [16], [17]) present an alternative approach to hysteretic models: only the stress and strain accumulated at the end of one cycle of loading are modelled, while the load cycle characteristics enter indirectly in the formulation. Typical simple constitutive laws of this type correlate accumulated stresses, strains and pore pressure with the number of cycles; cyclic laboratory test results are necessary to choose the above correlations. Urzua [6] briefly discusses representative analyses of this group.

Simplicity is the major advantage from using the cumulative approach; the effective stress fields, average and cyclic, are determined in advance and then only the accumulation of strains and stresses has to be calculated. It is also possible to work with updated effective stresses which are necessary in the case of significant stress redistribution, or nonuniform cyclic loading [6],[16].

As is commonly the case, the trade-off for simplicity is loss in generality. The correlations among permanent stress, strain and number of cycles are mostly empirical and, as such are applicable only to stress and drainage conditions similar to those prevailing in the laboratory tests used to define the correlations. The effects from

different stress systems are usually considered secondary when solving complicated problems in Geomechanics, and test results from simple triaxial tests may be used under plane strain conditions (for example [6],[7]). Drainage effects, however, are too important to be overlooked; so far different sets of empirical equations have been used to predict permanent strain accumulation for drained and undrained cyclic loading ([5], [18] versus [17]).

Prediction of foundation performance under cyclic loading can also be made through centrifuge tests [19], [20] and small scale laboratory tests. Those methods, however, are experimental, and their review is out of the scope of this thesis.

1.3 OBJECTIVE OF RESEARCH

Section 1.2 indicates that a serious disadvantage of the cumulative strain approach is the lack of generality. The first objective of this thesis is to improve the generality of the approach by proposing a constitutive relation applicable to both drained and undrained problems. The key feature of the proposed relation is that it treats soil as a two phase material consisting of a solid phase and a liquid phase; it further assumes that the accumulation of strain depends on the average and cyclic effective state of stress.

Martin et al [21] conducted a fundamental study to link drained to undrained cyclic behavior of sand. They observed that the pore pressure increment during one cycle of undrained loading is equal to

the volume change that would happen during drained cyclic loading multiplied by the appropriate bulk modulus of the soil skeleton. Physically this means that during the undrained load cycle the volumetric strain increment caused by nonrecoverable slip deformation at grain contacts results in the transfer of intergranular stress to the more incompressible water. The corresponding reduction in effective stress results in release of recoverable volumetric strain stored in the sand skeleton. Hodge [22] has used a similar model to predict the pore pressure increase in cyclic triaxial tests of saturated sand; the proposed model in this thesis uses the same principles to link drained with undrained cyclic loading.

Effective stresses in the soil generally vary during repetitive loading either due to internal stress redistribution or due to external change the applied loads. To predict the rate of accumulation of permanent strain in a consistent way, the proposed model relates increments of strain and stress to increments of number of cycles. Depending on the nature of the problem, the total cyclic load history can be divided into a number of parcels of loading each containing one or more cycles, so that the requirement for constant effective stress is approximately met for each parcel.

Test data from an extensive laboratory study on cyclic behavior of Oosterschelde sand [5],[40] were used to determine the model's parameters and to evaluate its accuracy. The laboratory study included drained and undrained cyclic triaxial tests, consolidated under isotropic and non isotropic initial stresses. The model's predictions have not been evaluated for clays so far; therefore its

application is recommended for sands only.

The second objective of the thesis is the analytical prediction of foundation performance under cyclic loading. The Finite Element method (for example [24]) was chosen for this purpose mainly because it is capable of modeling consistently the interaction between the soil and the foundation. An existing Finite Element program [24] has been extensively modified to meet the special requirements of the analyses to be performed. The modifications were aimed to make the program handle

- (i) Undrained problems in addition to drained ones.
- (ii) Incremental solutions.
- (iii) Changing boundary conditions, loads, and soil properties during the analysis.
- (iv) Axisymmetric problems in addition to plane strain and plane stress ones.

The need for the modifications will become clearer in the chapters that follow.

1.4 THESIS ORGANIZATION

The thesis is organized into two parts:

(i) Chapters 2, 3, 4 and 5 belong in the first part which describes the proposed constitutive relationship.

(ii) The second part consists of chapters 6 and 7 which describe the Finite Element formulation and present the results of the case studies analysed.

Finally chapter 8 summarizes the major findings of the thesis and recommends directions for future research.

1.4.1 PART I

Drained cyclic loading of granular materials results in a steady densification together with accumulation of shear deformation; stabilization of strain is usually reached at large number of cycles [27]. It is possible, however, that steady dilation occurs during the cyclic loading, or that stabilization of shear strain is never reached [25]. Under undrained conditions excess pore pressure accumulates in addition to shear deformation. In most cases positive excess pore pressure reduces the average mean effective stress; large irreversible deformation may occur suddenly within one cycle, not necessarily the first, or the pore pressure stabilizes while shear deformation continues to accumulate [5]. Less often negative pore pressure accumulates followed by either shear failure or stabilization [5], [27].

Considerable research has been aimed in developing criteria for

gross soil behavior under cyclic loading, mainly for the prediction of large settlements during earthquakes. Chapter 2 reviews existing theories related to the specific problems of:

(i) What initial conditions will lead to contraction in volume, or dilation, during drained cyclic loading, and what is the limiting density that can be achieved by cycling the load.

(ii) What initial conditions will produce positive or negative pore pressure under undrained cyclic loading, and what is the limiting pore pressure that can be reached.

(iii) When do large irrecoverable strains occur within one cycle of loading.

The rate of accumulation of permanent strain is investigated in chapter 3. Data from drained cyclic triaxial tests on Oosterschelde Sand [5] are used to define the correlation of the rate of accumulation and the effective average and cyclic stress. The generality of the correlations is checked by test results reported by other investigators who used different material and different testing equipment.

The results of chapters 2 and 3 are used in chapter 4 to develop an analytical model of cyclic soil behavior. Static triaxial tests and drained cyclic triaxial tests are required for the determination of the model's parameters.

Evaluation of the model is obtained in chapter 5 through

comparison with cyclic one dimensional test results, where the model predicts accumulation of vertical strain accompanied by increase of the horizontal stress. Comparison is also done with cyclic undrained triaxial tests, where the model predicts the excess pore pressure increase in addition to the accumulation of shear strain.

1.4.2 PART II

Chapter 6 describes a two dimensional Finite Element computer program that incorporates the analytical model described in chapter 4. The Finite Element formulation is made in terms of effective stresses and can be used under either drained or undrained conditions. The computer program is checked by solving simple two dimensional boundary value problems with known solutions.

In chapter 7 the Finite Element program is used to study the permanent deformation of one of the piers of a barrier dam across the Oosterschelde inlet, located southwest of Rotterdam, Netherlands. Different combinations of static and cyclic loads were considered under drained and undrained conditions. The results of these analyses are compared with the permanent displacement patterns observed during the model caisson test in Neeltje Jans [4], as well as, with results obtained by Marr and Christian [7] and Urzua [6]. The effect on permanent deformations of applied loads, soil density, stress redistribution and drainage conditions is investigated.

Chapter 8 summarizes the results of the research and recommends

possible extensions of the work.

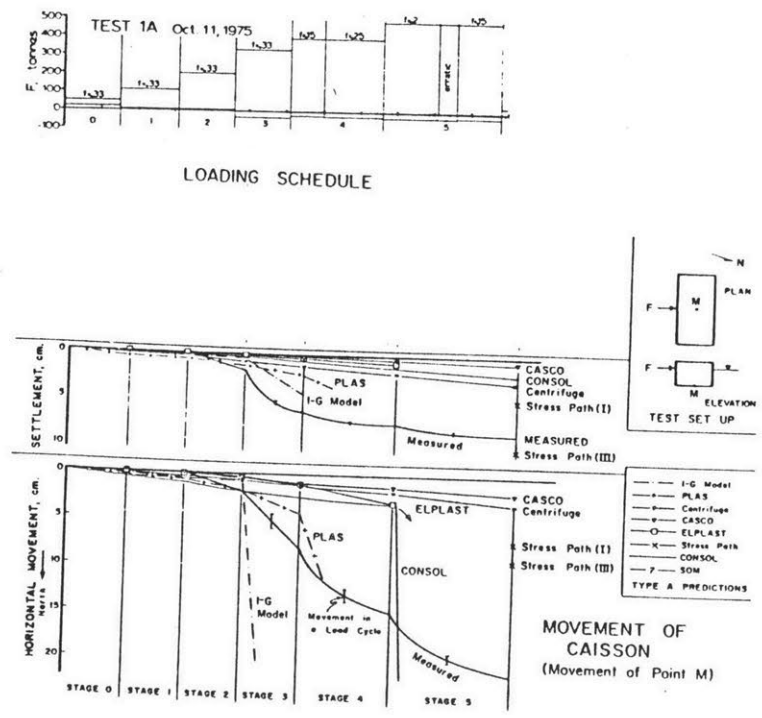
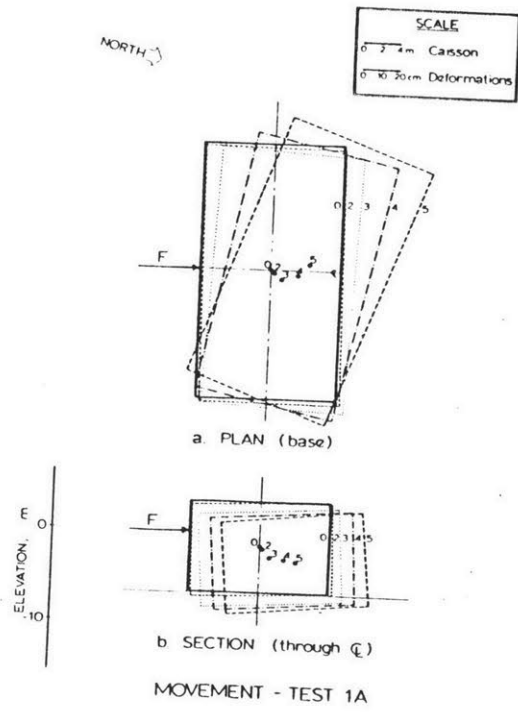


FIGURE 1.1 Observed and Predicted Movement of Model Test in Neeltje Jans (from Ref. 1)

CHAPTER 2

CONTRACTION AND DILATION IN CYCLIC LOADING2.1 INTRODUCTION

Cohesionless soils tend to change in volume during cyclic loading; this tendency results in pore pressure development when no volume change is allowed (i.e. Martin et al [21]). The term Contraction in this thesis is used to denote reduction in the volume of soil during drained cyclic loading, or development of positive pore pressure during undrained cyclic loading. The term Dilation is used to describe the opposite phenomenon, i.e. the increase in the volume of soil during drained cyclic loading or the development of negative pore pressure during undrained cyclic loading. The purpose of this chapter is to suggest a complete set of criteria for predicting contraction and dilation.

The literature reviewed was not particularly rich in complete studies of contraction and dilation of sands. In fact only a set of criteria proposed by Luong and Sidaner [25,26] defined clearly the initial conditions leading to contractive and dilative behavior of sands. Sangrey et al [29] and France and Sangrey [30] propose a

different set of criteria applicable to clays. Later attempts by Sangrey et al [31], to extend those criteria to cover silts and sands were unsuccessful, since the limited amount of data on cyclic loading of sands used in the study (Castro [28]) indicated significantly different behavioral patterns for sands and clays.

In the following paragraphs the behavioral model suggested by Luong and Sidaner will be reviewed, and compared with available cyclic triaxial test results on Oosterschelde Sand [39].

2.2 THE "CHARACTERISTIC THRESHOLD" MODEL

An experimental program using the conventional axisymmetric triaxial apparatus suggested the introduction of the concept of the "Characteristic Threshold" for cohesionless soils. This concept offers the framework for a set of criteria for cyclic behavior of sands proposed by Luong and Sidaner [25,26].

2.2.1 THE CHARACTERISTIC THRESHOLD - DEFINITION

During undrained Compression Loading of a dense sand in a triaxial test, the rate of pore pressure generation is positive initially and then becomes negative passing through zero (fig. 2.1). Large irreversible shear strain development corresponds to the negative rate of pore pressure generation. During a similar drained test an initial volume decrease is observed followed by a later increase, combined

with large irreversible shear strain (fig. 2.2).

The stress level corresponding to either the inversion of the rate of pore pressure generation in an undrained test, or the zero of the volume change rate in a drained one, defines the Characteristic Threshold (CT). This line lies below the failure envelope in the effective stress space (fig. 2.3) and divides it to two domains, the "surcharacteristic" and the "subcharacteristic."

2.2.2 DRAINED LOADING

Cyclic loading of the sand within the "Subcharacteristic" domain leads to steady densification and accumulation of permanent shear strain. The rate of accumulation decreases gradually as the number of cycles increases until stabilization of the shear and volumetric strain finally occurs. Cyclic loading within the "surcharacteristic domain," on the other hand, causes ratchet behavior and failure because of large dilatancy.

When the average stress point lies on the CT-line and cyclic stresses do not touch the failure line, no irreversible volume change occurs, while the accumulation of axial strain increases in proportion to the logarithm of the number of cycles. During cyclic loading crossing the CT-line, the behavior is interpolated between the three patterns described above.

Figure 2.4 summarizes the sand behavior during drained cyclic loading, as a function of the applied average and cyclic stress with

respect to the CT-line.

2.2.3 UNDRAINED LOADING

Undrained cyclic loading in triaxial tests is characterized by two distinct phases:

First pore pressure develops accompanied by a steady accumulation of shear strain; when the average effective stress meets the CT-line stabilization of the pore pressure occurs. For initial average effective stress states in the "subcharacteristic domain" the stabilized pore pressure is positive, while it is negative for initial average stress states in the "surcharacteristic domain."

Second, during cyclic loading around the stabilized position the pore pressure varies between two fixed values, and shear strain accumulates more or less proportionally to the logarithm of the number of cycles. The stabilized position is reached asymptotically, and large number of cycles is required to reach it, especially when the cyclic load amplitude is small.

Test data supporting this behavioral pattern are shown in figures 2.5 and 2.6 for Contractive and Dilative sands respectively.

2.3 CYCLIC BEHAVIOR OF SAND A

A four year testing program at M.I.T. between 1975 and 1979 on the cyclic behavior of Dutch sands, produced 328 cyclic triaxial tests, and 112 static tests on sand. Appendix A gives information about the history and the objective of this program, as well as, description of the soils tested and the testing procedures. Oosterschelde Sand A, or briefly Sand A, was the most extensively tested sand during this program. The present section compares cyclic test results from Sand A, with predictions of the Characteristic Threshold model.

2.3.1 THE CHARACTERISTIC THRESHOLD - SAND A

Static triaxial compression tests, drained and undrained, were used to locate the CT-line for Sand A; the test data were obtained from Document L-38 prepared by T.W. Lambe and Associates for the Dutch Government [39]. The location of the CT-line was defined using the procedures recommended by Luong and Sidaner [26] - described also in section 2.2.1 - and the results are portrayed through the "Characteristic Threshold Angle" (ϕ_{CT}) defined by the relation

$$\phi_{CT} = \sin^{-1} \left(\frac{\sigma_v - \sigma_h}{\sigma_v + \sigma_h} \right) \text{ on CT-line}$$

Tables 2.1 and 2.2 summarize the consolidation stresses and porosities for the tests analysed. In addition to the "Characteristic

Threshold Angle" in the above tables, the maximum friction angle is also presented, as estimated by the relation:

$$\phi_{\max} = \sin^{-1} \left(\frac{\sigma_v - \sigma_h}{\sigma_v + \sigma_h} \right)_{\max}$$

The effects of porosity on both angles is shown in figure 2.7. Despite the considerable scatter in the results the following conclusions can be drawn:

- (i) There is no pronounced effect of the drainage conditions - drained vs. undrained - on the estimated Φ_{CT} .
- (ii) The effect of porosity on Φ_{CT} is considerably less than its effect on Φ_{\max} .
- (iii) Φ_{CT} increases with decreasing porosity.

2.3.2 UNDRAINED LOADING

Document L-39 [40] summarizes the results from Undrained Cyclic Triaxial Tests on Sand A. The tests were performed under various average stresses, isotropic or not, various cyclic stresses and porosities. Relative to the Characteristic Threshold of Sand A all tests belong to the subcharacteristic domain, and therefore no information is available about the behavior of Sand A in the surcharacteristic domain.

In all tests positive pore pressure accumulated after each cycle

of loading, driving the effective stresses towards the failure envelope. The rate of accumulation decreased steadily during the cyclic loading until practically no additional accumulation occurred. Table 2.3 summarizes the friction angle where stabilization of the average state of effective stress occurred, for non-isotropic cyclic triaxial tests. Figure 2.8 compares this angle with the Characteristic Threshold angle (Φ_{CT}) determined by static tests; the data suggests that Φ_{CT} determined by the static tests is an upper bound to the angle where stabilization of pore pressure occurs. This is consistent with Luong and Sidaner's criterion stating that equilibrium on the CT-line is asymptotic; most undrained tests on Sand A, however, were stopped shortly after the rate of accumulation became "practically" zero so that it cannot be determined if perfect stabilization of the pore pressure was achieved during the test.

Figure 2.9 plots the cumulative vertical strain versus the logarithm of the number of cycles, from several undrained cyclic tests on Sand A. The rate of accumulation increases during each test; as the effective state of stress approaches to the CT-line - end portion of curves in figure 2.9 - accumulation of strain occurs approximately proportional to the logarithm of the number of cycles. Luong and Sidaner report the same behavior during cyclic loading back and forth across the CT-line.

In summary it can be concluded that that the criteria proposed by Luong and Sidaner for undrained cyclic loading of Contractive sands agree with the general behavior of Sand A under cyclic loading.

2.3.3 DRAINED LOADING

Drained Cyclic Triaxial Tests were also performed on Sand A and are described in Document L-39. During all tests the average and cyclic stresses were kept constant, inside the Subcharacteristic domain; no tests were run on the CT-line or in the surcharacteristic domain.

The accumulated volumetric and axial strain due to cyclic loading are plotted in figures 2.10 and 2.11 versus the number of cycles; the test conditions are summarized in table 2.4. In all tests the cyclic loading caused reductions of the volume of the sand with a steadily decreasing rate, similar to what Luong and Sidaner report. All tests were stopped before stabilization of volume occurred, so that no conclusions can be drawn with regard to the minimum volume that is reached due to cyclic loading of Sand A.

2.4 EVALUATION OF THE CHARACTERISTIC THRESHOLD MODEL

Luong and Sidaner were not the first to appreciate the significance of the CT-line for the cyclic behavior of sands. Ishihara, Tatsuoka, and Yasuda [33] defined a similar threshold, the "Phase Transformation Line" which was used as an index of initial liquefaction, and also as a criterion for beneficial preshearing in liquefaction [34]. Its use by Luong and Sidaner as a bound between dilative and contractive behavior has a sound experimental basis as well.

Although the Characteristic Threshold concept provides a complete description of the ultimate pore pressure that can be reached with undrained cyclic loading, it does not specify the ultimate volume that can be reached during drained cyclic loading. Youd [27a] studied the compaction of sands by repeated shear straining, and reports that high densities were achieved, which sometimes exceeded those determined by the standard ASTM procedures. Similar results were reported by the same researcher in a previous publication [27b].

Luong and Sidaner suggested that undrained cyclic loading in the subcharacteristic domain will always lead to stabilization of the pore pressure on the CT-line. Castro [78], however, shows experimental results where, during cyclic loading in the subcharacteristic domain, sudden failure of the sand occurred within one cycle of loading. This behavior was observed in sands that during static undrained loading develop a well defined peak shear strength followed by significant strain softening. Failure during undrained cyclic loading occurred when the maximum shear stress exceeds a critical limit, approximately equal to the ultimate undrained strength of the sand [31].

For Sand A, which follows the same trends reported by Luong and Sidaner, the ultimate shear strength is estimated in Appendix B as function of the porosity. For the tests analyzed the maximum shear was well below the ultimate strength. Although there is no information available about the ultimate drained strength of the sand(s) tested by Luong and Sidaner, it is reasonable to assume that their conclusion refers to cyclic loading at shear stress levels lower than the undrained strength of the sand.

Finally Luong and Sidaner's criteria do not describe behavior during cyclic loading touching the failure line. One such case is, for example, cyclic loading with average stresses on the CT-line and cyclic stresses that cause failure. It is reasonable to question if under such conditions no permanent volume change will occur and that the axial strain will not accumulate faster than the criteria define. To obtain a positive answer to similar questions, however, is generally difficult because of the numerous uncertainties associated with laboratory testing close to failure.

In the following chapters the set of criteria proposed by Luong and Sidaner will be used to distinguish Contractive from Dilative sands when the maximum shear stress during cyclic loading does not exceed the ultimate undrained strength. In addition it will be assumed that the minimum volume that can be reached with drained cyclic loading corresponds to the maximum density of the material determined by standard ASTM procedures. While this property is not a basic property of the soil its determination is part of most laboratory testing programs for sands.

Reference to Luong and Sidaner's criteria complemented by the definition of the minimum volume, will be made thereafter by the name "Characteristic Threshold" model, or "CT-model".

2.5 SUMMARY

The most complete set of criteria for contraction and dilation of sands, reported in the literature, is that suggested by Luong and Sidaner [26]. According to this set of criteria a sand may contract or dilate depending on its average effective stress state compared to the CT-line.

Data from drained and undrained cyclic triaxial tests on Sand A were in good agreement with the set of criteria for contractive sands. No tests were run in the surcharacteristic domain so that the validity of the criteria for this domain cannot be evaluated.

Test results reported by Castro [78] suggest that the CT-model does not apply to undrained cyclic loading with maximum shear stress larger than the ultimate undrained strength of the sand. Under such conditions stabilization of pore pressure is never reached, but sudden collapse of the sand can occur within one cycle of loading, not necessarily the first.

As a first approximation it was assumed that the ultimate volume that can be reached due to drained cyclic loading corresponds to the maximum density of the material determined by standard ASTM procedures. Luong and Sidaner's set of criteria do not specify the ultimate volume.

TEST #LS	TEST TYPE	$\bar{\sigma}_{vo}$ ksc	$\bar{\sigma}_{ho}$ ksc	n_o %	ϕ_{CT} (o)	ϕ_{MAX} (o)
65	CAU	1.41	1.99	44.4	28.0	30.1
67	CIU	2.00	2.00	45.1	33.7	34.1
68	CIU	5.00	5.00	45.5	29.0	30.4
74	CIU	1.00	1.00	41.4	32.0	35.0
79	CIU	2.00	2.00	45.9	28.0	31.1
90	CAU	2.50	1.50	41.1	36.0	39.2
99I	CAU	2.50	1.50	41.4	32.0	35.9
99II	CAU	2.50	1.50	41.4	32.0	37.3

TABLE 2.1: Critical Threshold Angle from Undrained Tests on Sand A

TEST #LS	TEST TYPE	$\bar{\sigma}_{vo}$ ksc	$\bar{\sigma}_{ho}$ ksc	n_o %	ϕ_{CT} (o)	ϕ_{MAX} (o)
58	CID	1.00	1.00	43.8	30.0	33.1
59	CID	1.02	1.00	37.9	30.0	43.3
60	CAD	.90	1.00	40.9	29.0	37.8
61	CAD	1.00	2.00	40.8	33.0	38.8
62	CID	1.18	1.18	41.1	29.0	38.8
70	CID	1.00	1.02	41.1	30.0	36.6
71	CAD	1.00	.50	41.1	33.0	38.2
72	CID	3.00	3.00	41.4	30.0	34.9
73	CID	.50	.50	41.2	33.0	39.5
75	CID	1.00	1.00	37.2	32.0	43.1
76	CID	1.00	1.00	41.3	30.0	36.9
86	CID	1.00	1.00	41.1	31.0	37.0
91	CID	1.00	1.00	40.6	28.0	34.2
95	CID	1.00	1.00	40.4	27.0	34.8
96	CID	1.00	1.00	40.9	28.0	33.7
97	CID	1.00	1.00	40.9	28.0	34.1
98	CAD	1.00	2.00	41.5	29.0	32.1
108	CID	5.00	5.00	41.8	31.0	32.7

TABLE 2.2: Critical Threshold Angle from Drained Tests on Sand A

TEST #LC	TEST TYPE	$\frac{\sigma_v - \sigma_h}{2}$ (ksc)	n_o (%)	ϕ_{CT} (o)
66	CAU	.25	40.40	28.0
97	CAU	.50	41.26	28.0
104	CAU	.50	41.90	28.0
129	CAU	.50	43.50	27.0
130	CAU	.50	43.20	28.0
131	CAU	.50	42.90	29.0
132	CAU	.75	41.40	28.0
135	CAU	.50	41.20	27.0
137	CAU	1.00	41.30	28.0
142	CAU	.50	41.70	28.0
148	CAU	.25	41.10	25.0
149	CAU	1.25	41.40	28.0
151	CAU	.50	41.40	29.0
156	CAU	.50	45.00	29.0
166	CAU	1.00	43.30	28.0
181	CAU	.50	41.30	29.0
219	CAU	.50	41.60	29.0
229	CAU	1.00	43.20	27.0
230	CAU	.50	42.20	30.0
242	CAU	1.00	41.90	28.0
251	CAU	1.75	41.10	26.0
260	CAU	1.00	44.30	29.0

TABLE 2.3: Characteristic Threshold Angle
from Undrained Cyclic Triaxial
Tests on Sand A

TEST #LC	TEST TYPE	σ_{vo} (ksc)	σ_{ho} (ksc)	Δq_{cyc}^* (ksc)	n_o (%)	n_f^{**} (%)
141	CAD	2.50	1.50	.45	43.1	42.0
176	CAD	3.00	2.00	1.00	43.0	40.6
187	CAD	4.20	2.80	.38	43.2	42.9
192	CAD	4.17	2.77	.63	43.1	42.7
198	CAD	3.00	2.00	.45	45.1	44.4
257	CAD	2.57	1.57	.45	42.0	41.2
282	CAD	3.01	2.01	.45	40.6	40.4
285	CAD	5.41	3.61	.45	43.1	42.7
290	CAD	5.42	3.62	.81	43.4	42.8
295	CAD	3.02	2.02	.45	43.3	42.4
297	CAD	2.51	1.51	.45	41.8	41.4
303	CAD	3.01	2.01	.21	42.6	42.4
305	CAD	3.04	2.04	.45	42.9	41.9
308	CAD	2.55	1.55	.45	42.8	41.6
316	CAD	2.50	1.50	.24	42.9	41.7
327	CAD	2.00	3.00	.45	43.3	42.3

$$* \Delta q_{cyc} = (\Delta \sigma_v - \Delta \sigma_h)_{cyc} / 2$$

** n_f : porosity at the end of cyclic loading

TABLE 2.4: Drained Cyclic Test Conditions - Sand A

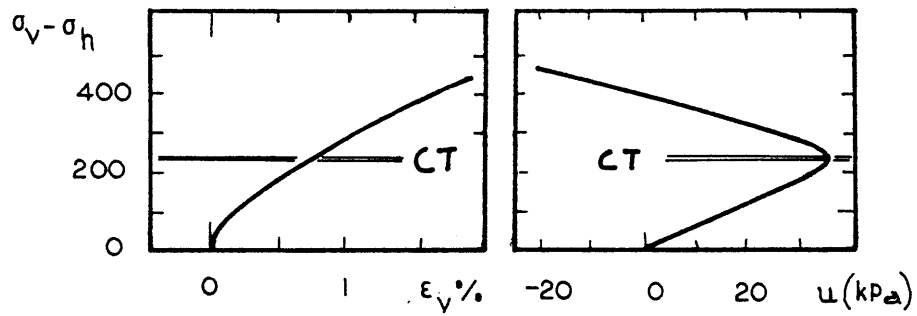


FIGURE 2.1: Determination of the Characteristic Threshold (CT) during an Undrained Test (Ref. 25)

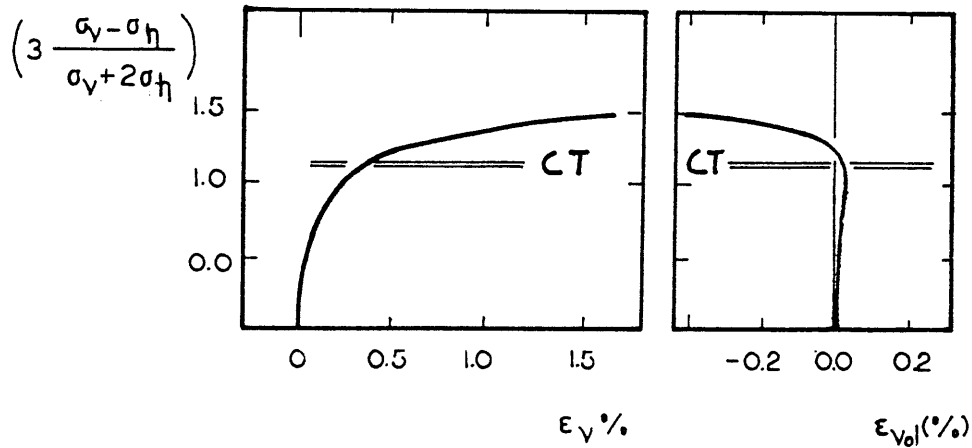


FIGURE 2.2: Determination of the Characteristic Threshold (CT) during a Drained Test (Ref. 25)

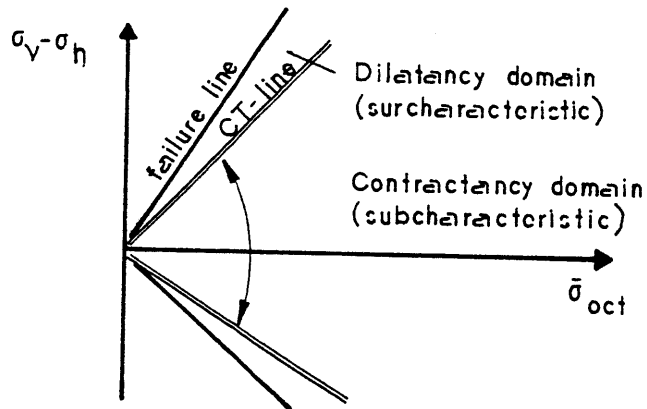


FIGURE 2.3 : Characteristic Criterion Bounding the Contractancy Domain of Granular Materials (Ref. 25)

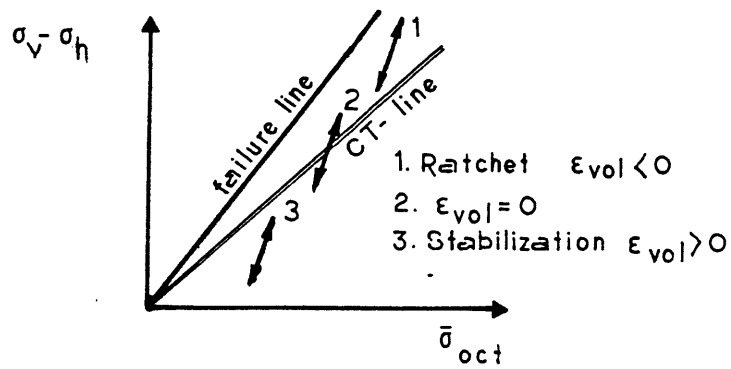


FIGURE 2.4 : Diverse Cyclic Behavior of Sand Observed during Drained Shearing under Constant Confinement Conditions (Ref. 25)

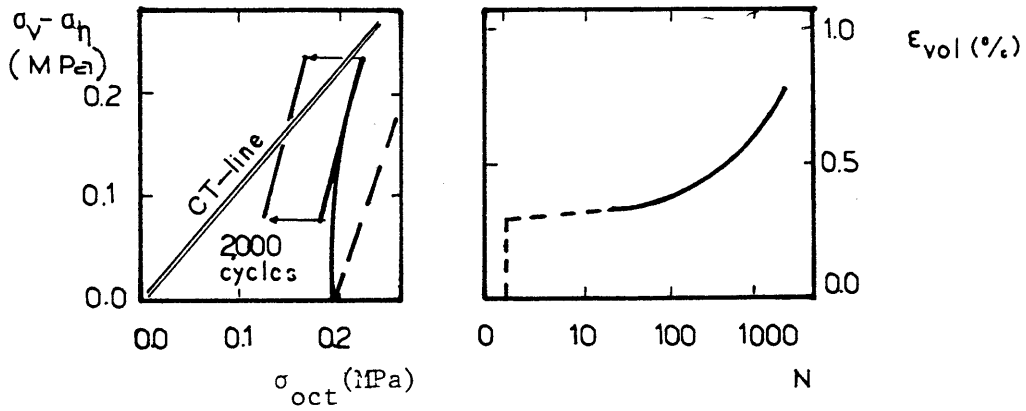


FIGURE 2.5 : Undrained Cyclic Shearing in the Subcharacteristic Domain (Ref. 25)

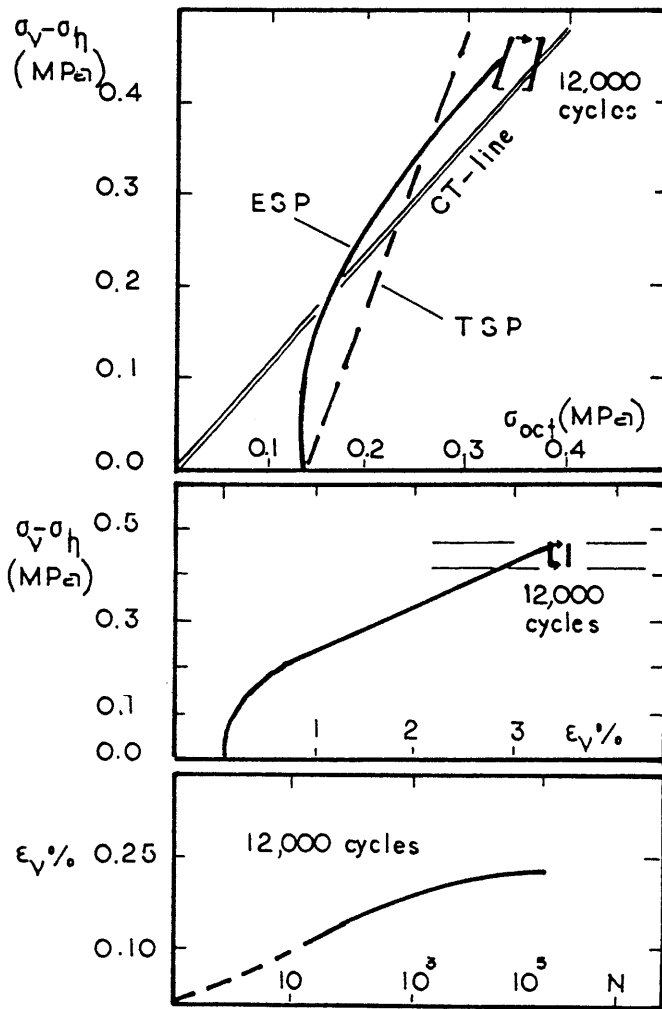


FIGURE 2.6 : Prolonged Cyclic Shearing (Ref. 25)

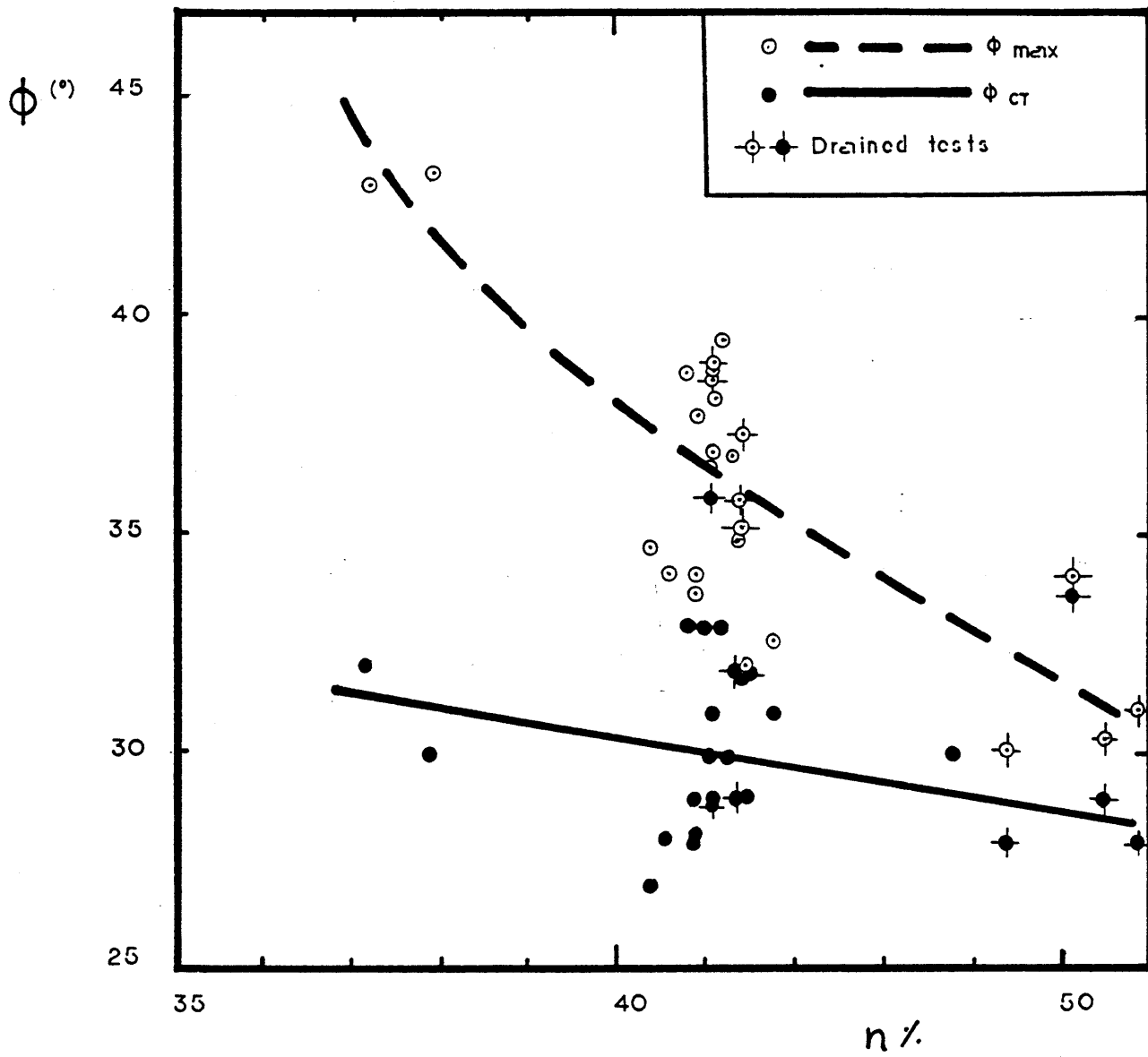


FIGURE 2.7 : Maximum Friction Angle and Characteristic Threshold-Angle of Sand A

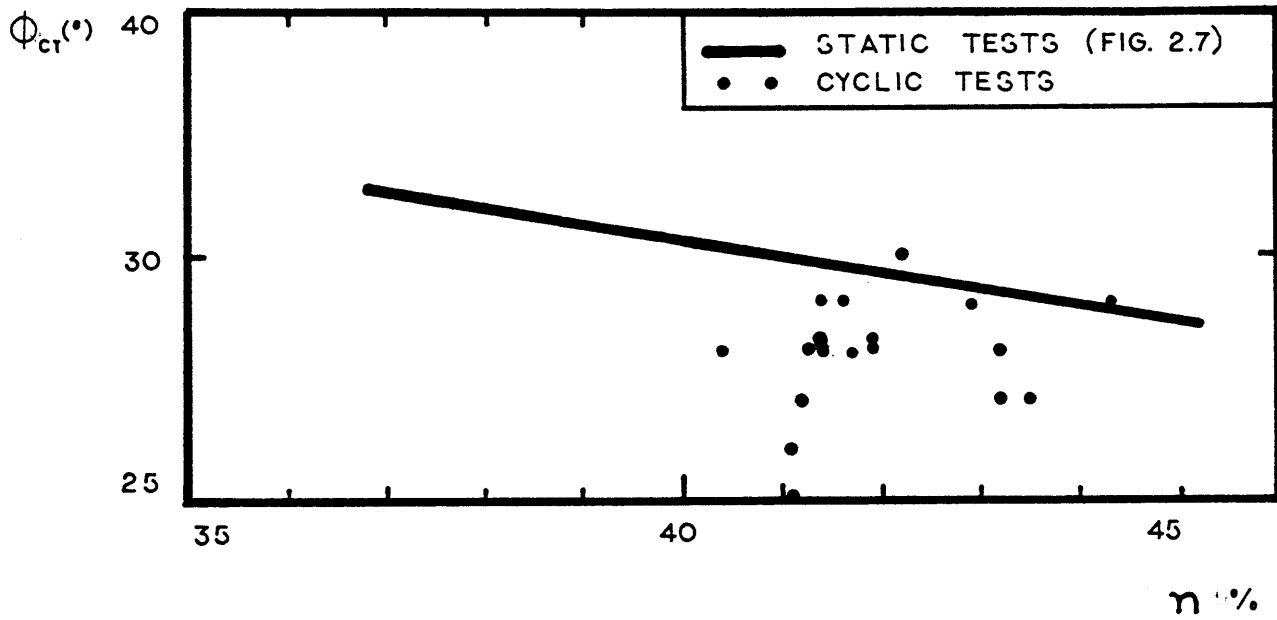


FIGURE 2.8 : Characteristic Threshold Angle Determined by Static and Cyclic Triaxial Tests on Sand A

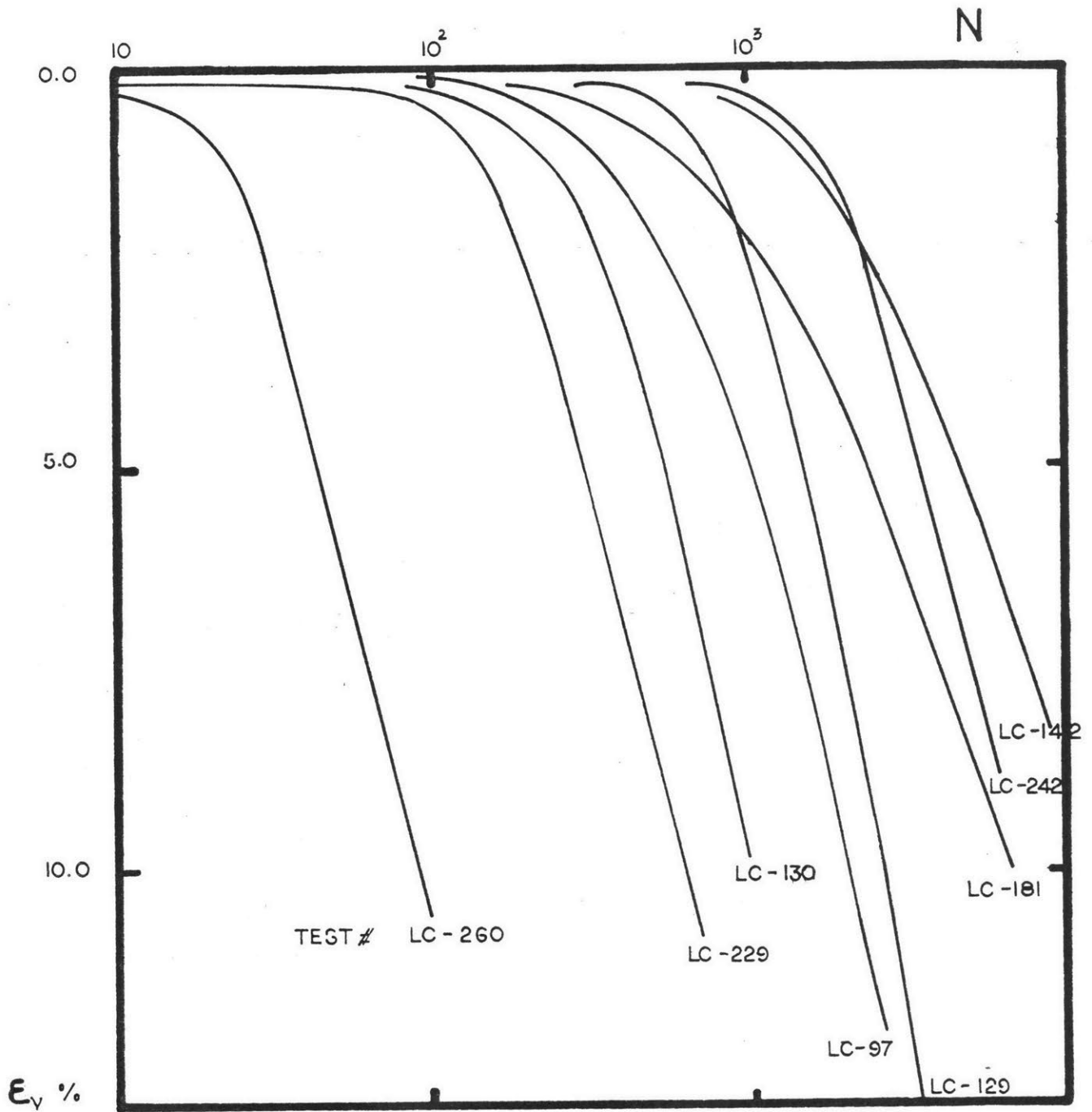


FIGURE 2.9 : Cumulative Vertical Strain in Undrained Cyclic Triaxial Tests on Sand A

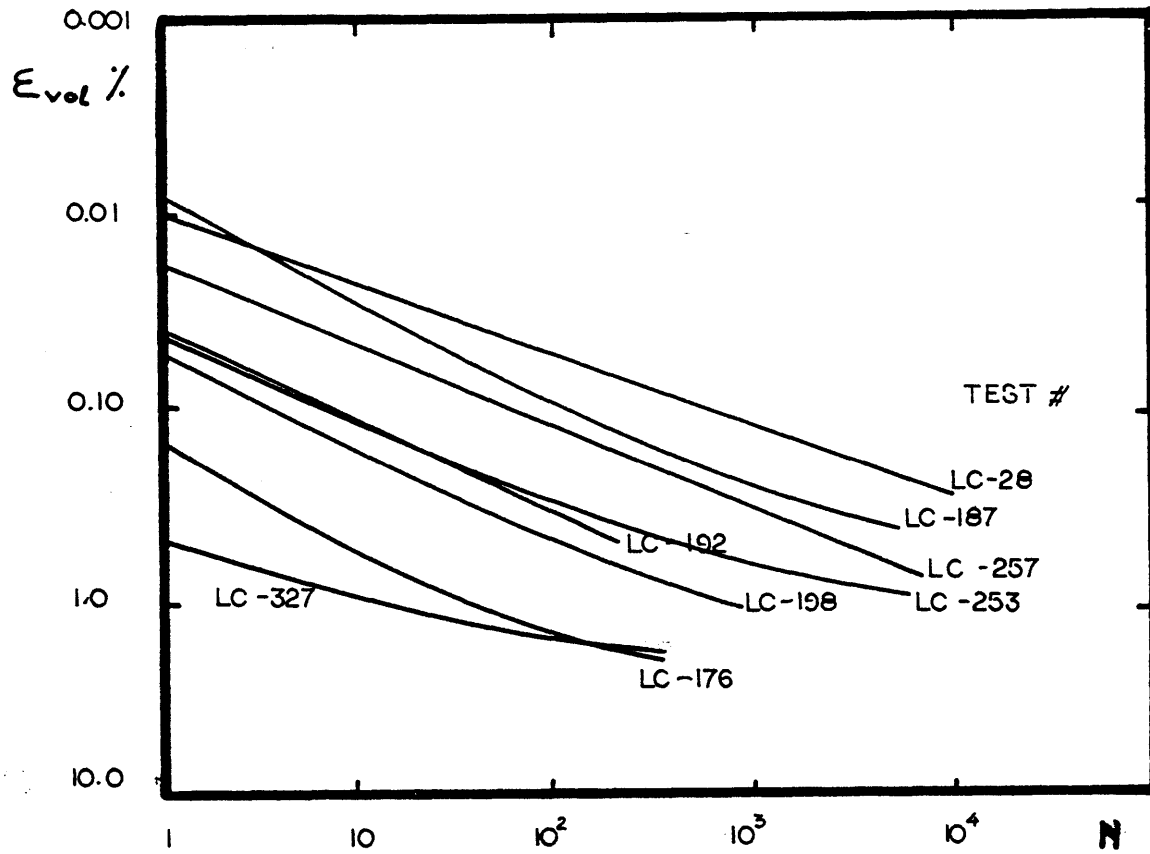


FIGURE 2.10 : Cumulative Volumetric Strain in Drained Cyclic Triaxial Tests

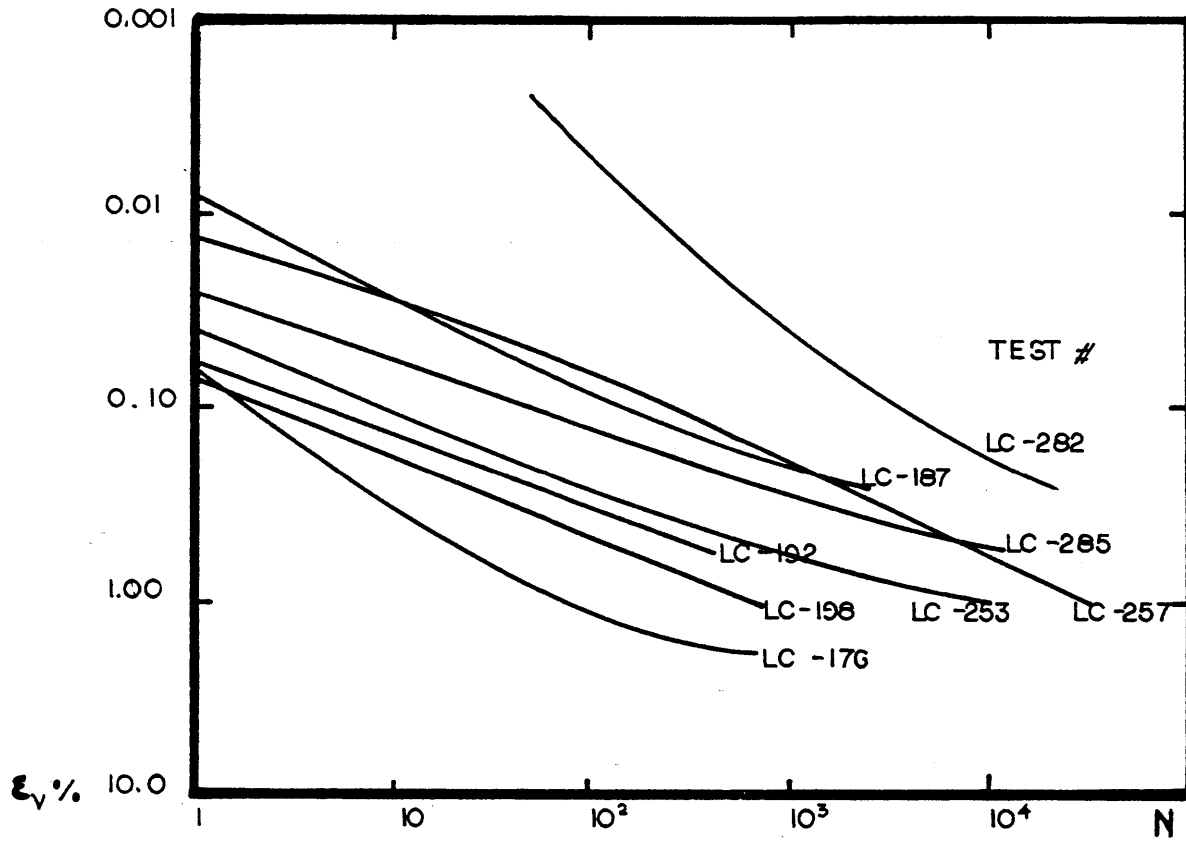


FIGURE 2.11 : Cumulative Vertical Strain in Drained Cyclic Triaxial Tests

CHAPTER 3

PERMANENT STRAIN IN THE DRAINED CYCLIC TRIAXIAL TEST

3.1 INTRODUCTION

The previous chapter discussed the limit states of strain and stress reached by cyclic loading. This chapter continues the description of cyclic sand behavior by defining the rate of accumulation of permanent strain in drained cyclic triaxial tests. Research in the past ([21], [22]) has shown that this information can lead to predictions of the performance of sand under undrained cyclic loading as well.

Results from drained Cyclic Triaxial tests on Sand A, run at M.I.T., will be used to derive empirical equations for the accumulation of permanent strain; comparison with test data reported by other researchers is aimed at ensuring more general applicability of the proposed relations.

There are definite advantages from using drained triaxial test results for this study:

(i) Since constant average effective stresses can be maintained throughout the test, the permanent deformation exclusively due to cyclic loading can be studied. The same is not true, for example, for Direct Simple Shear tests; in such tests average effective stresses change and thus deformations are caused partly by the change in the average effective stress and partly due to cyclic loading.

(ii) Since stresses are controlled, the dependence of the rate of accumulation of permanent strain on the average and cyclic state of stress can be investigated.

3.2 PERMANENT VOLUMETRIC STRAIN

Important factors that may affect cumulative volume change are the initial porosity of the sand, the average effective stresses, the cyclic stresses and the cyclic strains. Several researchers have found that repetitive changes in the effective hydrostatic stress contribute negligibly to permanent volume reduction in sand. Ko and Scott [41] and El Shoby and Andrawes [42] claim that the behavior of dense sand under hydrostatic stress change is nearly elastic, producing insignificant residual strain; the same is true for loose sands except that some permanent strain occurs during the first few cycles of loading.

Cyclic shearing, therefore, is the primary cause of change in

volume. Silver and Seed [43], Youd [27] using cyclic simple shear tests and Hodge and Marr [22b] using results from cyclic triaxial tests on Sand A, confirm this statement. Further they conclude that for a given initial density and cycle number, permanent volume change is a function only of the difference between the maximum and the minimum shear strain applied to the sample. This strain is called "cyclic shear strain" in the remaining of the thesis. Figure 3.1 shows results reported by Silver and Seed [43] and Hodge and Marr [44] which support a linear relationship between the logarithms of cyclic shear strain and permanent volume change, for small levels of cyclic shear strain (<1%) and for small number of cycles ($N < 1000$). The slope of the straight lines in figure 3.1 is not sensitive to changes in the initial density of the material and the cycle number. Consequently the relationship between the cumulative volume strain and the cyclic shear strain can be written as

$$\varepsilon_{vol} = C(n, N) \gamma_{cyc}^{\alpha} \quad (3.1)$$

Hodge and Marr [22b] used results from Drained Cyclic Triaxial tests on Sand A and found that under constant cyclic shear strain, a linear relationship exists between the logarithms of the permanent volume change and the cycle number (see figure 3.2). Their conclusion, however, must be limited to small level of permanent strains. According to the Characteristic Threshold model described in chapter 2, as the maximum density of the sand is approached the rate of accumulation of volumetric strain decreases gradually and eventually becomes zero. For small levels of permanent volumetric

strain equation 3.1 becomes:

$$\epsilon_{vol} = C(n) N^b \gamma_{cyc}^\alpha \quad (3.2)$$

For the narrow range of porosities tested by Hodge and Marr, no pronounced effect of the initial porosity on the accumulation of volumetric strain was observed; the empirical relation they propose for contractive Sand A is

$$\epsilon_{vol} (\%) = 0.685 N^{0.4} \gamma_{cyc}^{1.26} \quad (3.3)$$

Silver and Seed [43] tested sand under a wider range of initial densities and observed that the loose sand accumulated volumetric strain faster than the dense one. Part of their data, shown in figure 3.3, indicate that the function C in equation 3.2 has the form

$$C = C_o \exp \left[c \frac{Dr - Dr_o}{Dr_o} \right] \quad (3.4)$$

where C_o is the value of the function for Relative density equal to Dr_o . Available test data for Sand A are not adequate to verify equation 3.4; in the following chapters equation 3.3 will be used to describe the cumulative volumetric strain, for contractive Sand A, at small levels of permanent strain.

3.3 PERMANENT VERTICAL STRAIN

Test results from drained cyclic triaxial tests are commonly portrayed in terms of accumulated volumetric and vertical strain versus number of cycles, since the testing system facilitates direct measurement of these quantities. The horizontal permanent strain can be computed as a function of the vertical and volumetric strain. In order to complete the study of permanent strains in cyclic triaxial tests, the accumulation of vertical strain will be examined next.

The ratio of the measured vertical to the volumetric permanent strain for different number of cycles is summarized in table 3.1 for twenty five drained cyclic test on Sand A. The data suggest that for each test this ratio is approximately constant, independent of the number of cycles.

Factors that may affect the ratio of permanent strains are the porosity of the sand, the average effective stress and the cyclic stress or strain. The effect of initial porosity is shown in figure 3.4 and the effect of cyclic shear strain is shown in figure 3.5. Both factors have no pronounced effect on the ratio of permanent strains. The effect of the average effective stress is shown in figure 3.6 where the ratio of the vertical to the volumetric permanent strain is plotted versus the average stress ratio ($q/\bar{\sigma}_o$). Larger stress ratios result in larger proportions of vertical to volumetric permanent strain. An empirical relationship that fits the data is:

$$\frac{\epsilon_v^-}{\epsilon_{vol}} = 13.6 q \frac{|q|}{\bar{\sigma}_{oct}^2} + 0.33 \quad (3.5)$$

The test results in figure 3.6 correspond to contractive Sand A at small levels of permanent volume strain; application of equation (3.5), therefore, is restricted to small levels of permanent volumetric strain too.

3.4 LIMITS ON PERMANENT STRAIN ACCUMULATION

3.4.1 VOLUMETRIC STRAIN

According to the CT-model described in chapter 2, a sand has no tendency to change in volume due to cyclic loading under two conditions:

- (i) When the average effective stress lies on the Critical Threshold line.
- (ii) When the density of the sand is equal to the maximum density defined by standard ASTM procedures.

In section 3.1 it was shown that the accumulation of volumetric strain of contractive Sand A can be described by an empirical relationship, namely:

$$\epsilon_{vol}^- = 0.685 \gamma_{cyc}^{1.26} N^{0.4} \quad (3.3)$$

Differentiation of equation 3.3 with respect to the number of cycles

gives an empirical equation for the rate of volumetric strain accumulation:

$$\dot{\epsilon}_{vol} = 0.274 \gamma_{cyc}^{1.26} N^{-0.60} \quad (3.6)$$

Equations 3.3 and 3.6 do not satisfy conditions (i) and (ii) above; to complete the description of permanent volume change, equation 3.6 will be multiplied by a function f such that:

$$f = \begin{bmatrix} 0.0 & \delta / \delta_{max} = 0.0 \\ 1.0 & \delta / \delta_{max} = 1.0 \end{bmatrix} \quad (3.7)$$

where δ denotes the distance of the volume and average effective stress state of the sand from the limit states described by conditions (i) and (ii); δ_{max} denotes the maximum δ during the loading history (see figure 3.7). One function with the above properties (equation 3.7) is

$$f = 1. - \exp(-\ell.S) \quad \ell > 0 \quad (3.8)$$

with

$$s = \frac{\delta}{\delta_{max} - \delta}$$

The maximum distance (δ_{max}) is defined either as volume or as stress depending on the definition of the distance (δ) to which it must be compatible.

The function f is plotted in figure 3.8 for different values of the parameter " ℓ ". This parameter defines the extent of the influence of the limit state and is determined through tests approaching the limit states. No such drained tests were available for Sand A; an estimation of the appropriate value of " ℓ " will be obtained from

undrained cyclic triaxial tests where the average effective stress stabilizes on the Critical Threshold line.

3.4.2 VERTICAL STRAIN

With respect to the vertical permanent strain, the behavioral model suggests that the rate of accumulation becomes zero when the maximum density of the sand is reached; on the CT-line, strain accumulates in proportion to the logarithm of the number of cycles:

$$\dot{\epsilon}_v = \begin{bmatrix} 0.0 & \text{Dr} = \text{Dr}_{\max} \\ K \frac{1}{N} & \text{on CT-line} \end{bmatrix}$$

The shear component of the vertical strain rate is:

$$\dot{\epsilon}_v = \dot{\epsilon}_v - \frac{1}{3} \dot{\epsilon}_{\text{vol}} = 3.73 q \frac{|q|}{\sigma_{\text{oct}}^2} \gamma_{\text{cyc}}^{1.26} N^{-0.6} \quad (3.9a)$$

To make this expression consistent with the behavioral model it will be multiplied by the same function "f" used for volumetric strain (eq. 3.8). The distances Σ and Σ_{\max} , will be defined only with respect to the minimum volume of the sand; thus equation (3.9a) becomes

$$\dot{\epsilon}_v = 3.73 q \frac{|q|}{\sigma_{\text{oct}}^2} \gamma_{\text{cyc}}^{1.26} N^{-0.6} f \quad (3.9b)$$

implying that

$$\dot{\epsilon}_v = \begin{bmatrix} 0.0 & \text{Dr} = \text{Dr}_{\max} \\ K \frac{1}{N^{0.6}} & \text{on CT-line} \end{bmatrix}$$

It is possible to modify equation 3.9 so that it will agree exactly

with the CT-model. Such modification, however, will complicate the empirical relation, without improving essentially its accuracy, since cyclic loading back and forth across the CT-line is a rather extreme situation.

3.5 CYCLIC SHEAR STRAIN IN TRIAXIAL TESTS

Earlier in this chapter it has been shown that the accumulation of permanent deformation depends on the cyclic shear strain among other factors. In triaxial tests the maximum shear strain is equal to the difference between the major and the minor principal strains:

$$\gamma = \epsilon_1 - \epsilon_3$$

The cyclic shear strain in equation 3.3 was defined by Hodge and Marr [22b] as:

$$\begin{aligned} \gamma_{cyc} &= \text{peak-to-peak shear strain} = \gamma_{max} - \gamma_{min} \\ \gamma_{max} &= \text{shear strain at maximum shear stress} \\ \gamma_{min} &= \text{shear strain at minimum shear stress} \end{aligned}$$

In the following paragraphs, two empirical equations for the cyclic shear strain will be presented: one proposed by Hodge and Marr and also used by Urzua [6], and another which is based on the hyperbolic constitutive model, and is proposed by the author.

The applicability of both models will be examined with respect to drained and undrained cyclic triaxial tests of Sand A [62]. In the

drained tests the average and the cyclic effective stress were kept constant throughout the test (figure 3.9). Hodge and Marr observed that while values of γ_{max} and γ_{min} in equation (3.10) continually increased with cycling, the cyclic shear strain remained relatively constant (figure 3.9). In the undrained test total stresses are controlled; under constant total average and cyclic stresses excess pore pressure development changes the effective stress during the test and results in varying cyclic shear strain (figure 3.10). For undrained tests in the "subcharacteristic domain," the cyclic shear strain increases as the effective stress path moves towards the critical threshold line.

3.5.1 PEAK TO PEAK CYCLIC SHEAR STRAIN

Hodge and Marr suggest that the effects of porosity, cyclic shear stress ratio and mean effective stress on are approximately independent of each other, and proposed the following relationship for Sand A:

$$\gamma_{cyc} (\%) = -0.488 + 0.01 n (\%) + 0.562 \frac{\Delta q_{cyc}}{\bar{p}} + 0.016 \bar{p} \quad (3.11)$$

Application of this relation is strictly limited to stress and porosity conditions similar to those existed in the laboratory study:

$$41.0 < n\% < 43.6$$

$$0.06 < \frac{\Delta q_{cyc}}{\bar{p}} < 0.28$$

$$1.0 \leq \bar{p} \leq 5.0 \quad \text{ksc}$$

$$0.15 \leq \frac{q}{\bar{p}} \leq 0.30$$

$$\Delta q_{\text{cyc}} = \Delta p_{\text{cyc}}$$

Hodge proposed equation (3.11) for application with drained cyclic triaxial tests where the mean stress (p) remains constant. For undrained cyclic triaxial tests, where p continuously changes, the cyclic shear strain in one cycle of loading is computed according to the stresses existing at the beginning of the cycle.

Figures 3.11 through 3.14 compare predictions based on equation 3.11, with measured values of cyclic shear strain from drained and undrained tests on Sand A. The following trends can be identified:

- (i) Equation 3.11 is reasonably accurate for drained cyclic triaxial tests within the limitations described previously.
- (ii) For undrained cyclic compression tests (figure 3.12), equation 3.11 gives satisfactory predictions for small values of cyclic strain ($\gamma_{\text{cyc}} \leq .2\%$); for larger values it underestimates the measured cyclic strain.
- (iii) For undrained cyclic isotropic tests (figure 3.13) the empirical model predicts reasonably well the small cyclic strains, but it underpredicts larger ones.
- (iv) For undrained cyclic extension tests (figure 3.14) the model consistently underestimates the cyclic shear strain.

3.5.2 THE HYPERBOLIC MODEL

3.5.2.1 DRAINED CYCLIC TRIAXIAL TESTS -

Kondner ([48], [49]), Duncan ([50], [51]) with their colleagues have found that the plot of shear stress versus strain in Triaxial compression tests is nearly a hyperbola. Hardin and Drnevich [45], have shown that the same is true for isotropically consolidated simple shear tests. In this section the cyclic shear strain will be estimated assuming that the shear stress strain relationship for Sand A is described by a hyperbola:

$$\Delta\gamma = \frac{\Delta q}{G_o} \frac{1.}{1. - \frac{\Delta q}{\Delta q_{max}}} \quad (3.12a)$$

where

G_o : tangent shear modulus for $q=0$

Δq_{max} : maximum change in shear stress required to reach failure

Rearrangement of terms in equation 3.12 results in a different expression:

$$\frac{\Delta\gamma}{\Delta q} = \frac{1.}{G_o} + \frac{\Delta\gamma}{\Delta q_{max}} \quad (3.12b)$$

Equation 3.13) represents a straight line in a " $\frac{\Delta\gamma}{\Delta q}$ vs. $\Delta\gamma$ " plot, when G_o and Δq_{max} are constant (see figure 3.15).

The initial shear modulus G_o is usually related to the confining effective stress applied to the soil; in addition Duncan and Chang [50] suggest that the initial modulus for unloading-reloading is

different from that for first loading. Desai and Christian [] and Hardin [44] suggest that during unloading-reloading the initial modulus is approximately equal to the shear modulus of soil at very small strain ($\gamma = 10^{-5}$ to 10^{-6}); a popular expression of this modulus for sands has been proposed by Richart [47]:

$$G_{\max} = 326 p_{\alpha} \frac{(2.973 - e)^2}{1 + e} \left(\frac{\bar{\sigma}_{\text{oct}}}{p_{\alpha}} \right)^{0.5} \quad (3.13)$$

Equation 3.13 was obtained using data from many different sands and is followed by considerable scatter. For Sand A it will be assumed that

$$G_o = \mu G_{\max} \quad (3.14)$$

The calibration factor " μ " will be determined from drained cyclic triaxial test data from Sand A.

The second parameter of the hyperbola, Δq_{\max} , is related to the shear stress required to reach failure, (Δq_{ult}). Duncan and Chang [50] suggest that

$$\Delta q_{\max} = \frac{\Delta q_{\text{ult}}}{R_f}$$

with constant value of R_f between 0.70 and 0.90. To ensure a smooth transition from the pre-peak to the post-peak behavior, Hardin [44] suggests that R_f is a function of the shear stress which tends asymptotically to 1. as the peak shear stress is approached.

To find the most appropriate definition of Δq_{\max} for Sand A the strain in drained cyclic triaxial tests was compared with equation 3.12. A definition that led to consistent prediction of cyclic shear strain for reloading and unloading is shown in figure 3.16. The

predicted and measured strain are compared in figure 3.17. For this comparison it was assumed that the calibration factor μ in equation 3.14 is equal to one and a half.

3.5.2.2 UNDRAINED CYCLIC TRIAXIAL TESTS

Prediction of the cyclic shear strain with Hodge's model requires knowledge of the average effective stress and the cyclic shear stress only; according to the hyperbolic model, the direction of cyclic effective stress path is also important. To apply this model, therefore, to undrained loading a prediction method for the effective stress path followed during each load cycle is necessary.

Extensive studies, concerning the deformation characteristics of a sand under static and cyclic triaxial loading, have been performed in the laboratory of University of Tokyo under the supervision of Professor Ishihara ([67], [68], [69], [70], [71]). The major findings, related to undrained stress paths are shown in figure 3.18; in summary

- (i) The line of "Phase Transformation" (PT), separates contractive from dilative sands during static loading. This line is essentially the same with the CT-line proposed by Luong and Sidaner ([25],[26]) and presented in detail in chapter 2.

(ii) Static shearing below the PT-line (subcharacteristic domain) results in pore pressure increase (path 1-4-7); above the PT-line (surcharacteristic domain) dilation of the sand occurs and decrease of the pore pressure (paths 7-8,9-10-11).

(iii) Unloading-reloading within the subcharacteristic domain is approximately elastic with the change of pore pressure equal to the change of the total octahedral stress (paths 2-3-4, 5-6-7). Unloading from a point within the surcharacteristic domain produces significant positive "plastic" pore pressure in addition to the elastic one (paths 8-9, 11-12).

Figure 3.19 shows representative stress paths from undrained loading of Sand A which agree with Ishihara's findings.

The effective stress path during unloading and reloading in the subcharacteristic domain will be represented by a straight line parallel to the "q" axis in a "q vs. $\bar{\sigma}_{oct}$ " plot (see Figure 3.20a). This is equivalent with assuming that unloading and reloading in this domain are elastic. After the effective stress path crosses the critical threshold line it changes direction, following the straight line connecting the point of intersection with the ultimate state of stress (see Figure 3.20b). Description of the ultimate state of stress and volume for Sand A is presented in Appendix B. A stress path starting within the surcharacteristic domain and moving towards the CT-line (see figure 3.20c) will follow the straight line

connecting the initial point (A in figure 3.20c) with the point corresponding to the average stresses at the beginning of the cycle (B in figure 3.20c). There is little physical meaning in this assumption, but it is consistent with the observed cyclic sand behavior as will be shown next.

In figure 3.21 the model is compared with the stress paths observed in undrained cyclic compression, isotropic and extension tests on Sand A; the sand properties required by the model are summarized in Table 3.2. To illustrate the sensitivity of cyclic shear strain to the assumptions concerning stress paths, the hyperbolic model was used to predict the cyclic shear strains along the stress paths in Figure 3.21; the results are summarized in table 3.3. For eight out of the nine stress paths considered, the error in the prediction was below 12%; for one of the stress paths the error was 71%.

Evaluating the data in figure 3.21 and table 3.3, one has to keep in mind that the proposed model will be used in the prediction of the cyclic shear strain when the average effective stresses and the cyclic shear stress are known. Further sophistication would be necessary if the model was used directly to predict the strain and pore pressure accumulation due to cyclic loading (for example [70], [71], [73]).

With a method to predict the cyclic effective stress path due to undrained loading, cyclic shear strain can be predicted through the hyperbolic model. Figures 3.22 to 3.23 compare the predicted with the measured cyclic shear strain in undrained triaxial tests. The following conclusions can be drawn from the comparison:

(i) The hyperbolic model predicts well the cyclic shear strain in undrained compression tests.

(ii) There is considerable scatter in the model's predictions for isotropic tests; the model overpredicts the cyclic shear strain when it is larger than 0.1% .

(iii) for undrained extension tests the model's predictions are in good agreement with the test data for small and large values of cyclic strain; for medium strains, between 0.10 and 0.25%, the predicted values exceed the measured ones.

3.5.3 SUGGESTED MODEL FOR CYCLIC SHEAR STRAIN

In choosing between Hodge's relation for cyclic shear strain and the hyperbolic model, three major factors will be considered

(i) accuracy

(ii) number of parameters defining the model

(iii) computational effort required for the application of the model

(iv) generality

Accuracy

Review of figures 3.11 and 3.17 indicates that both models fit the available data from drained cyclic triaxial tests equally well. The models' predictions for undrained tests are summarized in figures 3.25 to 3.27. It is evident that the hyperbolic model is more accurate, especially in predicting the large cyclic shear strain which, according to figure 3.10, occurs during shearing close to the failure envelope.

Number of parameters

To define Hodge's empirical relation (equation 3.11) four parameters are required; they can be determined from series of drained cyclic triaxial tests where each of the important quantities ($n, \frac{\Delta q}{\bar{p}}, \bar{p}$) varies at the time and the rest are kept constant.

The hyperbolic model is defined through two parameters (see equations 3.12, 3.14): the calibration factor " μ " for the initial shear modulus, and the friction angle of the soil which is used to define the ultimate shear stress " Δq_{max} ". To apply the model to undrained cyclic loading the location of the phase transformation line has to be defined as well. This line, however, has been already defined in chapter 2 under the name "CT-line", as a distinction between contractive and dilative sands; thus, it does not introduce one additional parameter.

Computational Effort

The computational effort required from the two models is summarized in table 3.4; it is evident that the hyperbolic model is

more computationally involved.

Generality

Hedges relation is purely empirical and contradicts two basic concepts of soil behavior:

(i) The soil stiffness increases as the applied confining stress increases; Hedges equation predicts instead that the cyclic shear strain will increase if the applied mean effective stress increases.

(ii) There is a peak shear stress that can be reached, after which large strains occur. Hedges equation does not account for the peak stress, and for this reason consistently underpredicts the cyclic strain due to loading close to the failure envelope.

The hyperbolic model is consistent with the two concepts previously described, and is generally accepted as a simple but meaningful model for the prediction of shear strain in soils (for example [44], [74]).

In summary, the hyperbolic model is more accurate, needs fewer parameters and is consistent with basic soil mechanics concepts; the only disadvantage compared with Hedges' model is that it requires larger computational effort. In the present thesis the hyperbolic model will be used to predict the cyclic shear strain, since it

appears to be more advantageous, over all, than Hodge's empirical relation.

3.6 SUMMARY

The more important findings of this chapter can be summarized as follows:

(i) The volumetric permanent strain is drained cyclic triaxial tests is related to the cyclic shear strain, the number of cycles and the initial stress ratio by a log-linear relation; for Sand A:

$$\epsilon_{vol}(\%) = 0.685 \gamma_{cyc}^{1.26} N^{0.40} \quad (3.3)$$

(ii) The vertical permanent strain is proportional to the volumetric with proportionality constant depending on the initial stress ratio:

$$\frac{\epsilon_v}{\epsilon_{vol}} = 13.6 q \frac{|q|}{\bar{\sigma}_{oct}^2} + 0.33 \quad (3.5)$$

(iii) The rate of permanent volume change becomes zero when the average effective stresses lies on the CT-line; the rate of vertical strain accumulation, however, remains unaffected.

(iv) The cyclic shear strain in drained and undrained cyclic triaxial tests can be successfully estimated, by a two parameter hyperbolic stress strain relationship.

(v) A proposed model for the prediction of effective stress paths during undrained cyclic loading fits sufficiently well the data from cyclic triaxial tests on Sand A.

TEST #LC	γ_{cyc} meas.	$\frac{q}{\sigma_{oct}}$	n%	$\epsilon_v / \epsilon_{vol}$								N_f	$\epsilon_v / \epsilon_{vol}$ mean
				N=5	10	50	150	550	1050	2000			
127	0.174	0.00	41.2	0.16	0.18	0.23	0.26	0.28	0.28	0.27	0.27	0.24	
141	0.088	0.27	43.1	1.49	1.45	1.30	1.13	1.04	1.01	1.04	1.06	1.19	
168	0.077	0.18	43.0	0.80	0.80	0.75	0.69	0.65	0.79	0.76	0.79	0.75	
169	0.084	0.21	43.2	1.16	1.12	1.01	0.96	1.06	1.14	0.97	0.99	1.05	
170	0.077	0.30	43.0	1.73	1.56	1.26	0.94	1.04	1.13	1.11	1.12	1.24	
171	0.106	0.00	43.2	0.05	0.11	0.20	0.26	0.29	0.36	0.35	0.34	0.25	
175	0.129	0.21	43.2	0.94	0.89	0.81	0.79	0.85	0.84	0.83	0.79	0.84	
177	0.061	0.21	42.9	1.12	1.08	1.01	1.03	0.90	0.88	0.98	0.91	0.99	
178	0.106	0.21	43.5	1.10	1.07	1.00	0.97	0.87	0.78	0.83	0.82	0.93	
179	0.040	0.21	42.8	0.95	0.97	1.05	1.27	1.26	0.74	1.04	1.05	1.04	
180	0.078	0.46	42.6	5.45	4.77	3.72	3.16	2.67	3.06	2.78	2.62	3.53	
196	0.073	0.21	41.9	-	-	-	0.77	0.69	0.69	0.73	1.01	0.78	
197	0.079	0.41	43.1	-	-	-	1.94	1.77	1.72	1.84	1.75	1.80	
212	0.096	0.21	43.4	-	-	-	0.67	0.65	0.71	0.78	0.87	0.74	
257	0.058	0.27	42.0	0.66	0.60	0.56	0.58	0.56	0.56	0.65	0.68	0.61	
261	0.019	0.21	43.4	0.56	0.51	0.67	0.60	0.51	0.68	0.36	0.37	0.53	
285	0.054	0.21	43.1	1.17	1.19	1.07	0.99	0.91	0.89	0.87	0.88	1.00	
290	0.106	0.21	43.4	1.14	1.08	1.06	1.05	1.02	1.01	1.07	1.18	1.08	
297	0.066	0.27	41.8	1.24	1.12	1.02	1.09	1.07	1.05	1.13	1.26	1.12	
303	0.029	0.21	42.6	1.27	1.13	1.05	1.02	0.97	0.90	1.14	1.58	1.13	
305	0.077	0.21	42.9	0.99	0.94	0.86	0.84	0.82	0.82	0.89	0.95	0.88	
308	0.087	0.27	42.8	1.47	1.34	1.20	1.18	1.15	1.14	1.11	1.10	1.21	
316	0.034	0.27	42.9	1.55	1.35	1.09	1.00	0.89	0.86	0.85	0.87	1.06	
321	0.068	0.21	41.1	0.84	0.86	0.85	0.89	0.96	1.04	1.15	1.27	0.98	
327	0.170	-0.19	43.9	-2.69	-2.41	-1.91	-1.57	-1.36	-1.27	-1.18	-1.14	-1.69	

TABLE 3.1: Ratio of Vertical to Volumetric Permanent Strain in Drained Cyclic Triaxial Tests on Sand A

TEST #	POROSITY (%)	(1) ϕ_{\max} (o)	(2) ϕ_{CT} (o)	(1) S_u (ksc)
LC-77	41.0	37	30	200
LC-73	41.3	36	30	150
LC-74	41.3	36	30	150

- (1) Estimated in Appendix B
(2) From Figure 2.7

TABLE 3.2: Summary of Basic Parameters Required to Define the ESP during Undrained Cyclic Loading

TEST # LC-	CYCLE NUMBER	γ_{cyc} predicted (%)	γ_{cyc}^* (%)	$\frac{\gamma_{cyc}^* - \gamma_{cyc}}{\gamma_{cyc}^*}$ (%)
77	1	.051	.052	1.75
	2500	.073	.052	3.95
	9500	.162	.145	-11.72
73	1	.103	.116	+11.21
	12	.252	.270	6.67
	32	3.490	3.490	0.00
74	1	0.066	.071	7.04
	10	.133	.133	0.00
	60	.285	.981	70.95

* For Measured ESP

TABLE 3.3: Predicted γ_{cyc} along the Estimated and Measured ESPs

	HADGE	HYPERBOLIC
step 1	$\bar{p} = \frac{\bar{\sigma}_v + \bar{\sigma}_h}{2}$	$\bar{\sigma}_{oct} = \frac{\bar{\sigma}_v + 2\bar{\sigma}_h}{3}$
step 2	$\Delta q_{cyc} = \frac{\Delta\sigma_{v\ cyc} - \Delta\sigma_{h\ cyc}}{2}$	G_o (eq. 3.13, 3.14)
step 3	γ_{cyc} (eq. 3.11)	Effective stress path (section 3.5.2.2)
step 4	—	Δq_{max} (Figure 3.16)
step 5	—	γ_{cyc} (eq. 3.12)

TABLE 3.4: Computational Steps Required for the Prediction of γ_{cyc}

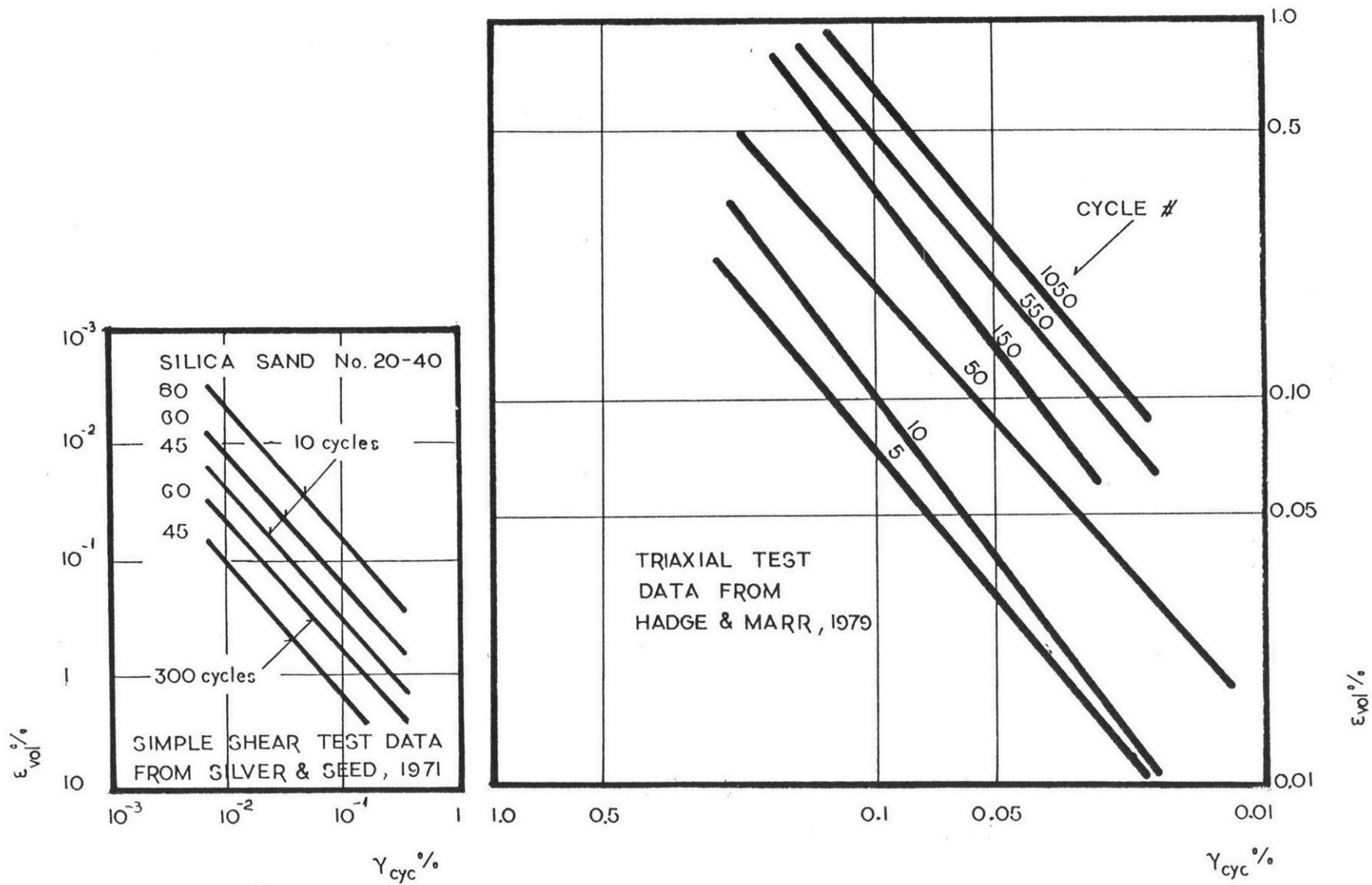


FIGURE 3.1 : Permanent Volumetric Strain versus Cyclic Shear Strain

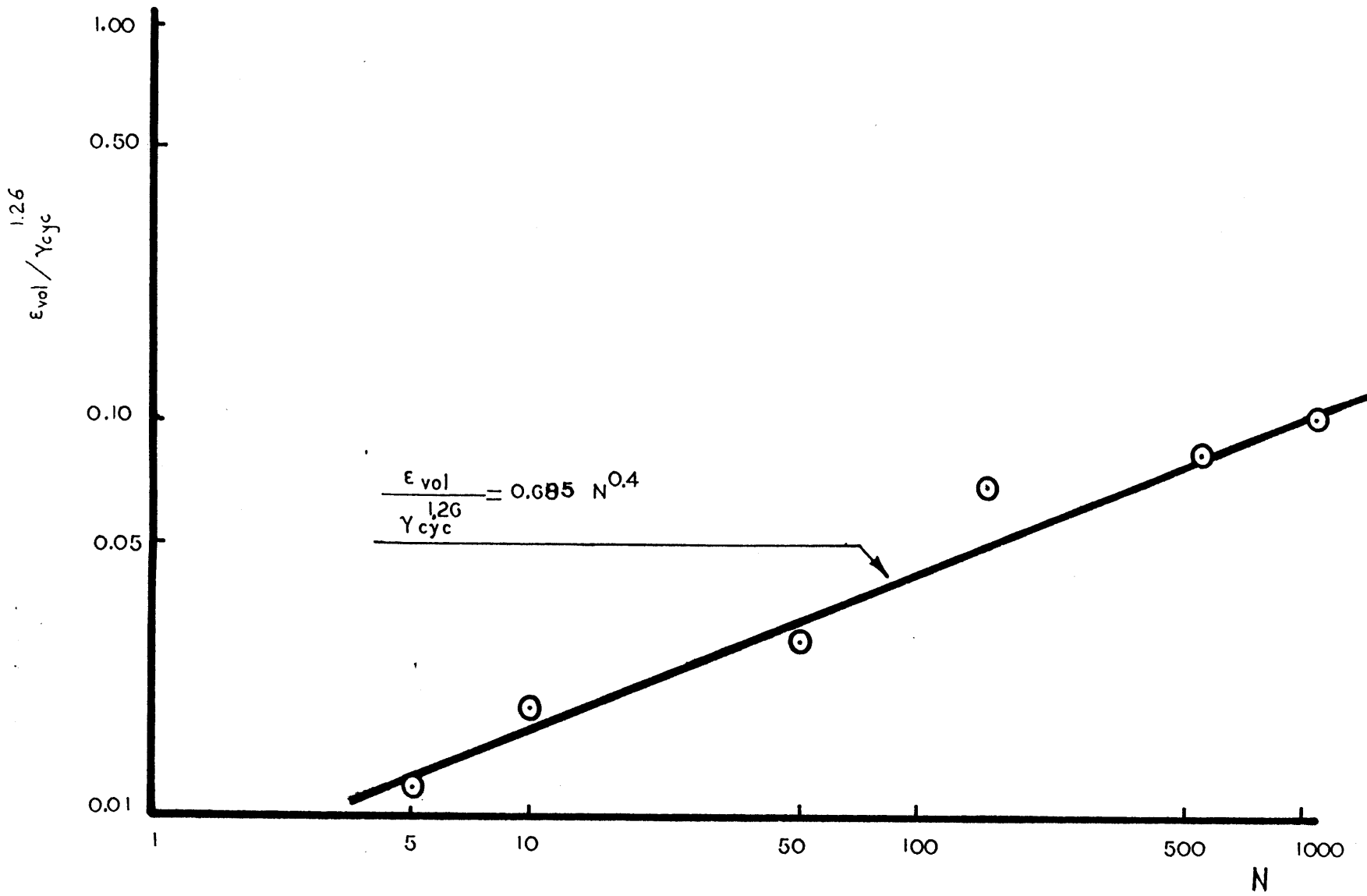


FIGURE 3.2 : Permanent Volumetric Strain versus Cycle Number (Ref. 22)

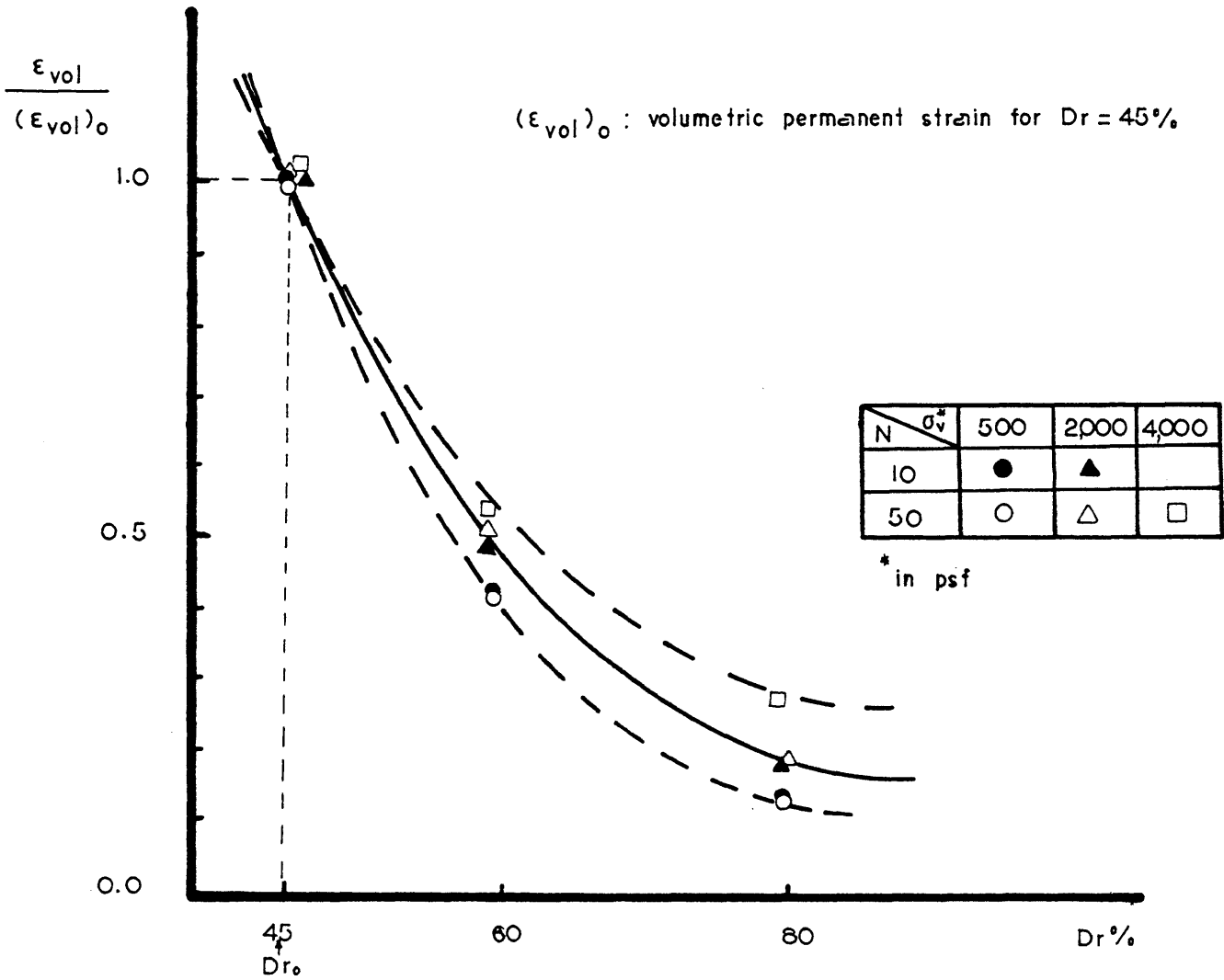


FIGURE 3.3 : Effect of Initial Density on Permanent Volumetric Strain
(data by Silver and Seed, 1971)

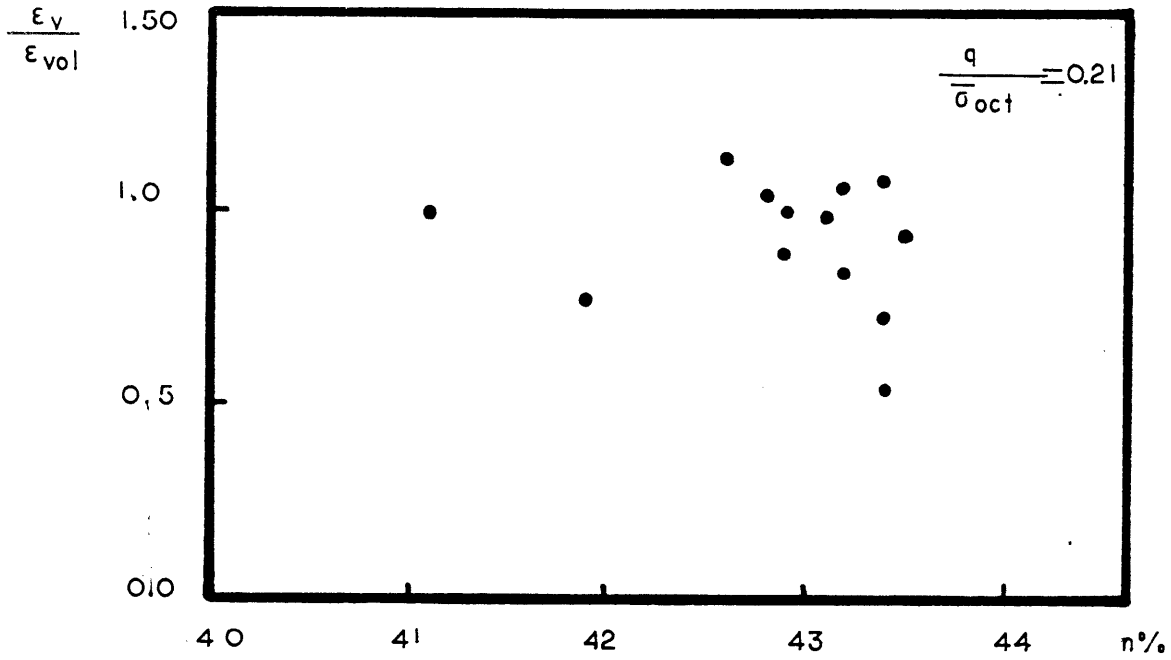


FIGURE 3.4 : Effect of Initial Porosity on Vertical Permanent Strain

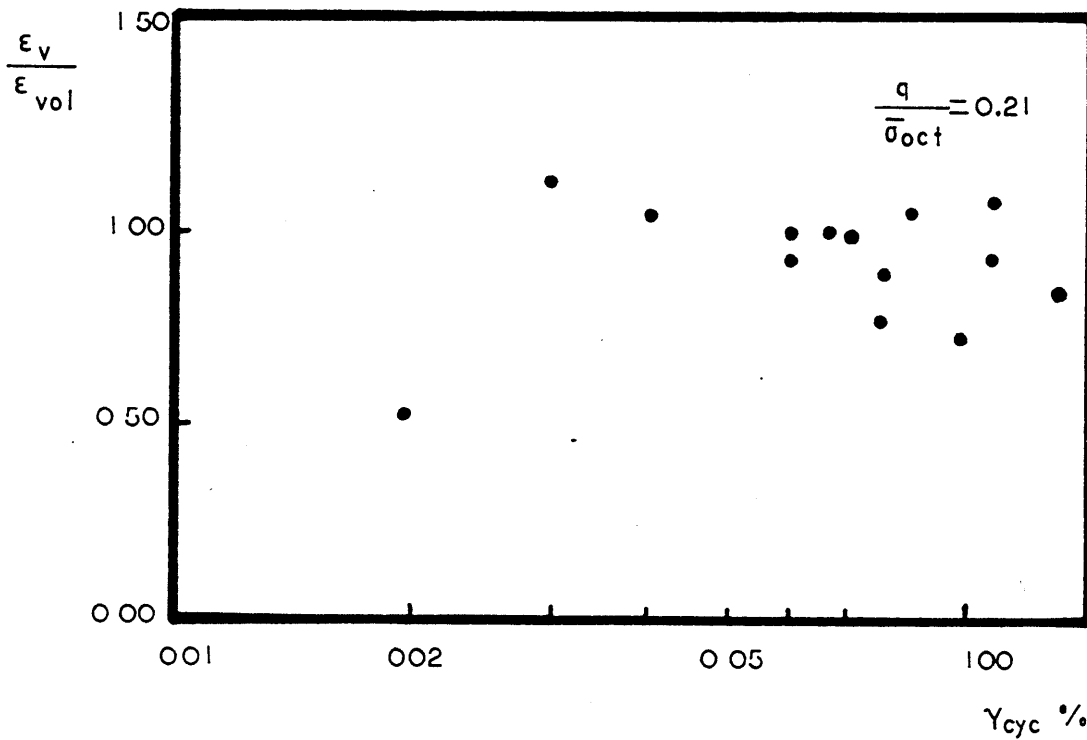


FIGURE 3.5 : Effect of Cyclic Shear Strain on Vertical Permanent Strain

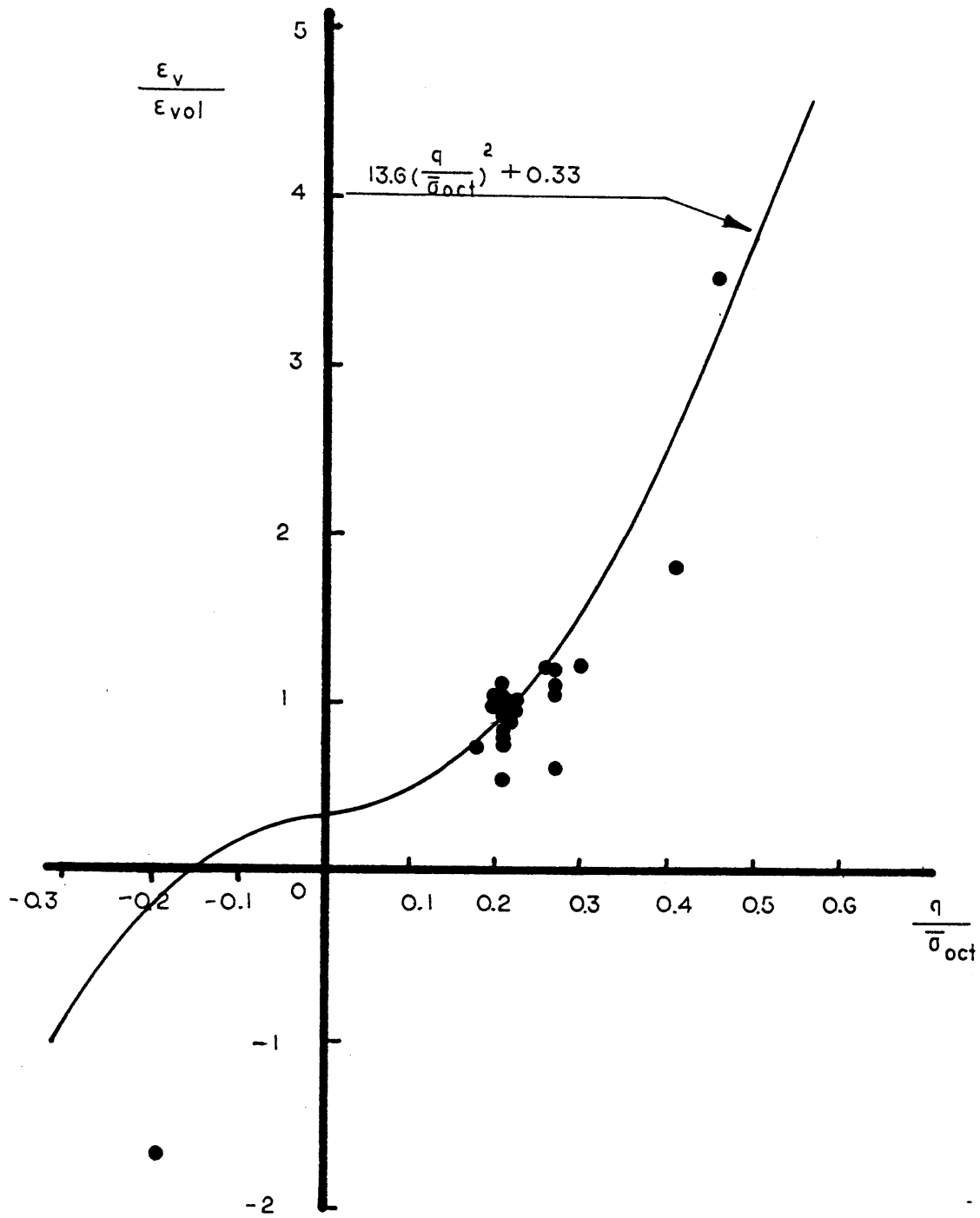


FIGURE 3.6 : Effect of Stress Ratio on Permanent Vertical Strain

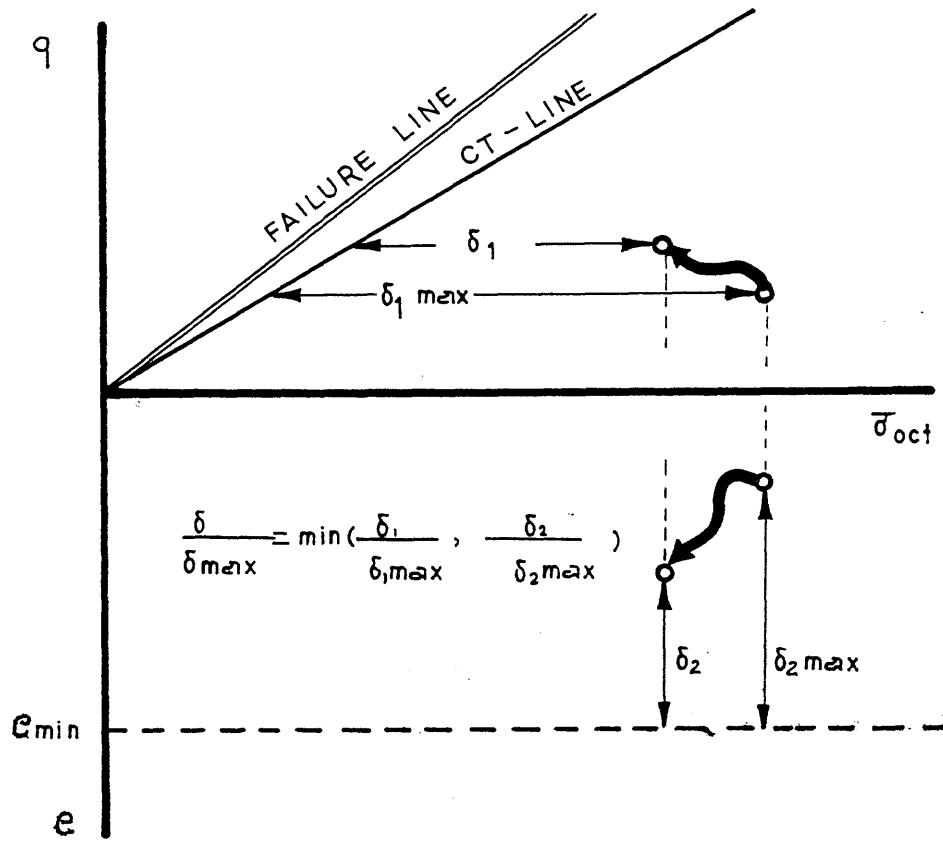


FIGURE 3.7 : Definition of Normalized Distance away from the Limit States

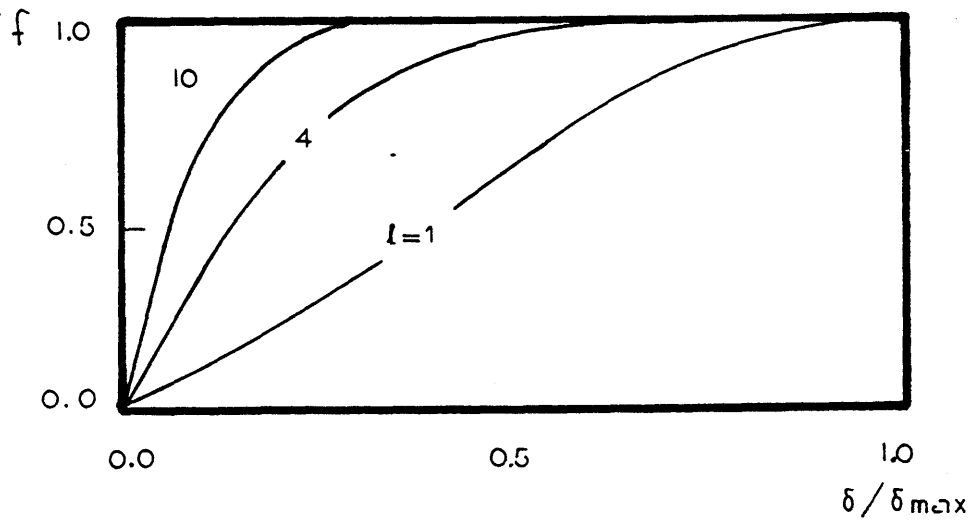


FIGURE 3.8 : Effect of Limit State

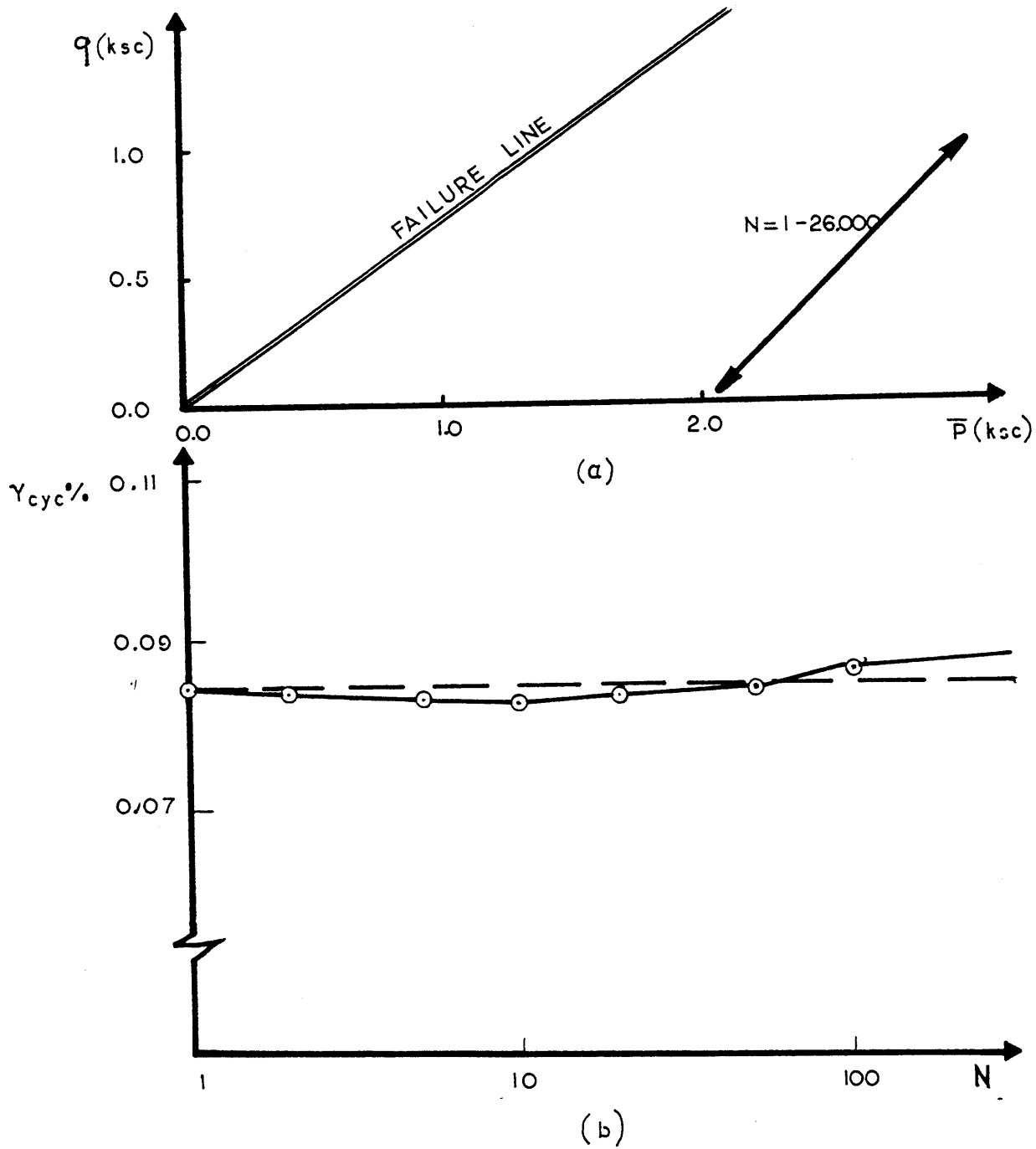


FIGURE 3.9 : Typical Effective Stress Path (a), and Cyclic Shear Strain (b) in Drained Cyclic Triaxial Tests

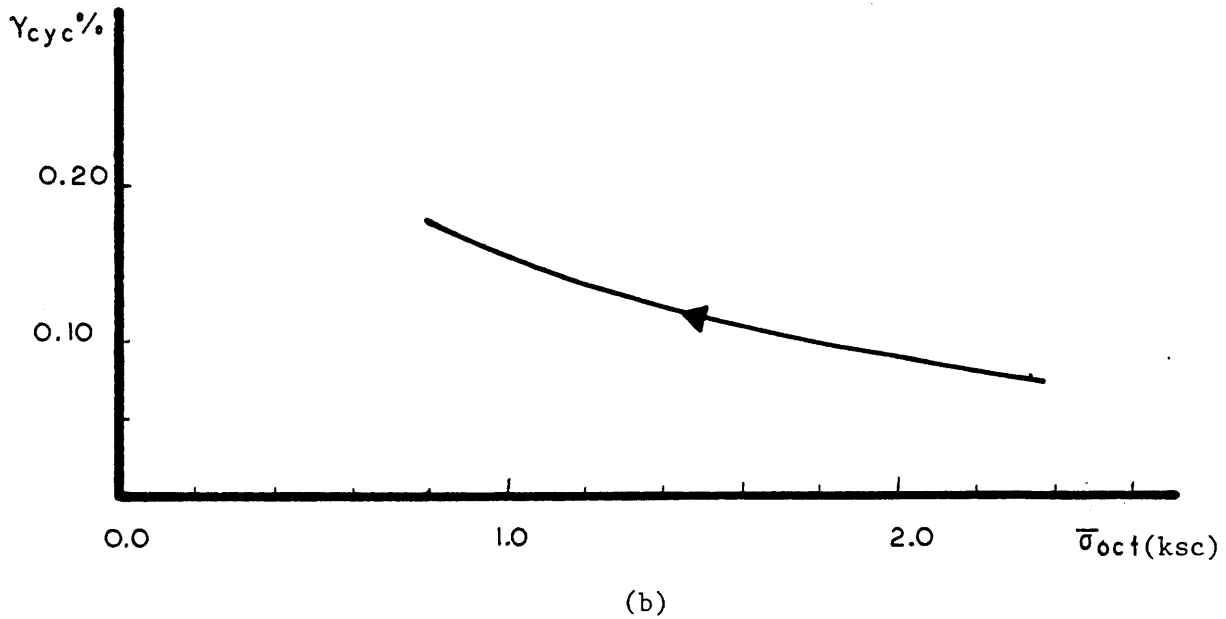
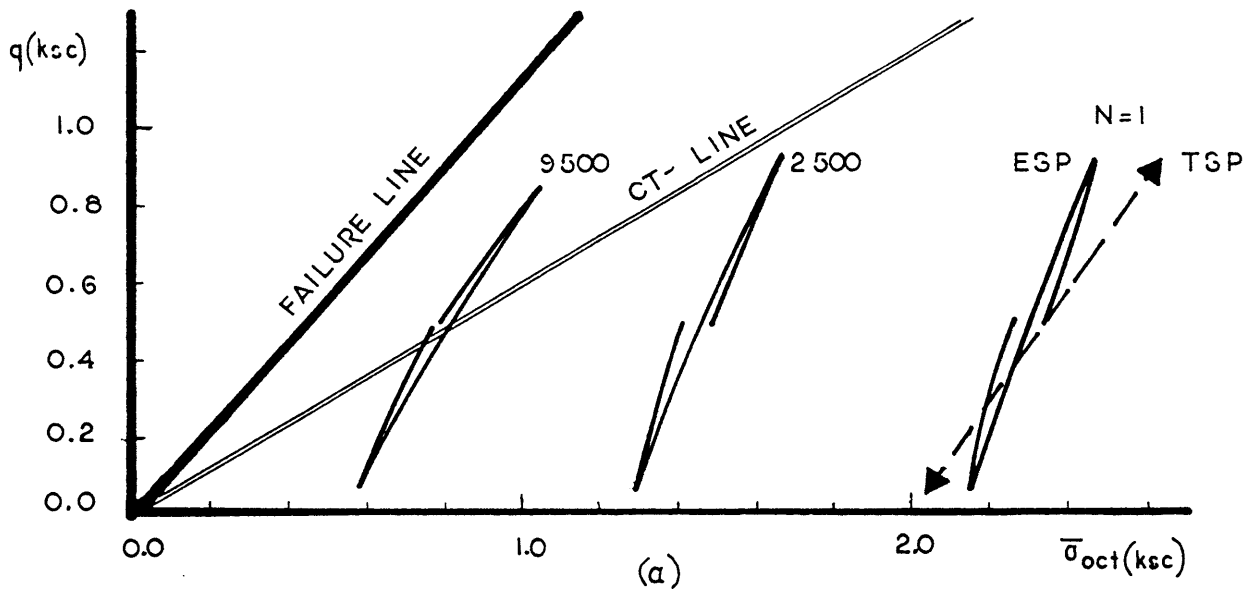


FIGURE 3.10 ; Typical Effective Stress Paths (a), and Cyclic Shear Strain (b) in Undrained Cyclic Triaxial Tests

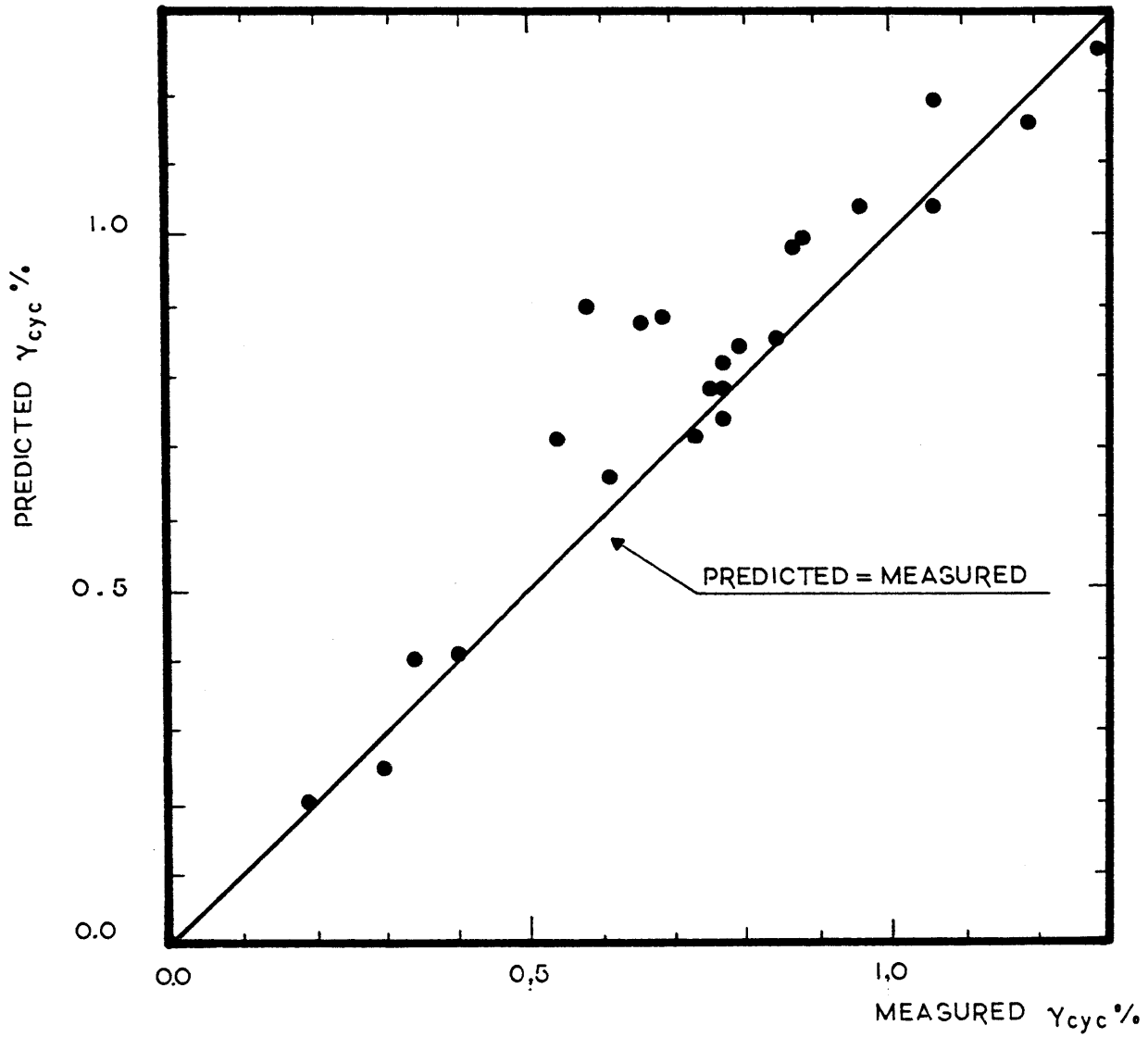


FIGURE 3.11 : Comparison of Hodge's Empirical Equation with Data from Drained Cyclic Triaxial Tests

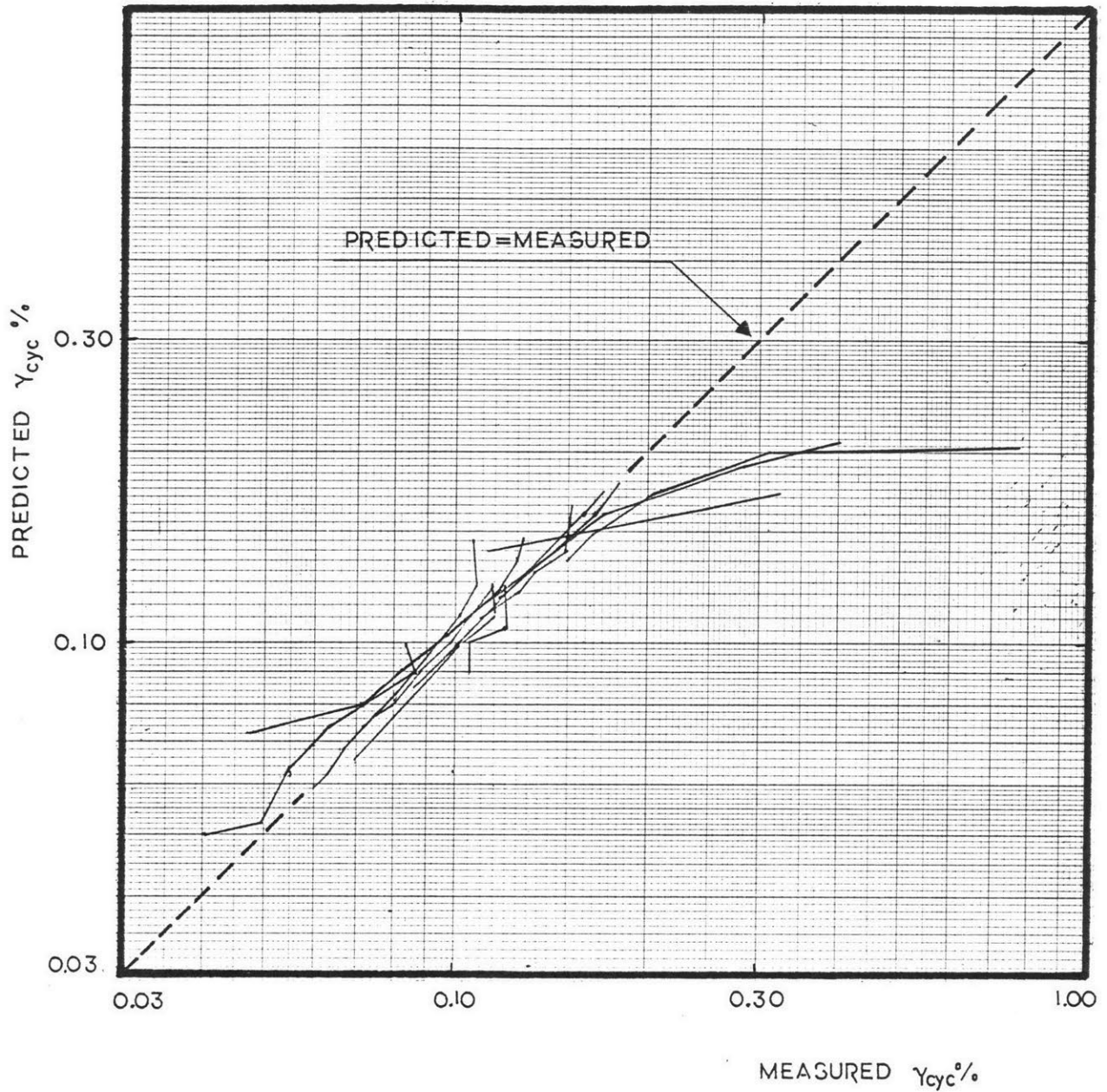


FIGURE 3.12 Comparison of Hodge's Empirical Equation with data from Undrained Cyclic Compression tests

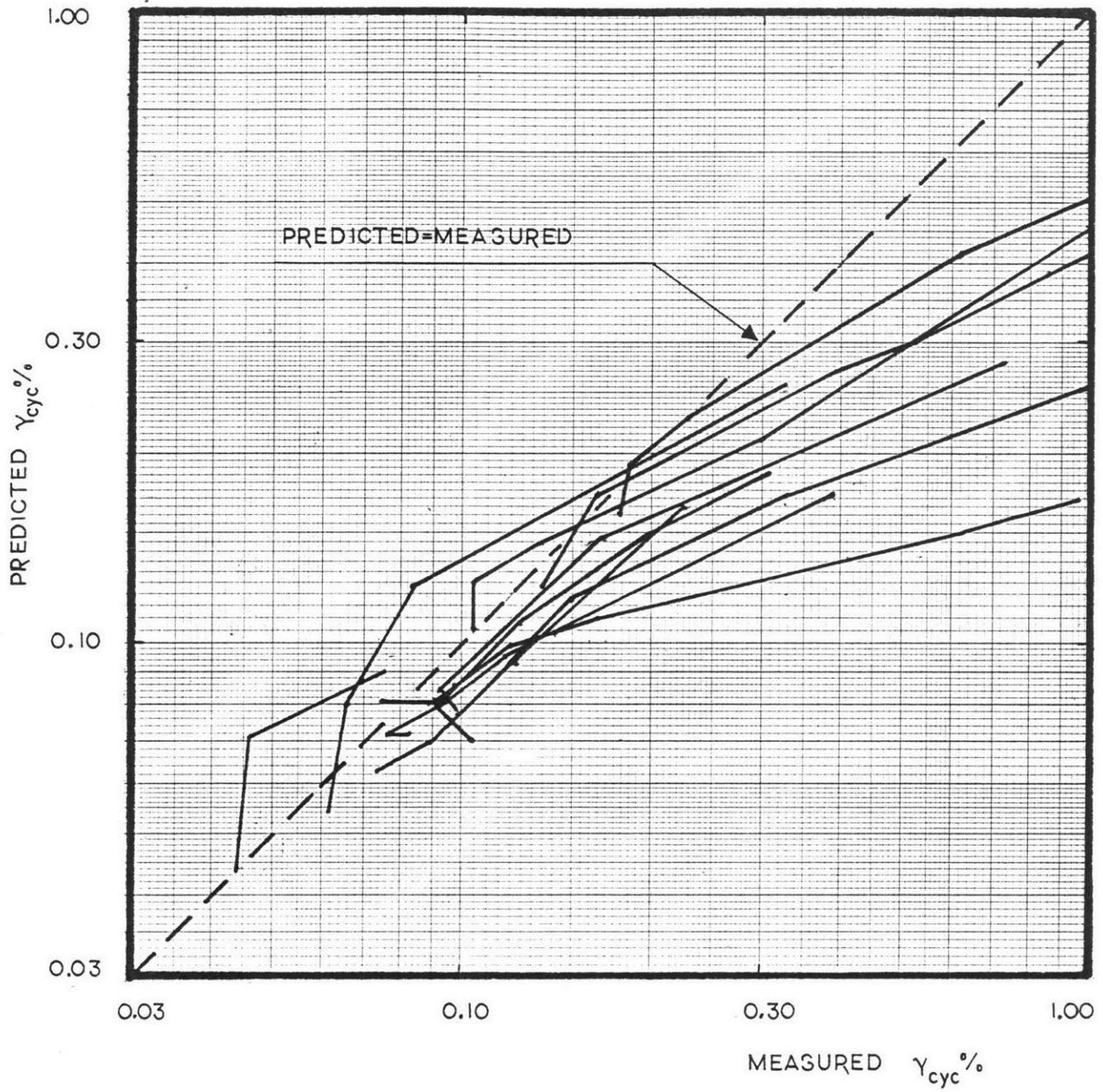


FIGURE 3.13 Comparison of Hodge's Empirical Equation with data from Undrained Cyclic Isotropic Tests

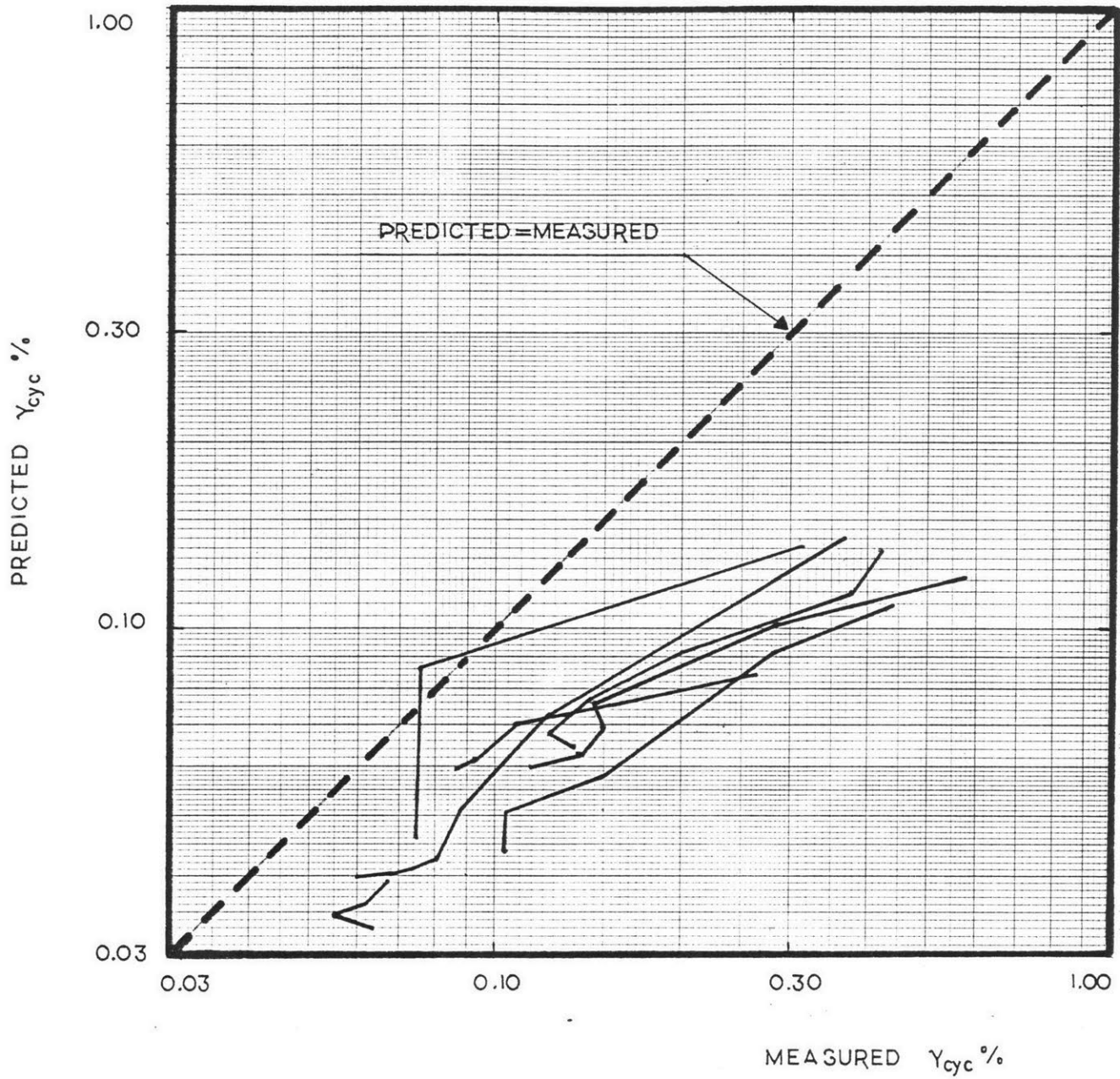


FIGURE 3.14 Comparison of Hodge's Empirical Equation with data from Undrained Cyclic Isotropic Tests

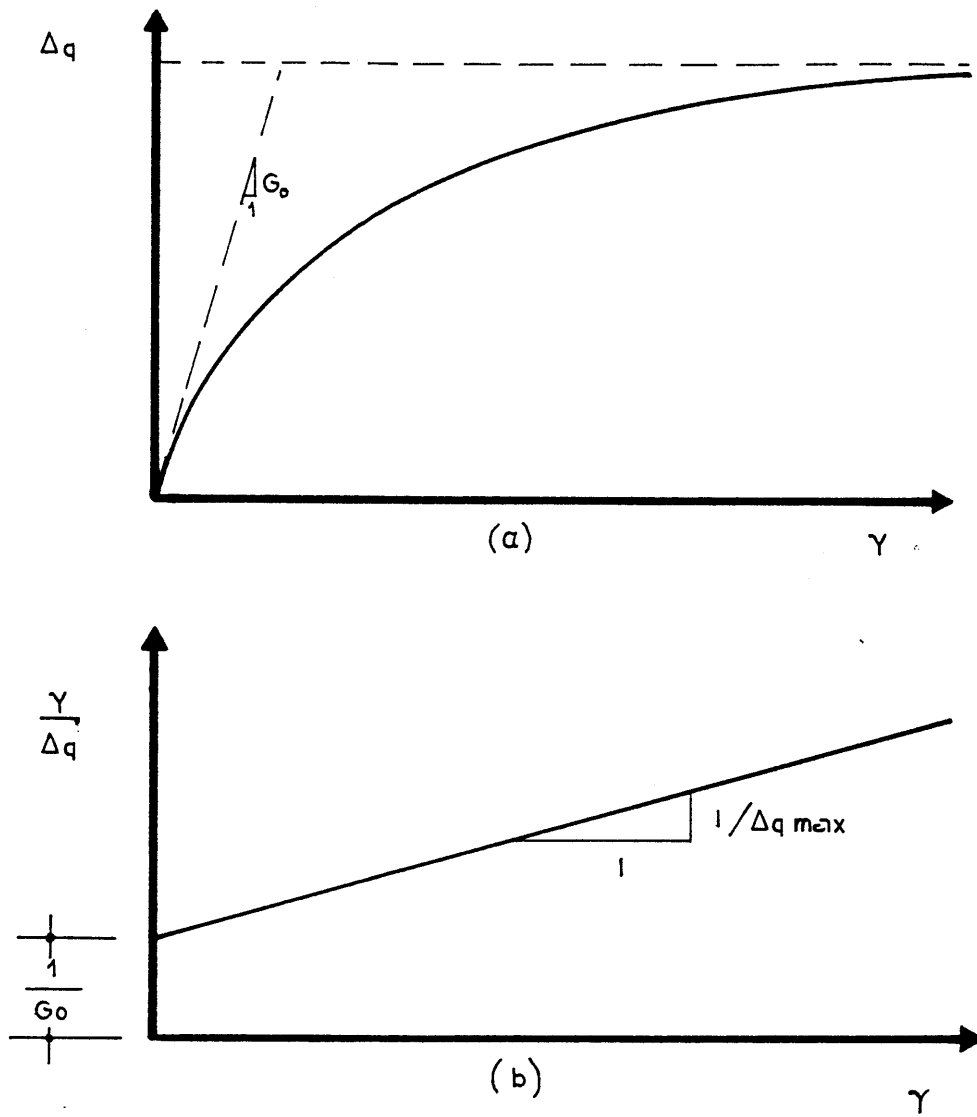


FIGURE 3.15 : Hyperbolic Stress-Strain Relationship : (a) Equation 3.12
 (b) Equation 3.13

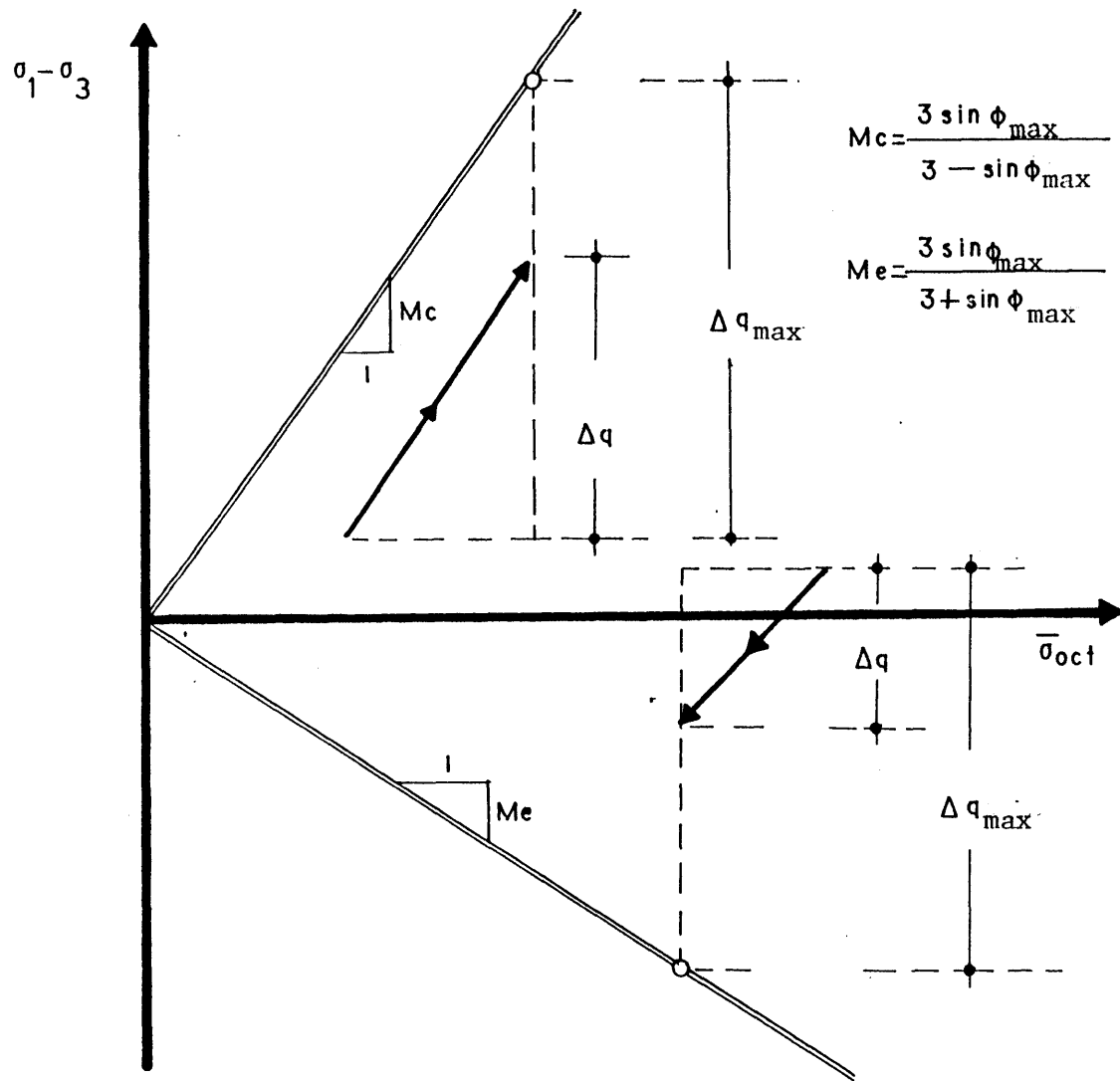


FIGURE 3.16 : Definition of Δq_{\max} for the Hyperbolic Stress - Strain Relationship

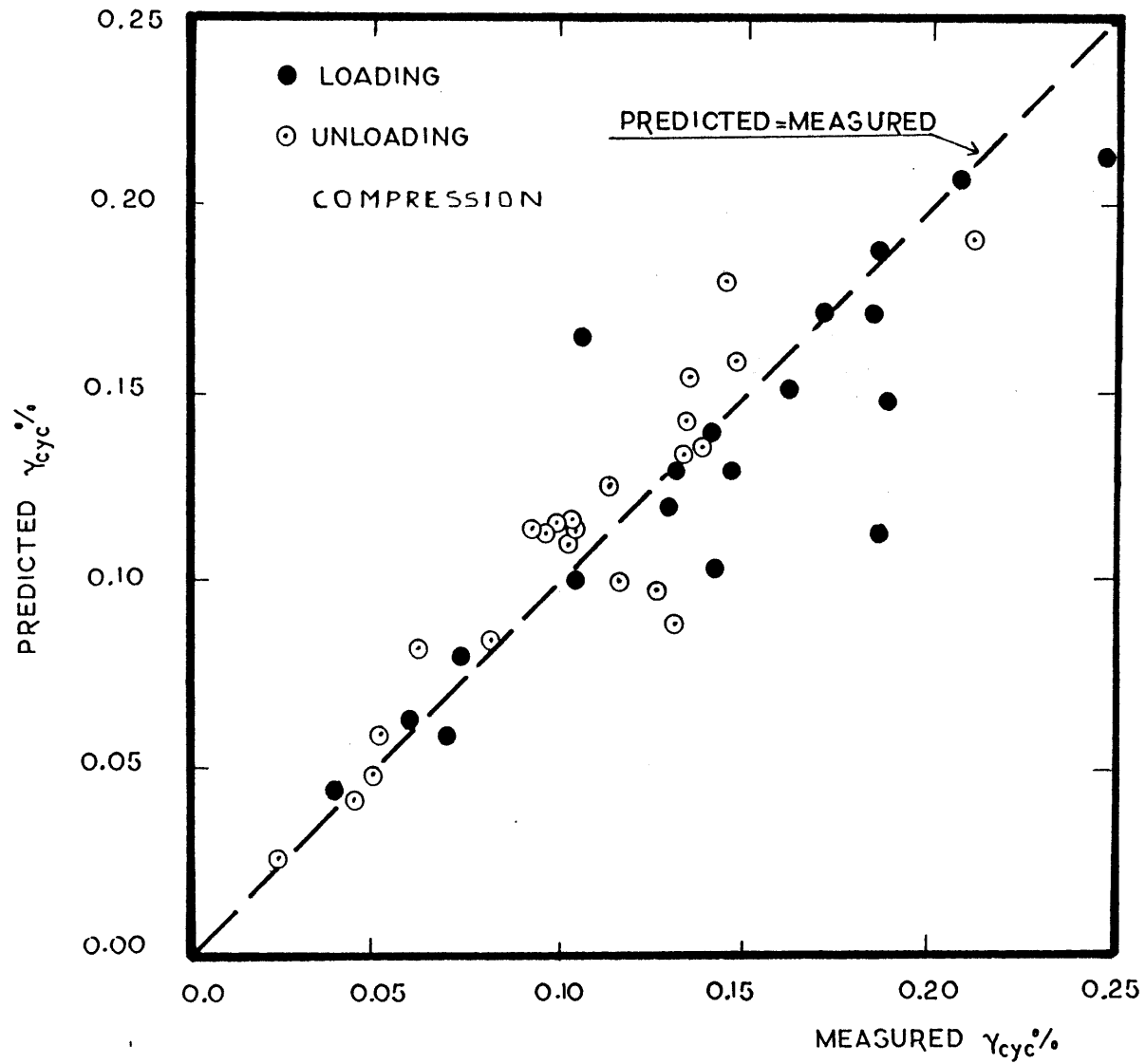


FIGURE 3.17 ; Comparison of the Hyperbolic Model with Data from Drained Cyclic Triaxial Tests

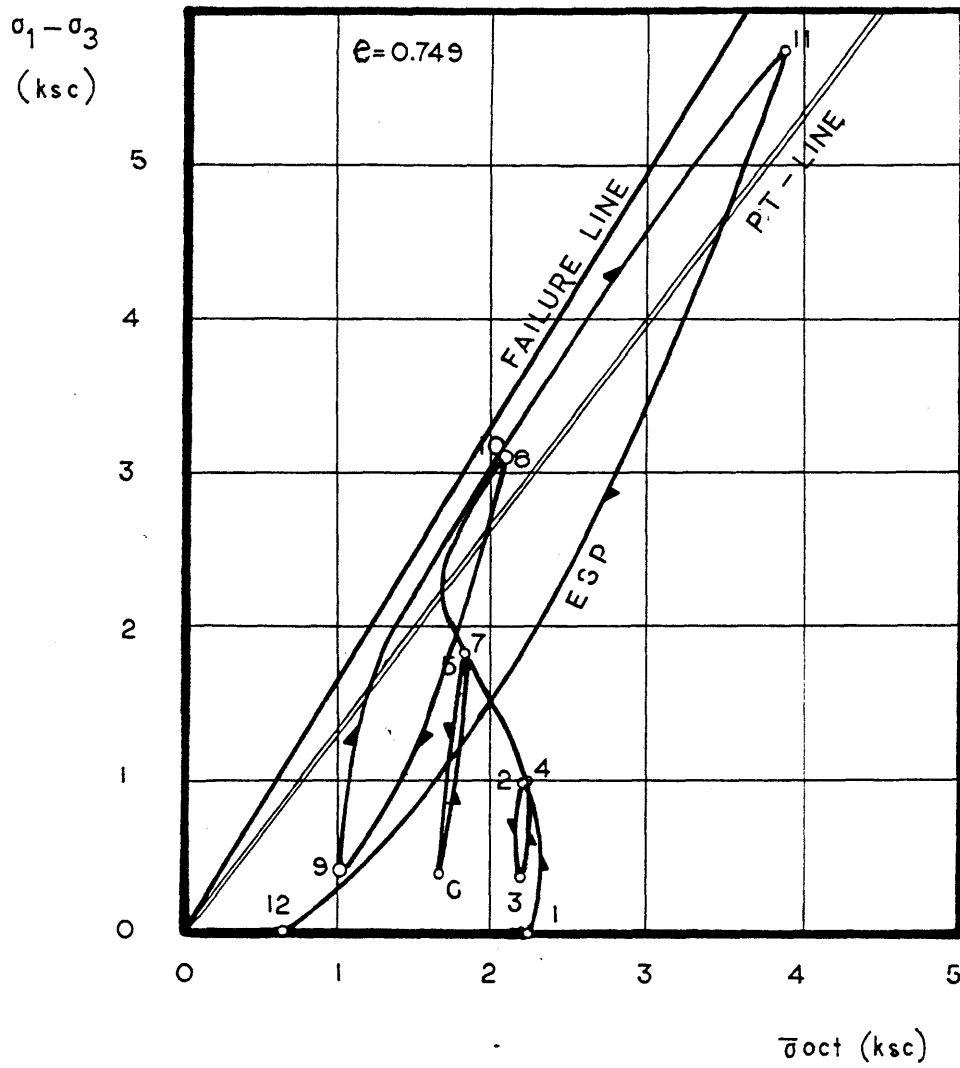


FIGURE 3.18 : Undrained Test on a Loose Sand Cycled with Varying Amplitude of Stress Ratio (Ref. 70)

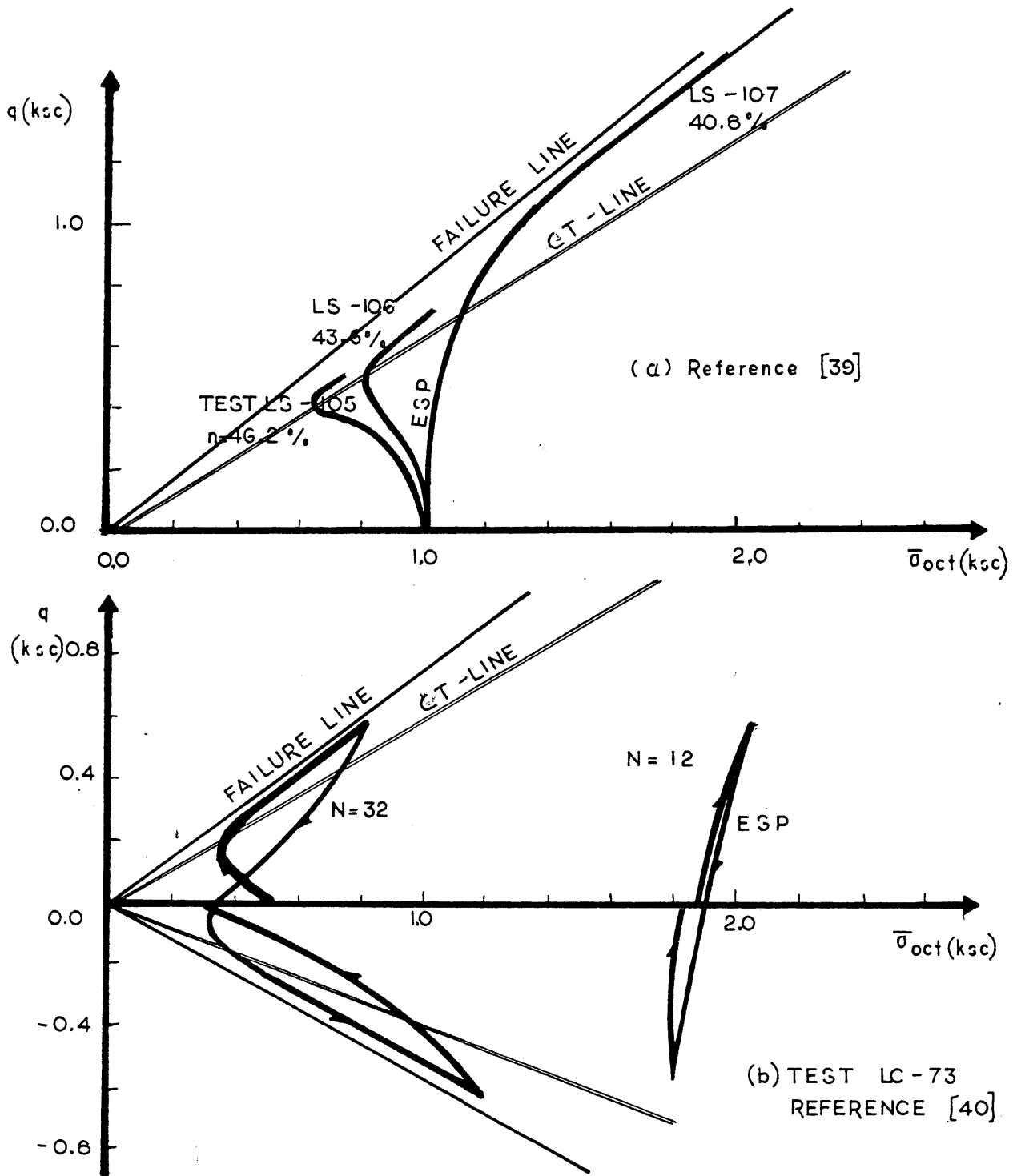


FIGURE 3.19 : Undrained Effective Stress Paths for Sand A: (a) Static Loading (b) Cyclic Loading

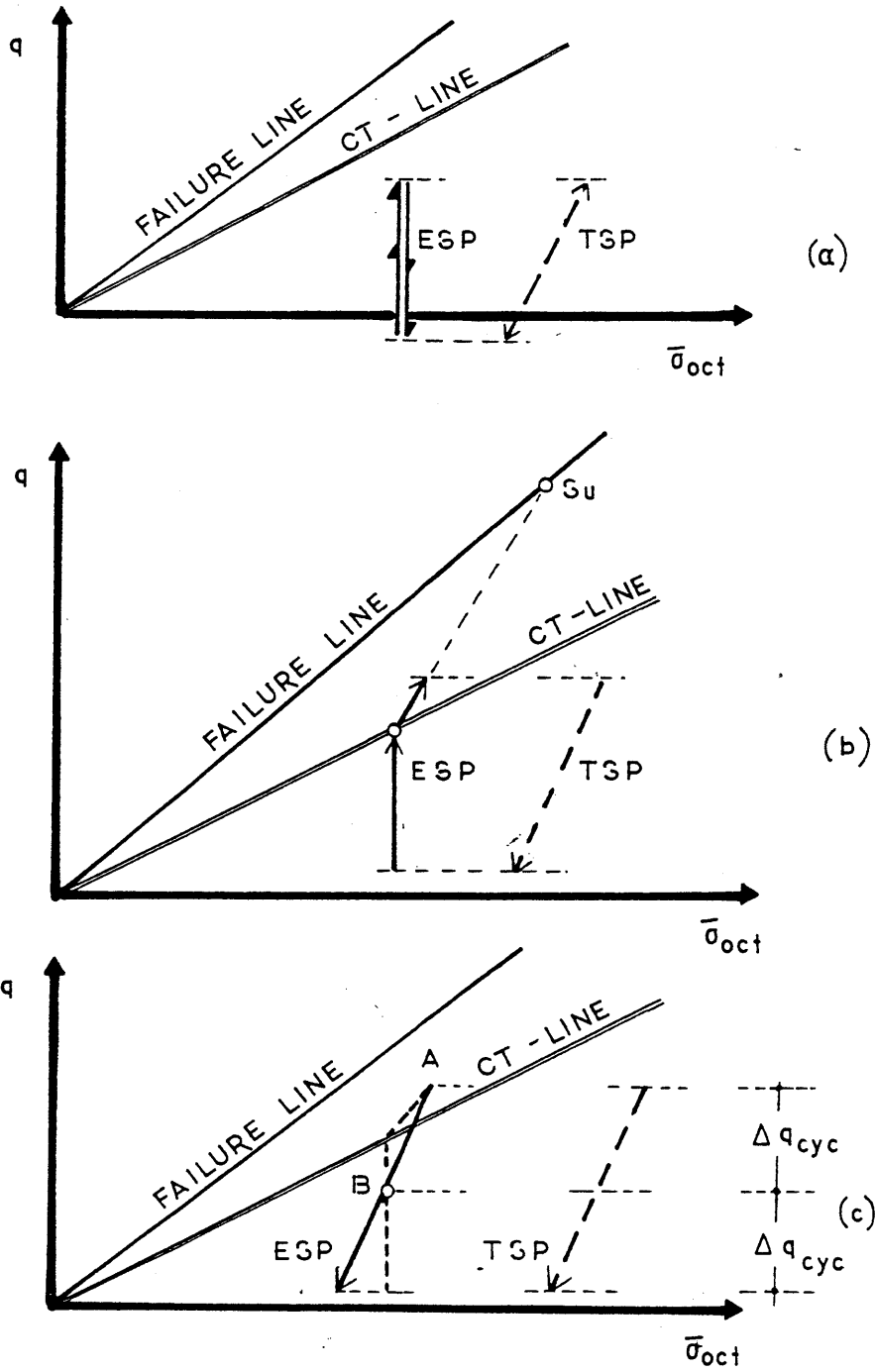


FIGURE 3.20 : Estimation of Effective Stress Paths during Undrained Cyclic Loading

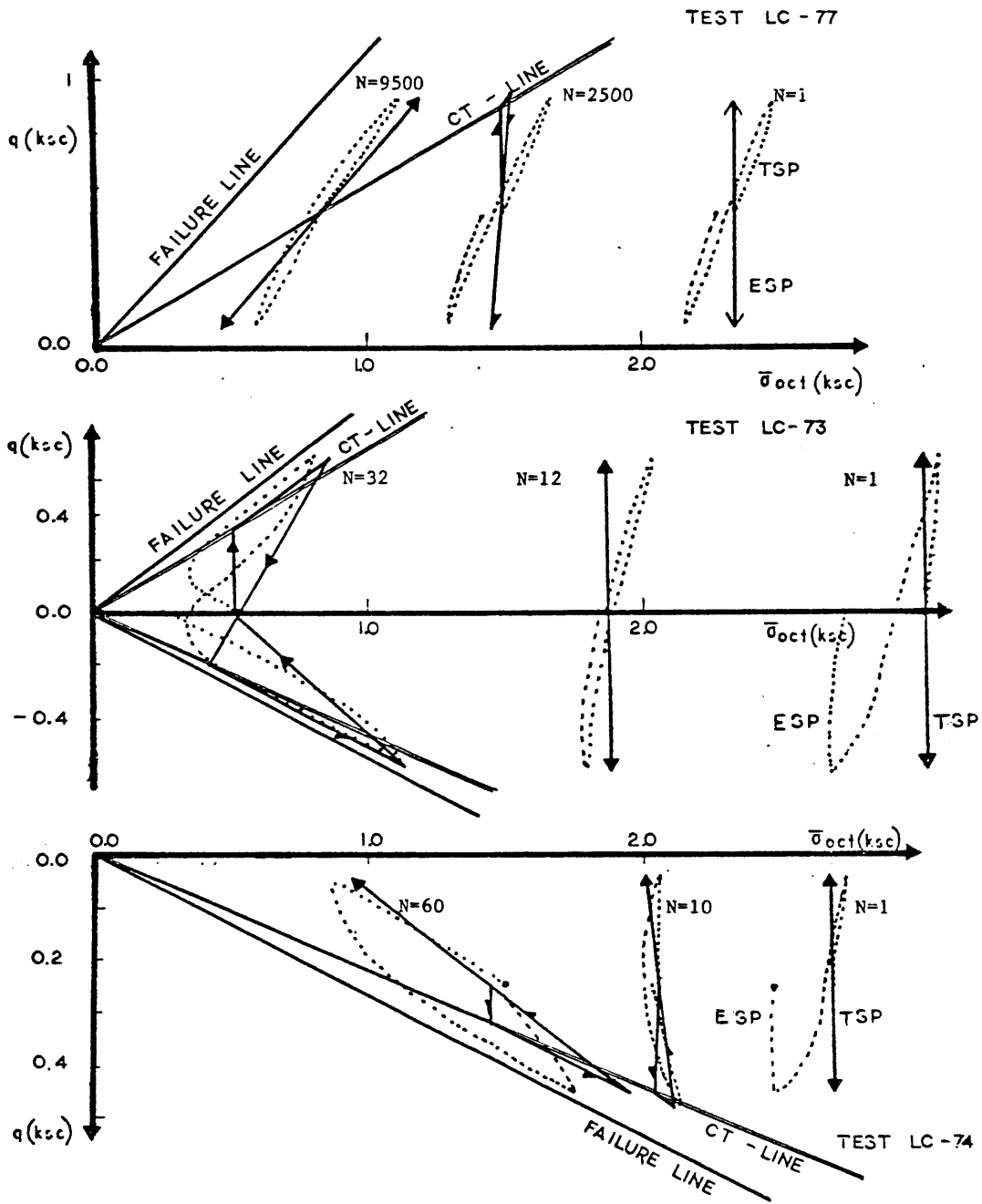


FIGURE 3.21 : Predicted and Measured ESP for Undrained Cyclic Loading of Sand A

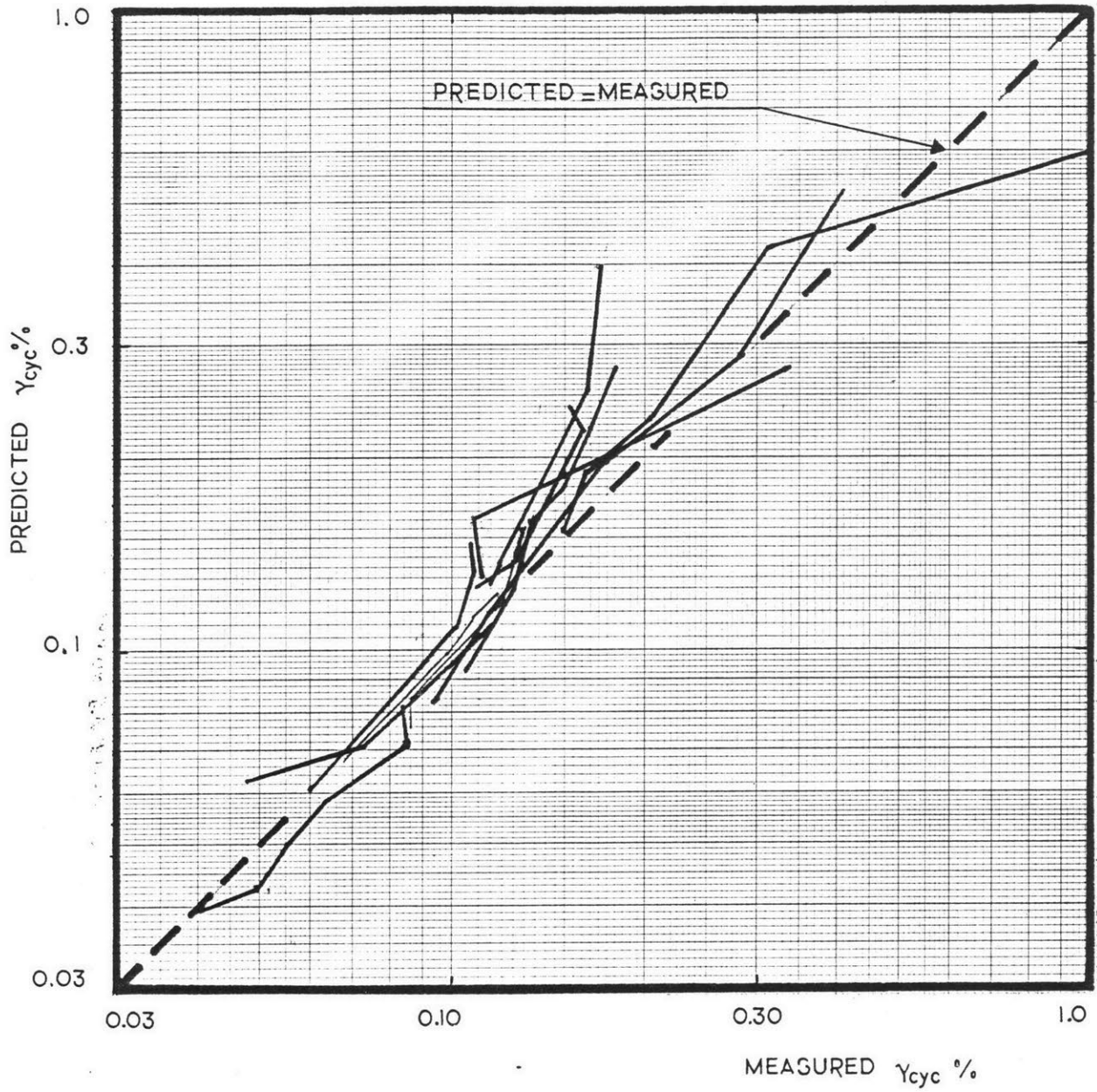


FIGURE 3.22 Comparison of the Hyperbolic Model with data from Undrained Cyclic Compression Tests

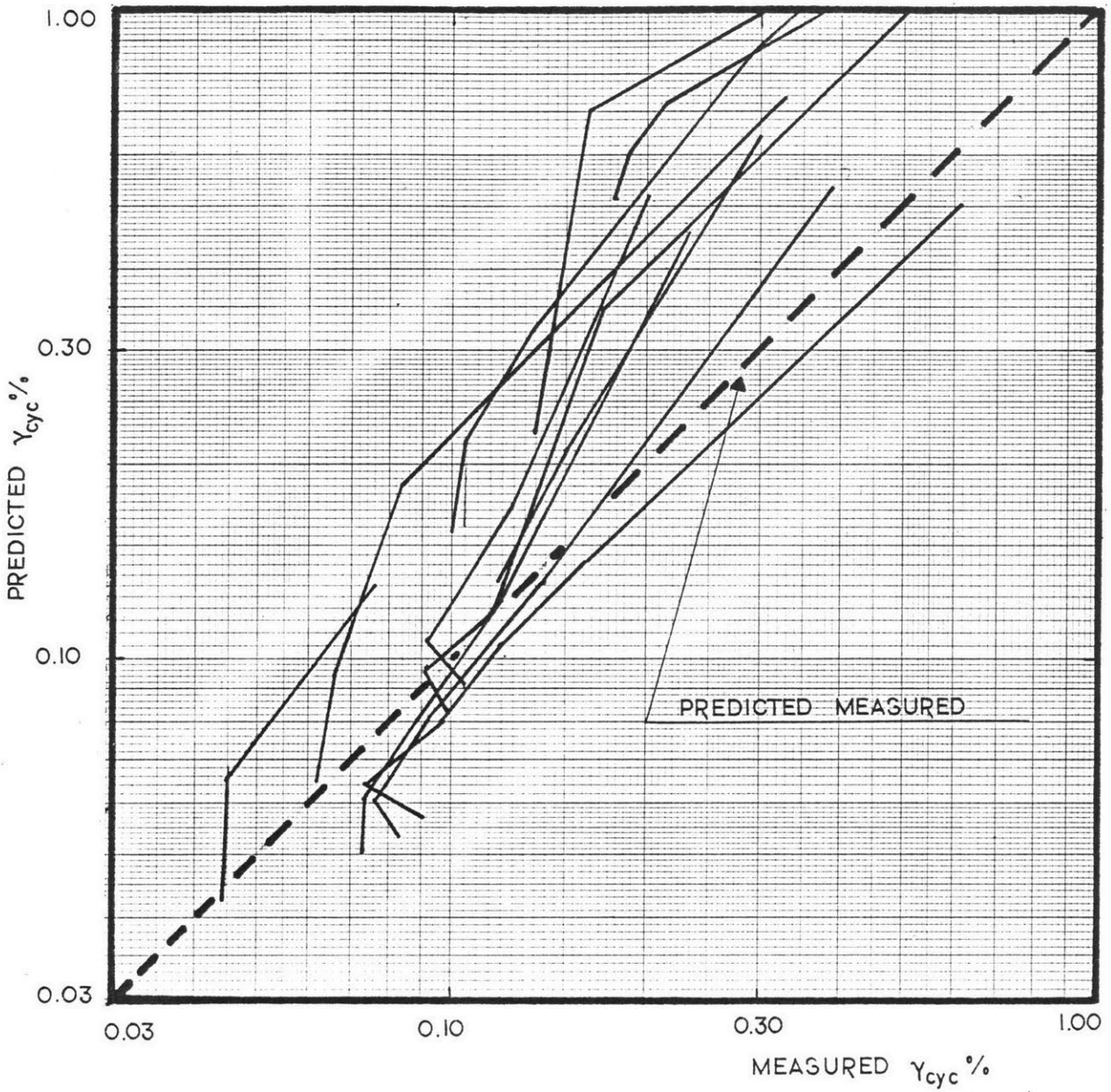


FIGURE 3.23 Comparison of the Hyperbolic Model with data from Undrained Cyclic Isotropic Tests

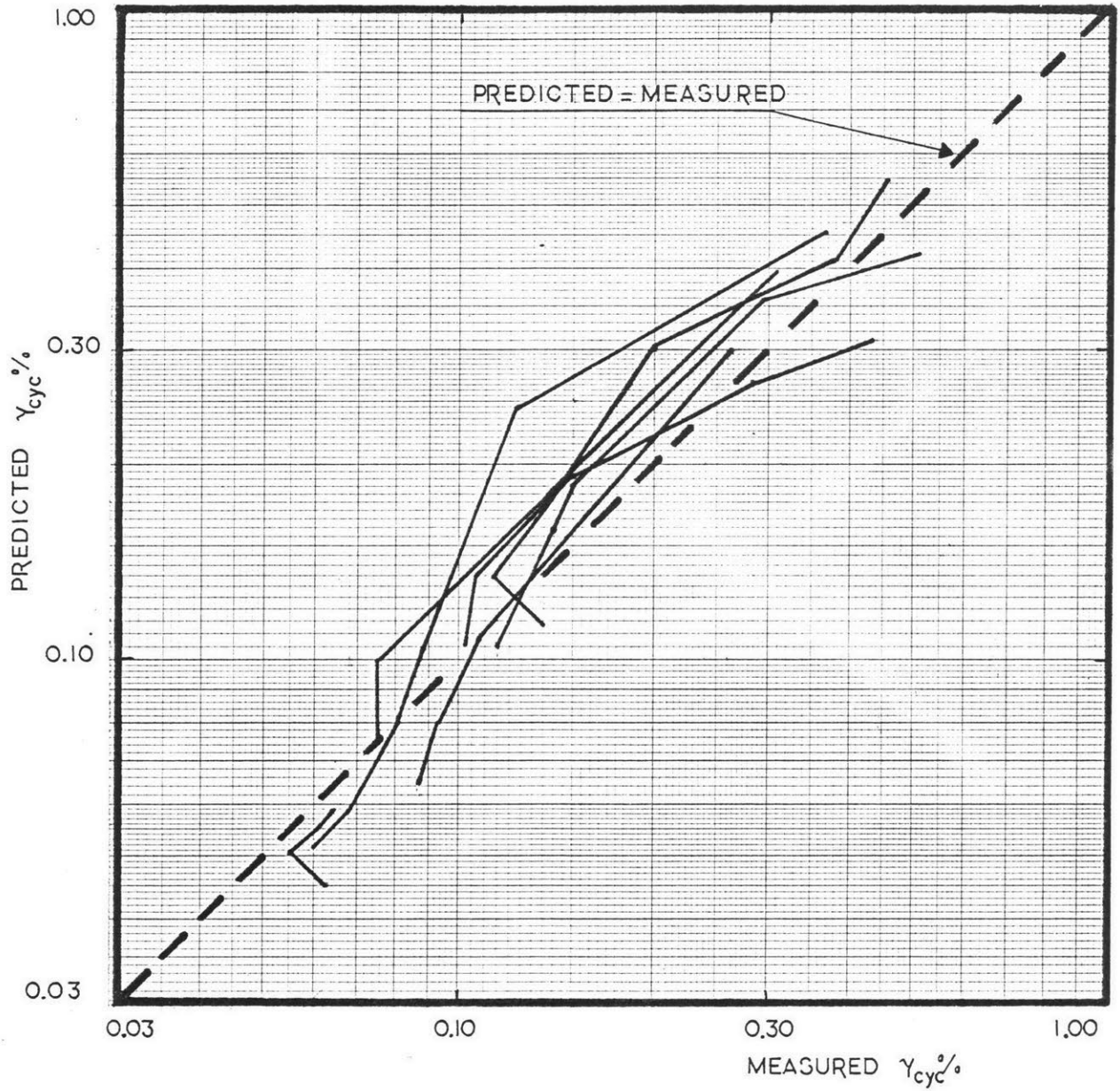


FIGURE 3.24 Comparison of the Hyperbolic Model with data from Undrained Extension Tests

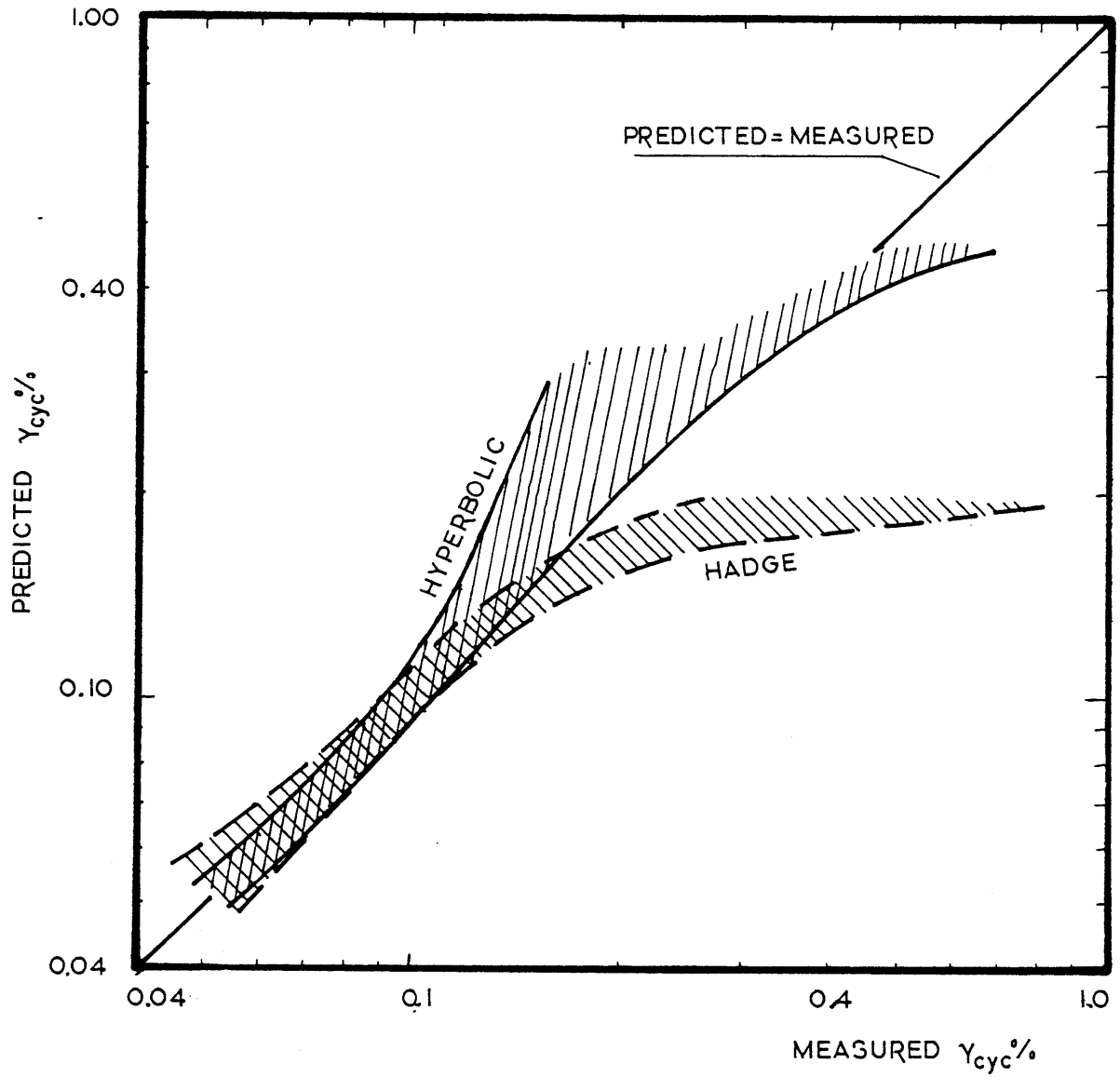


FIGURE 3.25 : Prediction of γ_{cyc} for Undrained Cyclic Compression Tests by Hadge's Model and by the Hyperbolic Model

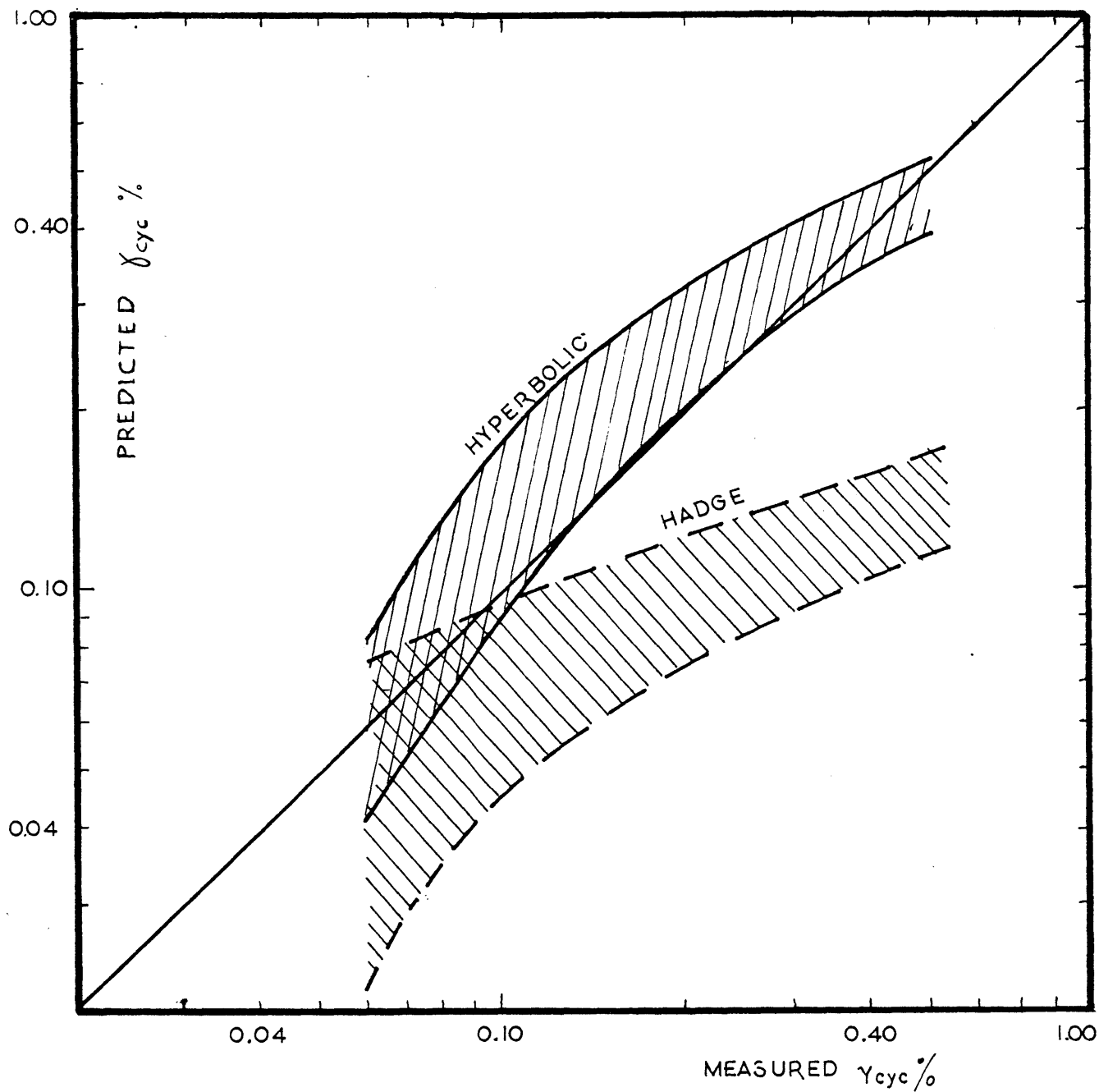


FIGURE 3.26 : Predicted γ_{cyc} for Undrained Cyclic Isotropic Tests by Hadge's Model and by the Hyperbolic Model

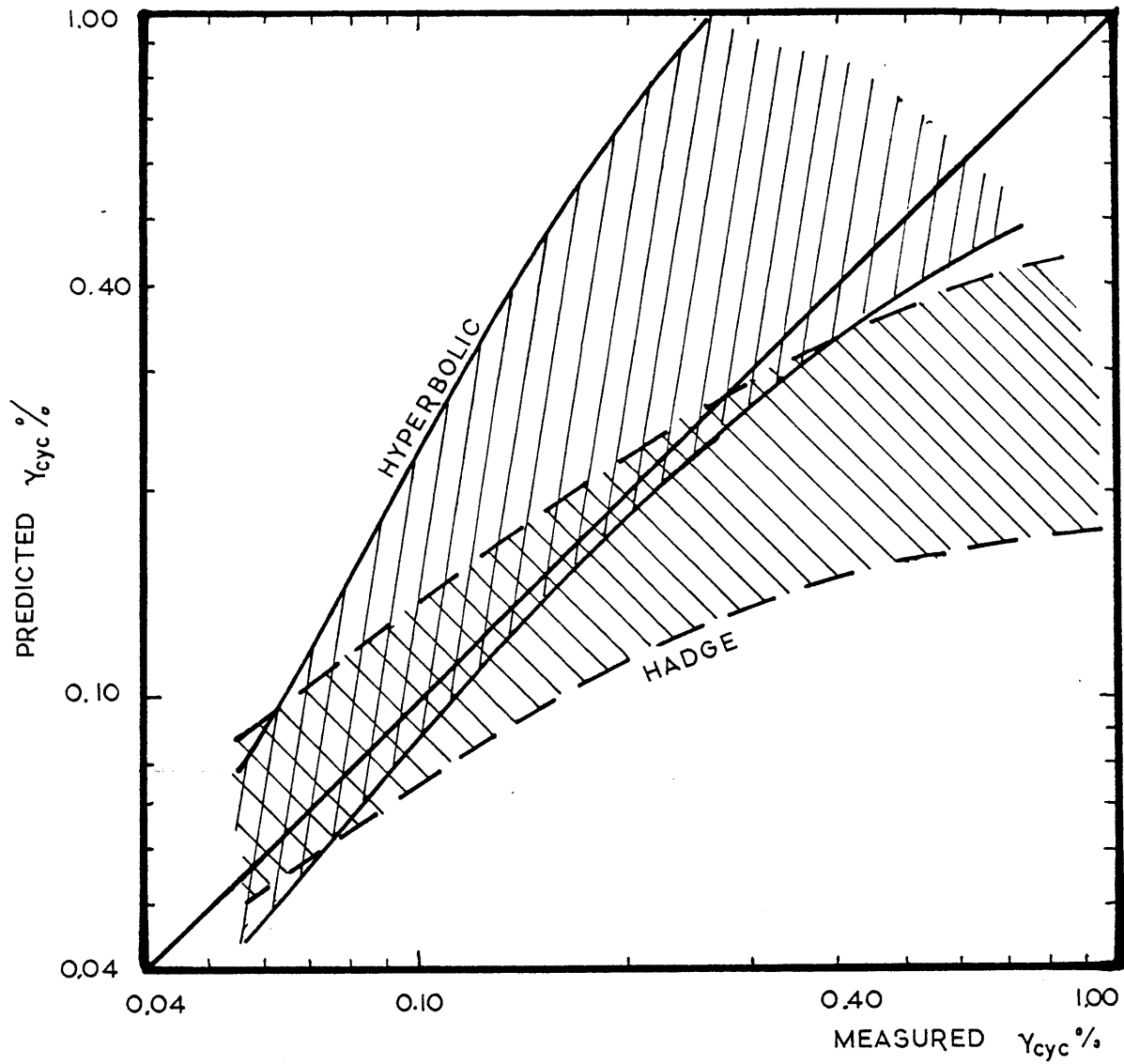


FIGURE 3.27 : Predicted γ_{cyc} for Undrained Cyclic Extension Tests by Hadge's Model and by the Hyperbolic Model

CHAPTER 4

A CONSTITUTIVE MODEL FOR CYCLIC LOADING OF SAND

4.1 INTRODUCTION

In previous chapters 2 and 3, the accumulation of strain due to drained triaxial cyclic loading of Sand A was studied, and empirical relations were suggested. Prediction of the performance of foundations under cyclic loads, however, cannot be based directly on those relations for the following reasons:

(i) In the tests analyzed the average effective stress remained constant during cycling and thus the measured strain was caused exclusively by cyclic shearing. In general, the average effective stress changes during cyclic loading due to the displacement constraints; the final strain, therefore, is the combined result of cyclic straining and static change in the average effective stress:

$$\tilde{\epsilon} = \tilde{\epsilon}^R + \tilde{\epsilon}^{\Delta\bar{\sigma}}$$

$\tilde{\epsilon}^R$ = residual strain under no displacement constraints

$\tilde{\epsilon}^{\Delta\bar{\sigma}}$ = strain due to change in average effective stresses

A complete description of cyclic sand behavior requires coupling of the empirical equation for cumulative strains with a stress-strain relationship for static loading.

(ii) In chapter 3 it was found that the accumulated strain depends on the average effective stress, the cyclic shear strain and the straining history expressed through the number of cycles. In the tests analyzed the effective stress, both average and cyclic, was kept constant allowing the total cumulative strain to be related to the number of cycles. For general analyses it is more appropriate to assume that the average stress remains constant during small parcels of cycles only. For the description of cyclic sand behavior, therefore, an incremental relation between strain and number of cycles is required.

(iii) The proposed relations were developed for triaxial tests where

$$\sigma_1 \neq \sigma_2 = \sigma_3 \quad , \quad \varepsilon_1 \neq \varepsilon_2 = \varepsilon_3$$

or

$$\sigma_1 = \sigma_2 \neq \sigma_3 \quad , \quad \varepsilon_1 = \varepsilon_2 \neq \varepsilon_3$$

Thus they describe the behavior of sand under cyclic loading in terms of the major and minor principal strain and stress only. Analysis of three dimensional problems, however, requires a complete constitutive relation of all the components of strain and stress.

This chapter presents a constitutive model that fulfills the requirements described above.

4.2 CYCLIC LOADING VERSUS CREEP

Striking similarity exists between creep and cyclic loading of soils as described by the "cumulative strain" approach:

- for creep, under constant stress, the deformation of the material increases as time increases
- for cyclic loading under constant average effective stress, deformation accumulates as the number of cycles increases.

Urzua [6] observed this similarity and used series of Kelvin-Voigt elements to predict the strain accumulation during drained cyclic loading. Using the Boltzman's superposition principle [80], Urzua was able to account for the effect of change of the average stresses on the strain accumulation (equation 3.5b). Boltzman's principle, however, applies only to material with constant compliances. This is not true for soil, whose material properties depend strongly on the effective state of stress; the method proposed by Urzua, therefore, accounts only in part for the effect of stress redistribution.

A simple means to describe creep is the Maxwell Fluid model consisting of a spring and a dashpot connected in series. Under axial stress (σ) the strain rate predicted by the model is

$$\frac{de}{dt} = \frac{1}{E} \frac{d\sigma}{dt} + \frac{\sigma}{F} \quad (4.1)$$

where

E = spring constant

F = viscosity constant

Since equation 4.1 is in incremental form, it allows for continuous updating of the model parameters E and F, and can thus include completely the effects of stress redistribution on strain accumulation. The Maxwell Fluid model will be used to describe the permanent strain accumulation due to repeated loading. The stress and strain quantities used in the model's description are summarized in table 4.1 for general three dimensional states and for triaxial test conditions.

For isotropic soil two equations, similar to 4.1, are necessary; one for the volumetric strain and stress rate and one for the deviatoric:

$$\dot{\epsilon}_{vol} = \frac{\dot{\bar{\sigma}}_{oct}}{K} + \frac{\bar{\sigma}_{oct}}{V} \quad (4.2)$$

$$\dot{e}_{ij} = \frac{\dot{S}_{ij}}{2G} + \frac{S_{ij}}{R}$$

The spring constants, K,G, correspond to the bulk and shear modulus and depend on the average effective state of stress; the "viscosity constants" V and R are non-linear functions of the average effective state of stress, the cyclic shear strain and the strain history.

Equation 4.2b suggests that the viscosity function R is common for all deviatoric components of strain, which is true for isotropic materials only. Soil is not isotropic primarily because of the

initial consolidation process and subsequent plastic flow; application of the proposed model, therefore, will be approximate as far as material isotropy is concerned.

4.3 DETERMINATION OF VISCOSITY FUNCTIONS

For repeated straining under constant average effective stress ($\bar{\sigma}_{oct} = S_{ij} = 0$) equations 4.2a and 4.2b simplify to

$$\dot{\epsilon}_{vol} = \frac{\bar{\sigma}_{oct}}{V} \quad (4.3a)$$

$$\dot{\epsilon}_{ij} = \frac{S_{ij}}{R} \quad (4.3b)$$

For triaxial tests equation 4.3b can be expressed as

$$\dot{\epsilon}_v - \dot{\epsilon}_h = \frac{\sigma_v - \sigma_h}{R}$$

or

$$\dot{\epsilon}_v - \frac{1}{3} \dot{\epsilon}_{vol} = \frac{2}{3} \frac{q}{R} \quad (4.3c)$$

Substitution of the strain rates in equations 4.3a and 4.3c with the empirical equations 3.6 and 3.9 leads to expression of the viscosity functions for Sand A:

$$V = \frac{\bar{\sigma}_o}{0.274 \gamma_{cyc}^{1.26} N^{-0.6} f} \quad (4.4a)$$

$$R = \frac{1}{2.795 \frac{|q|}{\sigma_{oct}} \gamma_{cyc}^{1.26} N^{-0.6} f} \quad (4.4b)$$

An invariant measure of shear stress for general stress conditions is

the shear stress intensity T defined as

$$T = (J_2^\sigma)^{\frac{1}{2}} \quad (4.5)$$

J_2^σ : second invariant of the deviatoric stress

For triaxial tests (see table 4.1)

$$\tau = \frac{2}{\sqrt{3}} |q|$$

Substitution of equation 4.5 into equation 4.4 results in expression of the viscosity functions only in terms of the stress invariants:

$$V = \frac{\bar{\sigma}_{oct}}{0.274 \gamma_{cyc}^{1.26} N^{-0.6} f} \quad (4.6a)$$

$$R = \frac{1.}{2.421 \frac{T}{\bar{\sigma}_{oct}^2} \gamma_{cyc}^{1.26} N^{-0.6} f} \quad (4.6b)$$

The above relations are based on data from cyclic tests with constant amplitude, where the strain history is completely defined by the number of cycles. In many important practical problems - such as loading resulting from wave forces on offshore structures, or from earthquake ground motion - the cyclic load amplitude is variable. Such problems are usually handled by converting the irregular time history into an equivalent number of cycles of uniform load.

There are different ways to do so depending on the objective of the study. Annaki and Lee [53] and others [52], [54] use fatigue concepts to define the equivalent number of cycles: for a reference cyclic shear stress they find the number of uniform cycles that will cause the same damage, with respect to liquefaction, as the irregular loading. The basic premises are two:

(i) The cyclic strength of the material is known.

(ii) The energy applied during any stress cycle has cumulative damaging effect which is independent of where in the time history that particular stress cycle occurs.

This procedure is meaningful for repeated loading under undrained conditions, and has been successfully used to determine safety against liquefaction.

Urzua [6] applies a similar approach to irregular cyclic loading of dry soils. For a reference cyclic shear strain he defines the number of uniform cycles which will produce the same accumulation of volume change as the irregular loading. This procedure, similar to the previous one, assumes that each strain cycle has a cumulative effect which is independent of the sequence of loading.

A different way of treating irregular loading is to describe the cyclic history with a strain measure. This approach is widely used to describe monotonic loading of soils through classical plasticity ([9], [10] etc.) and endochronic models ([55], [56] etc.). Martin, Finn and Seed [56] propose that the accumulation of strain or pore pressure due to one cycle of loading depends, among other factors, on the permanent volume that would have occurred prior to this cycle if free drainage had been allowed. This method, in contrast to the two previously described, takes into account the sequence of the irregular loading; in addition it is applicable to both drained and undrained loading. Martin et al used this method with success to study the effect of the membrane penetration and the partial saturation on the results of

cyclic undrained triaxial tests.

The effect of cyclic history on equation 4.6 will be introduced with the method of Martin et al. If at the beginning of one cycle of loading the permanent volume change that would have occurred under drained conditions and no other displacement constraints is ϵ_{vol}^R , and the cyclic shear strain amplitude of the cycle is γ_{cyc} then the equivalent number of cycles with uniform amplitude γ_{cyc} is

$$N_{eq} = \left[\frac{\epsilon_{vol}^R}{0.685 \gamma_{cyc}^{1.26}} \right]^{2.50} \quad (4.7)$$

The number of cycles N , in equation 4.6 has to be replaced with N_{eq} to make the equation applicable to irregular cyclic loading; if the amplitude of cyclic shear strain remains constant during the loading period the equivalent number of cycles is equal to the true one.

4.4 DETERMINATION OF SOIL MODULI

The change in strain due to an average effective stress increment can be predicted with different degree of accuracy depending on the soil model used and the kind of loading. Linear elastic is the simplest model that can be used, since it requires the definition of two parameters only: The Young's modulus and the Poisson's ratio, or any other equivalent pair. Soil, however, is highly non linear and application of linear elasticity must be restricted to problems where small change of stress is expected.

Improved predictions of stress-strain behavior can be achieved if

the elastic parameters are related to the effective stress. One example of this category is the widely used hyperbolic model ([48], [49], [50] etc.) which uses five parameters to define the variation of the elastic soil properties. Simplicity is the major advantage from using those models; their application, however, is limited to stress paths not significantly deviating from the laboratory tests used to fit the model parameters [58]. The description with such models of the post-peak behavior of soils with strain softening requires the introduction of large number of parameters which complicates the model [74].

Recent application of plasticity and viscoplasticity concepts to soil mechanics produced models able to predict characteristic features of soil behavior such as: strain softening, change in volume due to shearing and anisotropy effects. Models, however, which are also realistic in predicting those features quantitatively are usually defined through a large number of parameters (for example Prevost [8], [9]), and also require relatively large computational effort.

The use of an endochronic or a plasticity model to describe the soil moduli in equations 4.2 would rather complicate the proposed model. Instead simple relationships of the soil moduli to the effective state of stress can yield sufficiently accurate predictions, since:

- (i) simple aspects of the pre-peak response of sands is of primary interest here

(ii) the stresses in the foundation can be estimated in advance so that appropriate stress conditions can be used in the laboratory to define the stress-strain relations.

4.4.1 SHEAR MODULUS

Since the deviatoric stresses and strains are related through the shear modulus:

$$e_{ij} = \frac{S_{ij}}{2G}$$

the same will be true for their invariants. A non linear elastic relation will be assumed between the shear stress and the shear strain intensities (see definitions in table 4.1):

$$\dot{\Gamma} = \frac{\dot{T}}{2G}$$

with tangent shear modulus, G , defined as

$$G = G_{50} \quad (4.8)$$

$$G_{50} = \text{Secant Modulus for } T = 1/2 T_{\text{failure}}$$

It is worth noting that the definition of shear modulus is independent of the direction of load increment as far as loading and unloading is concerned; this characteristic considerably simplifies the numerical application of the model. The proposed modulus is not affected by the applied shear stress; consequently possible stress redistribution in the foundation cannot be modeled for the case of local failures due to monotonic or cyclic loading.

Christian and Marr [59] report the following approximate relationship between Young's modulus confining stress and porosity, for Sand A:

$$E_{50} = (6507.0 - 134.0 n) p_{\alpha} \left(\frac{\bar{\sigma}_{oct}}{p_{\alpha}} \right)^{0.5} \quad (4.9)$$

where n = porosity in. %
 p_{α} = atmospheric pressure

The shear modulus can be computed from equation 4.9 as

$$G_{50} = (6507.0 - 134.0 n) \frac{p_{\alpha}}{2(1+\nu)} \left(\frac{\bar{\sigma}_{oct}}{p_{\alpha}} \right)^{0.5} \quad (4.10)$$

ν = Poisson's ratio

Figure 4.1 compares equation 4.9 with the general relation for the shear modulus at small strains (G_{max}) proposed by Richart [47] (equation 3.12) for a wide range of initial void ratios. The correlation of the expressions depends on the void ratio of the sand; for the range of porosities tested by Christian and Marr it is approximately

$$G_{50} = 0.35 G_{max} \quad (4.11)$$

4.4.2 BULK MODULUS

From theory of elasticity the Bulk and the Shear moduli are related by the equation

$$K = \frac{2(1+\nu)}{3(1-2\nu)} G$$

with values of Poisson's ratio smaller than 0.5. This relation,

however, is realistic at small strains only, when the stress-strain relationship of the soil is approximately elastic. When plastic strain starts developing, the above equation is not valid any more and the Bulk modulus must be determined independently from the Shear modulus using results from appropriate laboratory tests (e.g. [50,51]).

Duncan et al [51] suggest that the Bulk Modulus of sands is related to the minor effective stress in triaxial tests by the equation

$$K = B p_{\alpha} \left(\frac{\bar{\sigma}_3}{p_{\alpha}} \right)^m$$

Duncan based his conclusions on isotropically consolidated triaxial tests where the minor effective stress is also equal to the initial hydrostatic effective stress. Similar to the proposed relation for the shear modulus, the Bulk Modulus will be expressed in terms of the hydrostatic effective stress which is an invariant quantity:

$$K = B p_{\alpha} \left(\frac{\bar{\sigma}_{oct}}{p_{\alpha}} \right)^m \quad (4.12)$$

Duncan and Chang [50] accept that the parameter B must be related to the porosity of the soil but they avoid proposing any empirical relation due to lack of experimental data. The same researchers suggest that B for reloading and unloading is different than B for primary loading, but the exponent m is the same. Duncan and Chang express concern over the effective stress path followed in triaxial compression tests; it is very likely that the direction of loading has to be added to the factors affecting the Bulk Modulus. Due to

those complexities, it is recommended that the appropriate values for the parameter B and m in equation (4.13) be estimated through laboratory tests along effective stress paths similar to those expected during cyclic loading.

4.5 EVALUATION OF MODEL'S PARAMETERS

This section summarizes the laboratory tests required for the determination of the model's parameters. The tests will be grouped according to the parameter(s) they are used to evaluate.

Strength Characteristics

Drained and Undrained static triaxial tests are required to determine the maximum friction angle and the undrained shear strength of the soil (Appendix B). It is desirable that those tests cover a wide range of initial porosities since both the friction angle and the undrained shear strength are related to porosity.

Limits on Permanent Strain Accumulation

In chapter 2 the boundary between contractive and dilative behavior due to cyclic loading was defined by the CT-line and the minimum void ratio of the soil. The static triaxial tests run to determine the strength characteristics of the soil can also be used to define the CT-line, in the way described in chapter 2. The minimum void ratio must be determined from vibratory compaction tests

according to ASTM D-2049-69 requirements.

Viscosity Functions

In section 4.3 it was shown that two empirical relations are required to describe the viscosity functions V and R; one for the volumetric and one for the vertical strain accumulation. Those relations must be derived from two series of drained cyclic triaxial tests:

- one where the initial state of stress is kept constant and the cyclic stress amplitude varies

- a second where the initial stresses vary

For the second series of tests it is important to run tests varying the distance from the CT-line systematically, so that the function expressing the effect of limit state on permanent strain accumulation (see section 3.3) can be determined.

For both series a large number of cycles of loading ($N > 1000$) must be applied.

Soil Moduli

The soil moduli G and K are used by the model to determine the permanent strain resulting from stress redistribution during cyclic loading. For their evaluation, therefore, stress-strain data are required from static tests run along stress paths simulating the expected stress redistribution. Sample evaluation of soil moduli are

presented in the following chapter, which compares the model's predictions with data from test where the average state of stress changes during cyclic loading.

4.6 SUMMARY

A constitutive model was developed which relates the change in cumulative strain to the change of the number of cycles and to the change of the average effective state of stress. The most important features of the model are listed below:

(i) It is formulated in terms of six components of stress and strain and can thus be applied under general loading and boundary conditions

(ii) It is formulated in terms of the effective state of stress and applies to both drained and undrained analyses

(iii) It is incremental and can thus account effectively for the effects of stress redistribution on permanent strain accumulation

(iv) It assumes isotropic material properties

(v) Relatively simple laboratory tests are required to determine the model's parameters, which include static triaxial tests and drained cyclic triaxial tests.

GENERAL	TRIAXIAL TESTS	
$\epsilon_{vol} = \epsilon_{xx} + \epsilon_{yy} + \epsilon_{zz}$	$\epsilon_{vol} = \epsilon_v + 2\epsilon_h$	Volumetric Strain
$e_{ij} = \epsilon_{ij} - 1/3 \delta_{ij} \epsilon_{vol} \quad i,j=x,y,z$	$\epsilon_v = 2/3 (\epsilon_v - \epsilon_h)$ $\epsilon_h = -1/3 (\epsilon_v - \epsilon_h)$	Deviatoric Strain
$\sigma_{oct} = \frac{\sigma_{xx} + \sigma_{yy} + \sigma_{zz}}{3}$	$\sigma_{oct} = \frac{\sigma_v + 2\sigma_h}{3}$	Octahedral Stress
$S_{ij} = \sigma_{ij} - 1/3 \delta_{ij} \sigma_{oct} \quad i,j=x,y,z$	$\sigma_v = 2/3 (\sigma_v - \sigma_h) = 4/3 q$ $\sigma_h = -1/3 (\sigma_v - \sigma_h) = -2/3 q$	Deviatoric Stress
$\delta_{ij} = \begin{bmatrix} 1. & i=j \\ 0. & i \neq j \end{bmatrix}$		Kronecker Delta
$J_2^{\sigma} = 1/2 S_{ij} S_{ij} \quad i,j=x,y,z$	$J_2^{\sigma} = 1/3 (\sigma_v - \sigma_h)^2 = 4/3 q^2$	Second Invariant of the Deviatoric Stress
$T = (J_2^{\sigma})^{1/2}$	$T = \frac{ \sigma_v - \sigma_h }{\sqrt{3}} = \frac{2 q }{\sqrt{3}}$	Shear Stress Intensity
$J_2^{\epsilon} = 1/2 e_{ij} e_{ij} \quad i,j=x,y,z$	$J_2^{\epsilon} = 1/3 (\epsilon_v - \epsilon_h)^2 = 1/3 \gamma^2$	Second Invariant of the Deviatoric Strain
$\Gamma = (J_2^{\epsilon})^{1/2}$	$\Gamma = \frac{ \epsilon_v - \epsilon_h }{\sqrt{3}} = \frac{ \gamma }{\sqrt{3}}$	Shear Strain Intensity

TABLE 4.1: Definitions of Stress and Strain Quantities Used with the Proposed Model

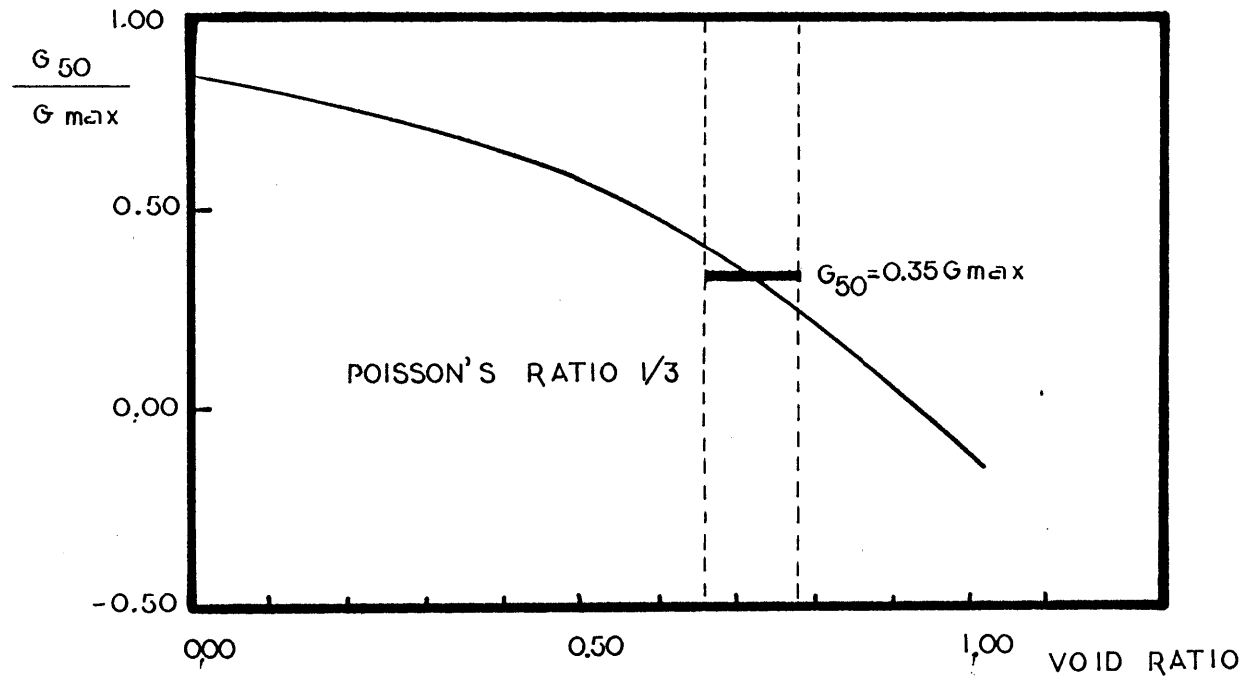


FIGURE 4.1 ; Comparison between G_{50} for Sand A and G_{max} by Richart (ref. 40)

CHAPTER 5

EVALUATION OF MODEL'S PREDICTIONS

5.1 INTRODUCTION

So far it has been shown that the model fits the behavior of Sand A under drained cyclic triaxial test where the average effective stress and the cyclic shear strain remained constant throughout the test. Those tests, however, are not representative of the stress conditions in a foundation subjected to repeated loading, as has been already discussed in chapter 4. In the following paragraphs the applicability of the proposed model will be evaluated through comparison with results from cyclic oedometer tests and undrained cyclic triaxial tests.

5.2 CYCLIC OEDOMETER TESTS

5.2.1 TEST RESULTS

Wooten [60] reports test results from cyclic oedometer tests on Sand A where the applied vertical stress varied between two fixed limits; the stress and porosity conditions for the tests are summarized in table 5.1. The ratio of the horizontal to the vertical stress, and the accumulated vertical strain, measured in all of the tests are portrayed in Figure 5.1.

Similar as in drained cyclic triaxial tests, permanent vertical strain in oedometer tests accumulates at a decreasing rate with respect to number of cycles. The magnitude of permanent strain, however, is smaller in oedometer tests than in drained triaxial tests (see Figure 5.2). At small numbers of cycles ($N < 40$) the log strain log number of cycles plot for the oedometer test is slightly shallower than that corresponding to triaxial test under the same stress and porosity conditions; the plots become approximately parallel at larger numbers of cycles ($N > 40$). In all tests a small increase, up to 9%, in horizontal stress is observed during the first cycles of loading ($N < 40$). Thereafter the horizontal stress either remains constant or decreases.

Measurements of the horizontal stress during cyclic oedometer tests of Ottawa sand reported by Finn [61], are shown in Figure 5.3. For normally consolidated samples ($D_r = 45\%$) cyclic loading increased the horizontal stress by 50%; for overconsolidated samples ($\alpha_{CR} = 4$) cyclic loading decreased the applied horizontal stress by 30%. The results show that the ratio of the horizontal to the vertical stress

tends to a limiting value approximately equal to 0.63. For initial stress ratios smaller than the limiting value, cyclic loading will increase the horizontal stress, while it will have the opposite effect when the value of initial stress ratio is larger than the limiting value.

The normally consolidated Ottawa sand tested by Finn has similar density and initial stress ratio to Sand A tested by Wooten. Finn, however, reports a much larger increase in horizontal stress than Wooten does. In addition his results suggest a steady increase of the horizontal stress towards a limiting value, in contrast to the initial increase followed by decrease in horizontal stress observed by Wooten.

In interpreting his results, Wooten considered three possible factors to account for the measured decrease in horizontal stress:

- (i) Measurement errors
- (ii) Equipment characteristics
- (iii) Actual soil behavior

He concluded that the test results reflect actual soil behavior.

There are reasons, however, to believe that measurement errors and equipment characteristics may play a more significant role. In Figure 5.4 the ratio of the vertical to the volumetric permanent strain in the oedometer tests is plotted versus the average stress ratio ($q/\bar{\sigma}_{\alpha t}$); in the same figure data from drained cyclic triaxial tests on the same sand are shown for comparison. It is evident that the sand behavior observed in the triaxial tests is not compatible with

the results from the oedometer tests.

5.2.2 MODEL PREDICTION

Under constant average vertical stress ($\dot{\bar{\sigma}}_v = 0$) and no lateral strain ($\dot{\epsilon}_h = 0$) equations 4.2 take the form:

$$\dot{\epsilon}_v = \frac{2}{3} \frac{\dot{\bar{\sigma}}_h}{K} + \frac{\bar{\sigma}_{oct}}{V}$$

$$\dot{\epsilon}_v = - \frac{\dot{\bar{\sigma}}_h}{2G} + \frac{\bar{\sigma}_v - \bar{\sigma}_h}{R}$$

Solution of this system of equations yields the expressions for the two unknowns $\dot{\bar{\sigma}}_h$ and $\dot{\epsilon}_v$:

$$\dot{\bar{\sigma}}_h = \frac{\bar{\sigma}_v - \bar{\sigma}_h}{R} - \frac{\bar{\sigma}_{oct}}{V} \left(\frac{2}{3K} + \frac{1}{3G} \right) \quad (5.1)$$

$$\dot{\epsilon}_v = \frac{\bar{\sigma}_v - \bar{\sigma}_h}{R} - \frac{\bar{\sigma}_{oct}}{V} \left(1 + \frac{3}{4} \frac{K}{G} \right) + \frac{\bar{\sigma}_{oct}}{V} \quad (5.2)$$

The results reported by Wooten and Finn show that during cyclic loading under one-dimensional conditions of Sand A will increase the average horizontal stress, and will decrease the volume of the sand. As it is shown in Figure 5.5 the average stress and volume state of Sand A will move away from the "Virgin compression line" (VCL) where it originally belonged. The appropriate moduli in equations 5.1 and 5.2, then, are those corresponding to unloading and reloading.

Paragraph 4.4.1 describes completely the shear modulus for Sand A.

Data from 1-D monotonic loading and unloading of the same sand are reported by Wooten [60]; it is suggested (see Figure 5.6) that the Bulk Modulus can be estimated from the following expression:

$$K = 2250.0 p_{\alpha} \left(\frac{\bar{\sigma}_{\text{oct}}}{p_{\alpha}} \right)^{1.70} \quad (5.3)$$

Figure 5.7 summarizes characteristic predictions of the model for two cyclic oedometer tests with different initial stress ratios. In both cases the horizontal stress changes until a limiting value of the stress ratio is reached; thereafter the average effective stress remains constant and the vertical permanent strain equals to the volumetric since no lateral deformation is allowed. The limit stress ratio then can be defined from the empirical equation 3.5a as

$$\frac{\epsilon_v}{\epsilon_{\text{vol}}} = 13.6 \left(\frac{q}{\bar{\sigma}_{\text{oct}}} \right)^2 + 0.33 = 1.0$$

or

$$\frac{\epsilon_v}{\epsilon_{\text{vol}}} = 13.6 \frac{3}{2} \left(\frac{1-K}{1+2K} \right) + 0.33 = 1.0 \quad (5.4)$$

Solution of equation 5.4 yields the limiting stress ratio for Sand A

$$K_{\text{limit}} = \left(\frac{\bar{\sigma}_h}{\bar{\sigma}_v} \right)_{\text{limit}} = 0.66 \quad (5.5)$$

When the initial stress ratio is larger than the limiting value, the average horizontal stress decreases due to cyclic loading, but it increases when the initial stress ratio is smaller than the limiting value. This behavioral pattern is in good agreement with the test

results reported by Finn [61] and shown in Figure 5.3. Comparison of the limiting values of the stress ratio measured by Finn and predicted by the model, 0.63 and 0.66 respectively, shows a remarkably good agreement.

Vertical strains in Figure 5.7 accumulate continuously at a decreasing rate. For small initial stress ratio the slope of the log strain-log N plot is initially small and increases as the number of cycles of loading increases; the same response is reported by Wooten [60] (see Figure 5.2). In the case with large initial stress ratio the opposite response is predicted. At a large number of cycles the strain rates of both cases become similar.

Figure 5.8 compares measured horizontal stress and vertical permanent strain in cyclic oedometer tests on Sand A with the model predictions. The model predicts larger changes in horizontal stress, and a smaller accumulation of vertical strain. To examine the sensitivity of the predictions to the value of Bulk Modulus, a modulus equal to one tenth of that defined by equation 5.3 was used to predict the cyclic response; the results are summarized in Figure 5.9. Although the comparison with the measured response has been improved, especially at small number of cycles, still the model predicts larger horizontal stress and smaller vertical strain.

Earlier in section 5.2.1 it was shown that there are reasons to believe that testing errors may have altered the measured response. One assumption that seems to explain the divergence between the predicted and measured behavior is that testing conditions in the cyclic oedometer tests are not purely one dimensional. Lateral

flexibility of the stress measuring ring, or dilation caused by temperature increase during the test, may have allowed horizontal strain, thus leading to small change in horizontal stress and large vertical deformation.

To check the validity of this assumption, predictions of cyclic response were made, allowing free lateral strain. Figure 5.10 compares the test data with model predictions under both assumptions of no lateral strain and free lateral strain; the results reported by Wooten [60] correspond to an intermediate situation. It is reasonable, then, to believe that despite the great care taken by Wooten to maintain one dimensional conditions throughout the test, some lateral strain developed during cyclic loading.

5.2.3 SUMMARY

Comparison of the model's prediction presented with test results from cyclic oedometer tests reported by Finn [61] and Wooten [60]. The model was able to predict all the basic trends reported by the two researchers:

- (i) There is a limiting value of the ratio of horizontal to vertical stress that can be reached with cyclic loading.
- (ii) When the initial stress ratio is smaller than the limiting one cyclic loading results in increase of the horizontal stress. The effect of cyclic loading on

horizontal stress is opposite when the initial stress ratio is larger than the limiting value.

(iii) When the initial stress ratio is lower than the limiting one the slope of log strain-log N plot is smaller at small number of cycles than it is in large number of cycles.

Model predictions overestimate the stress and underestimate the strain measured by Wooten. Evidence has shown that lateral expansion of the testing device used by Wooten resulted in conditions different than one dimensional, as the model assumes.

5.3 UNDRAINED CYCLIC TRIAXIAL TESTS

5.3.1 MODEL'S PREDICTION

Undrained cyclic triaxial tests on Sand A were run at M.I.T. as part of research on the behavior of Oosterschelde soils, sponsored by the Government of the Netherlands. The test conditions and procedures are summarized in reference [62].

The total average stresses were kept constant throughout each test ($\dot{\bar{\sigma}} = 0$); this condition when combined with the volume incompressibility ($\dot{\bar{\epsilon}}_{vol} = 0$) and equation 4.2a yields an expression for the rate of accumulation of pore pressure:

$$\dot{u} = K \frac{\bar{\sigma}_{oct}}{V} \quad (5.6)$$

Equation 4.2b or its simplified version 4.3b defines the vertical

strain accumulation rate:

$$\dot{\epsilon}_v = \frac{2}{3} \frac{\sigma_v - \sigma_h}{R} \quad (5.7)$$

The bulk modulus in equation 5.6 must be estimated according to stress-strain data from laboratory tests along the path followed by the average state of stress during undrained cyclic loading.

For initial stress conditions in the subcharacteristic domain, positive pore pressure will develop due to cyclic loading, reducing the octahedral effective stress under constant shear stress. Hodge and Marr [22b] measured the volume increase of Sand A, in static tests along just such a stress path. Their results are presented in Figure 5.11 in terms of the tangent bulk modulus and the effective octahedral stress; a simple relation that fits the data is

$$K = 280.0 \bar{\sigma}_{\text{oct}} \quad (5.8)$$

Equation 5.8 overestimates the modulus for effective octahedral stress smaller than 1.20 ksc. For most of the cyclic triaxial tests on sand A (see table 5.2), however, the initial octahedral stress is larger than this value. In addition typical data from undrained triaxial tests (e.g. figure 5.13) show that the rate of pore pressure accumulation is larger during the initial stages of cyclic loading than it is later. For both reasons it is preferable to fit the experimental data over the range of effective octahedral stresses larger than 1.20 ksc.

It is possible that initial stresses and volume conditions affect the bulk modulus. The analyzed tests, however, cover a limited range

of porosities and initial shear stress ratios:

$$41.1 \leq n\% \leq 43.8$$

$$0.21 \leq \frac{q}{\bar{\sigma}_{\text{oct}}} \leq 0.36$$

and do not permit evaluation of those effects.

One parameter of the model that has not been determined so far is the parameter " ψ " in the expression for the effect of the Cyclic limit state on permanent strain accumulation (see section 3.3). The value of " ψ " must be determined from series of drained cyclic tests with varying distance away from the CT-line. Such tests, however, were not available for Sand A and a crude estimation of the value of " ψ " will be made through test data from a representative undrained cyclic triaxial test in compression.

Figure 5.12 compares predicted pore pressures and vertical strains with values measured in test LC-104. A wide range of " ψ " values was considered to determine the sensitivity of the model's predictions to this parameter. It can be concluded that:

- (i) both strain and pore pressure predictions are sensitive to the value of " ψ "
- (ii) the effect of " ψ " is more pronounced at large number of cycles as the effective state of stress moves close to the CT-line due to the increase in pore pressure

(iii) values of " η " between 0.40 and 2.50 provide a reasonably good fit of the data. In the following sections a value equal to 1.0 is used to predict the cyclic response of Sand A.

5.3.2 PREDICTED VERSUS MEASURED RESPONSE

To evaluate the model's validity under undrained conditions, the predicted and measured response was compared for twenty eight undrained cyclic triaxial tests: ten of the tests are in compression ($\sigma_v > \sigma_h$), eleven are isotropic, and seven are in extension ($\sigma_v < \sigma_h$). The initial stress and porosity conditions for all tests are summarized in table 5.2.

CYCLIC COMPRESSION TESTS

Figure 5.13 presents typical results for vertical strain, pore pressure and mean effective stress versus number of cycles. Positive pore pressure accumulates at a continuously decreasing rate until stabilization occurs. Compressive vertical permanent strain develops at an initially increasing rate. After stabilization of pore pressure the rate of accumulation remains more or less constant as the number of cycles increases. The model's predictions for the same test are shown in Figure 5.14; the predicted strain and pore pressure accumulation are in very good agreement with the trends identified in Figure 5.13.

A summary of the quantitative comparison between predicted and measured values of pore pressure and residual permanent strain is shown in Figure 5.15; the model's predictions generally agree with the average measured response. The scatter in the prediction is larger for strain than it is for pore pressure; also the scatter in pore pressure prediction is independent of the number of load cycles, while for permanent strains, it increases with the number of load cycles.

CYCLIC ISOTROPIC TESTS

Typical values of residual strain, pore pressure and effective octahedral stress versus number of cycles for isotropic triaxial tests are shown in Figure 5.16. According to the test results pore pressure increases and mean effective stress decreases at an approximately constant rate during most of the test. Close to the end of the test, pore pressure starts accumulating rapidly, and finally stabilizes at a value equal to the total confining stress; the corresponding value of the average mean effective stress is equal to zero.

Practically no residual vertical strain accumulates during most of the test; at the final stage of the test and in parallel with the rapid accumulation of pore pressure, extension strains start developing.

The model's predictions for the same test described above are presented in Figure 5.17; there is striking similarity between all aspects of predicted and measured response. The only qualitative difference lies in the extension residual vertical strains measured

before the effective stresses become zero. Castro [79], however, suggests that those strains are not realistic but have been caused by the non-uniform density and displacement distribution in the sample developing during cyclic loading close to failure. Cassagrande and Rendon [78] also present results supporting this view.

Quantitative comparison between the predicted and measured values of residual pore pressure and vertical strain is summarized in Figure 5.18. Permanent strains developed in the final stage of cyclic loading are not included in the comparisons for reasons explained above. The magnitude of predicted pore pressure and vertical strain is in very good agreement with the test measurements.

CYCLIC EXTENSION TESTS

Typical measured results from cyclic extension tests are summarized in Figure 5.19. According to the test results positive pore pressure develops due to cyclic loading, followed by residual extensive strain. The pore pressure accumulation initially increases with the number of load cycles, then levels off and finally decreases slightly. Hedberg [5] attributes the observed decrease to dilatancy, as well as, possible decrease in strength of the sample. The rate of vertical strain accumulation continuously increases with the number of load cycles throughout the test.

A summary of model predictions for the same test is presented in Figure 5.20. The model predicts the development of positive pore pressure and extensive residual vertical strain. The way the rate of accumulation of both quantities changes with the number of cycles is

also predicted correctly except for the observed decrease of pore pressure at the end of cyclic loading.

Quantitative predictions of pore pressure and residual vertical strain values are compared in Figure 5.21; the model consistently predicts smaller pore pressure and strain values than those measured in the tests. The pore pressure is underpredicted by an average amount of 70%. To eliminate this difference either the Bulk modulus (K) has to be increased by 70% or the volumetric viscosity function (V) has to be decreased by the same amount (see equation 5.6). Figures 5.22 and 5.23 summarize the model's predictions for increased Bulk modulus and decreased viscosity function respectively. The elimination of the consistent difference between the predicted and measured value of pore pressures, results in significant improvement of the prediction for residual vertical strain as well. Among the two ways suggested to improve the predictions, reduction of the volumetric viscosity constant gave better predictions of vertical permanent strain.

The fact that different model parameters must be used for extension tests than for isotropic and compression tests implies that the tested sand is not isotropic material as the model assumes, but anisotropic. Hedberg [5] confirms also the anisotropic nature of Sand A, presenting data from static and cyclic triaxial tests.

The model's parameters were determined primarily through data from drained triaxial tests either isotropic or in compression, due to lack of similar data from extension tests. To be able to fit the cyclic response in extension, data from drained cyclic and static triaxial

tests in extension are required.

5.3.3 SUMMARY

Test results from undrained cyclic triaxial tests on Sand A were compared with predictions made by the proposed model. It was found that the model successfully predicts the basic trends identified in the test results. Namely,

(i) During cyclic compression tests positive pore pressure accumulates with continuously decreasing rate until stabilization occurs. In parallel compressive vertical strain accumulates during the tests at an initially increasing rate

(ii) During cyclic isotropic tests positive pore pressure accumulates at an approximately constant rate; stabilization of pore pressure occurs at zero effective octahedral stress following a rapid increase of the accumulation rate. The permanent vertical strain accumulated due to cyclic loading is practically zero

(iii) In cyclic extension tests positive pore pressure builds up at a decreasing rate. In parallel residual extension strains accumulate with an increasing rate per cycle throughout the test.

The model is also successful in predicting the magnitude of the accumulated pore pressure and vertical permanent strain for cyclic isotropic and compression tests. The scatter in the predictions is larger in compression than in isotropic tests.

Permanent pore pressure and vertical strain are underpredicted in cyclic extension tests. Increase of the value of the Bulk modulus or decrease of the value of the volumetric viscosity function significantly improve the fit of the data.

The fact that good quantitative prediction of cyclic behavior in extension tests cannot be made with the same parameters used for compression and isotropic tests implies that the tested Sand A is not isotropic, as the model assumes, but anisotropic.

5.4 CONCLUSION

In chapter 4 a constitutive model has been proposed to describe behavior of sand during cyclic loading. The required parameters are determined from drained cyclic triaxial compression tests under constant static and cyclic stresses. The objective of this chapter has been to examine whether the proposed model can also predict cyclic response under boundary constraints, which partially prevent permanent strain accumulation and lead to change in the static and/or cyclic stresses.

Comparison of the model's predictions were presented with test data from cyclic oedometer tests and from cyclic undrained triaxial

tests in compression, in extension and with isotropic average states of stress (compression and extension stress change). In the cyclic oedometer tests no lateral displacement is allowed while in the cyclic undrained tests no volume change is permitted.

The model is able to predict the basic trends that strain and stress accumulation followed in both the cyclic oedometer tests and the undrained cyclic triaxial tests. It also gave generally good quantitative predictions for permanent strain and pore pressure in undrained cyclic triaxial tests in compression and compression/extension.

The model's quantitative predictions do not agree well with one of the two sets of test data from cyclic oedometer tests, and with the test data from undrained cyclic extension tests. Evidence shows that testing errors may have seriously affected the test results from one of the sets of cyclic oedometer tests. For undrained cyclic extension tests the difference between measured and predicted response is attributed to the anisotropic nature of the sand, which is not taken into account by the model.

After reviewing all comparisons presented in this chapter, one concludes that the proposed model works reasonably well for cyclic loading under various boundary constraints. This feature of the model makes it a valuable tool for analyzing the behavior of foundations under cyclic loading conditions, either drained or undrained.

TEST	SAND	σ_v (ksc)	$\Delta\sigma_v$ (ksc)	κ_o	n %	Dr %
KO1	A	1.019	0.298	0.380	43.2	28.1
KO2	A	2.021	0.282	0.411	42.8	31.9
KO3	A	2.030	0.592	0.400	43.0	30.0
KO6	A	2.031	0.894	0.405	42.9	31.0
KO7	M	2.020	0.595	0.413	43.4	29.6
KO8*	A	2.023	0.600	0.398	42.9	31.0
KO9*	A	2.017	0.596	0.485	43.2	28.1
KO10*	A	2.021	0.601	0.398	42.9	31.0
KO11*	A	2.013	0.594	0.409	42.0	39.4

Monterey Sand: $e_{max} = 0.852$, $e_{min} = 0.564$ (Ref. 60)

A = Sand A

M = Monterey Sand

*Sample Preparation Series

KO8 3 layers, tamped moist, tested wet
 KO9 3 layers, rodded dry, tested wet
 KO10 6 layers, tamped moist, tested wet
 KO11 3 layers, tamped dry, tested dry

TABLE 5.1 : Summary of Cyclic Oedometer Test Conditions - Sand A

TEST LC-	σ_v (ksc)	σ_h (ksc)	$\Delta\sigma_v$ (ksc)	n %	REMARKS
104	2.50	1.50	0.90	41.90	COMPRESSION
129	2.50	1.50	0.50	43.50	COMPRESSION
130	2.50	1.50	0.70	43.20	COMPRESSION
132	3.00	1.50	0.90	41.40	COMPRESSION
135	3.00	2.00	0.90	41.20	COMPRESSION
142	2.50	1.50	0.70	41.71	COMPRESSION
143	2.50	1.50	1.10	43.20	COMPRESSION
152	3.00	1.50	1.20	41.41	COMPRESSION
294	3.03	2.03	0.90	43.60	COMPRESSION
299	3.01	2.01	0.90	42.80	COMPRESSION
61	1.01	1.01	0.60	41.10	ISOTROPIC
63	0.99	0.99	0.60	40.80	ISOTROPIC
73	3.00	3.00	1.20	41.20	ISOTROPIC
78	0.50	0.51	0.20	41.20	ISOTROPIC
123	1.00	1.00	0.80	38.60	ISOTROPIC
138	1.00	1.00	0.40	41.40	ISOTROPIC
139	2.00	2.00	0.80	41.50	ISOTROPIC
144	2.50	2.50	0.90	41.40	ISOTROPIC
231	4.03	4.03	0.90	43.30	ISOTROPIC
241	4.02	4.02	0.90	42.20	ISOTROPIC
273	4.00	4.00	0.90	44.20	ISOTROPIC
71	1.00	1.30	0.40	41.20	EXTENSION
74	1.00	1.50	0.40	41.30	EXTENSION
79	1.00	1.81	0.40	41.20	EXTENSION
136	3.00	4.50	1.20	39.90	EXTENSION
147	3.00	4.50	1.20	40.00	EXTENSION
240	3.50	4.50	0.90	42.10	EXTENSION
250	3.49	4.49	0.86	40.30	EXTENSION

TABLE 5.2 : Summary of Test Conditions for Undrained Cyclic Triaxial Tests - Sand A

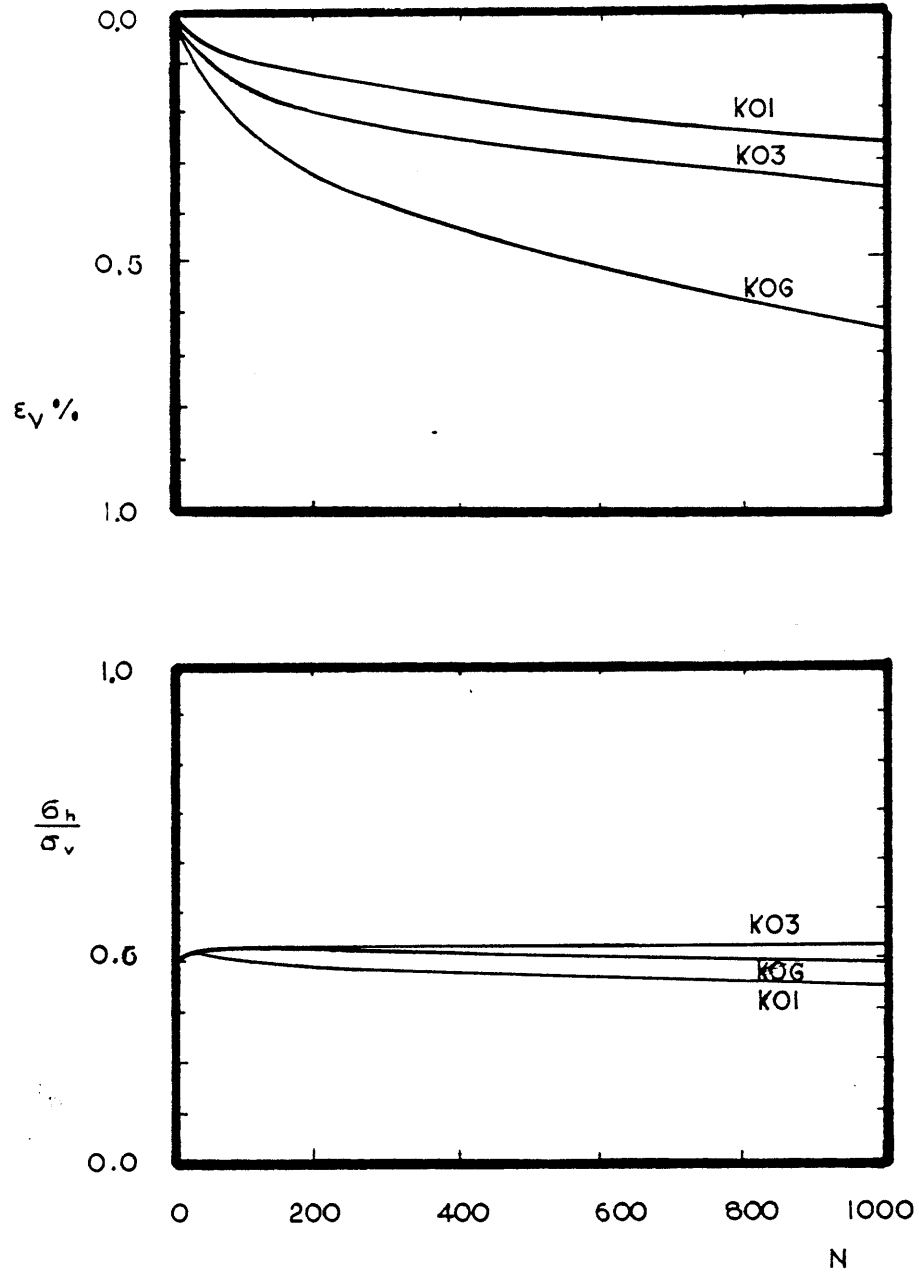


FIGURE 5.1 : Typical Results from Cyclic Oedometer Tests on Sand A (Ref. 60)

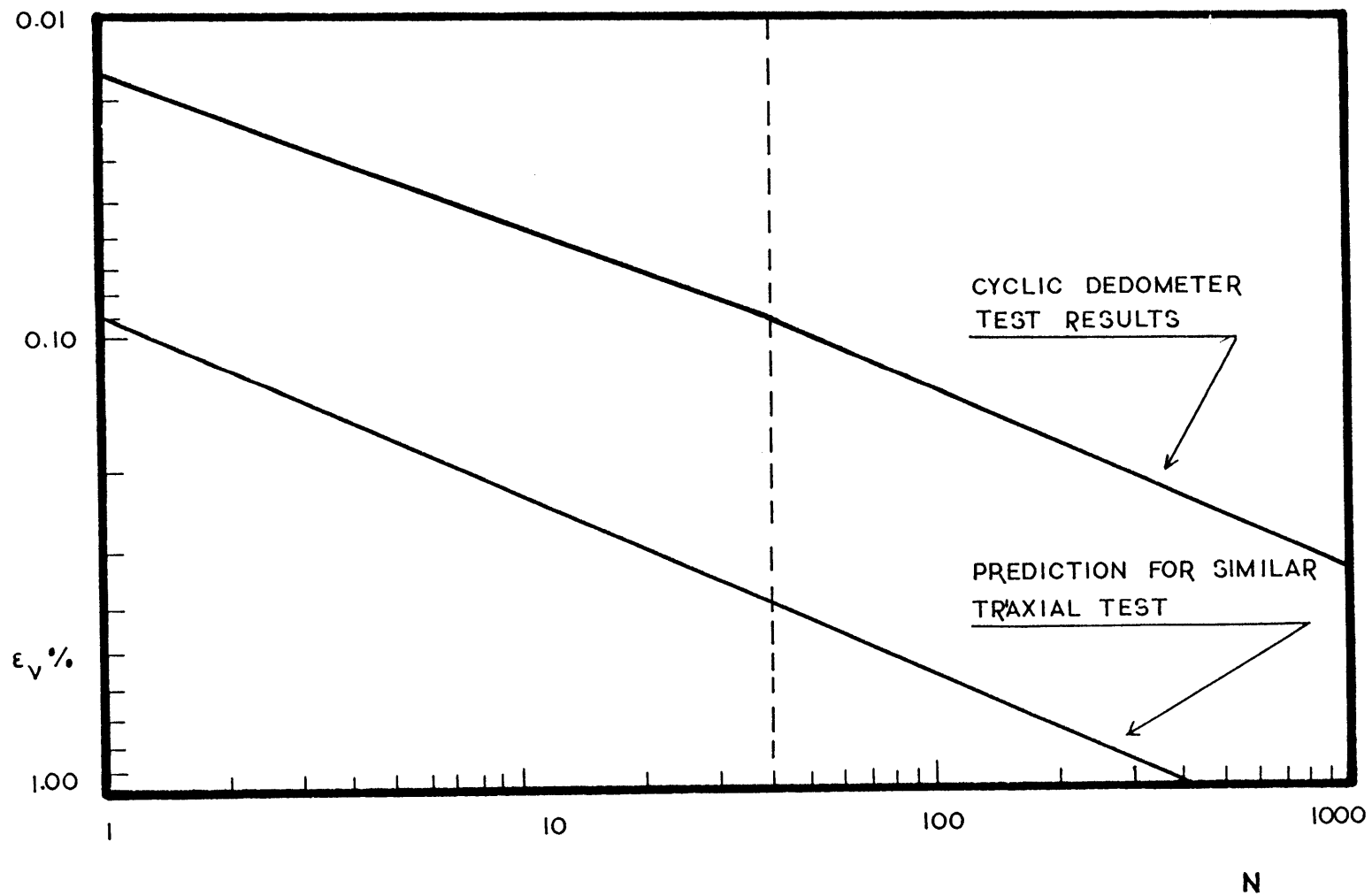
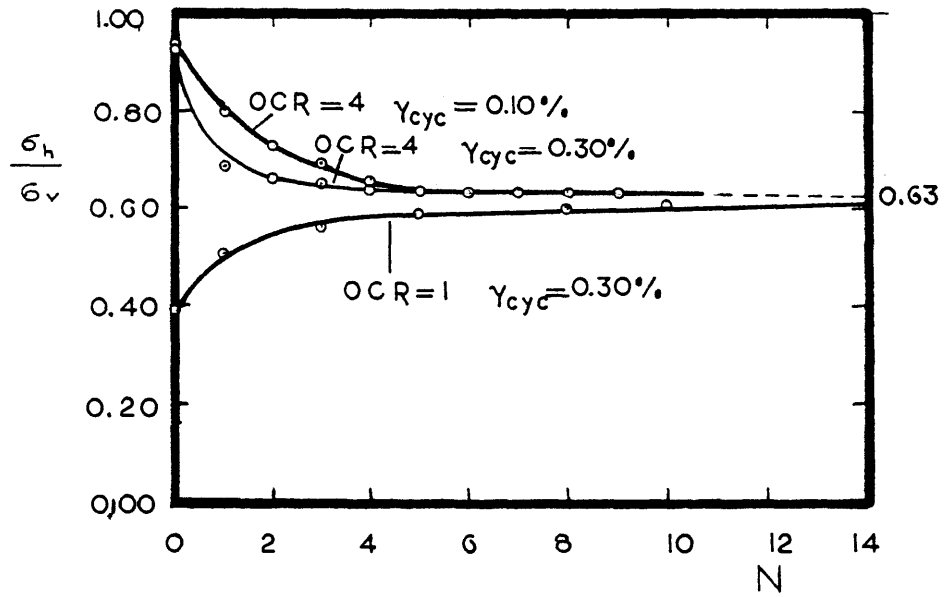


FIGURE 5.2 ; Comparison of Strain Accumulation in Cyclic Oedometer and Drained Triaxial Tests



OTTAWA SAND (C - 109)
 $D_r = 45\%$ $\sigma_{v_0} = 200 \text{ kN/m}^2$

FIGURE 5.3 : Change in Horizontal Stress during Cyclic Oedometer Tests

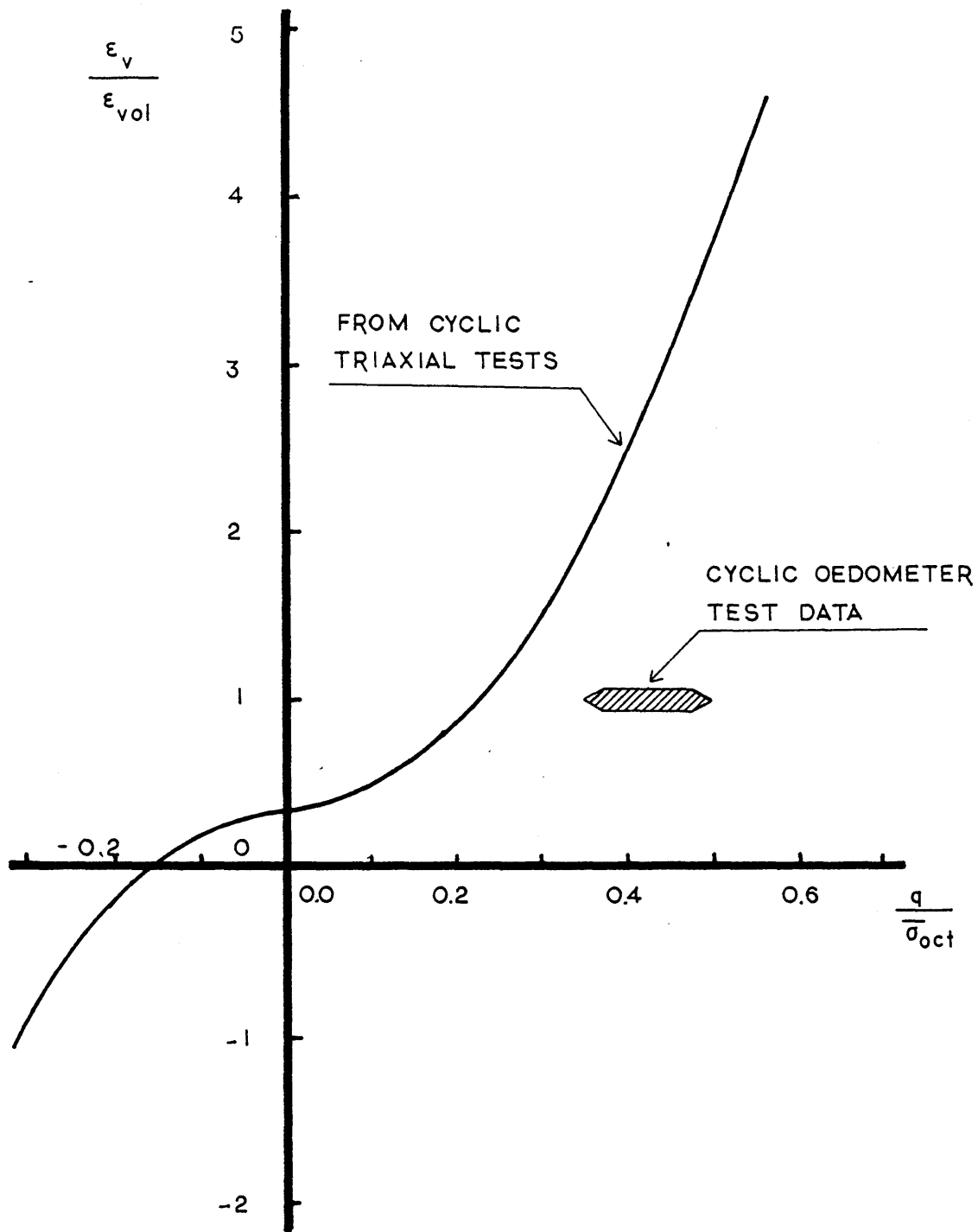


FIGURE 5.4 : Comparison between Cyclic Oedometer and Cyclic Triaxial Test Results

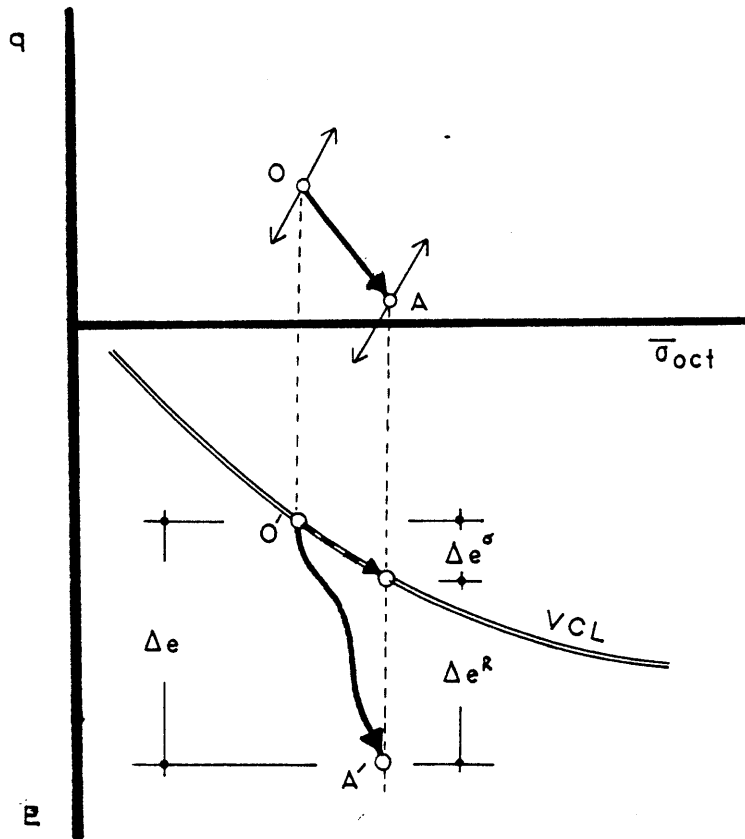


FIGURE 5.5 : Change of Stress and Volume during Cyclic Oedometer Test on Normally Consolidated Sand

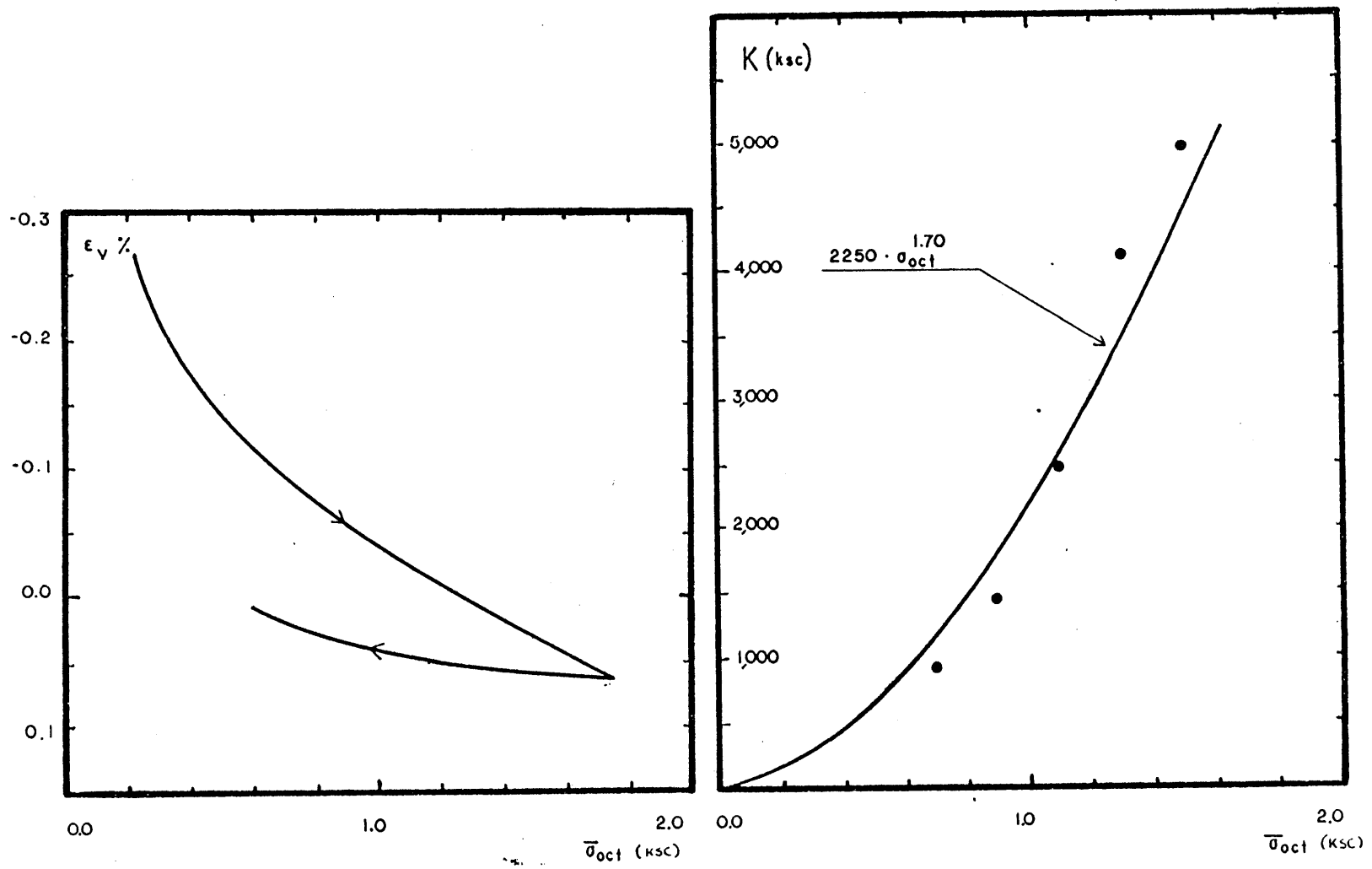
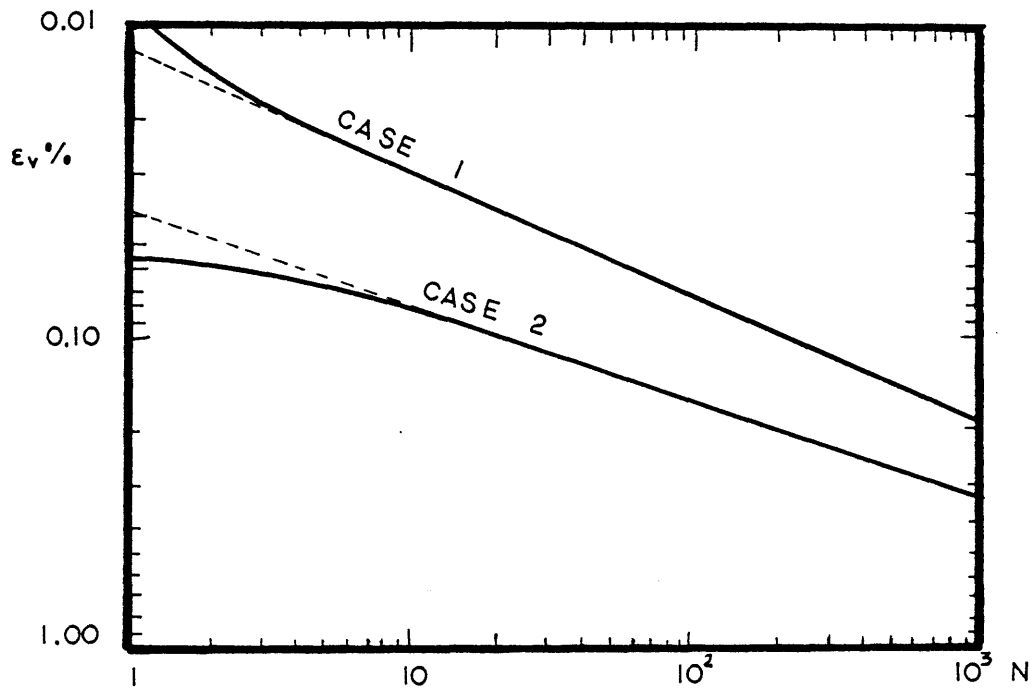
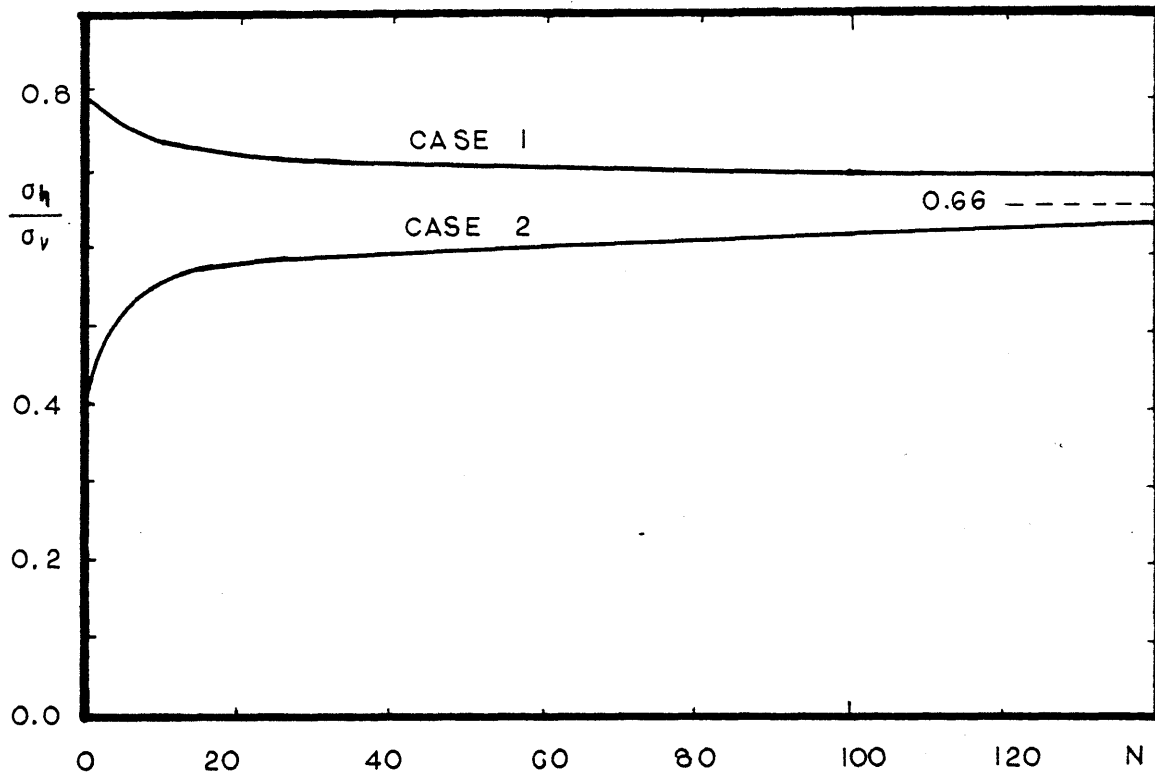


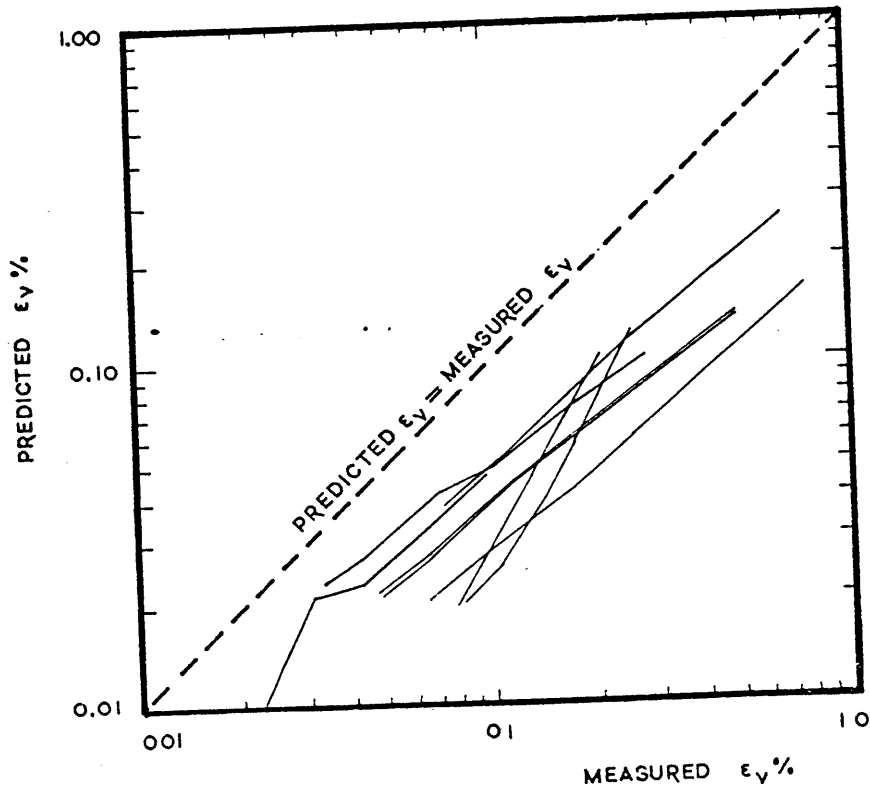
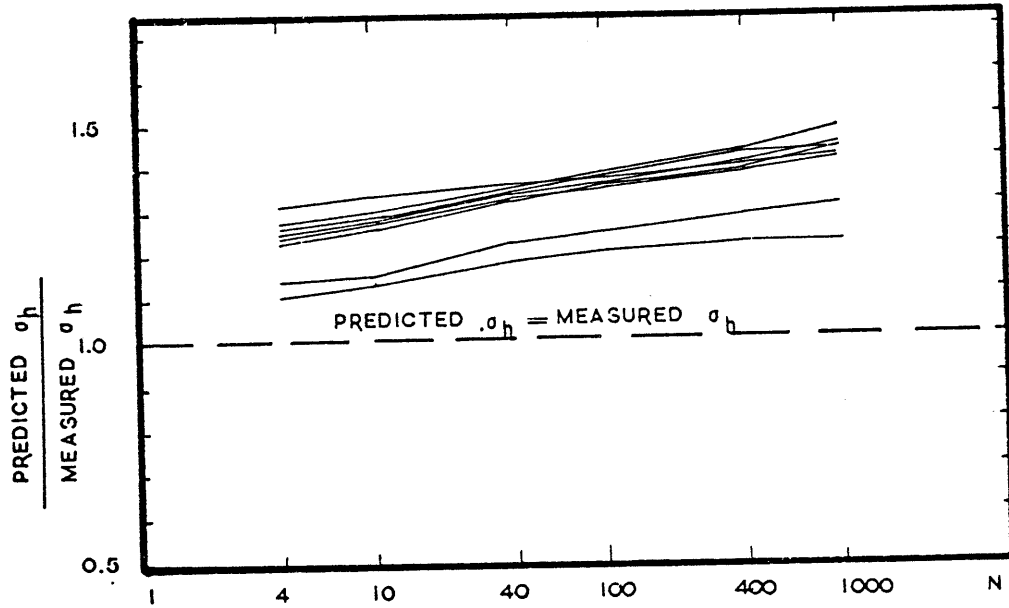
FIGURE 5,6 ; Bulk Modulus for One-Dimensional Unloading (Stress-Strain Data by Ref. 61)



CASE	$\bar{\sigma}_v$ (ksc)	$(\Delta\sigma_v)_{cyc}$ (ksc)	k_o	π %	SOIL
1	2.031	0.894	0.405	42.9	SAND A
2	2.031	0.894	0.800	42.9	SAND A

FIGURE 5.7 : Typical Model Prediction for Cyclic Oedometer Tests

FIGURE 5.8 : Comparison between Predicted and Measured Cyclic Response for Oedometer Tests on Sand A



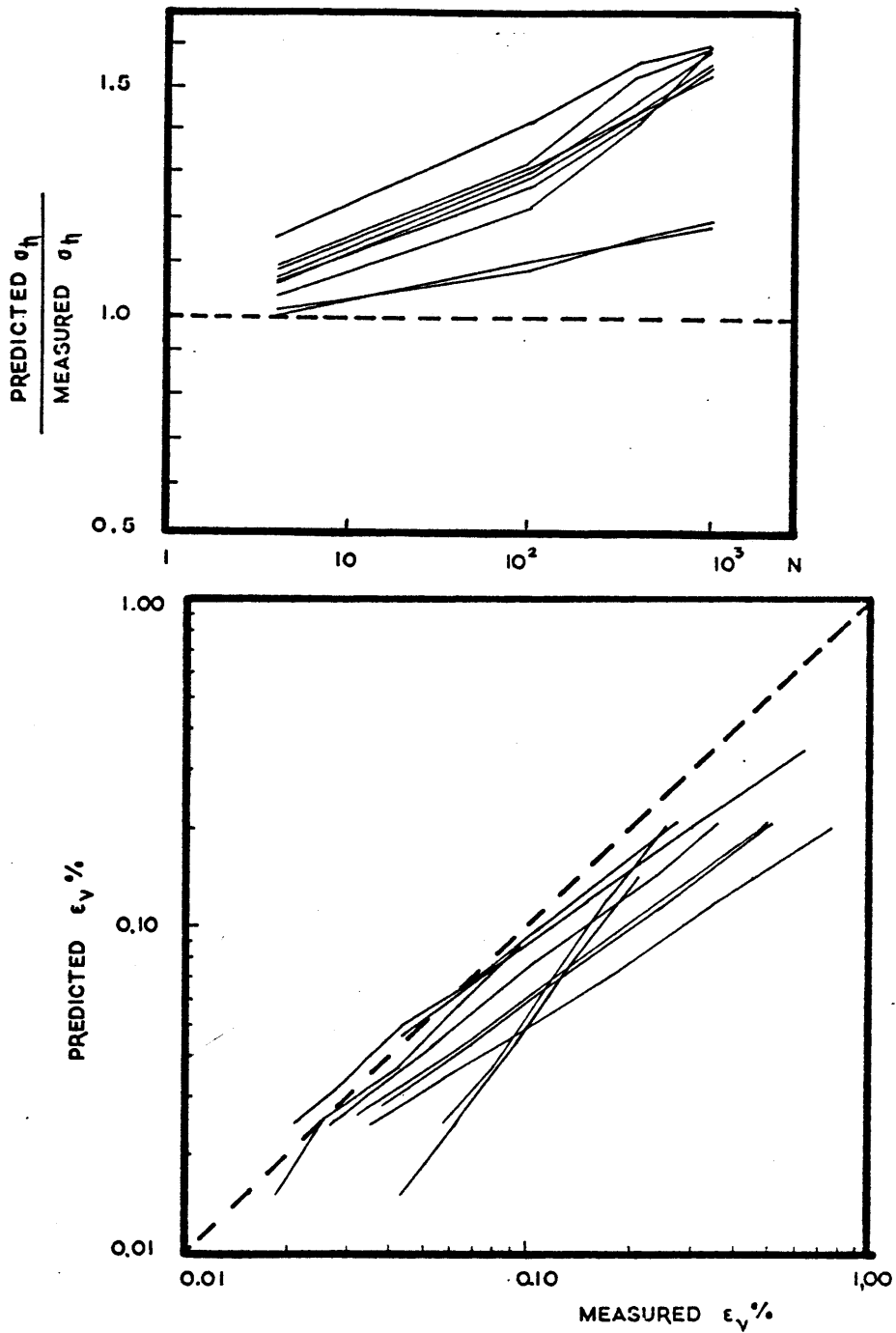


FIGURE 5.9 : Comparison between Measured and Predicted Cyclic Response in Oedometer Tests - REDUCED BULK MODULUS

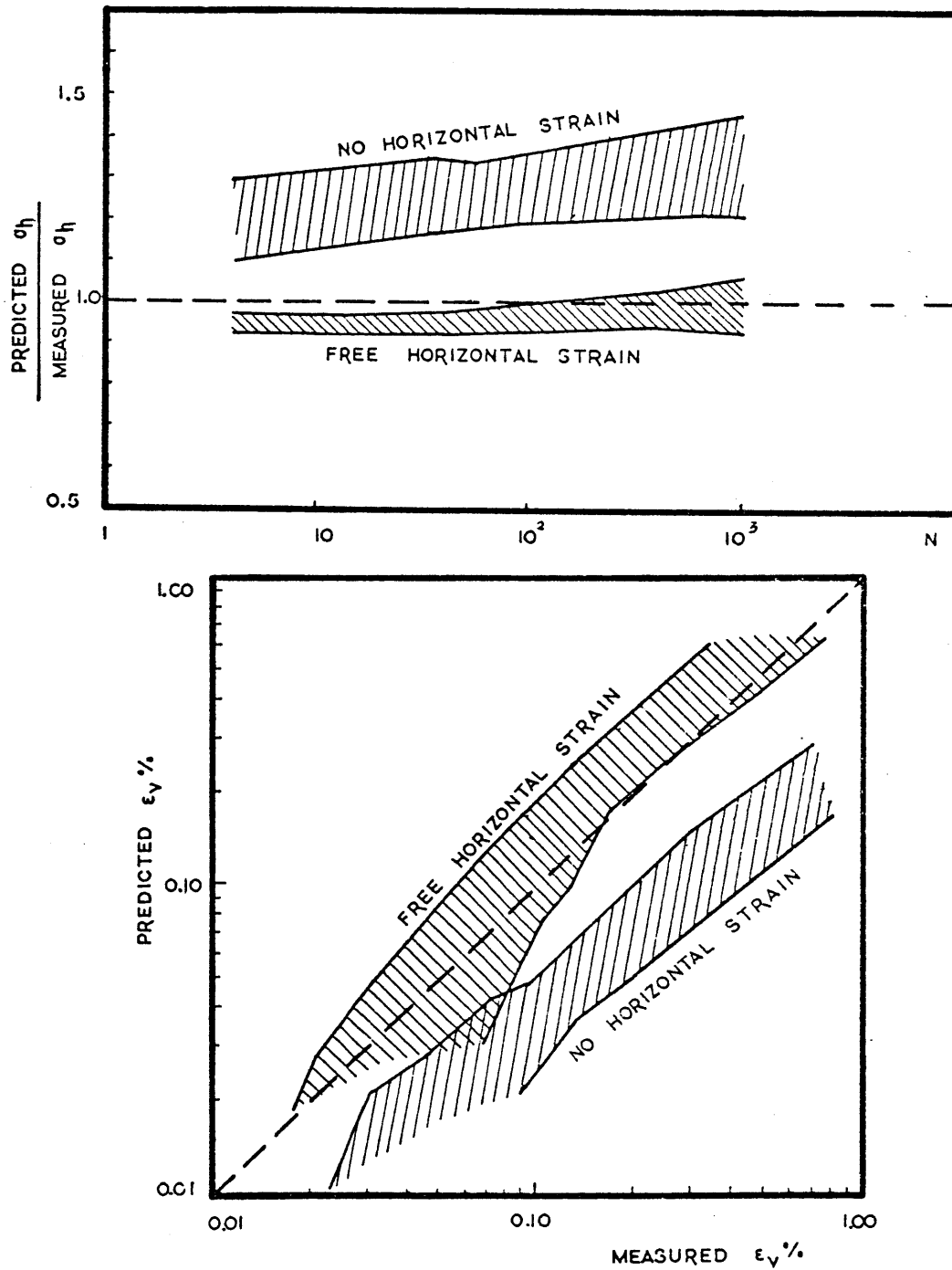


FIGURE 5.10 : Prediction of Cyclic Response in Oedometer Tests under Free Horizontal Strain and under no Horizontal Strain

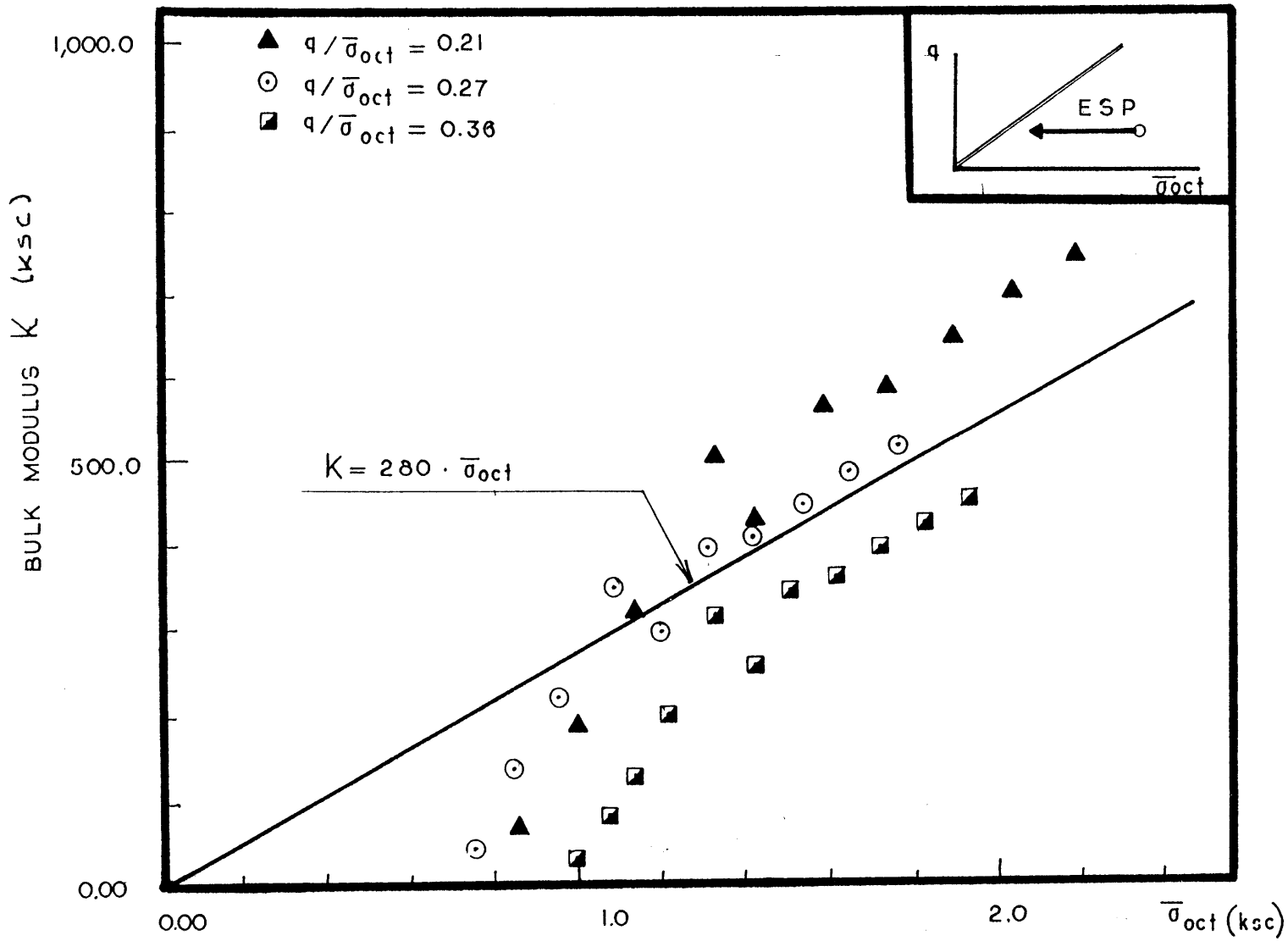
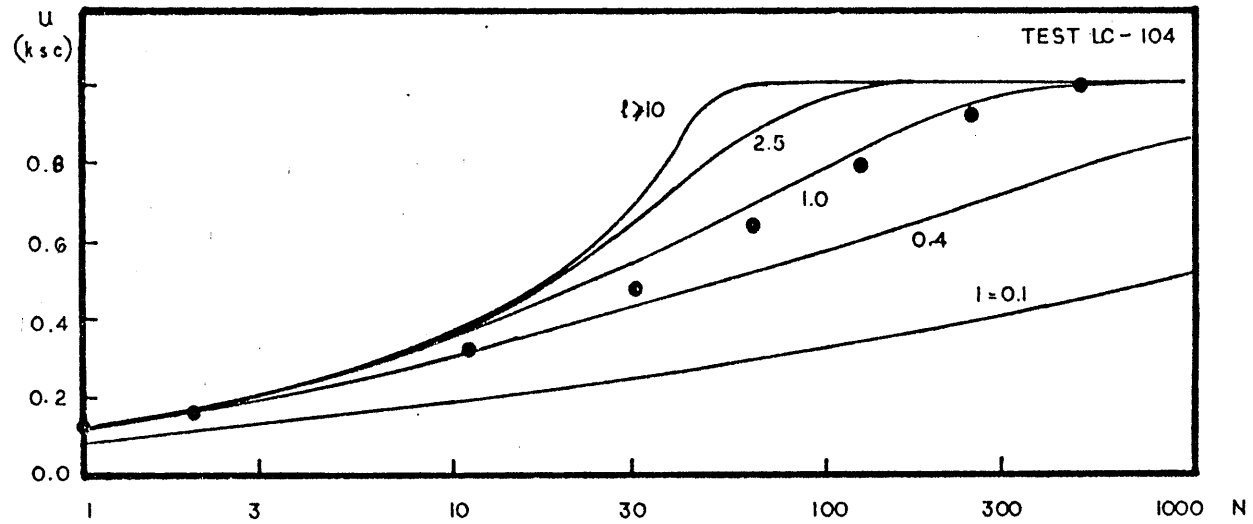
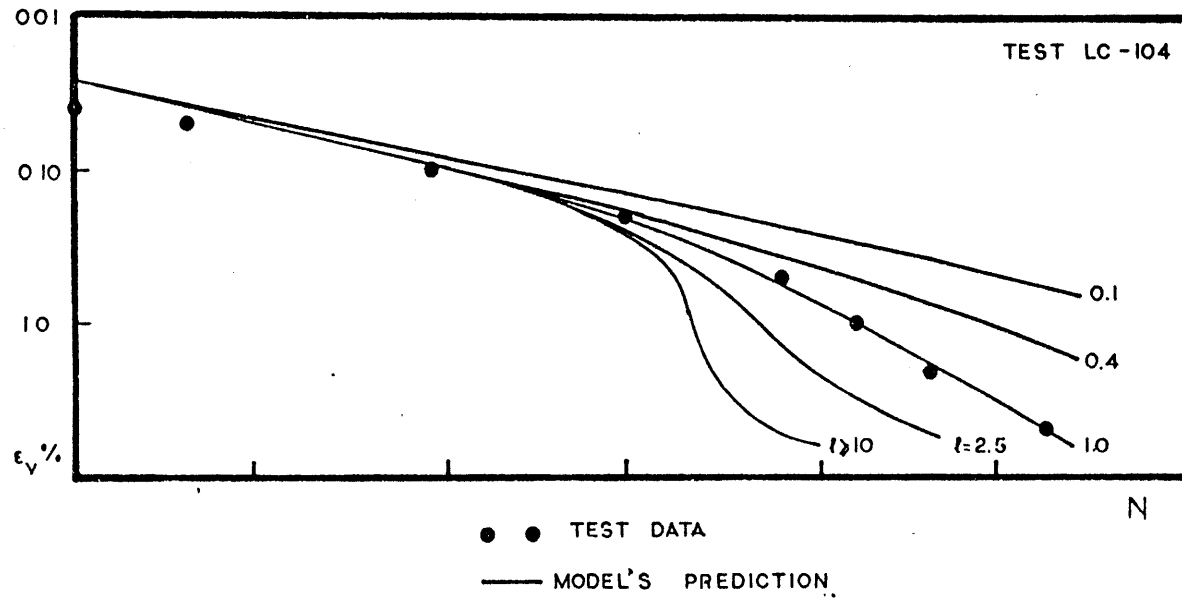


FIGURE 5.11 : Bulk Modulus for Cyclic Undrained Triaxial Tests

FIGURE 5.12 : Estimation of the Parameter " l "



TEST LC - 104

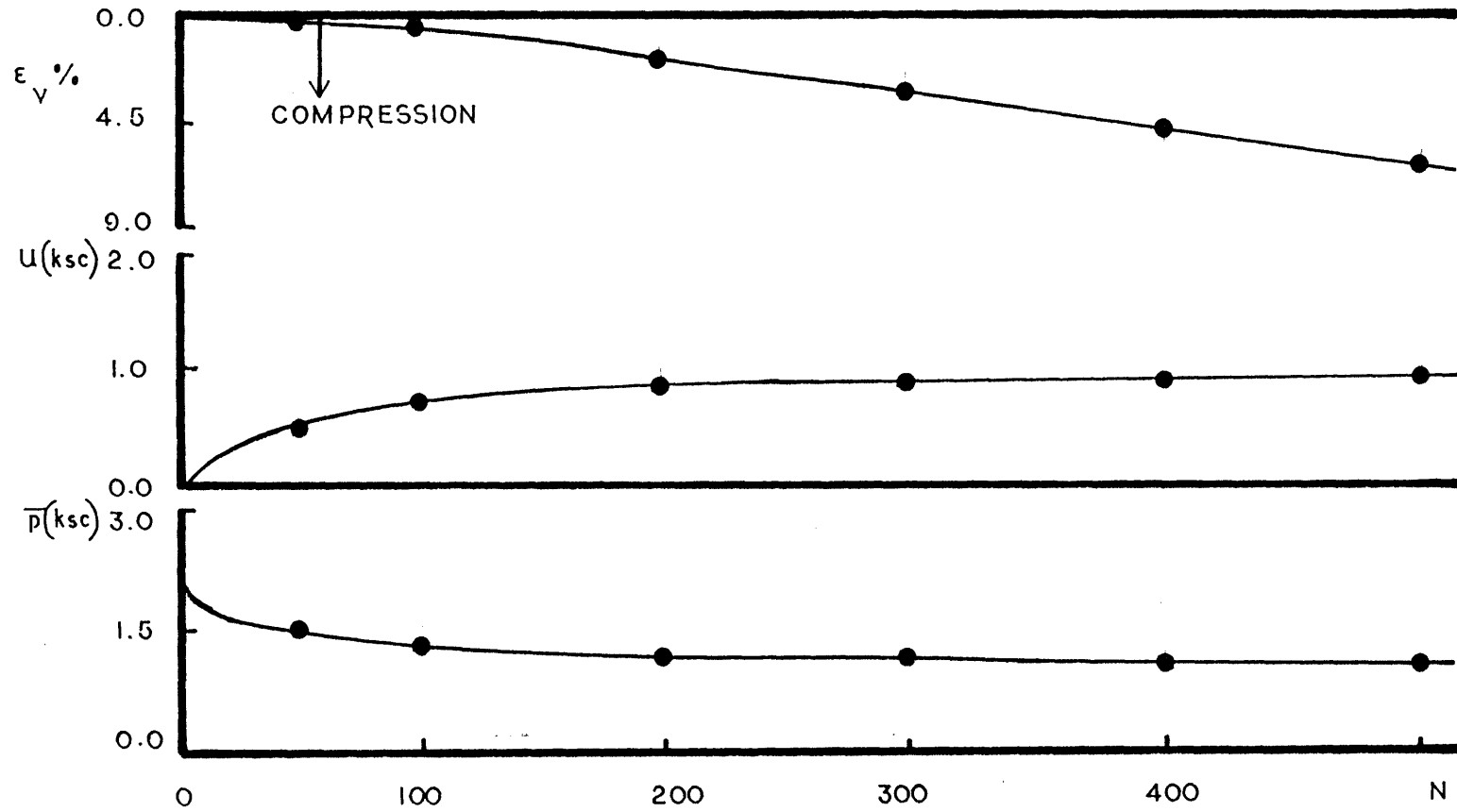


FIGURE 5.13 : Typical Cyclic Response in Undrained Compression Tests

TEST LC - 104

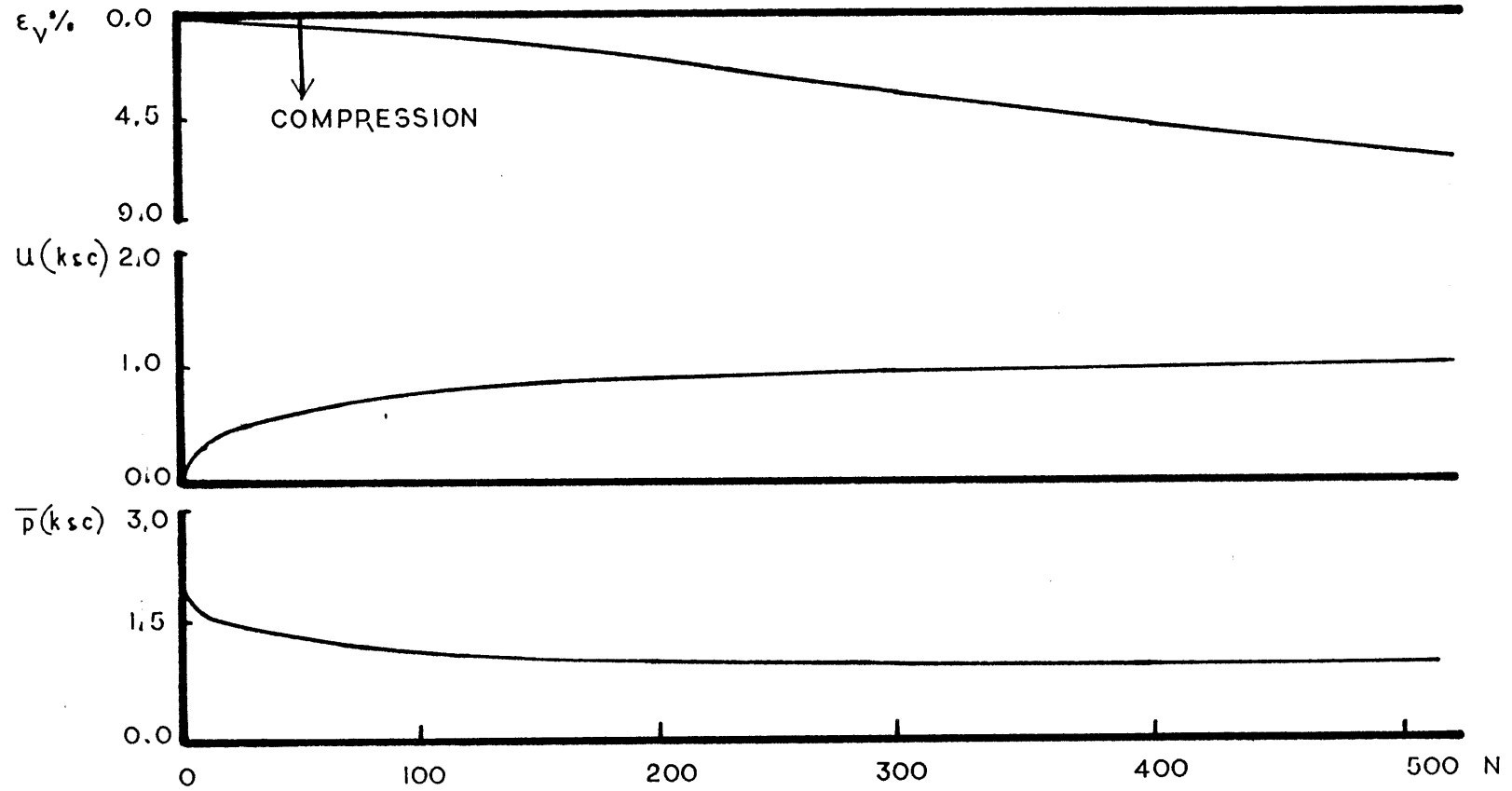


FIGURE 5.14 : Typical Model Prediction for Undrained Cyclic Triaxial Compression Tests

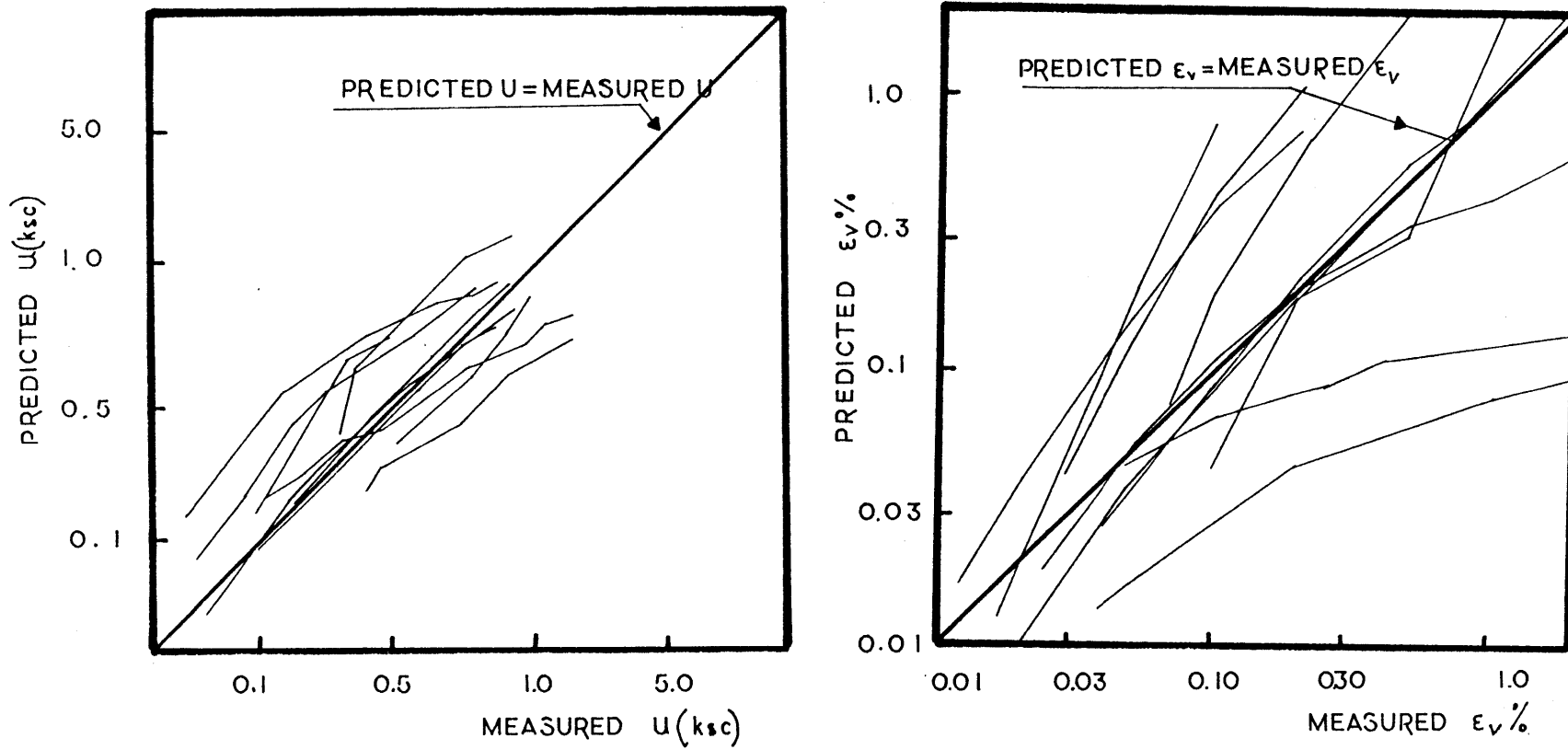


FIGURE 5.15 : Comparison between Predicted and Measured Cyclic Response in Undrained Triaxial Compression Tests

TEST LC - 144

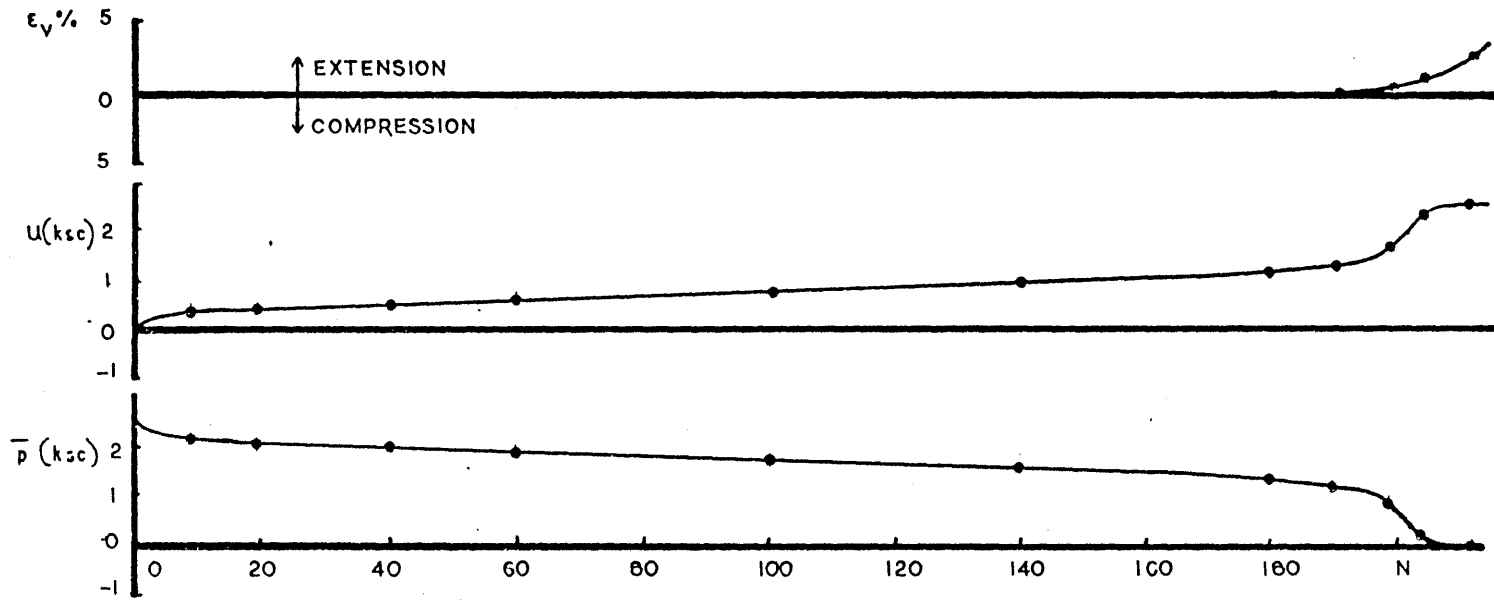


FIGURE 5.16 ; Typical Cyclic Response in Undrained Isotropic Tests

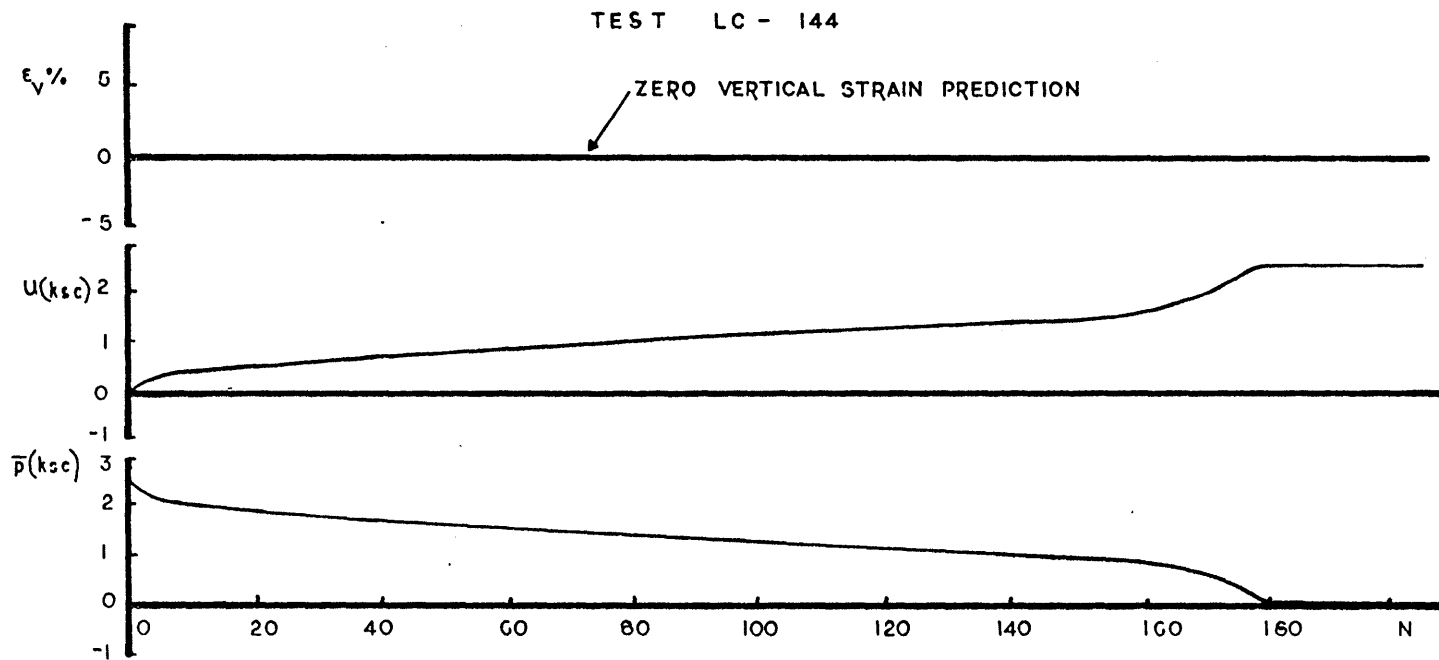


FIGURE 5.17 ; Typical Model Predictions for Undrained Cyclic Triaxial Isotropic Tests

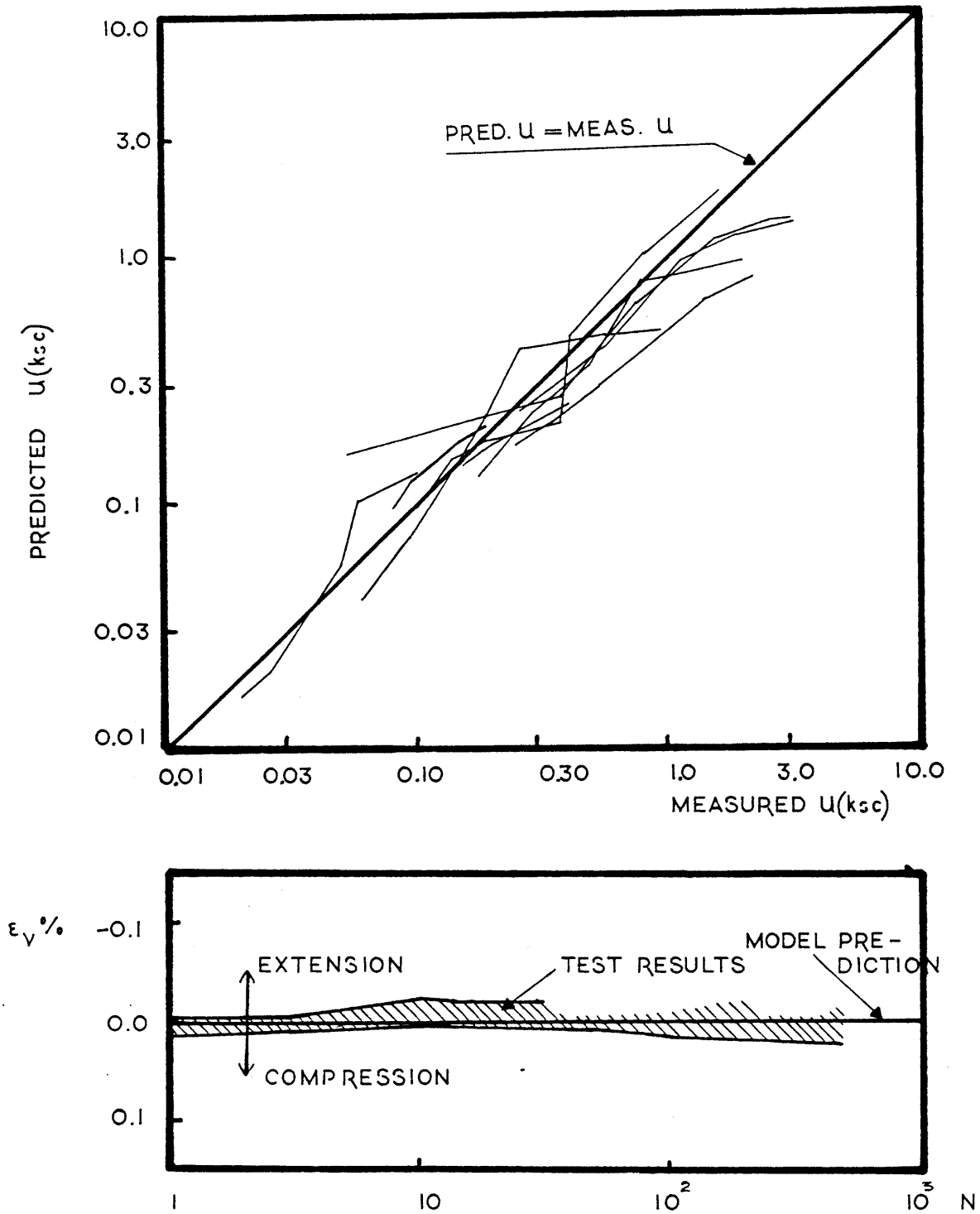


FIGURE 5.18 : Comparison between Predicted and Measured Response in Cyclic Undrained Isotropic Tests

TEST LC-147

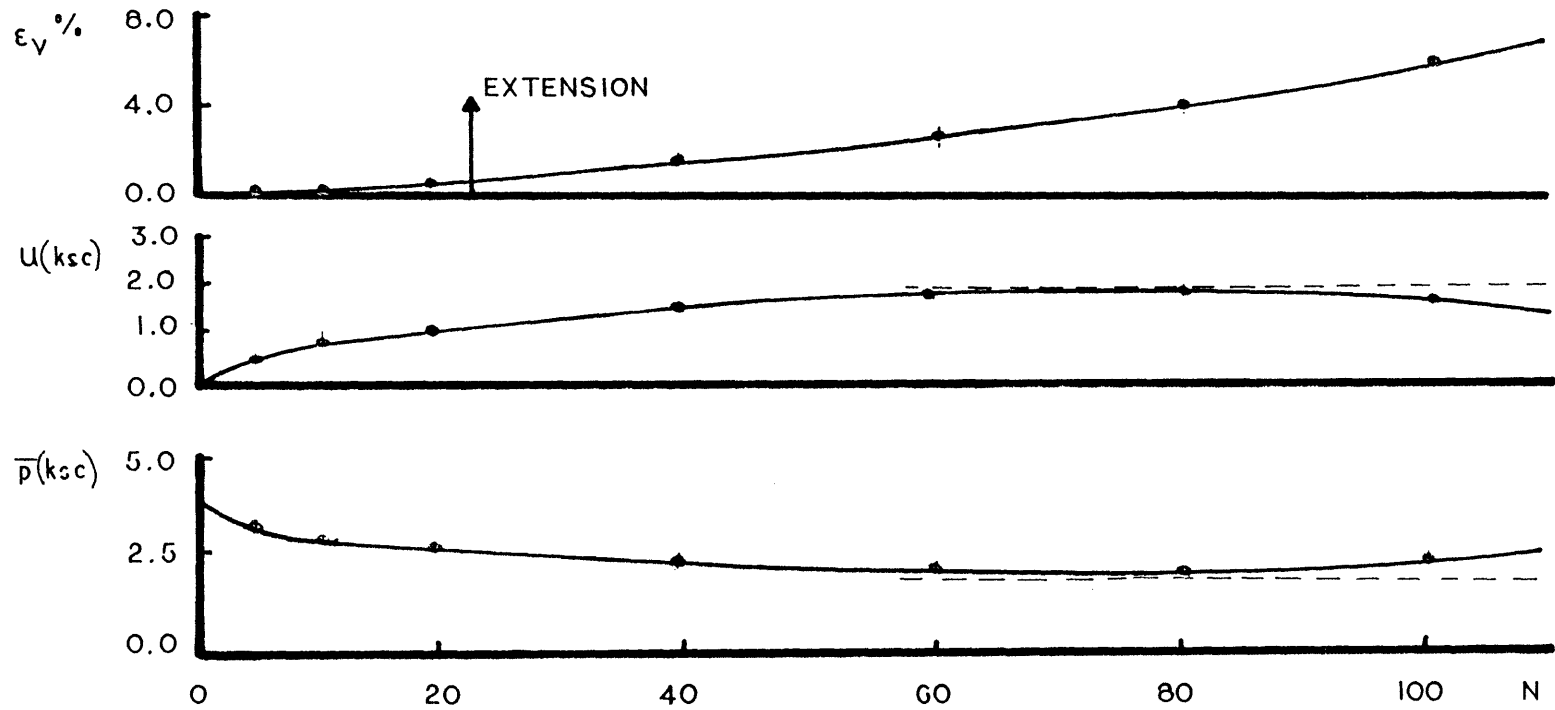


FIGURE 5.19 : Typical Response from Undrained Cyclic Extension Tests

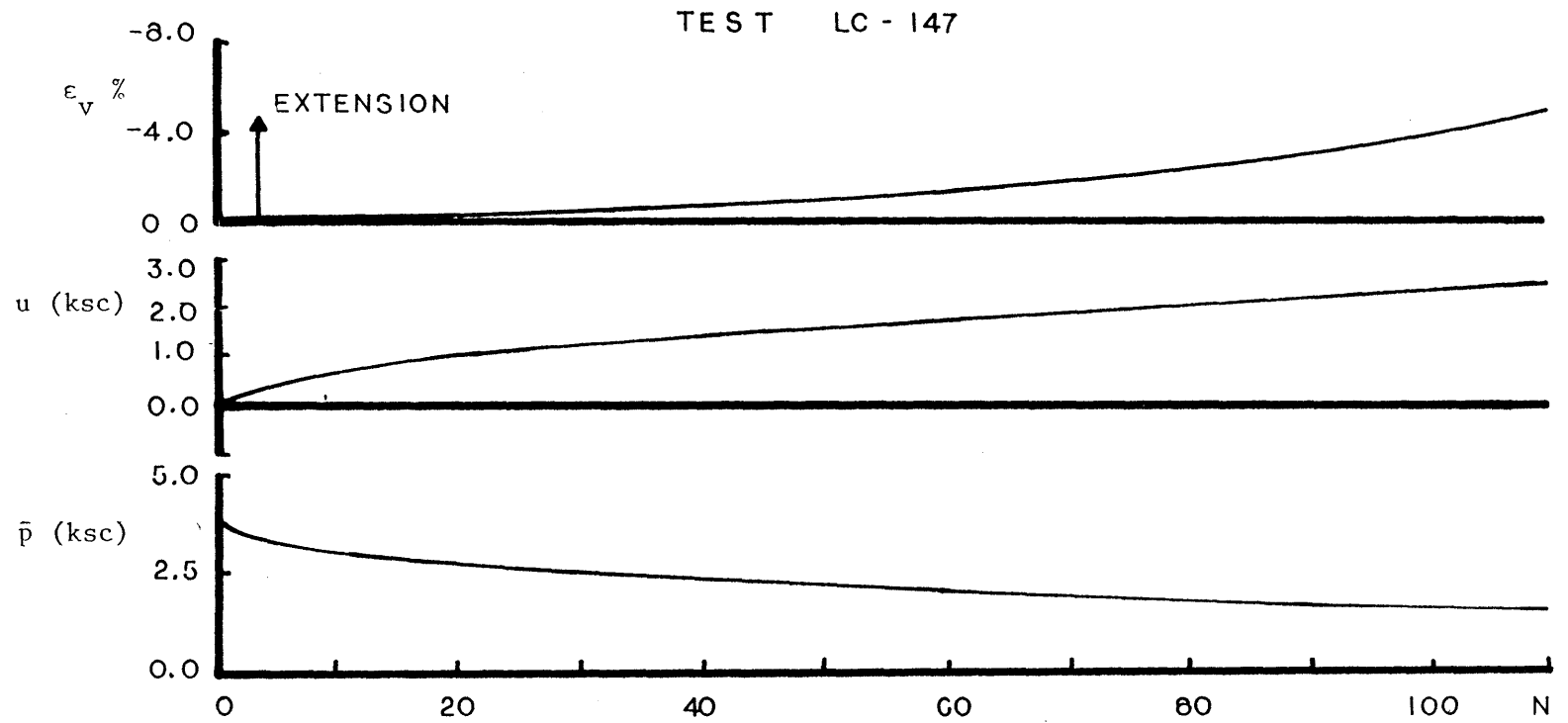


FIGURE 5.20 ; Typical Prediction of Cyclic Response for Undrained Cyclic Extension Tests

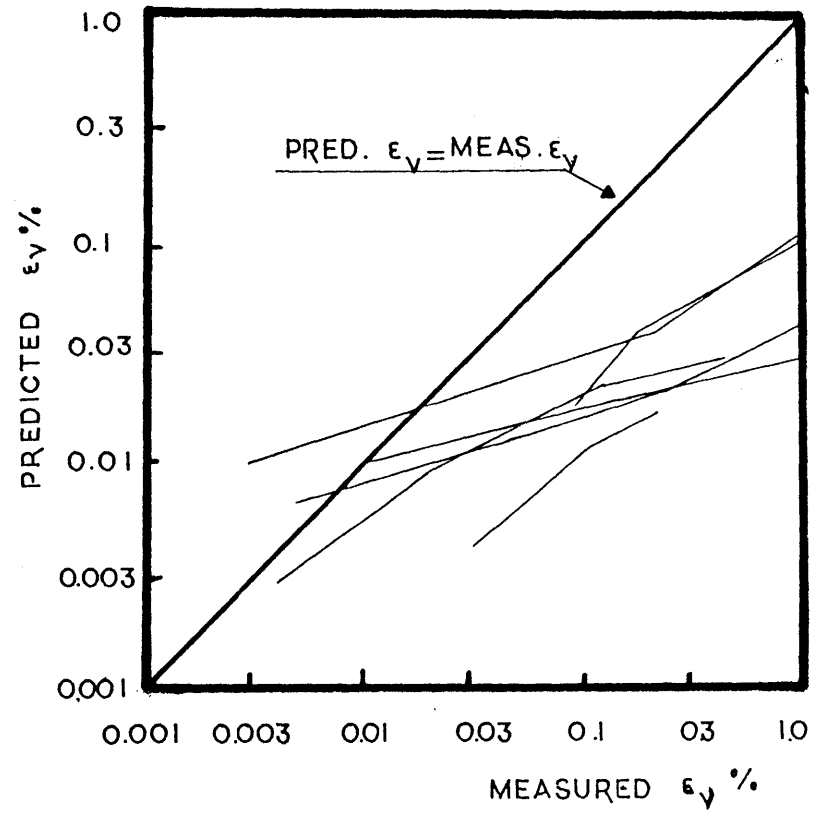
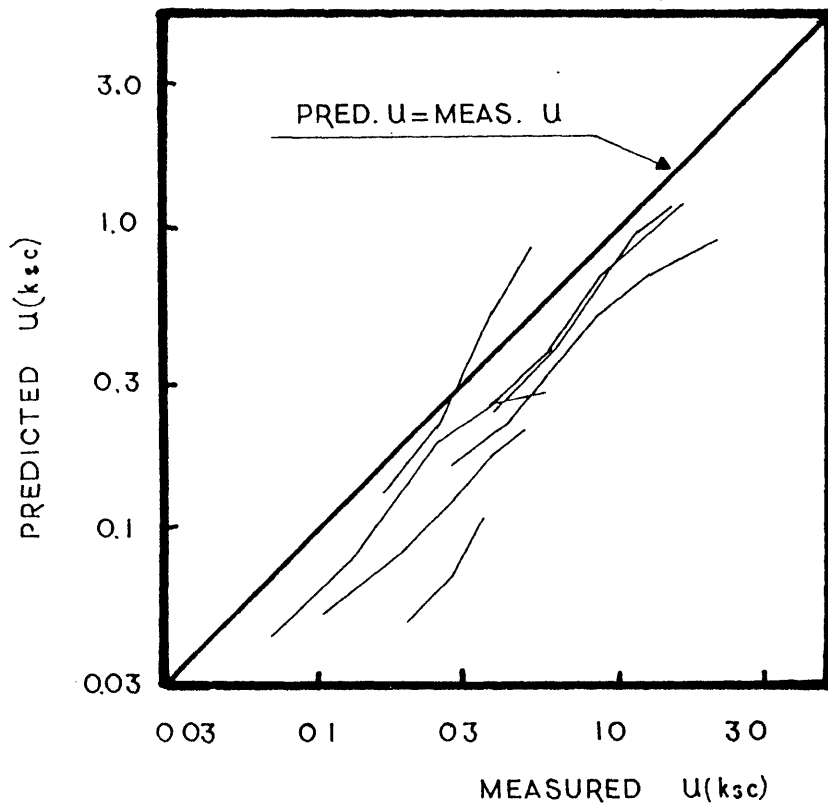


FIGURE 5.21 ; Comparison between Predicted and Measured Response in Undrained Cyclic Extension Tests

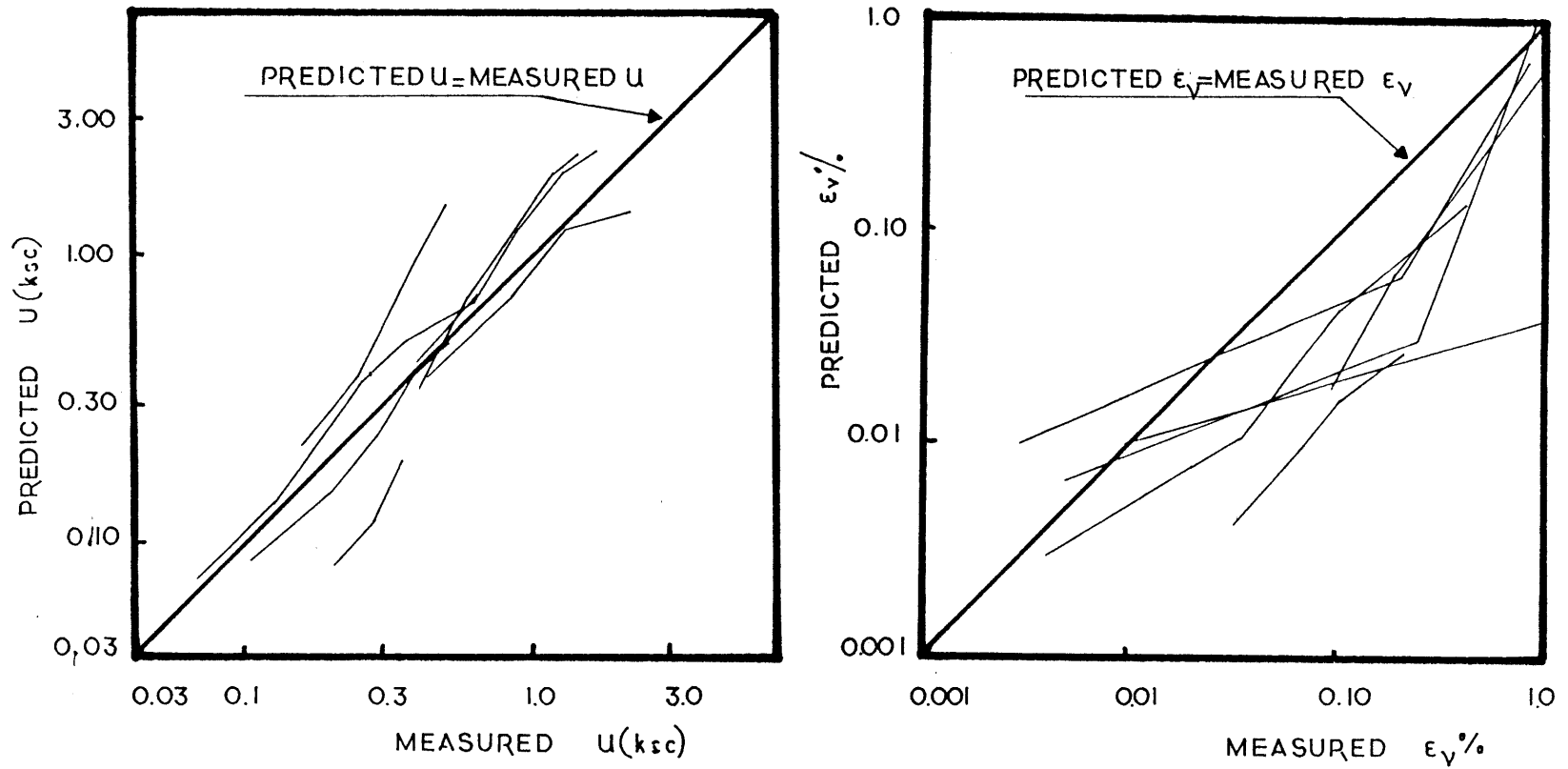


FIGURE 5.22 : Comparison between Predicted and Measured Cyclic Response in Undrained Extension Tests - INCREASED BULK MODULUS

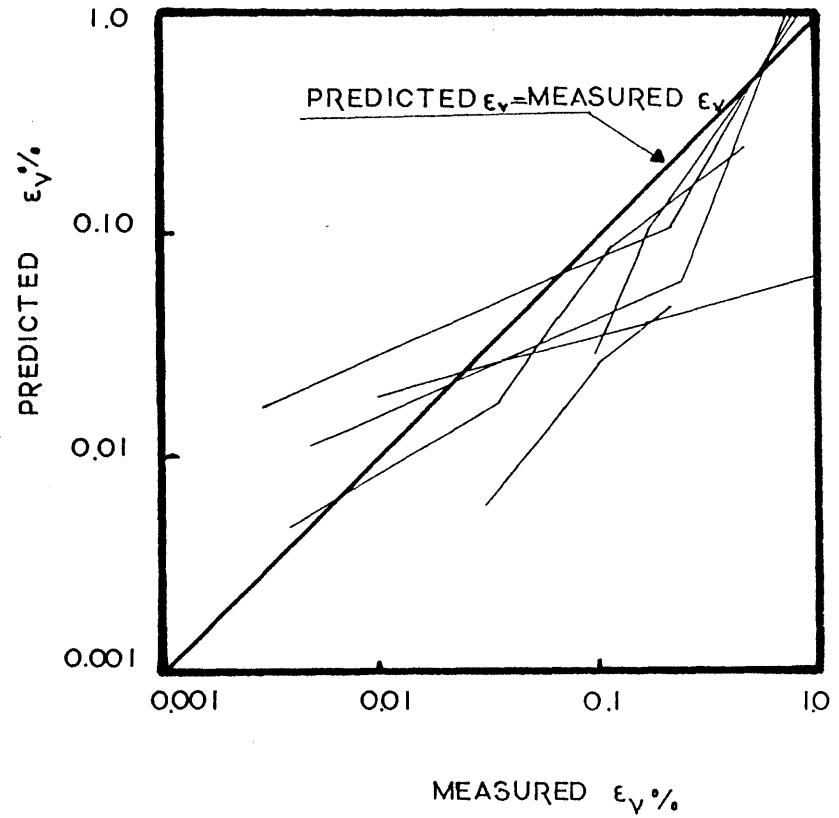
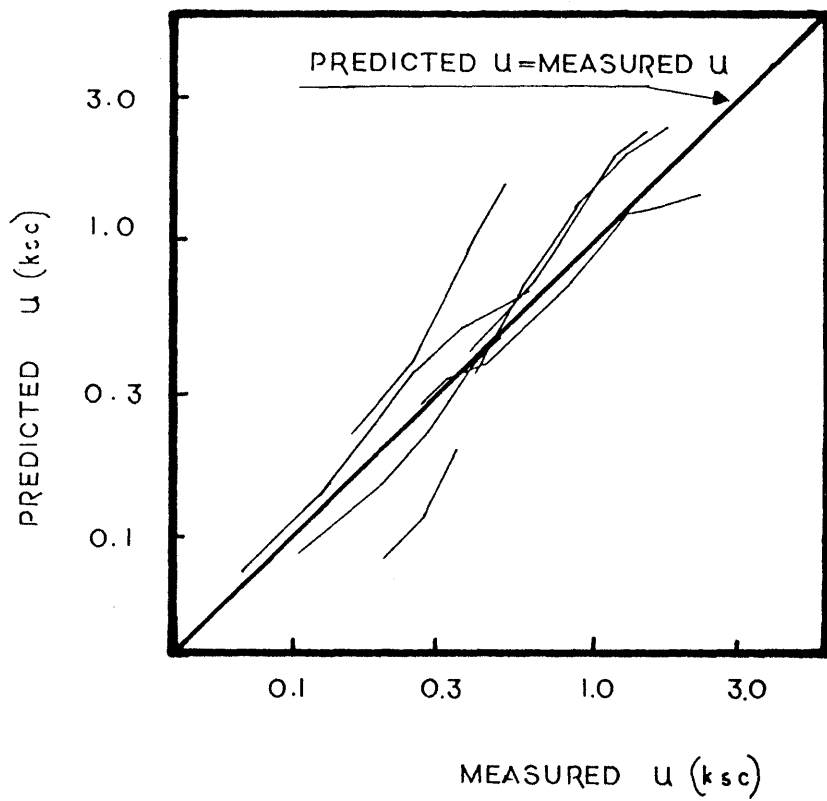


FIGURE 5.23 : Comparison between Predicted and Measured Cyclic Response in Undrained Extension Tests - DECREASED VISCOSITY FUNCTION

CHAPTER 6FINITE ELEMENT MODELING OF CYCLIC LOADING OF FOUNDATIONS6.1 INTRODUCTION

Previous chapters describe a constitutive model of the stress-strain accumulation in Sand A due to cyclic loading. This chapter presents the application of the constitutive model to the prediction of foundation performance due to repeated loading, through the finite element method.

To solve a boundary value problem in continuum Mechanics, the following field equations need to be satisfied:

- equilibrium equations
- stress-strain relationship
- strain-displacement relations satisfied on the surface of the body.

Closed form solutions under those requirements are possible for very simple problems only; for most problems the solution is achieved by using different numerical techniques. The most popular among them is the discretization of the continuum into a number of finite elements ([64], [65]).

The field equations for cyclic loading of foundations and their solution by the finite element method are described in sections 6.1 and 6.2 respectively. The computer implementation of the solution is described in section 6.3 and its accuracy is evaluated in section 6.4.

6.2 PRINCIPLE OF VIRTUAL WORK

6.2.1 DEFINITION

External forces that may act on a three-dimensional body include the surface tractions f , body forces f and concentrated forces F . These forces have three components corresponding to the three coordinate axes x , y and z :

$$\underset{\sim}{f}^S = \begin{Bmatrix} f_x^S \\ f_y^S \\ f_z^S \end{Bmatrix} ; \quad \underset{\sim}{f}^B = \begin{Bmatrix} f_x^B \\ f_y^B \\ f_z^B \end{Bmatrix} ; \quad \underset{\sim}{F}^i = \begin{Bmatrix} F_x^i \\ F_y^i \\ F_z^i \end{Bmatrix}$$

The displacements are:

$$\underset{\sim}{U}^T = \{U_x, U_y, U_z\}$$

the strains corresponding to $\underset{\sim}{U}$ are:

$$\underset{\sim}{\varepsilon}^T = \{\varepsilon_{xx}, \varepsilon_{yy}, \varepsilon_{zz}, \varepsilon_{xy}, \varepsilon_{yz}, \varepsilon_{zx}\}$$

and the stresses corresponding to $\underset{\sim}{\varepsilon}$ are:

$$\underset{\sim}{\sigma}^T = \{\sigma_{xx}, \sigma_{yy}, \sigma_{zz}, \sigma_{xy}, \sigma_{yz}, \sigma_{zx}\}$$

The principle of Virtual Work states that the equilibrium of the body requires that for any compatible, small virtual displacement imposed into the body, the total internal virtual work is equal to the

total external virtual work (Bathe and Wilson [63]).

$$\int_V \delta \underline{\varepsilon}^T \underline{\sigma} dV = \int_V \delta \underline{U}^T \underline{f}^B dV + \int_S \delta \underline{U}^T \underline{f}^S dS + \sum_i \delta U^i \underline{F}^i \quad (6.1)$$

The internal virtual work is given on the left side of equation 6.1 and is equal to the actual stress times the virtual strains ($\delta \underline{\varepsilon}$) that correspond to the imposed virtual displacements; the external work is given on the right side of the equation and is equal to the actual forces times the virtual displacements ($\delta \underline{U}$). Equation 6.1 is the cornerstone for the calculation of the displacements (\underline{U}) via the finite element method.

6.2.2 VOLUME INCOMPRESSIBILITY

Applying the finite element method to equation 6.1 directly, is appropriate only when compressible materials are considered. For nearly incompressible materials, as is soil under undrained condition, the Poisson's ratio, ν , approaches one-half, and certain terms in the total stress-strain relationship tend to infinity. This results in loss in accuracy of the finite element method.

The first step to overcome this difficulty is to replace the total stress ($\underline{\sigma}$) in equation 6.1 by the sum of the effective stress ($\underline{\bar{\sigma}}$) and the pore pressure (u):

$$\int_V \delta \underline{\varepsilon}^T \underline{\sigma} dV + \int_V \delta \underline{\varepsilon}^T u dV = \int_V \delta \underline{U}^T \underline{f}^B dV + \int_S \delta \underline{U}^T \underline{f}^S dS + \sum_i \delta U^i \underline{F}^i \quad (6.2)$$

The pore pressure vector is defined as

$$\underline{u} = \{u, u, u, 0, 0, 0\} = u \underline{I}^T$$

where

$$\underline{I}^T = \{1, 1, 1, 0, 0, 0\}$$

so that it will be compatible with the stress and strain definition.

In equation 6.1 the unknown quantities are the displacements (U) since total stress is function of displacement. Equation 6.2, however, includes additional unknowns which are the pore pressures (u). Condensation of the additional unknowns is achieved using the incompressibility condition:

$$\varepsilon_{vol} = \underline{I}^T \underline{\varepsilon} = 0. \quad (6.3)$$

To avoid numerical instabilities during the solution of the system of equations 6.2 and 6.3 it is often assumed that a very small change in volume occurs, equal to a change in volume of the pore fluid (Penalty Method):

$$\varepsilon_{vol} = \underline{I}^T \underline{\varepsilon} = \frac{u}{K_p} \quad (6.4)$$

The inverse of K_p will be called hereafter the "Penalty Constant"; K_p must be chosen much larger than the drained Bulk Modulus of the soil but is otherwise arbitrary.

It is worth noting that there is no physical meaning of the "Penalty Method" and that the constant K_p is not equal to the Bulk Modulus of water. It will be shown in later paragraphs that, with the appropriate solution technique and finite element discretization direct solution of equations 6.2 and 6.3 can be achieved for an infinite value of K_p .

6.3 FINITE ELEMENT IMPLEMENTATION

The finite element method approximates a continuous body as an assemblage of discrete finite elements, interconnected at nodal points. The unknown quantities, displacements and pore pressures in the present case, vary within each element according to a predefined function of the spatial coordinates. Usually polynomial expansions are assumed with coefficients determined from the values of the unknown quantities at the nodes of the element. It is evident that the order of the expansions of the unknowns and the number of nodal points per element are directly related.

In choosing the appropriate order polynomials for displacements and pore pressures, the following considerations were made:

Stresses are proportional to the first derivatives of displacements and consequently their polynomial expansion is always one order lower than the displacement expansion. Stresses and pore pressures are additive quantities and it is desirable to be estimated with the same order of accuracy. Consequently the expansion of pore pressures must be also one order lower than that of displacements.

Linear expansion will be assumed for the pore pressures and quadratic for the displacements; this requires specification of pore pressures in four nodes per element and specification of displacement in eight nodes [63], [64], [65]. For element "m":

$$\tilde{U}^m = \tilde{N}^m(x, y, z) \tilde{q}^m$$

$$\underline{\underline{u}}^m = \underline{\underline{N}}^{*m}(x, y, z) \underline{\underline{p}}^m$$

$\underline{\underline{q}}^m$: nodal displacement vector for element (m)

$\underline{\underline{p}}^m$: nodal pore pressure vector for element (m)

The strain can be expressed as the first derivative of displacement:

$$\underline{\underline{\varepsilon}}^m = \underline{\underline{D}} \underline{\underline{N}}^m(x, y, z) \underline{\underline{q}}^m = \underline{\underline{B}}^m(x, y, z) \underline{\underline{q}}^m$$

Equation (6.2) can now be rewritten as

$$\delta \underline{\underline{q}}^T \sum_m \left(\int_V \underline{\underline{B}}^m T \underline{\underline{\sigma}} dV + \int_V \underline{\underline{B}}^m T \underline{\underline{N}}^{*m} \underline{\underline{p}}^m dV \right) = \delta \underline{\underline{q}}^T \sum_m \left(\int_V \underline{\underline{N}}^m T \underline{\underline{f}}^B dV + \int_V \underline{\underline{N}}^m T \underline{\underline{f}}^S dV + \sum_i \underline{\underline{N}}^i F_i \right) \quad (6.8)$$

For cyclic loading the total strain ($\underline{\underline{\varepsilon}}$) is the sum of three components

$$\underline{\underline{\varepsilon}} = \underline{\underline{\varepsilon}}^{\Delta \bar{\sigma}} + \underline{\underline{\varepsilon}}^R + \underline{\underline{\varepsilon}}^0$$

where

$\underline{\underline{\varepsilon}}^{\Delta \bar{\sigma}}$: strain due to change in average effective stress

$\underline{\underline{\varepsilon}}^R$: cumulative strain due to cyclic loading

$\underline{\underline{\varepsilon}}^0$: initial strain

The effective stress is related to the total strain as

$$\underline{\underline{\bar{\sigma}}} = \underline{\underline{C}} \underline{\underline{\varepsilon}}^{\Delta \bar{\sigma}} = \underline{\underline{C}} (\underline{\underline{\varepsilon}} - \underline{\underline{\varepsilon}}^R - \underline{\underline{\varepsilon}}^0) \quad (6.9)$$

The matrices $\underline{\underline{C}}$ and $\underline{\underline{\varepsilon}}^R$ are completely defined by the constitutive model described in chapter 4. Combining equations 6.7, 6.8 and 6.9 finally gives:

$$\underline{\underline{K}} \underline{\underline{q}} + \underline{\underline{H}}^T \underline{\underline{p}} = \underline{\underline{R}} \quad (6.10)$$

where

$$\underline{\underline{K}} = \sum_m \int_{V_m} \underline{\underline{B}}^m \underline{\underline{C}} \underline{\underline{B}}^m dV \quad (6.11)$$

$$\underline{\underline{H}} = \sum_m \int_{V_m} \underline{\underline{B}}^m \underline{\underline{I}} \underline{\underline{N}}^* dV \quad (6.12)$$

$$\underline{\underline{R}} = \sum_m \left(\int_{V_m} \underline{\underline{N}}^m \underline{\underline{f}}^B dV + \int_{S_m} \underline{\underline{N}}^m \underline{\underline{f}}^S dV + \int_{V_m} \underline{\underline{B}}^m \underline{\underline{C}} (\underline{\underline{\epsilon}}^R + \underline{\underline{\epsilon}}^O) dV \right) \quad (6.13)$$

Substitution of equation 6.6 and 6.7 into the volume incompressibility equation 6.4 yields

$$\underline{\underline{I}}^T \underline{\underline{B}} \underline{\underline{q}} - \frac{1}{K_p} \underline{\underline{N}}^* \underline{\underline{p}} = 0 \quad (6.14)$$

multiplication by $\underline{\underline{N}}$ and integration over the volume of the continuum finally gives:

$$\underline{\underline{H}} \underline{\underline{q}} + \underline{\underline{G}} \underline{\underline{p}} = \underline{\underline{0}} \quad (6.15)$$

$$\underline{\underline{G}} = -\frac{1}{K_p} \sum_m \int_{V_m} \underline{\underline{N}}^{*T} \underline{\underline{N}}^* dV \quad (6.16)$$

Equations 6.10 and 6.16 can be written in compact form as

$$\begin{bmatrix} \underline{\underline{K}} & \underline{\underline{H}}^T \\ \underline{\underline{H}} & \underline{\underline{G}} \end{bmatrix} \begin{Bmatrix} \underline{\underline{q}} \\ \underline{\underline{p}} \end{Bmatrix} = \begin{Bmatrix} \underline{\underline{R}} \\ \underline{\underline{0}} \end{Bmatrix} \quad (6.17)$$

Cyclic loading under drained conditions can be solved as a special case of undrained cyclic loading if the nodal pore pressures in equation 6.17 are constrained. The nodal displacements in that case will be described by the following relation:

$$\underline{\underline{K}} \underline{\underline{q}} = \underline{\underline{R}}$$

The matrices $\underline{\underline{K}}$, $\underline{\underline{H}}$, $\underline{\underline{G}}$, $\underline{\underline{R}}$ are known functions of the soil properties the geometry of the continuum and the applied loads; a more detailed description of their structure is given in Appendix B, for plane strain, plane stress and axisymmetric problems.

6.4 A COMPUTER PROGRAM FOR FINITE ELEMENT ANALYSIS

The basic steps in any finite element solution are:

- (i) To read the input data provided by the user and store them, so that they can be used in later steps.
- (ii) For every element "m" to compute the arrays \underline{K} , \underline{H} , \underline{G} , \underline{R} (see section 6.2) and add them to the total arrays.
- (iii) To solve the resulting system of equation (equation 6.17)
- (iv) To print the computed values of the unknowns

Each of the steps is, in practice, subdivided in smaller steps which are executed separately by subprograms connected with the main program.

The numerical solution of the finite element equation 6.17 is based on a computer program written by Taylor and described in detail in reference [65]. According to Taylor the program is "written specifically as a research and educational tool in which the various 'modules' can be changed or added to as desired. Indeed quite different combinations of the subroutines for purposes which may even today not be obviously needed are possible."

This flexibility of the program makes it appropriate for the present study, since extensive modifications and additions were necessary as is described next. In the following paragraphs, the original program will be referred to as FEAP, abbreviation for Finite

Element Analysis Program, and the modified version as FEAP-CYC.

The first major modification applied to FEAP was aimed to make it capable of handling undrained loading of soils in addition to drained ones. According to the "Penalty Method" described in section 6.1.2, undrained loading of soil is governed by the system of equations:

$$\begin{bmatrix} K & H^T \\ \sim & \sim \\ H & G \\ \sim & \sim \end{bmatrix} \begin{Bmatrix} q \\ \sim \\ p \\ \sim \end{Bmatrix} = \begin{Bmatrix} R \\ \sim \\ 0 \\ \sim \end{Bmatrix}$$

FEAP was built for the analysis of compressible materials where only the stiffness matrix K and the loading vector R need to be calculated. In FEAP-CYC the coupling matrix H and the pore pressure matrix G are computed in addition to K and R .

The loading vector R for cyclic loading, has in general the following components (see equation 6.13):

$$\underset{\sim}{R} = \underset{\sim}{R}^B + \underset{\sim}{R}^S + \underset{\sim}{R}^R + \underset{\sim}{R}^O$$

$$\underset{\sim}{R}^B = \text{nodal loads due to body forces}$$

$$\underset{\sim}{R}^S = \text{nodal loads due to surface tractions}$$

$$\underset{\sim}{R}^R = \text{nodal loads due to cumulative strain}$$

$$\underset{\sim}{R}^O = \text{nodal loads due to initial displacement}$$

FEAP was intended to solve static and transient problems and consequently it computes all loading components except from the cyclic one. FEAP-CYC computes the cumulative strain for each element according to the proposed constitutive relation, and then finds the equivalent nodal forces ($\underset{\sim}{R}^R$) required to prevent those strains. This

is a method commonly used to compute the equivalent loading in finite element analyses, when the material tends to strain itself due to either change in temperature or creep [65].

In modeling the cyclic behavior of Sand A it was assumed that it greatly depends on the applied average and cyclic effective stress. This requires that the finite element solution follows all the major events of the life of the foundation (see figure 6.1):

(i) Geostatic conditions

(ii) Installation

(iii) Static loading

(iv) Cyclic loading

The effective stresses at the end of each event are used to compute the soil properties for the following event and have to be saved. In addition different drainage conditions may prevail during the events, so that the boundary conditions of the problem have to be changed between two consequent steps of the solution; those options are not available in the original program. FEAP-CYC can perform many analyses in sequence, and keep the solution of each of them in the memory; at the end of each analysis all or part of the input data can be changed, except for those defining the finite element discretization.

Except for the calculation of the geostatic effective stresses the solution for all the major events described previously needs to be obtained incrementally due to nonlinearity of the soil. In modeling

the installation of the foundation and its static loading with FEAP-CYC a load increment has to be specified; when modeling the cyclic loading the definition of a cycle number increment is necessary instead. An option of variable cycle step is available which permits the use of small cycle steps at the beginning of the solution when strain rates are high.

The static stiffness of the soil can be computed according to stresses anywhere between the initial and the final state of stress of each step according to the user's preference. Since only the initial stresses are known a priori, iterations within each step are necessary during the solution. The iterations follow the "Predictor-Corrector" method:

if for a step "n" the initial stresses are $\bar{\sigma}_{n-1}$ and the final $\bar{\sigma}_n$, then for the next step n+1 the first estimation of the final stress - "Predictor" - is:

$$\bar{\sigma}_{n+1} = \bar{\sigma}_n + (\bar{\sigma}_n - \bar{\sigma}_{n-1})$$

correction of this value - "Corrector" - is done iteratively.

The version of FEAP described in Reference [65] can handle linear elastic problems under plane stress and strain; FEAP-CYC can analyze axisymmetric problems as well. A problem is axisymmetric when both the geometry of the structure and the applied loads are symmetric about one axis; an example of this category is the axial loading of vertical piles.

A complete listing of FEAP-CYC is provided in Appendix E. For detailed information about the computational techniques used by the

program - solution of the system of equations, numerical integration etc. - the reader is referred to the description of FEAP by Taylor [65].

6.5 CHECKING THE FINITE ELEMENT PROGRAM

To ensure the correctness of the proposed computer program FEAP-CYC, simple problems for which closed form solutions are available, were solved numerically. Figure 6.2 summarizes the boundary conditions and the loads for the static problems considered, as well as their exact solution. Plane strain and axisymmetric cases were analyzed under drained and fully undrained conditions. The load was applied either as a uniform boundary pressure, or as a uniform boundary displacement. In all cases the agreement between the numerical and the closed - form solution was exact.

In addition to the static tests, four cyclic tests were run with FEAP-CYC, which are summarized in figure 6.3. They simulate plane strain and triaxial cyclic laboratory tests under drained and undrained conditions. The analytical solutions for all cases have been obtained in chapter 4 in conjunction with the evaluation of the proposed constitutive relation and also in Appendix D. The numerical solution followed two steps: first the initial stresses were computed due to static drained loading and, second, the effects of cyclic loading under drained or undrained conditions were estimated. As with the "static" cases, the agreement between the numerical and the

analytical solution for all "cyclic" cases was exact.

Undrained loading was simulated by the "Penalty Method" (see section 6.1.2) assuming that the Penalty Constant ($1/K$ in equation 6.16) is equal to zero. This is equivalent to the assumption that saturated soils are perfectly incompressible or that the Poisson's ratio for a total stress analysis is equal to one half. In the left hand side of the finite element equation

$$\begin{bmatrix} \tilde{K} & \tilde{H}^T \\ \tilde{H} & \tilde{G} \end{bmatrix} \begin{Bmatrix} \tilde{q} \\ \tilde{p} \end{Bmatrix} = \begin{Bmatrix} \tilde{R} \\ 0 \end{Bmatrix}$$

the assumption of perfect volume incompressibility makes the elements of matrix G equal to zero. Solution of equation (6.17) however is obtained by the Gaussian Elimination technique [64], [65], and the zero terms are gradually replaced by nonzero ones as the solution proceeds. A solution will be impossible only if the first diagonal term in equation 6.17 is zero; this happens, for example, when all displacement degrees of freedom for the first node number are constrained.

The finite element method is approximate for two main reasons:

- (i) The variation of the unknowns - nodal displacements and pore pressure here - is approximated by a polynomial expansion within each element

(ii) The element matrices are usually computed by numerical integration over the volume of each element which may not be exact.

In the examined static and cyclic cases the displacements and the pore pressure were uniformly distributed so that the previous approximations were, in fact, exact. For this reason the agreement between the numerical and the analytical solution was perfect within the numerical accuracy of the computer. The purpose of the analyses, however, was not to evaluate the finite element method but to check the computer program FEAP-CYC; the applicability of the method in solid mechanics has been thoroughly investigated by different researches (for example [65]) and further evaluation of it is out of the scope of the present research.

6.6 SUMMARY

This chapter formulated the solution of cyclic loading of foundations using the finite element method and the constitutive model proposed in chapter 4. The formulation of undrained problems followed the Penalty Method of incompressibility which allows for the calculation of pore pressure and effective stresses in the soil in addition to displacements.

A computer program FEAP-CYC was described which combined with the suggested constitutive model predicts the performance of foundations under repeated loads. The program was checked against simple static

and cyclic loading problems where an analytical solution is available.

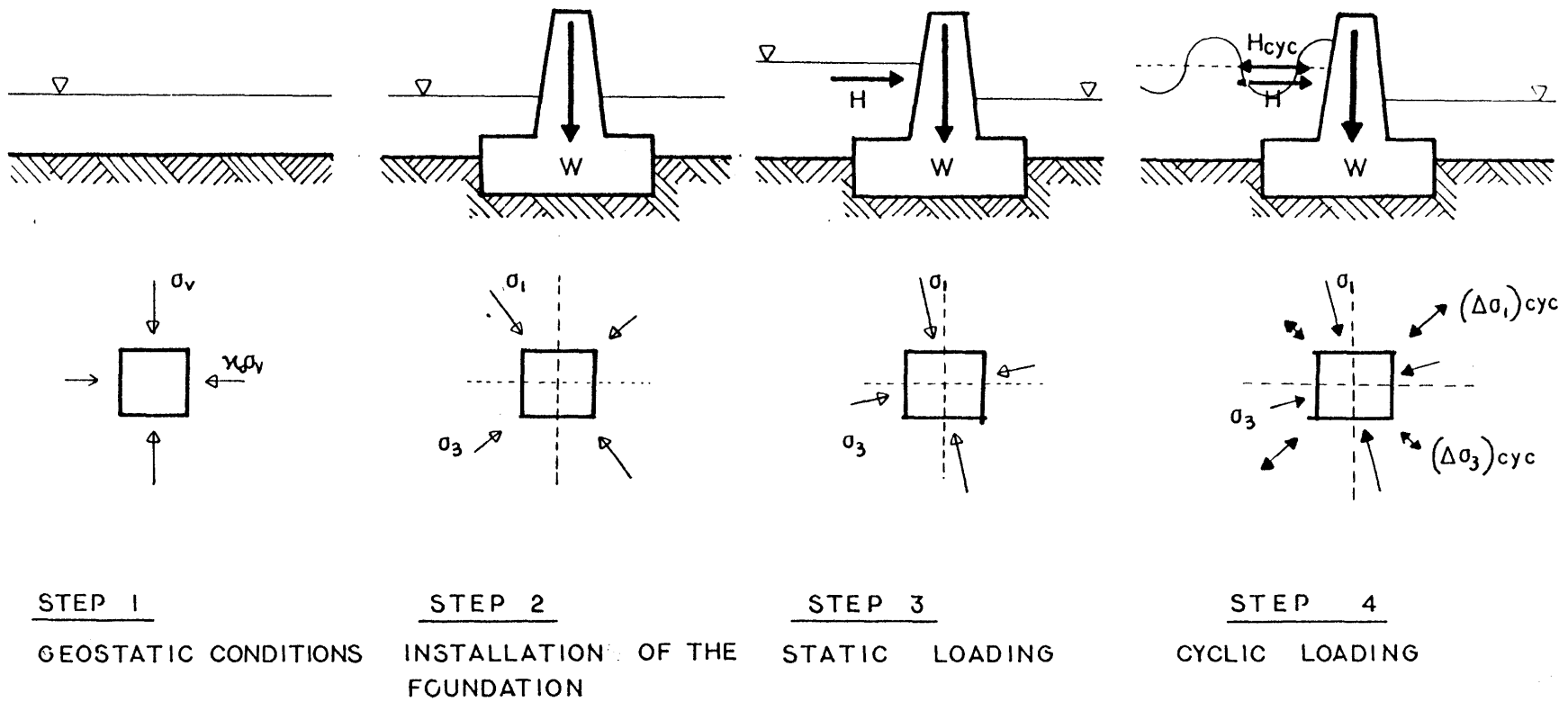


FIGURE 6.1 ; Major Events in the Life of a Foundation

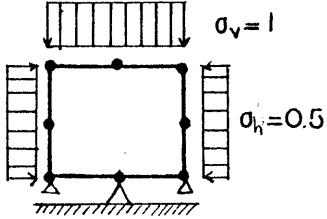
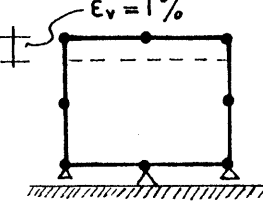
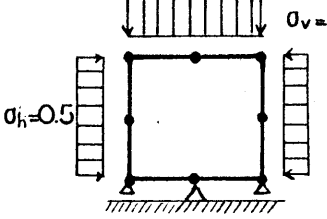
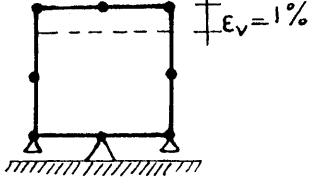
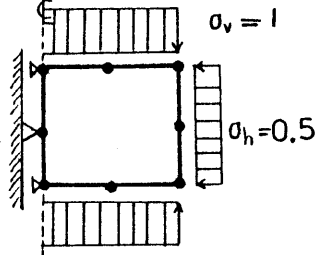
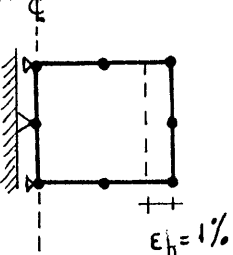
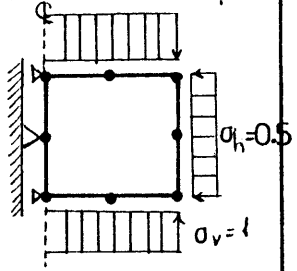
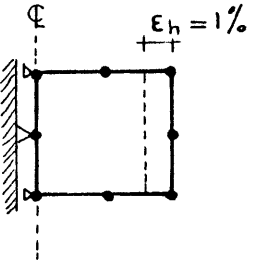
	DRAINED		UNDRAINED	
PLANE STRAIN				
	$\epsilon_v = \frac{(1+\nu)(2-3\nu)}{2E}$ $\epsilon_h = \frac{(1+\nu)(1-3\nu)}{2E}$	$\epsilon_h = -\frac{\nu}{1-\nu^2}$ $\sigma_v = \frac{E}{1-\nu^2}$	$\epsilon_v = 3/8E$ $\epsilon_h = -3/8E$ $u = 0.75$ $\bar{\sigma}_v = 0.25$ $\bar{\sigma}_h = -0.25$ $\bar{\sigma}_2 = 0.00$	$\epsilon_h = -1\%$ $u = 2/3E$ $\bar{\sigma}_v = 2/3E$ $\bar{\sigma}_h = -2/3E$ $\bar{\sigma}_2 = 0.00$
AXISYMMETRIC				
	$\epsilon_v = \frac{1-\nu}{E}$ $\epsilon_h = \frac{1-3\nu}{2E}$	$\epsilon_v = \frac{2\nu}{1-\nu}$ $\sigma_h = E$	$\epsilon_v = 1/2E$ $\epsilon_h = -1/4E$ $u = 2/3$ $\bar{\sigma}_v = 1/3$ $\sigma_h = -1/6$	$\epsilon = -2\%$ $u = E/3$ $\bar{\sigma}_v = -E/3$ $\bar{\sigma}_h = 2/3E$

FIGURE 6.2 : Summary of Simple Static Problems solved with FEAP-CYC

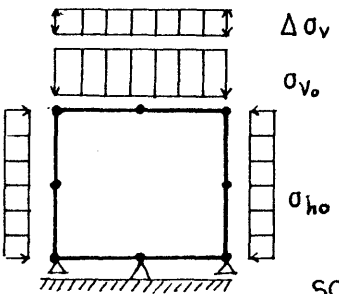
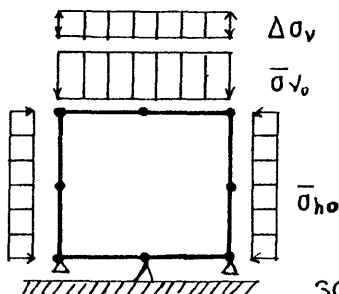
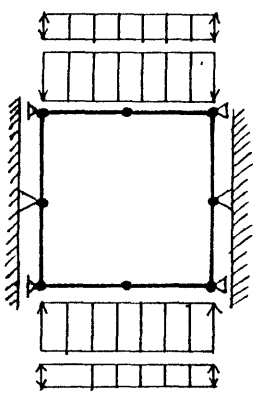
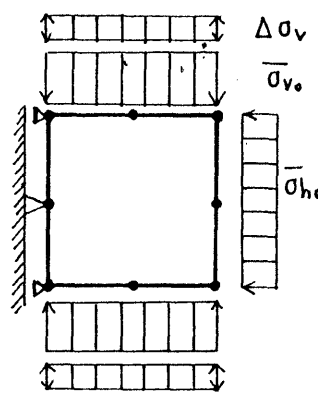
	DRAINED	UNDRAINED
PLANE STRAIN	 <p>SOLUTION DESCRIBED BY EQUATIONS D.7, D.14, D.17</p>	 <p>SOLUTION DESCRIBED BY EQUATIONS D.21, D.25, D.33, D.34</p>
AXISYMMETRIC	 <p>SOLUTION DESCRIBED BY EQUATIONS 5.1, 5.2</p>	 <p>SOLUTION DESCRIBED BY EQUATIONS 5.6, 5.7</p>

FIGURE 6.3 : Summary of Simple Cyclic Problems Solved with FEAP-CYC

CHAPTER 7

CASE STUDY: THE OOSTERSCHELDE BARRIER7.1 INTRODUCTION

The Netherlands government has the responsibility to design a barrier dam across the Oosterschelde inlet located southwest of Rotterdam. The closure which links with dikes must allow tidal flow during normal sea states and resists storm tides and waves [7]. The design chosen consists of large gates resting on reinforced concrete piers. Figure 7.1 portrays a pier section with base plan dimensions of 25m wide and 50m long. The piers are being constructed on shore, floated into position, sunk into a dredged trench, and ballasted. Erosion of the foundation materials will be prevented by placing a protective cover or sill.

The foundation materials consist of fine to medium sand of uniform gradation over most of the closure. The upper part, of an average depth of 20 meters, has been deposited in the Holocene epoch and is loose to medium dense. The underlying sand, deposited in the Pleistocene epoch, is medium dense to very dense.

The objective of this chapter is to predict the performance of one of the piers, for four different load combinations, under drained or fully undrained soil conditions. The results will be evaluated through the following comparisons:

(i) Comparisons with the trends predicted by one model test sponsored by the Dutch government, and presented by Lambe et al [4]

(ii) Comparison with analytical predictions presented by Marr and Christian [7] and Urzua [6]

(iii) Comparison with approximate solutions used in the past

Table 7.1 presents the four combinations of loads which will be considered. Case A is the combination of head loss and wave loading predicted from hydraulic studies. In case B, the design static load has been increased by one half of the design cyclic load; the cyclic wave load is one half of the design cyclic load. In case C the design static head loss load is one half of the design static load and the cyclic load consist of the remaining half of the design static load plus the design cyclic load. Thus case B has the total load heavily biased toward the cyclic component. In case D, there is no static head loss load and the cyclic load has the design value.

7.2 CAISSON TESTS AT NEELTJE JANS, THE NETHERLANDS

The Dutch government sponsored and directed a series of tests on a caisson - 15 meters by 27.7 meters by 10 meters high - resting on the sea bottom in 7 meters of water, at Neeltje Jans, Netherlands. A plan view and a section view of the test caisson is shown in Figure 7.2. The foundation soils at the test site consist of sands similar to those met in the Oosterschelde basin interspersed with layers of silt; tests were run on a natural untreated foundation soil as well as on a foundation densified by a vibrational method. The test results were extensively presented by Lambe et al [4]; in this section only the most important aspects of the observed behavior will be summarized.

The loading program in one of the tests is shown in Figure 7.3; six consecutive parcels of horizontal cyclic loading were applied in which the magnitude of the average and the cyclic component of loading were increased gradually. The movement of the caisson is shown in Figure 7.4. The following trends can be identified:

- (i) The caisson moved both in the horizontal and vertical directions.
- (ii) The horizontal movement was in the direction of the applied average horizontal load.
- (iii) The caisson tipped toward the load with the base moving more horizontally than did the top.

Densification of the foundation greatly improved its behavior.

The movement of the caisson on the densified foundation reached only 1/10 of the movement of the caisson on the undensified foundation.

Pore pressure below the caisson changed within each cycle of loading but it remained unaffected by the number of cycles; no accumulation of pore pressure was measured. Analytical studies on the accumulation of pore pressure due to cyclic loading of Oosterschelde soils (for example, Christian and Audibert [76]) have shown that only small values of excess pore pressure are likely to develop because of the large permeabilities of the soils.

7.3 PREDICTED RESPONSE OF OOSTERSCHELDE BARRIER

Figure 7.5 shows the finite element mesh used for the calculations and indicates material types and locations. The elastic soil parameters used for the foundation materials are summarized in table 7.2.

The shear modulus of the loose Holocene sand and the densified Pleistocene sand are related to the porosity of the materials and the applied effective octahedral stress by equation 4.12. The Poisson's ratios are those used by Marr and Christian [7] and Urzua [6]. The bulk moduli are related to the applied effective octahedral stress by equation 3.13; the two factors (B, m) appearing in the equation were determined using the values of the shear modulus and the Poisson's ratio.

For the artificial materials a constant value of the Young's

modulus and Poisson's ratio was specified equal to those used by Marr and Christian [7] and Urzua [6]. The modulus for concrete was adjusted to reflect the difference in moment of inertia between the actual pier section and that of the solid concrete section used in the analysis.

The model caisson tests in Neeltje Jans, as well as, the consolidation analysis done by Christian and Audibert, both presented in the previous section, suggest that in the actual case drained conditions should prevail. Thus as a first step the performance of the pier under drained conditions will be studied.

Figure 7.6 shows the predicted permanent displacements of the pier for the four different load combinations (case A - case D) described in section 7.1; in all cases 5 cycles of maximum wave load were applied to the pier.

In cases A, B and C the pier settled vertically and also moved horizontally in the direction of the applied static horizontal force similar to what has been observed during the model caisson test in Neeltje Jans. In case D, where no horizontal static force was applied, no permanent horizontal displacement occurred.

In cases A and B the pier tipped slightly with the base of the pier moving horizontally less than the top of the pier. In case C the pier tipped in the opposite direction with its base moving horizontally more than its top; a similar behavior has been observed during the model test in Neeltje Jans. The predicted settlement for case D was symmetric.

Comparing the predicted permanent displacements for the different

combinations of loads and soil densities, one can observe the following trends:

- (i) The cyclic load controls the magnitude of average permanent settlement.
- (ii) The static horizontal force controls the direction of the horizontal displacement of the foundation.
- (iii) The magnitudes of the horizontal permanent displacement and differential settlement are controlled by both the static and the cyclic applied horizontal load.

To evaluate the effect of densification of the foundation on predicted permanent displacement, an analysis was done assuming that the top layer of Holocene sand has been densified. The properties used for the densified Holocene sand are the same with the properties of the Pleistocene sand. Comparison of the results for loading case A are shown in Figure 7.7. Densification of the soil reduces the horizontal displacement by an average factor of 4.3, and the vertical displacements by an average factor of 1.7. A similar effect of densification on permanent displacement was observed during the model test in Neeltje Jans.

7.4 STRESS REDISTRIBUTION DUE TO CYCLIC LOADING

The cyclic oedometer test results described in chapter 5 have demonstrated that when permanent displacement is prevented the effective stress changes to counteract the accumulation of permanent strain. The same behavior was observed during undrained cyclic triaxial tests where the effective octahedral stress decreased to balance the tendency for volume decrease. During drained cyclic loading of the pier, changes in the stresses applied to the underlying soil are expected mainly because:

- (i) The plane strain assumption restricts any deformation along the long axis of the pier (y direction).
- (ii) The pier is considerably stiffer than the soil, partially preventing permanent displacements in its neighborhood.

The proposed method takes into account the stress redistribution in the computation of permanent displacements. The objective of this section is to evaluate the effect of stress redistribution on the prediction of permanent displacement of the pier due to drained cyclic loading.

In the previous section permanent deformations were predicted for five cycles of the load combinations A, B, C and D. Five increments of the number of cycles were used, each equal to one cycle. To evaluate the importance of stress redistribution, predictions were also made using one increment equal with five cycles. Comparison of

the results obtained with the two approaches are portrayed in Figure 7.8 and tables 7.3 and 7.4. Neglecting the effect of stress redistribution overestimates the permanent displacement. The error in the prediction of vertical settlement ranged between 7.1% and 13.7%; the error was larger in the prediction of horizontal displacement where it ranged between 13.1% and 40.9%.

Figure 7.9 shows the stresses applied in the soil four meters below the base of the pier, before and after the cyclic loading for case A. Although no additional load was applied to the pier a change in the stresses is predicted due to cyclic loading. The horizontal stress increased by 12 - 50 %, while the vertical and shear stresses decreased and increased locally by a smaller amount. The corresponding stress paths for three elements below the pier are shown in Figure 7.10.

Figure 7.11 presents the contours of change in octahedral stress in the soil due to cyclic loading for case A of loading. The octahedral stress increases in the Holocene sand layer and also in the Pleistocene sand layer below the center of the pier; the octahedral stress decreases in the rest of the sand. The magnitude of the change in the octahedral stress is reduced as the radial distance away from the pier increases; no significant stress redistribution occurs at radial distance approximately larger than the base of the pier.

Figure 7.12 shows the contours of change in the maximum shear stress in the soil due to cyclic loading. Reduction of the maximum shear stress occurs in the Holocene sand layer and also in the Pleistocene sand away from the base of the pier. Increase in the

maximum shear stress occurs in the Pleistocene sand below the foundation. Significant changes in maximum shear stress occur within a radial distance from the pier equal to the length of its base.

The direction of the stress paths resulting from stress redistribution for the soil below the Oosterschelde pier are shown in Figure 7.13 for loading case A..

The results presented in this section allow one to draw the following conclusions, with respect to drained cyclic loading of the pier:

(i) Neglecting the effect of stress redistribution results in overestimation of the permanent displacements.

(ii) The relative effect of stress redistribution is larger on the predicted horizontal displacement than on the predicted vertical displacement, but the vertical displacements are much larger in any case.

(iii) The magnitude of stress redistribution decreases as the radial distance away from the foundations increases. No significant stress redistribution occurs at radial distance from the foundation larger than the width of the foundation.

7.5 COMPARISON WITH PREVIOUS ANALYSES

Prediction of the performance of the pier for the four different load combination were previously done by Marr and Christian [7] and Urzua [6]. As in the proposed approach both previous analyses model the cumulative effect of cyclic loading on stresses and strains. The Finite element discretization used in both analyses is very similar to that shown in Figure 7.5; the soil parameters are also similar to those used by the author.

Figure 7.14 compares the permanent vertical displacements of the foundation predicted with the three approaches. Settlements predicted with the proposed method are in good agreement with the settlements predicted by the two other analyses, particularly with that by Marr and Christian.

Figure 7.15 compares the permanent horizontal displacement predicted by the three methods. The proposed method predicts less horizontal displacements than the two others. Marr and Christian's predictions are larger by an average factor of two, while Urzuas are larger by an average factor of 5.7.

The predicted differential settlements are compared in Figure 7.16. The proposed method predicts little differential settlement compared with the two other methods. It also predicts that tilting of the foundation will not always occur in the direction of the applied static moment, as the two other methods predict. Tilting in the opposite directions is also possible depending on the combination of the static and the cyclic horizontal loads. The tilting occurred

during the model test in Neeltje Jans (see section 7.2) is one example of tilting opposite to the direction of the applied static moment.

The differences between the predictions can be partly explained by considering the differences between the methods used in the three analyses to estimate the static initial stresses in the foundation, as well as, the permanent strain accumulation in the soil.

Marr and Christian [7] used the computer program FEECON (Simon et al [77]) to calculate the initial stresses before the application of the repeated wave loading. In their approach they simulated the excavation, the construction of the caisson, and the application of the head loss load in the computation of initial stresses. Their computation included the effects of stress redistribution due to soil nonlinearity. In Urzua's approach none of the construction processes is modelled and stresses are computed using an elastic analysis. In the proposed approach the stresses are computed in three steps: one to compute the initial geostatic stresses, one to simulate the construction of the caisson, and one to simulate the application of the head loss load. A linear elastic analysis is performed in each of the two last steps, with elastic soil properties consistent with the stresses computed at the end of the previous step. It is very likely that the three different procedures yielded different estimations of the applied stress in the foundation before cyclic loading, thus affecting the prediction of permanent displacements.

Even though the three models are based on essentially the same soil data, differences exist in the way these data were synthesized for input to the computer. Marr and Christian followed the work by

Hedberg [5] and Urzua followed the work by Hadge [22a]. The proposed approach, also follows the work by Hadge, but extensive modifications were applied to make it applicable to cyclic loading close to failure. For the present case study soil elements under the edges of the pier and especially under the heel, are very close to failure due to the weight of the pier and the static head loss.

Finally the three approaches account in different degree for the effects of stress redistribution discussed in section 7.3. Marr and Christian include no effect of stress redistribution while Urzua partially accounts for it. The proposed approach takes full account of the effect of stress redistribution.

A detailed comparative study of the results of the three approaches is necessary in order to evaluate the degree in which each of the above differences affects the quantitative prediction of permanent displacements. In conclusion, however, it is worth noticing that despite all the differences of the three methods the predicted trends in the gross accumulation of permanent displacement of the pier are in good agreement.

7.6 UNDRAINED CYCLIC LOADING

In the previous sections the assumption was made that drained conditions would prevail during the static and the cyclic loading of the Oosterschelde barrier. It is usefull, however, to examine the differences in the performance of the barrier when undrained cyclic

loading is considered. In this section the performance of the barrier will be predicted assuming that no dissipation of excess pore pressure occurs during the repeated wave loading.

Predicted Permanent Displacements

The predicted permanent displacement of the pier for load combinations A, B, C, and D are shown in Figure 7.17. For all cases it was assumed that first the maximum tide force was applied to the pier under drained conditions, followed by five cycles of undrained repeated loading with the maximum wave load. The following trends are identified:

(i) The vertical settlements are controlled by the magnitude of the applied wave load.

(ii) The static horizontal force controls the direction of the horizontal displacement of the foundation, as well as the direction of the differential settlement.

(iii) The magnitude of the horizontal displacements and the differential settlement is controlled by both the applied static and cyclic horizontal loads.

Comparison with Displacements from Drained Cyclic Loading

Figures 7.18, 7.19 and 7.20 compare the displacements of the center of the pier's base predicted for drained and fully undrained cyclic loading. The vertical settlements due to undrained cyclic

loading are four to five times smaller than the settlements due to drained cyclic loading. The effect of drainage conditions on horizontal permanent displacements is not significant; horizontal displacements due to drained and due to undrained cyclic loading are approximately equal. Finally, the differential settlement due to undrained cyclic loading is up to six times larger than that predicted for drained cyclic loading, and has always the direction of the applied static moment.

Displacements, like strains, have two components: the volumetric and the shear-deviatoric-component. During undrained loading only the shear component is present because no change in volume is allowed while during drained loading both components are present.

The large reduction of vertical settlement under undrained conditions implies that the largest part of the vertical settlement predicted for drained cyclic loading is due to permanent volume reduction. The opposite must be true for the horizontal displacement; since the different drainage conditions have little effect on the predicted displacement, the shear component of displacement must dominate in the horizontal direction. Finally, the increase of differential settlement under undrained conditions, implies that volume reduction and shear distortion contribute in opposite ways to the differential settlement due to drained cyclic loading. The shear component tends to tilt the pier in the direction of the applied static moment, and the volumetric component tends to tilt it in the opposite direction. For loading under drained conditions the volumetric and shear components approximately cancel each other,

resulting in very small differential settlement. Under undrained conditions when only the shear component is present tilting occurs in the direction of the applied static moment.

Predicted Pore Pressure Accumulation

Figure 7.21 presents the stress paths followed during Undrained cyclic loading by a soil element four meters below the heel of the pier for loading case A. Cyclic loading decreases the maximum shear stress applied to the element, increases the total octahedral stress and decreases the effective octahedral stress. Excess pore pressure is generated equal to:

$$\Delta u = \sigma_{\text{oct}} - \bar{\sigma}_{\text{oct}} \quad (7.1)$$

Since the analysis performed is elastic, the excess pore pressure due to stress redistribution (Δu_s) is equal to the change in the total octahedral stress:

$$\Delta u_s = \Delta \sigma_{\text{oct}} \quad (7.2)$$

The pore pressure in excess of Δu_s is due to contraction of the sand under cyclic loading (Δu_c):

$$\Delta u_c = \Delta u - \Delta \sigma_{\text{oct}} \quad (7.3)$$

The cyclic component of excess pore pressure is positive when the average effective state of stress belongs to the subcharacteristic domain and it is negative when it belongs to the surcharacteristic domain (see definitions in chapter 2). The component due to stress redistribution may be positive or negative depending on the direction

of the total stress path. The total excess pore pressure is the sum of the two components and may be either positive or negative.

Figure 7.22 shows contours of excess pore pressure below the pier for loading combination A. Positive pore pressure develops in most of the foundation soil; negative pore pressure is restricted to one narrow area twenty meters below the corners of the pier, and in one area at large depth below the center of the pier. Comparing figure 7.11 and 7.22, note that the two zones of volumetric expansion in the drained case correspond closely to the two areas of reduced pore pressure in the undrained case. The magnitude of the excess pore pressure generally decreases as the radial distance away from the pier increases.

Comparison with Simplified Prediction of Pore Pressure Accumulation

A simplified method that has been used in the past for the prediction of excess pore pressures from cyclic loading follows two basic steps:

(i) Use an elastic finite element analysis to estimate the average and cyclic state of stress in a number of soil elements below the foundation.

(ii) Use the results from undrained cyclic laboratory tests to compute the excess pore pressure for each element.

Excess pore pressures appearing in the paper by Marr and Christian [7] were computed with this method; the results from undrained cyclic

triaxial tests presented by Hedberg [5], were used for the analysis.

Figure 7.23 presents excess pore pressure contours below the pier for loading case A, computed with the simplified approach. The model, described in chapter 4, was used to reproduce the results from undrained cyclic triaxial tests under constant static total stresses. Comparison of Figures 7.22 and 7.23 shows that the two approaches yield significantly different patterns of pore pressure development. Close to the pier the simplified method underpredicts the pore pressure as much as five times.

The observed differences are explained from the fact that the simplified method computes only the cyclic component of pore pressure (Δu_c) and totally neglects the component due to stress redistribution (Δu_s). From Figure 3.21 it is realized that this component is a significant part of the total accumulated pore pressure and cannot be neglected. Thus it is concluded that use of the simplified method must be avoided when stress redistribution due to cyclic loading occurs.

7.7 SUMMARY

Two dimensional analyses were performed to evaluate the permanent displacement of the Oosterschelde barrier due to the combined action of rising tide and sea waves. The most important findings of the analyses are summarized below:

(i) The predicted displacement patterns under drained loading agree with trends observed during the model caisson test at Neeltje Jans.

(ii) Redistribution of stresses in the foundation occur during drained cyclic loading. Displacement predictions neglecting this redistribution overestimated displacements by a maximum of 40% ; this error, however, applies to the smallest displacements.

(iii) The trends predicted by the proposed method for drained cyclic loading, agree with previous analyses by Marr and Christian [7] and Urzua [6]. The predicted magnitude of permanent settlement also agrees in the three analyses. The two previous analyses, however, predict larger horizontal displacement and differential settlement than the proposed approach.

(iv) Drainage conditions have a significant effect on predicted average and differential settlements: undrained cyclic loading yield five times less average settlement than drained cyclic loading, and two to six times larger differential settlement. The effect of drainage conditions on predicted horizontal displacement was not significant.

(v) The undrained analyses show that excess pore pressure develops during cyclic loading for two reasons: repeated shearing and change in the average state of stress, referred to as stress redistribution

(vi) Simplified methods for the prediction of pore pressure accumulation, by direct use of laboratory test results, neglect the pore pressure component due to stress redistribution and may lead to wrong predictions.

<u>CASE</u>	<u>MAXIMUM LOADS</u>		<u>CYCLIC WAVE LOAD</u>	
		(10 ⁶ N)	<u>Magnitude (10⁶ N)</u>	<u>Number of Waves</u>
DESIGN	MAX HEAD LOSS	76.8	15.9	284
			25.3	187
	MAX WAVE LOAD	70.2	36.5	90
			48.7	31
			61.8	9
			70.2	2
LARGE TIDE	MAX HEAD LOSS	111.9	8.0	284
			12.7	187
	1/2 MAX WAVE	35.1	18.3	90
			24.5	31
			30.9	9
			35.1	2
LARGE WAVE	1/2 MAX HEAD LOSS	38.4	24.6	284
			39.1	187
	MAX WAVE +1/2 MAX HEAD LOSS	108.6	56.5	90
			75.3	31
			95.6	9
			108.6	2
NO TIDE	NO HEAD LOSS	0.0	15.9	284
			25.3	187
	MAX WAVE	70.2	36.5	90
			48.7	31
			61.8	9
			70.2	2

TABLE 7.1 : Static Head Loss and Cyclic Wave Load Combinations

MATERIAL	n %	E (t/m ²)	v	γ_{t_3} (t/m ³)	k _o
HOLOCENE SAND	41.0	-	0.30	2.00	0.5
PLEISTOCENE SAND	39.4	-	0.45	2.00	1.0
SLAG	-	9950	0.45	1.00	-
SILL	-	1990	0.20	1.00	-
CONCRETE	-	300000	0.20	2.50	-

TABLE 7.2 : Material Properties for Oosterschelde Soils and Oosterschelde Closure

DISPLACEMENT (mm) AT THE CENTER OF THE PIER'S BASE

	WITH STRESS REDISTRIBUTION	WITH NO STRESS REDISTRIBUTION	DIFFERENCE %
CASE A	2.53	2.71	7.1
CASE B	0.93	0.97	4.3
CASE C	4.73	5.38	13.7
CASE D	2.56	2.75	7.4

TABLE 7.3 : Effect of Stress Redistribution on Predicted Settlement

DISPLACEMENT (mm) AT THE CENTER OF THE PIER'S BASE

	WITH STRESS REDISTRIBUTION	WITH NO STRESS REDISTRIBUTION	DIFFERENCE %
CASE A	0.85	1.10	29.4
CASE B	0.61	0.69	13.1
CASE C	0.66	0.93	40.9
CASE D	-	-	-

TABLE 7.4 : Effect of Stress Redistribution on Predicted Horizontal Displacement

DIFFERENTIAL SETTLEMENT (TOE-HEEL) (mm)

	WITH STRESS REDISTRIBUTION	WITH NO STRESS REDISTRIBUTION
CASE A	0.16	-0.09
CASE B	0.08	0.02
CASE C	-0.09	-0.40
CASE D	-	-

TABLE 7.5 : Effect of Stress Redistribution on Predicted
Differential Settlement

	VERTICAL SETTLEMENT ⁽³⁾ (mm)			HORIZ. DISPLACEMENT ⁽³⁾ (mm)			DIFFERENTIAL SETTLEMENT (mm) (TOE-HEEL)		
	D ⁽¹⁾	U ⁽²⁾	U/D	D	U	U/D	D	U	U/D
CASE A	2.53	0.43	0.17	0.85	1.00	1.18	0.06	0.41	6.83
CASE B	0.93	0.15	0.16	0.61	0.67	1.10	0.09	0.24	2.63
CASE C	4.76	0.82	0.17	0.66	0.86	1.30	-0.09	0.41	-4.55
CASE D	2.56	0.47	0.18	-	-	-	-	-	-

- (1) DRAINED CYCLIC LOADING
(2) UNDRAINED CYCLIC LOADING
(3) AT BASE CENTER

TABLE 7.6 : Effect of Drainage on Predicted Permanent Movement of the Pier

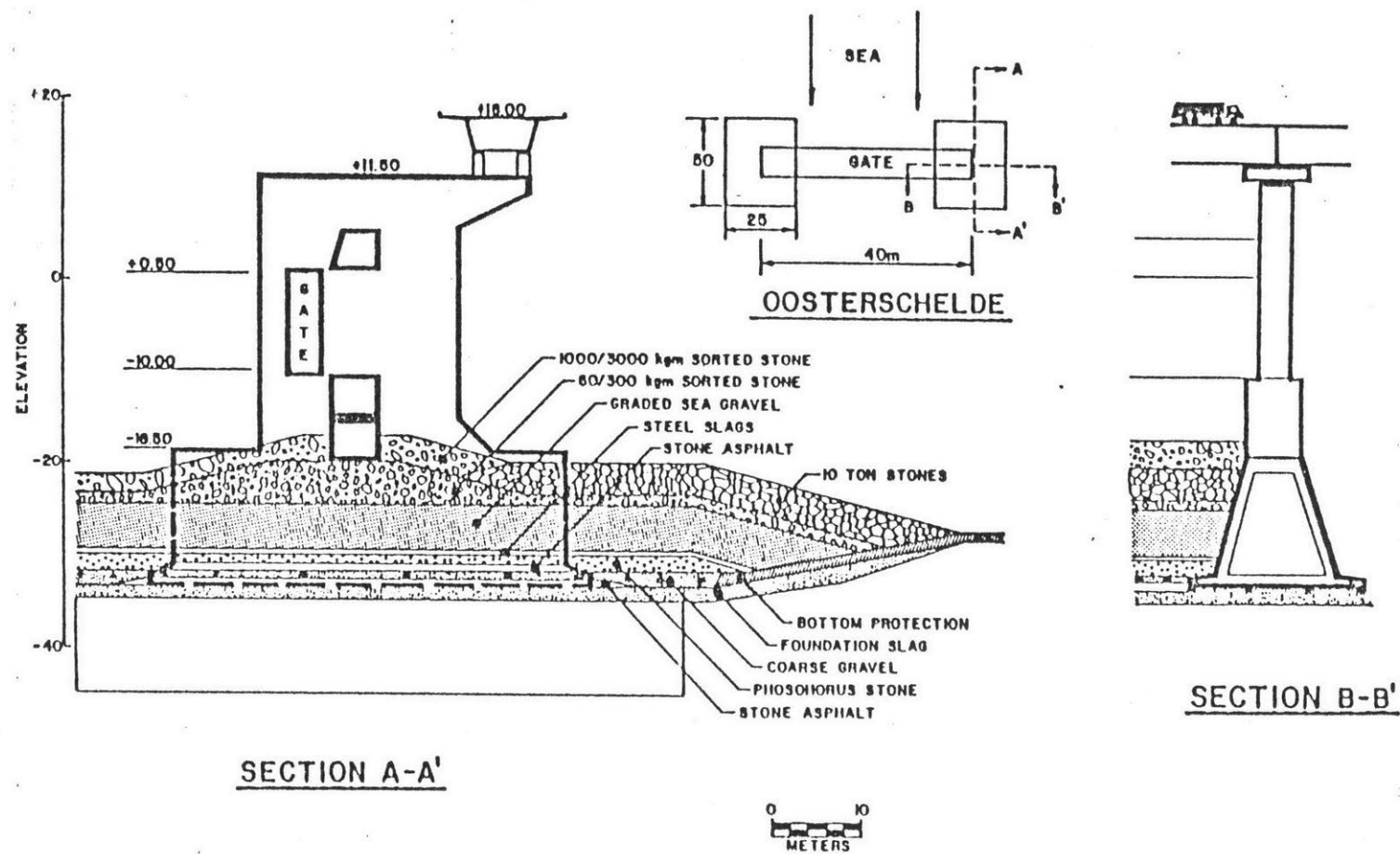
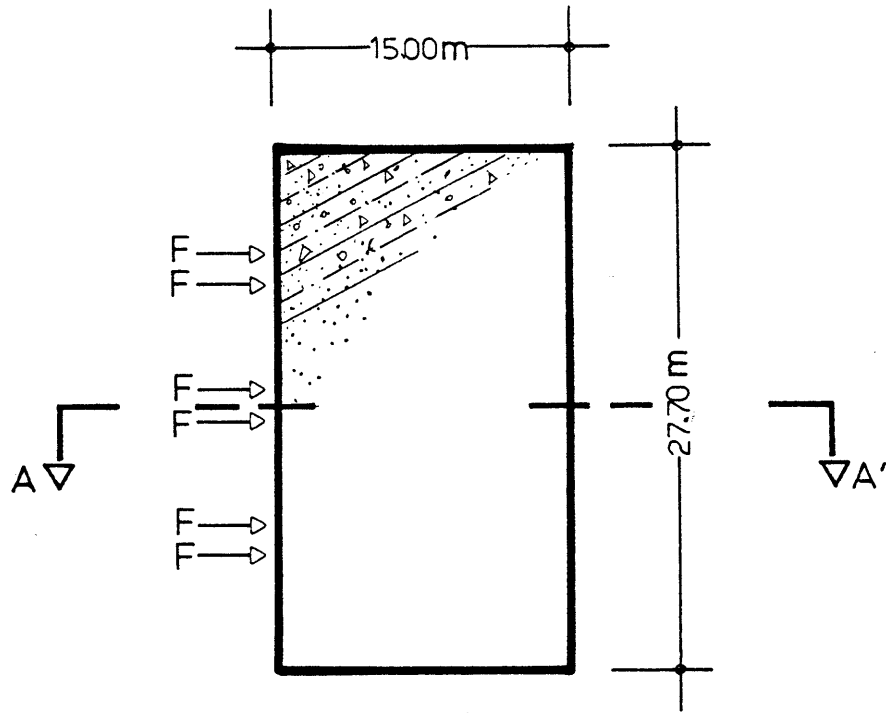
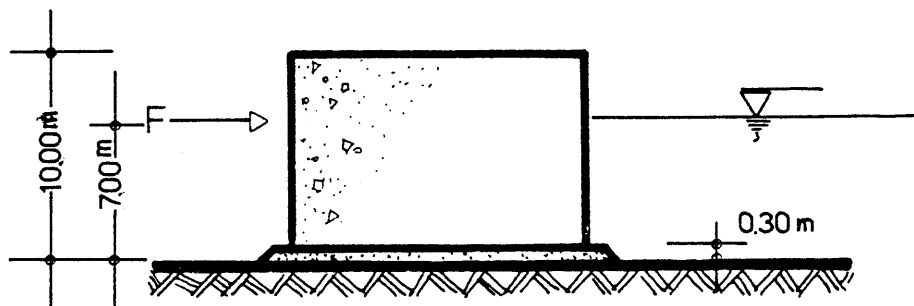


FIGURE 7.1. THE OOSTERSCHELDE BARRIER



A. PLAN OF TEST CAISSON



B. SECTION AA' OF TEST CAISSON

FIGURE 7.2

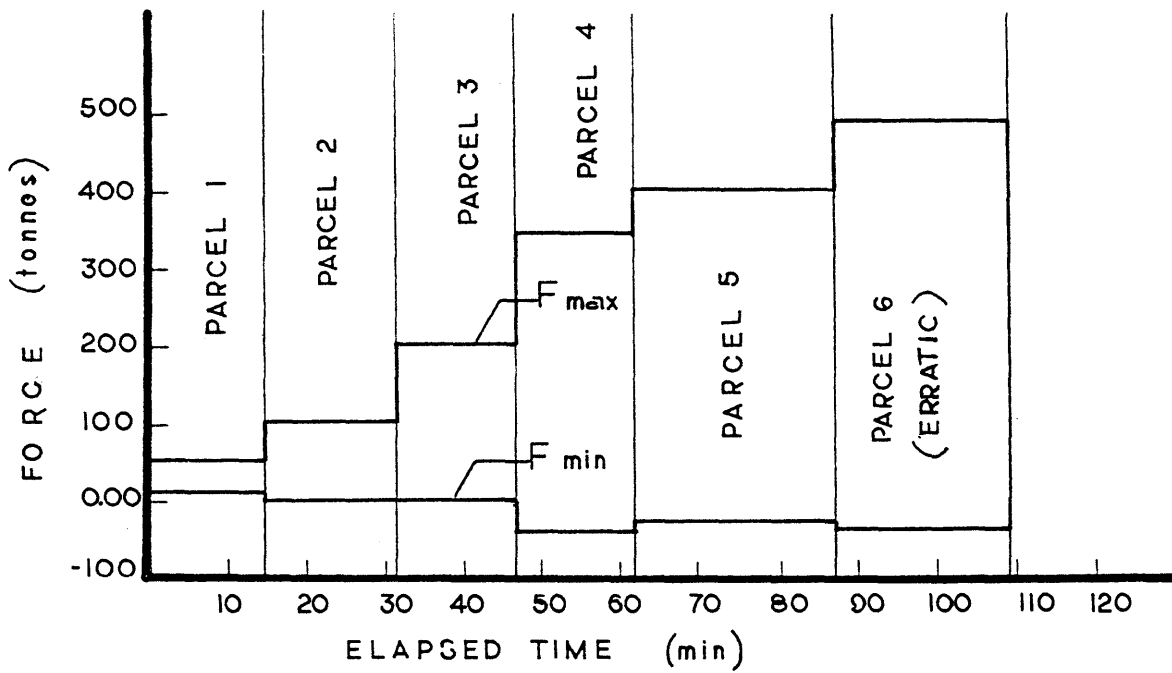


FIGURE 7.3 : Loading Schedule : TEST 1A

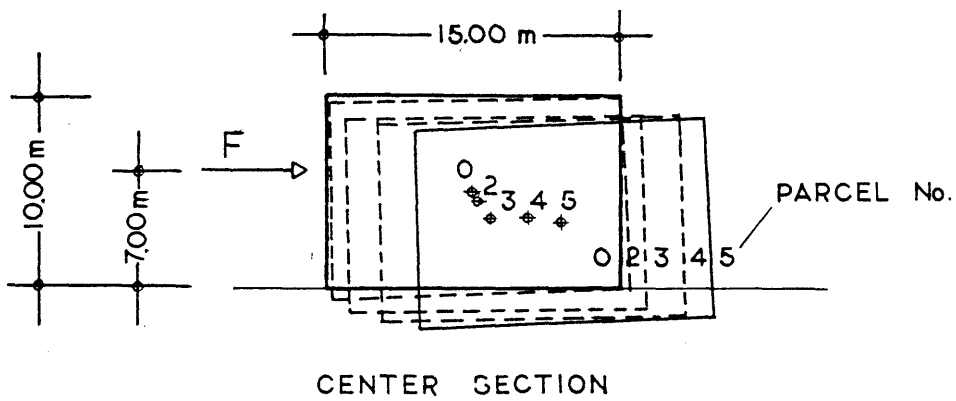


FIGURE 7.4 : Permanent Movement : TEST 1A

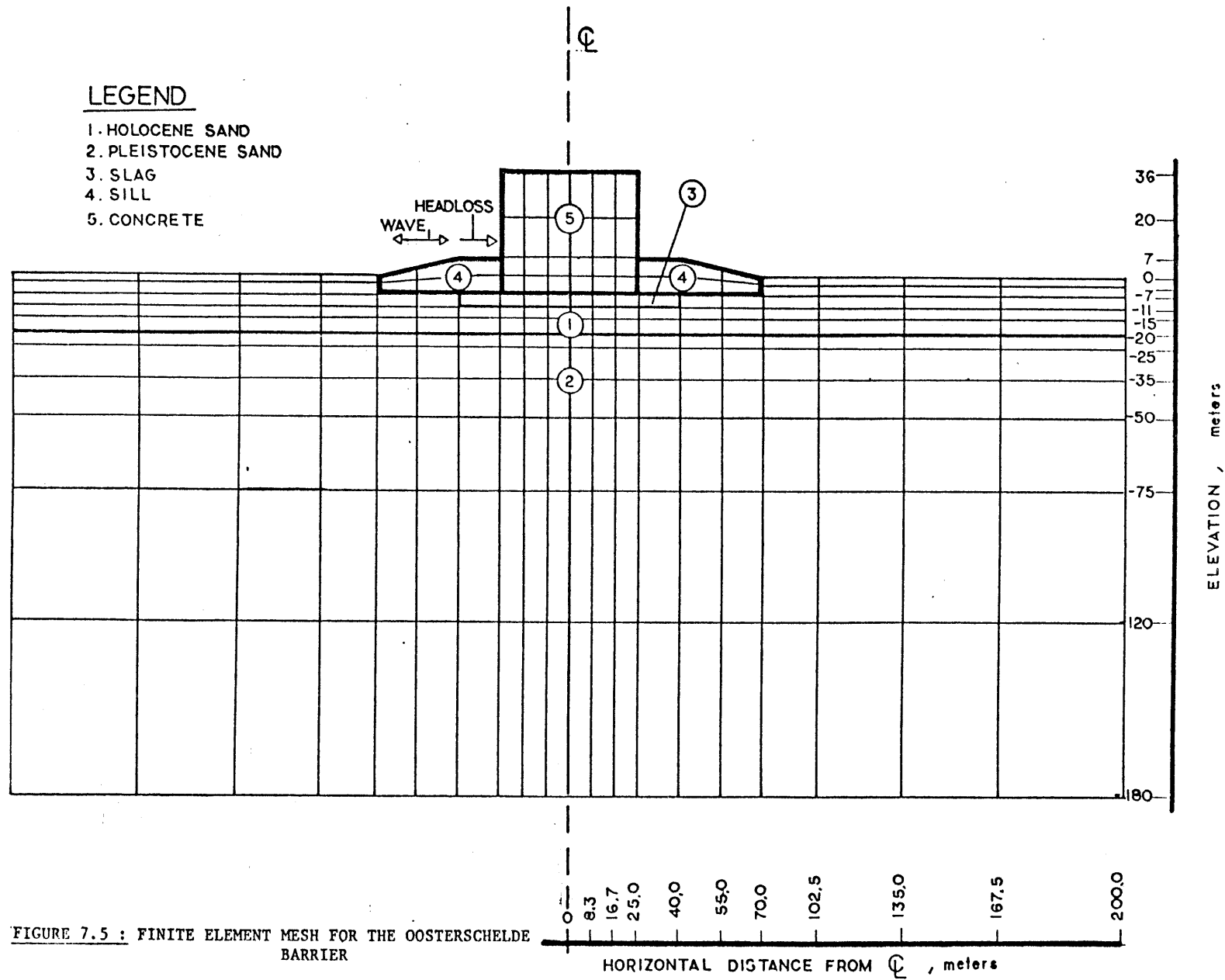


FIGURE 7.5 : FINITE ELEMENT MESH FOR THE OOSTERSCHELDE BARRIER

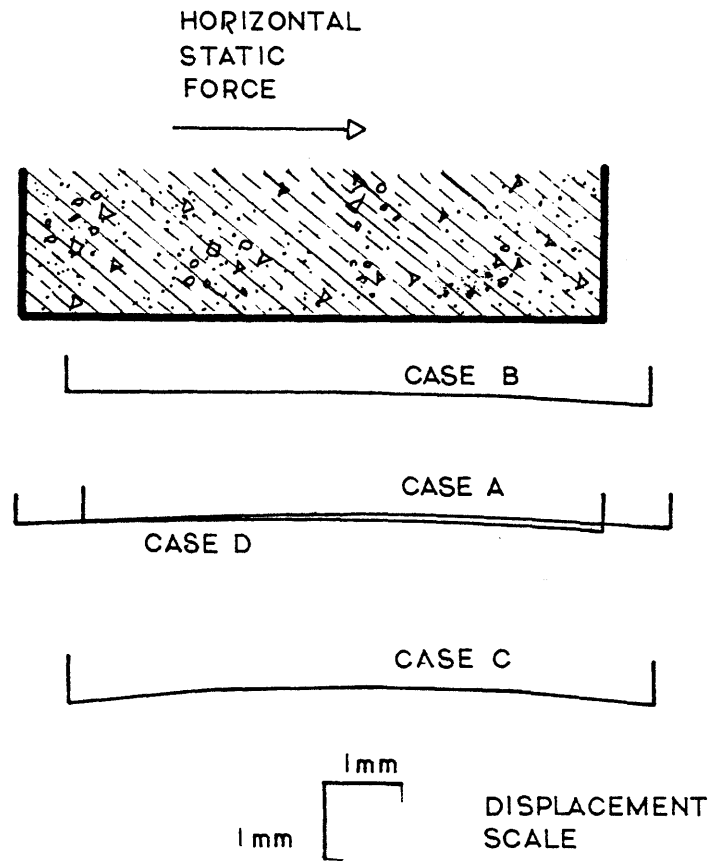


FIGURE 7.6 : Predicted Permanent Displacement of the Oosterschelde Barrier

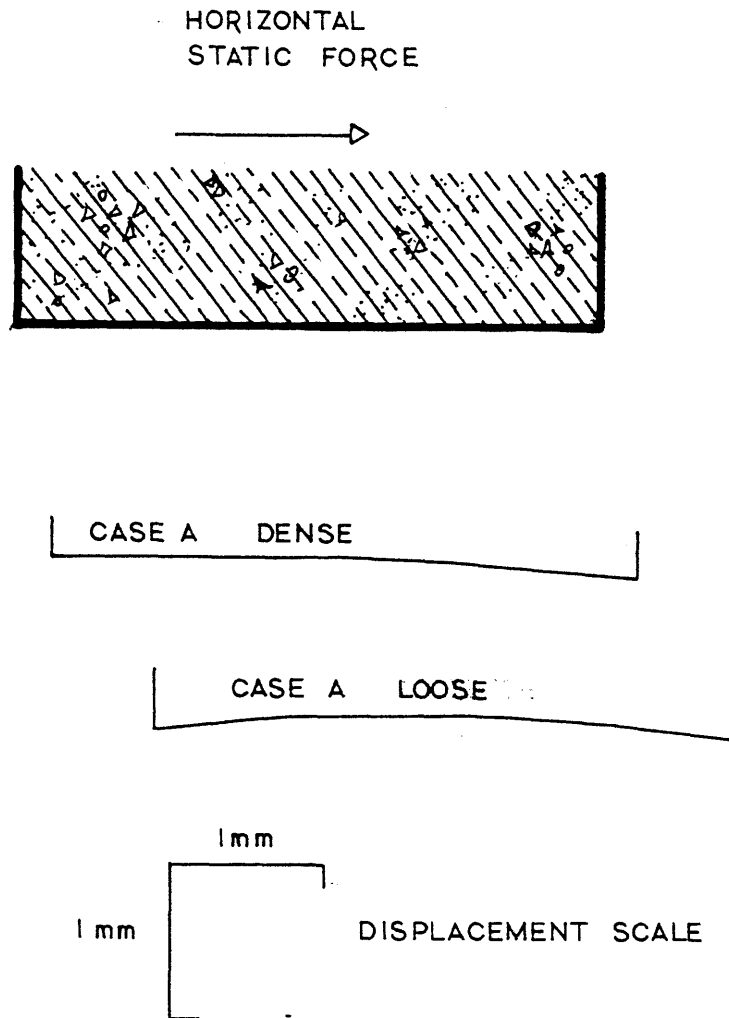


FIGURE 7.7 ; Effect of soil Densification on Predicted Permanent Movement

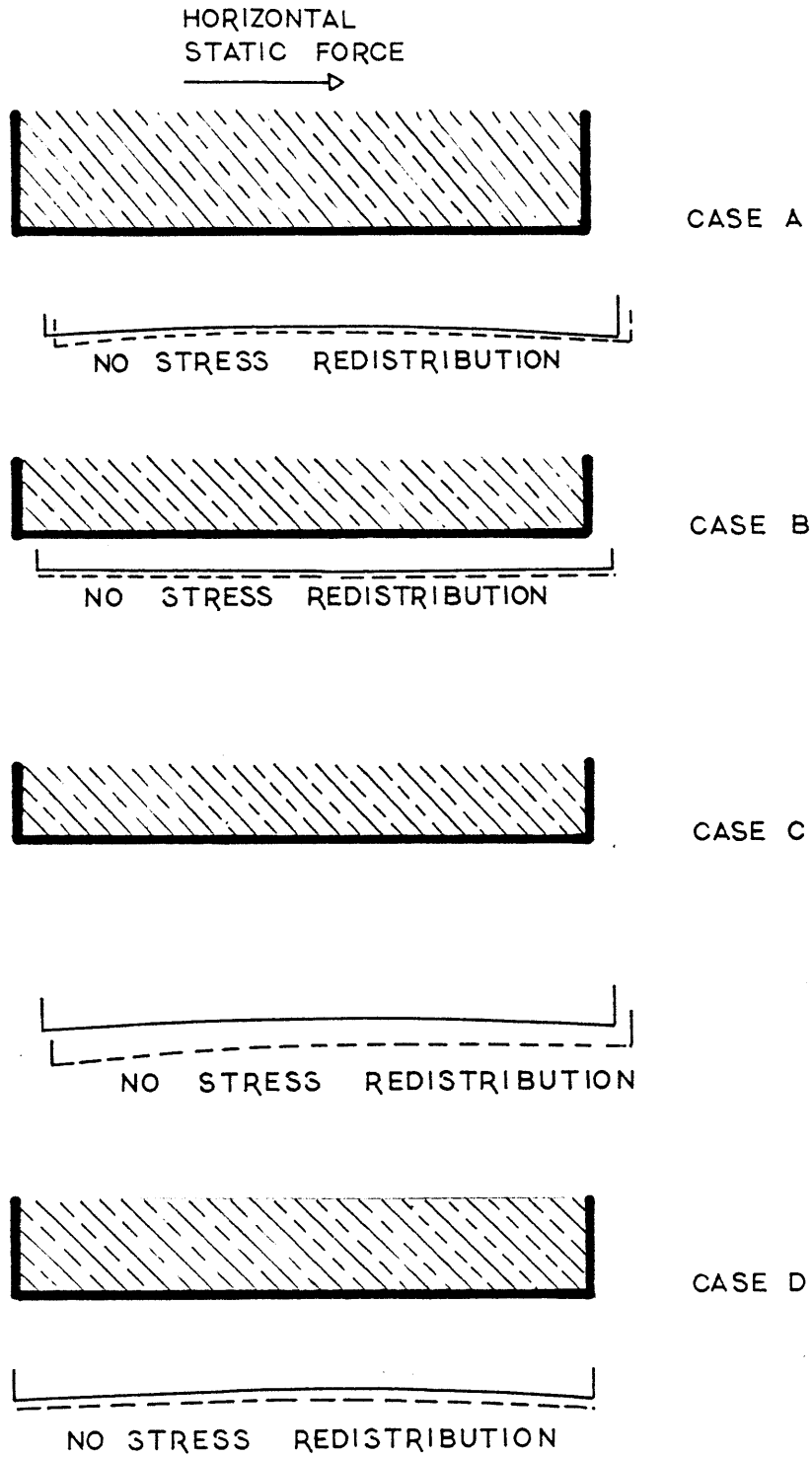


FIGURE 7.8 : Effect of Stress Redistribution on Predicted Permanent Movement

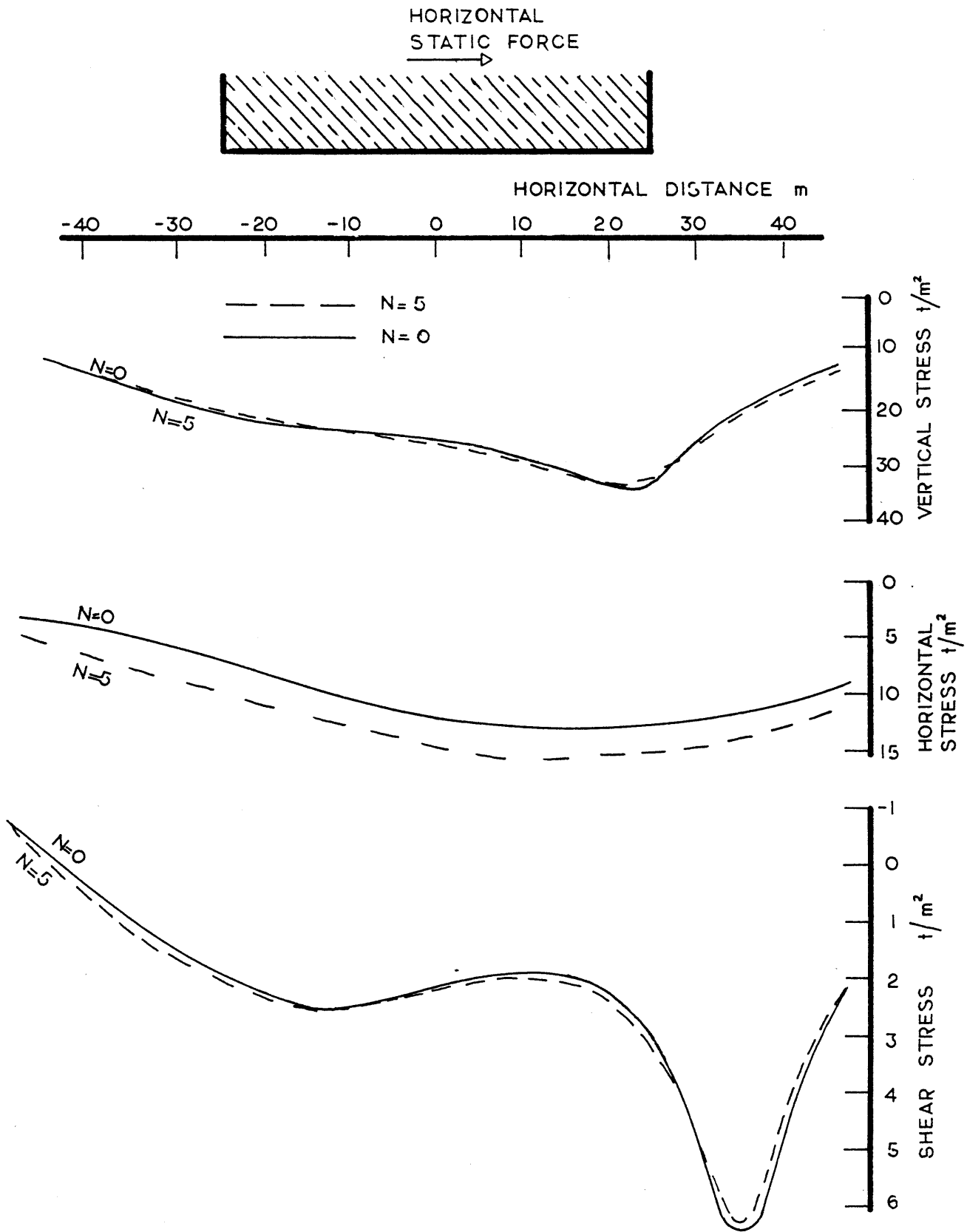


FIGURE 7.9 ; Stresses Applied 4m below the Base of the Pier (CASE A)

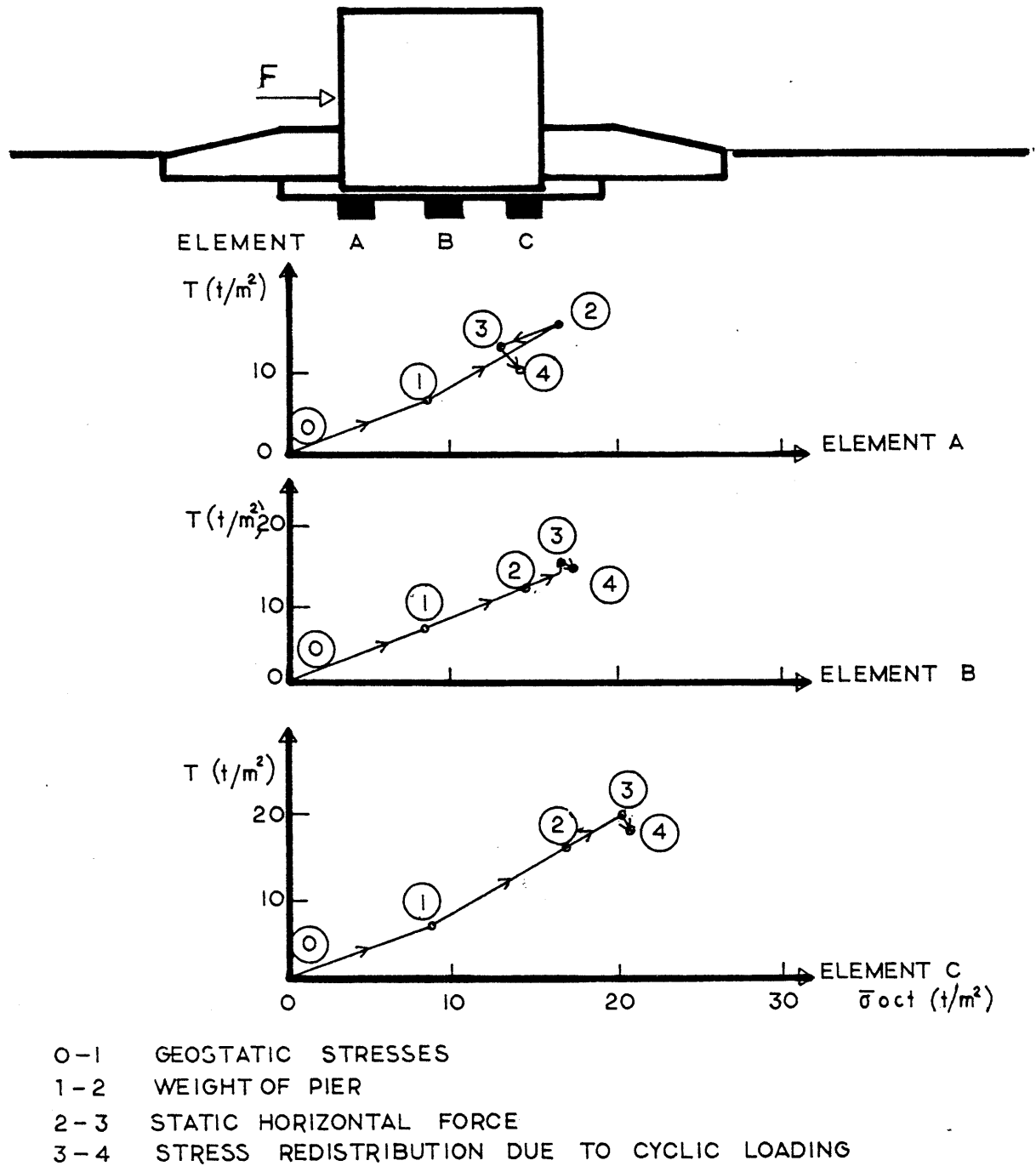


FIGURE 7.10 : Typical Stress Paths below the Base of the Pier

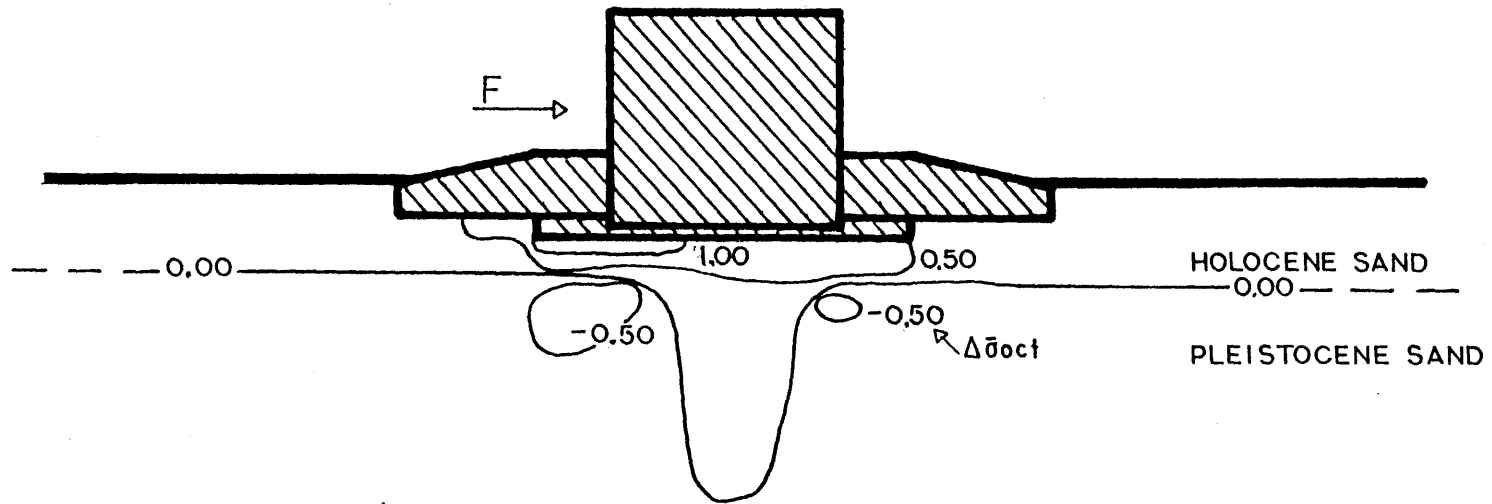


FIGURE 7.11: Contours of Change in Octahedral Stress due to Stress Redistribution (CASE A)

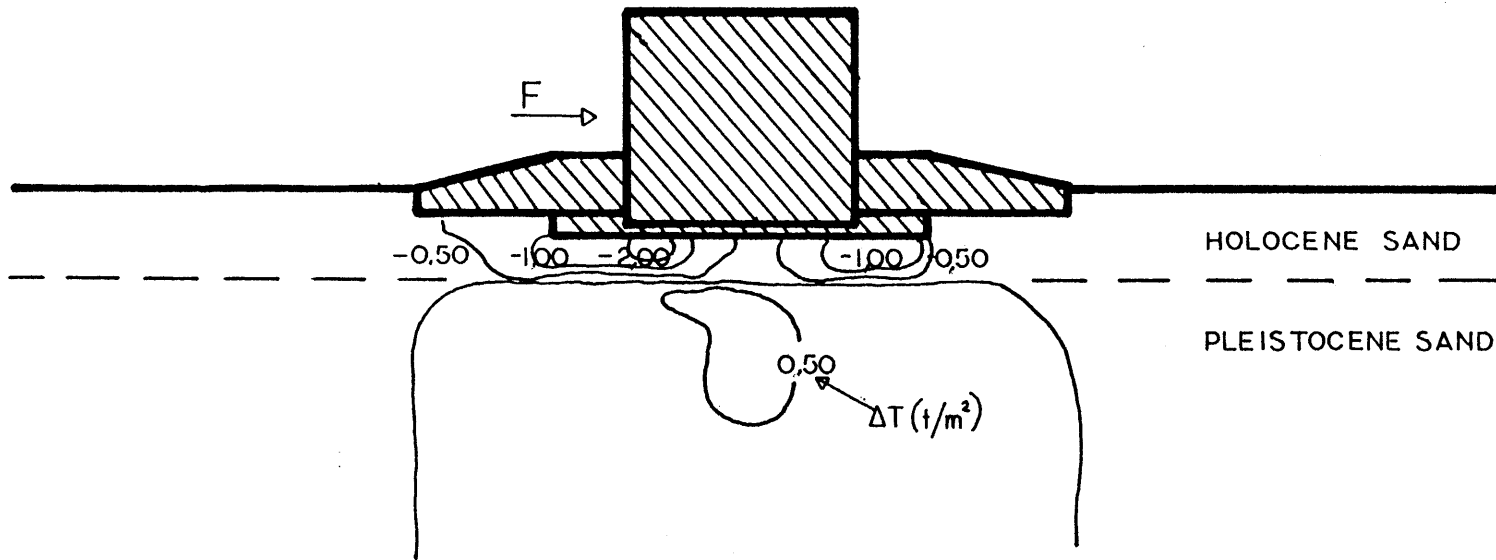


FIGURE 7.12 : Contours of Change in Maximum Shear Stress due to Stress Redistribution (CASE A)

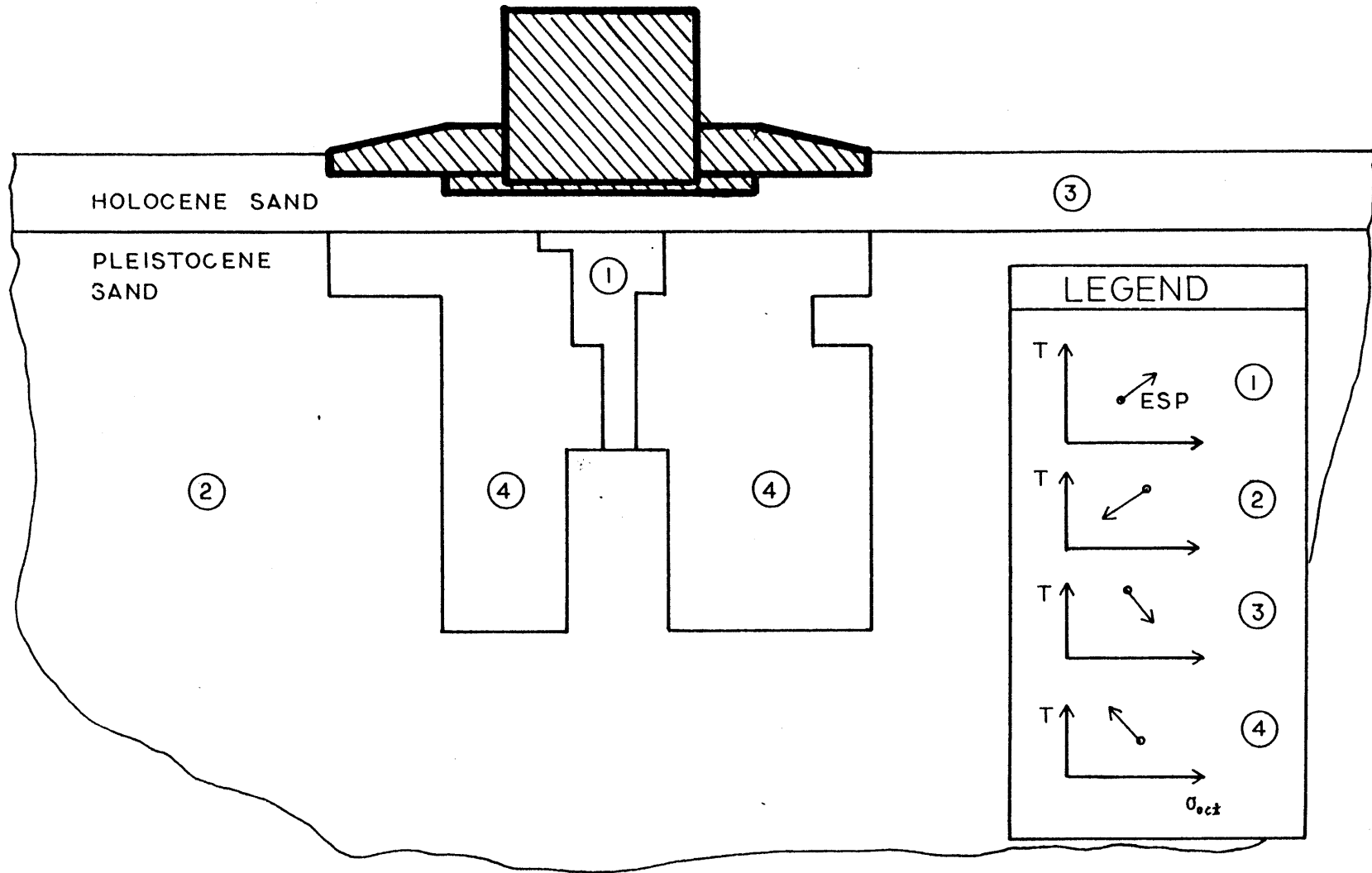


FIGURE 7.13 ; Stress Paths due to Stress Redistribution

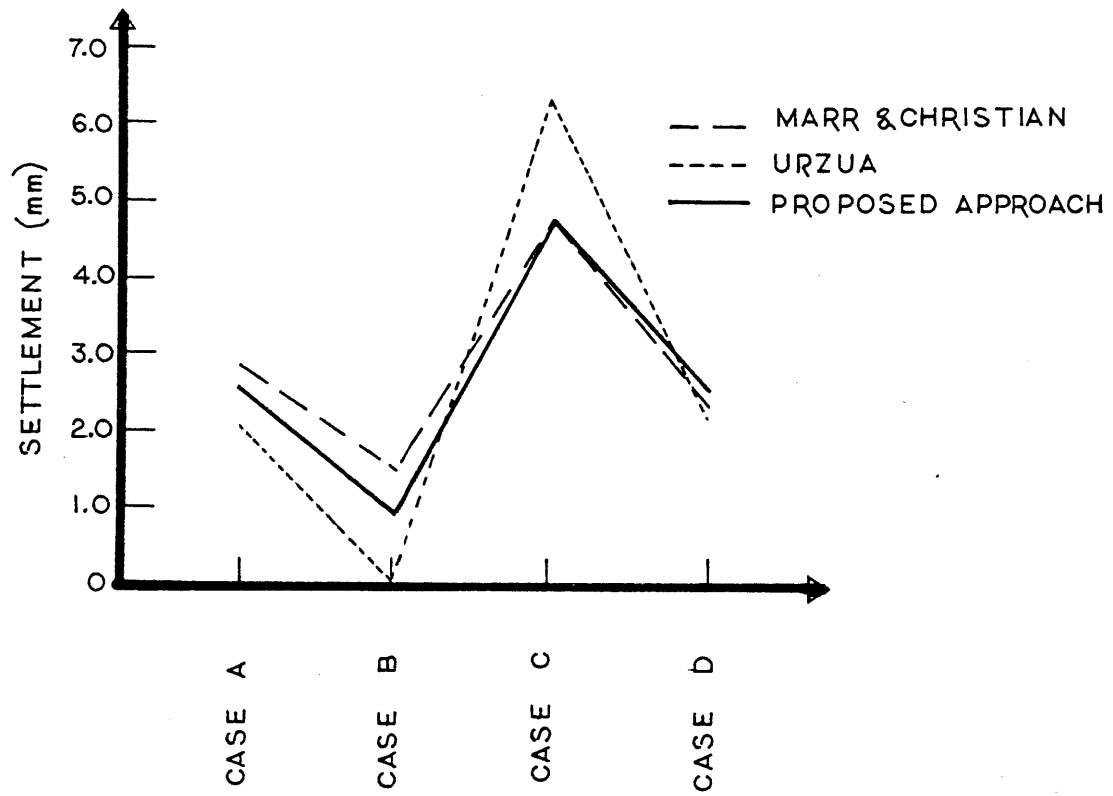


FIGURE 7.14 : Predicted Settlement of the Center of the Pier's Base

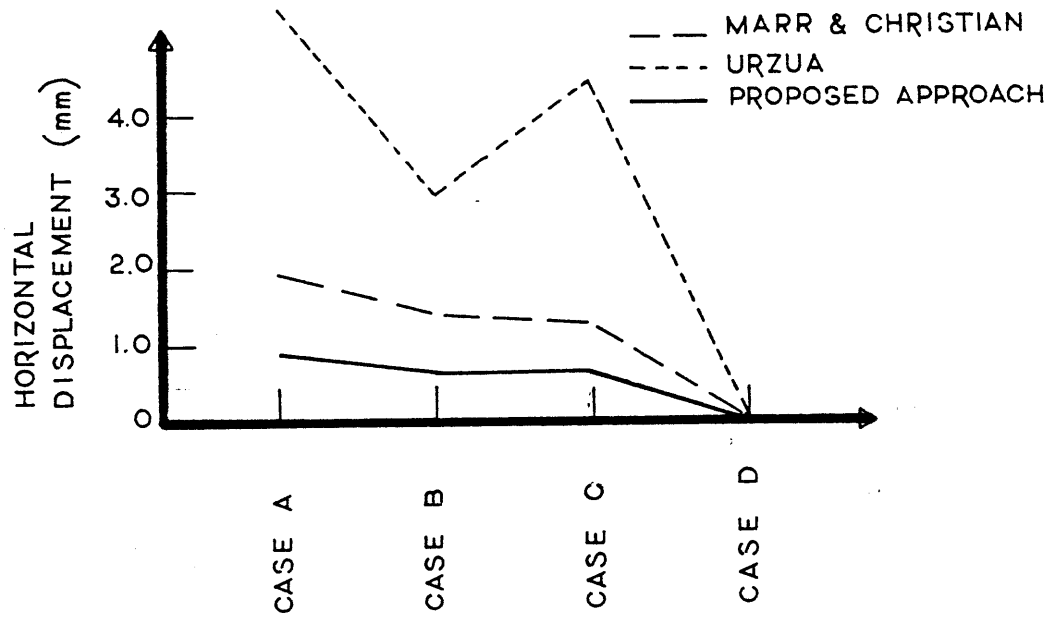


FIGURE 7.15 : Predicted Horizontal Displacement of the Center of the Pier's Base

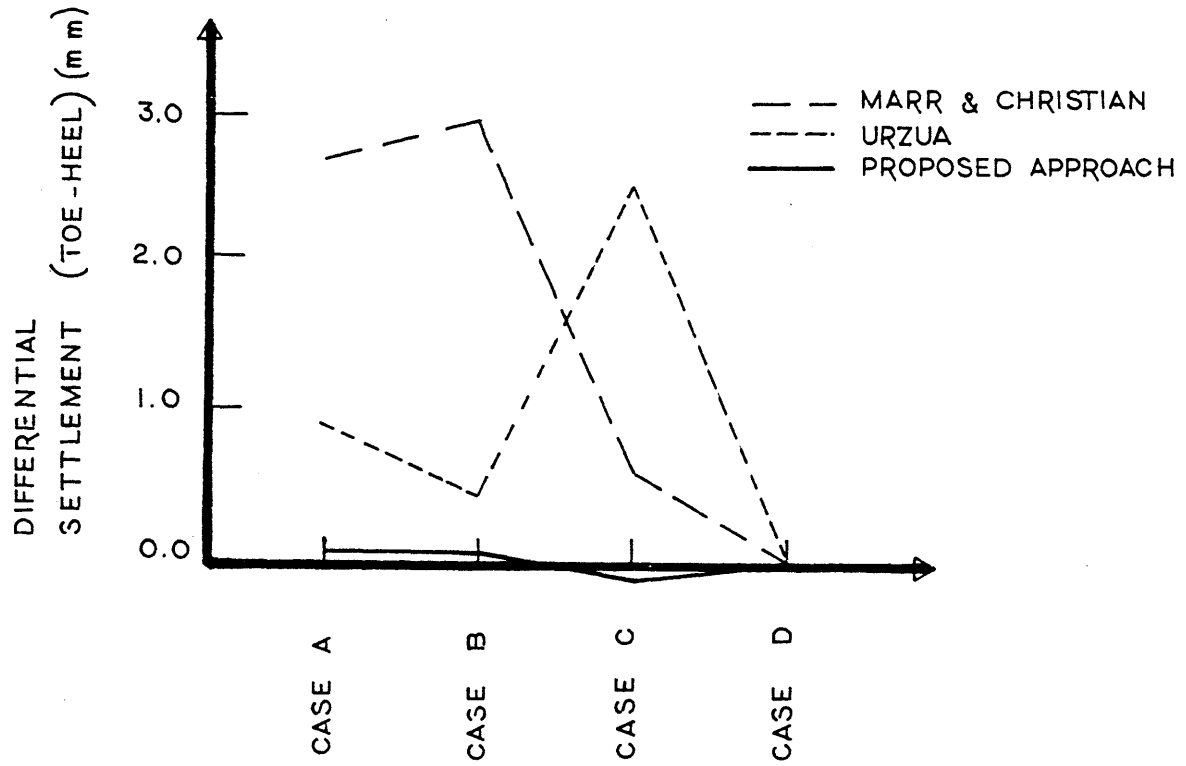


FIGURE 7.16 : Differential Settlement of the Base of the Pier

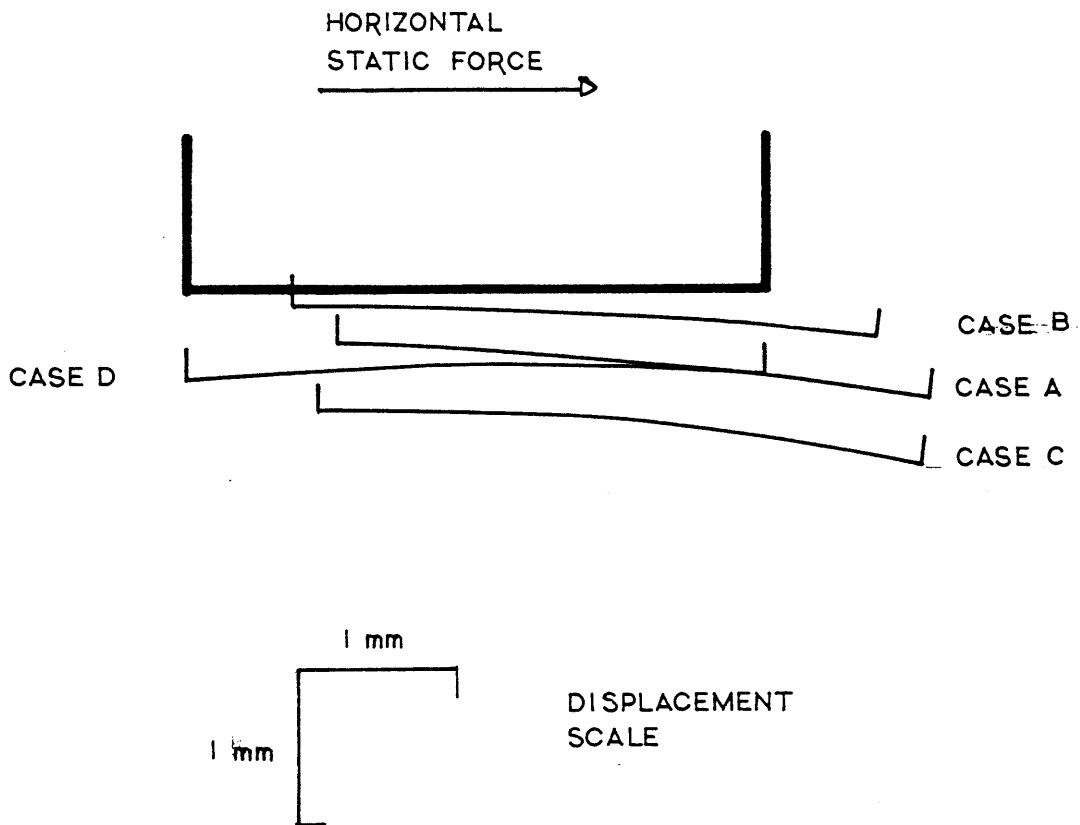


FIGURE 7.17 : Permanent Movement of the Pier due to Undrained Cyclic Loading

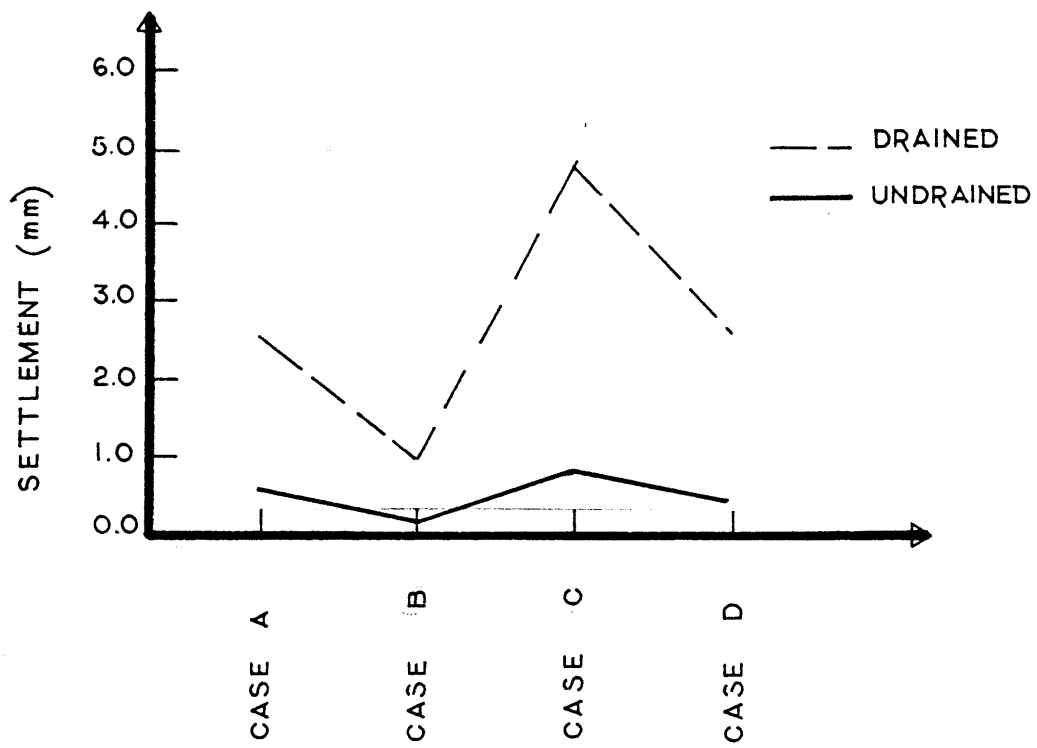


FIGURE 7.18 ; Permanent Settlement of the Center of the Pier's Base
- Effect of Drainage

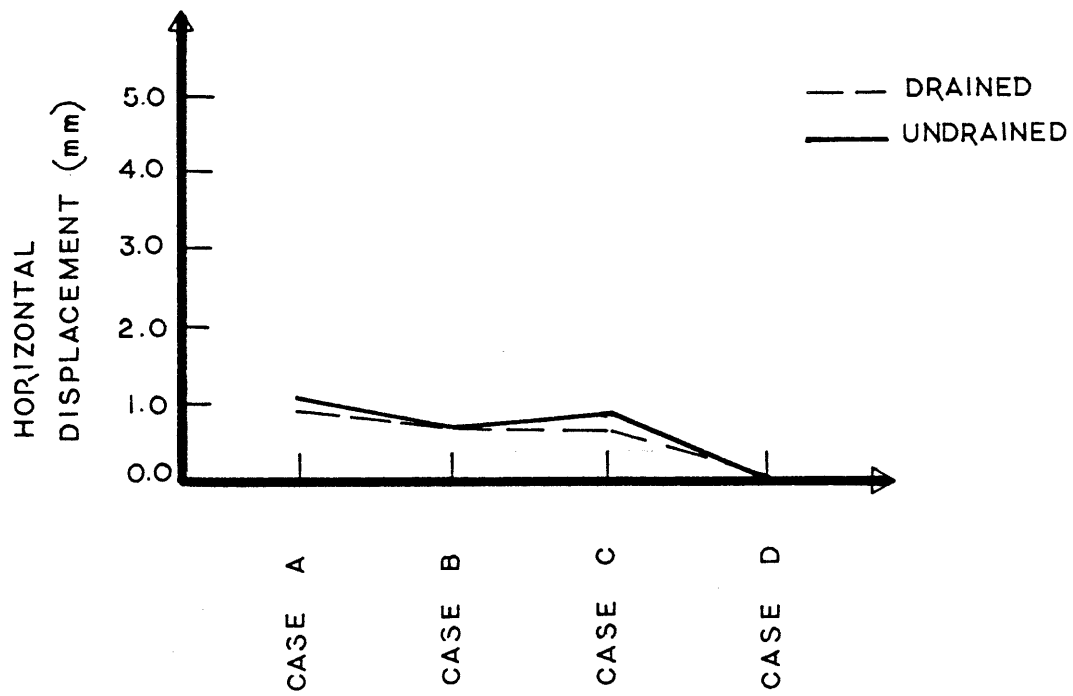


FIGURE 7.19 : Permanent Horizontal Displacement of the Center of the Pier's Base - Effect of Drainage

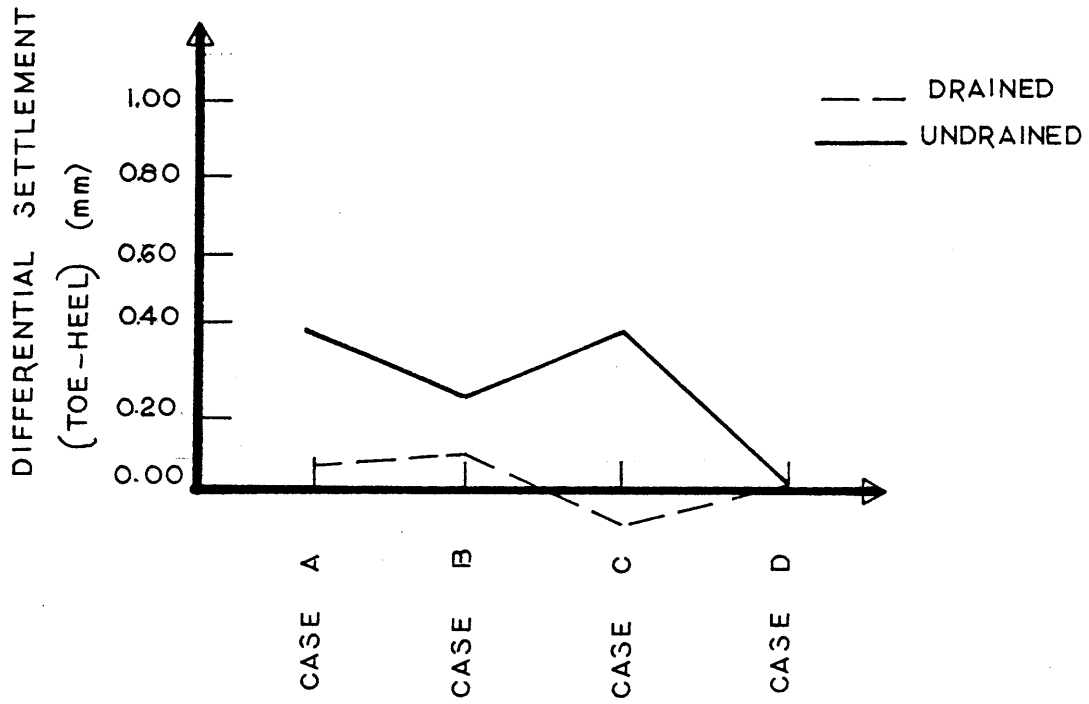
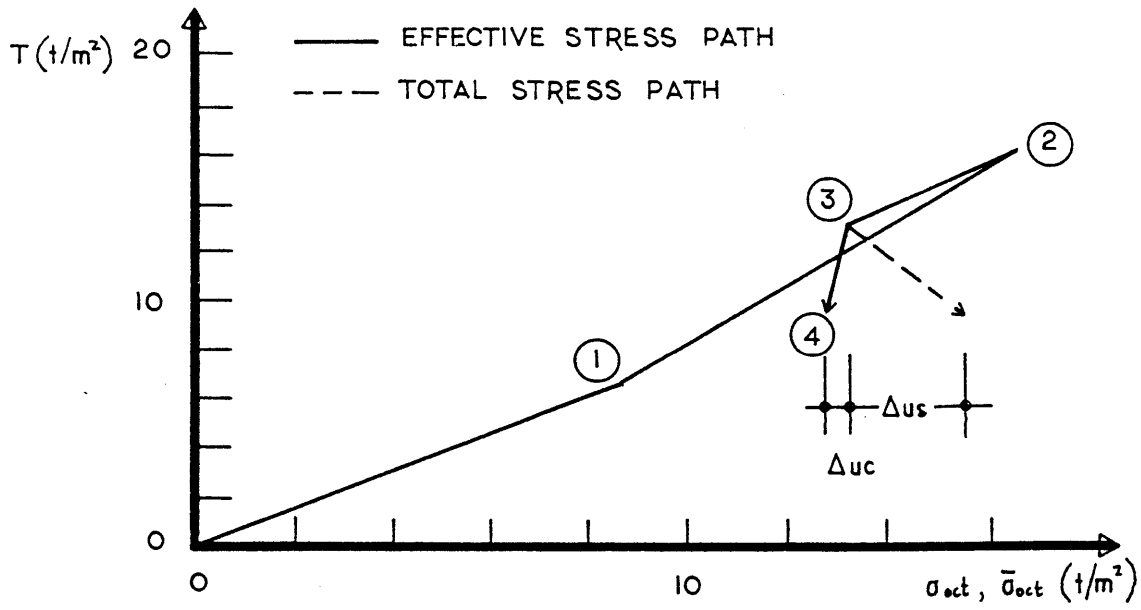


FIGURE 7.20 : Permanent Differential Settlement of the Base of the Pier
-Effect of Drainage



- Δu_c EXCESS PORE PRESSURE DUE TO CYCLIC LOADING
 Δu_s EXCESS PORE PRESSURE DUE TO STRESS REDISTRIBUTION
 0-1 GEOSTATIC STRESSES
 1-2 INSTALLATION OF PIER
 2-3 TIDE FORCE
 3-4 STRESS REDISTRIBUTION DUE TO CYCLIC LOADING

FIGURE 7.21 : Stress Paths 4 m below the Heel of the Pier during Undrained Cyclic Loading (CASE A)

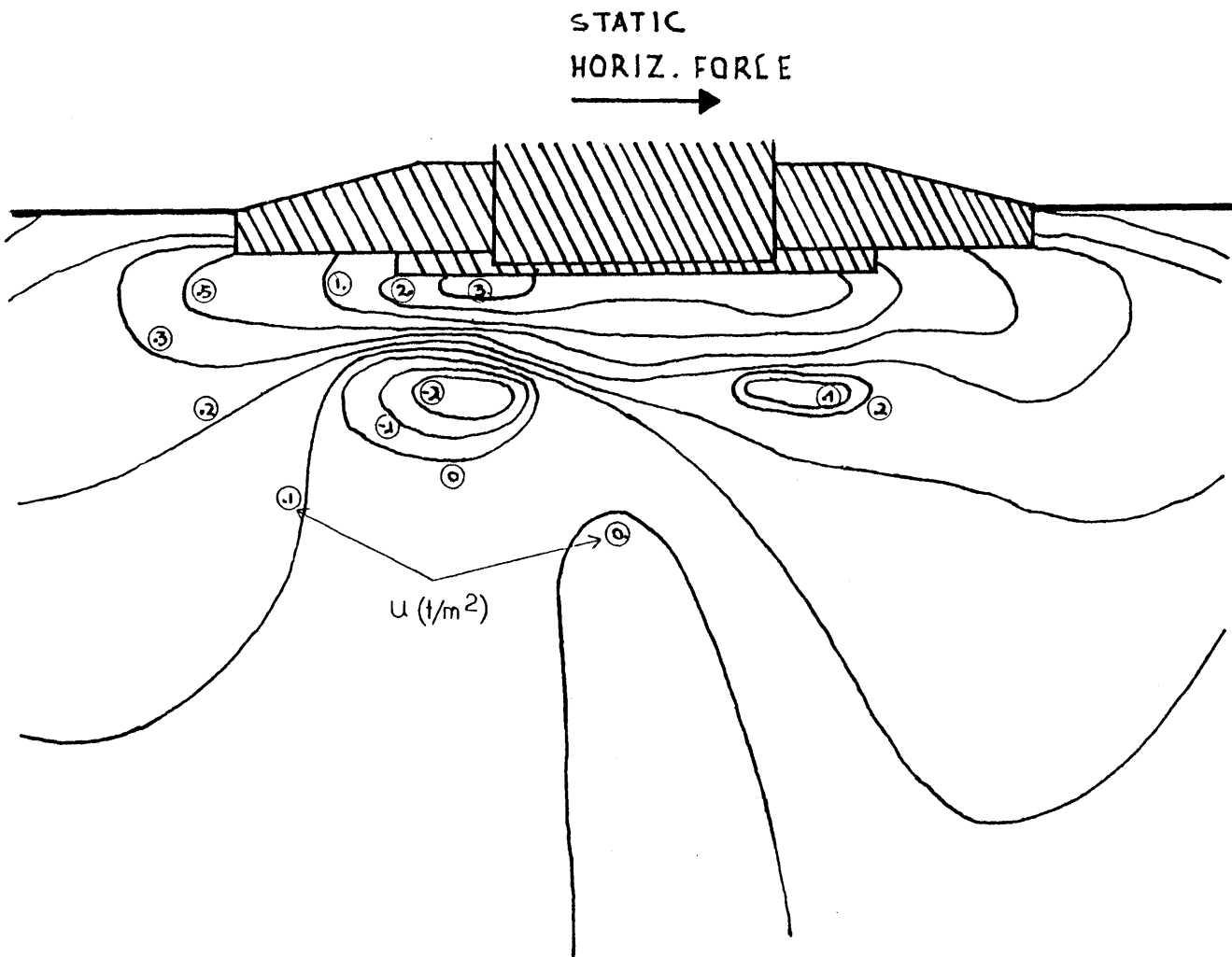


FIGURE 7.22 : Excess Pore Pressure Contours due to Cyclic
Loading (CASE A)

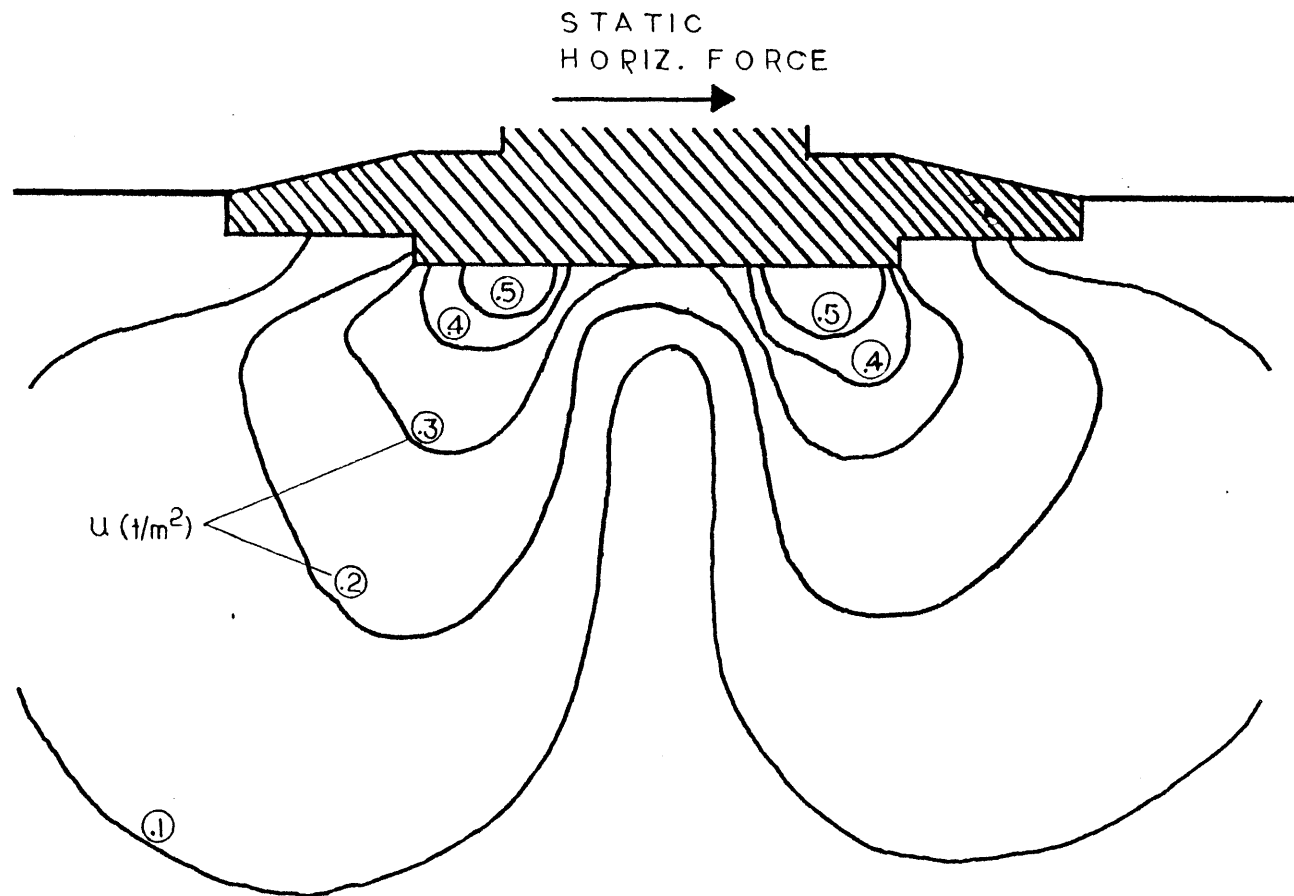


FIGURE 7.23 : Excess Pore Pressure Contours due to Cyclic Loading - Simplified approach (CASE A)

CHAPTER 8

SUMMARY AND CONCLUSIONS8.1 SUMMARY

An analytical method was developed to predict the permanent displacement of soils that results from cyclic loading under drained and undrained conditions. The basic characteristic of the method is that it focuses on the stress and strain accumulated at the end of one cycle of loading instead of predicting the soil response within the cycle.

The method is based on two empirical relations between permanent strain and number of cycles in drained cyclic triaxial compression tests: one for the permanent volumetric and one for the permanent vertical strain. For Sand A the relations proposed by Hodge [22] and Wooten [60] were used as a starting point. Major modifications were necessary in order to:

- (i) Include the effects of the direction of the cyclic stress path
- (ii) Cover cyclic loading with a negative mean shear stress
- (iii) Cover irregular cyclic loading
- (iv) Distinguish between contraction and dilation due to cyclic loading.

To be able to analyze cyclic loading under general boundary and loading conditions, the modified relations were used to define the viscosity constants of a three dimensional, isotropic Maxwell Fluid model where time has been replaced by the number of cycles. The elastic moduli appearing in the model are defined as functions of the effective octahedral stress, soil porosity and stress path direction. The resulting constitutive model is in incremental form, being thus able to account for changes in the average and cyclic state of stress, as well as in the soil properties during cyclic loading.

The model is evaluated by comparison with results from cyclic oedometer tests, and undrained cyclic triaxial tests in compression, in extension, and isotropic; those tests provide boundary conditions different from drained cyclic triaxial tests used to determine the required parameters.

The model predicted correctly the basic trends that stress and strain accumulation followed in the cyclic oedometer tests and the undrained cyclic triaxial tests. The magnitude of the predicted strain, pore pressure and stress accumulation was in good agreement

with values measured in part of the oedometer tests, and in all the undrained triaxial compression and isotropic tests

The model's quantitative predictions did not agree well with one of the two sets of oedometer test data and with cyclic undrained extension test data. Evidence was presented that testing errors may have seriously affected the test results from the cyclic oedometer tests. For undrained cyclic extension tests the difference between predicted and measured response is attributed to material anisotropy not taken into account by the model.

Two dimensional analyses were performed to predict the permanent displacement of the Oosterschelde barrier due to drained and undrained cyclic loading. The predicted permanent movement under drained conditions agrees well with the trends observed during a model caisson test in Neeltje Jans [4], as well as with results from previous analyses of the same structure [6], [7]. Displacement predictions neglecting the effect of stress redistribution around the foundation were generally conservative.

Permanent settlements predicted for undrained cyclic loading were five times less than for drained cyclic loading, while differential settlement was two to six times larger. The effect of drainage conditions on predicted horizontal displacement was not significant. Finally it was found that neglecting the effect of stress redistribution on pore pressure accumulation may lead to considerably wrong predictions.

8.2 CONCLUSIONS

Three major conclusions result from the presented analysis:

(i) The "cumulative strain" approach offers a rational means of solving the difficult problem of predicting permanent displacements from cyclic loading

(ii) Permanent displacements under various boundary conditions and drained or undrained constraints can be predicted by a simple model, fitted to the results of common static tests and relatively simple drained cyclic triaxial tests

(iii) Combination of the proposed model for cyclic sand behavior with the finite element method provides the means for the prediction of the permanent deformation of foundations due to cyclic loading.

8.3 FUTURE RESEARCH

Four different categories of research are recommended for the future: numerical analyses with the computer program FEAP-CYC, experiments, soil modeling and numerical modeling.

NUMERICAL ANALYSES

Use the computer program FEAP-CYC to evaluate the performance of

two dimensional foundations under various loading and drainage conditions. Earth dams under earthquake loading and tension or compression piles under cyclic axial loading are two examples of case studies of practical interest.

The proposed method can be also used to "calibrate" simple models for the prediction of permanent displacements of foundations, where soil is modelled by springs and dashpots. Such models cannot give much insight into the interaction of the different factors governing permanent displacement, but they are relatively simple and inexpensive to use.

EXPERIMENTS

Cyclic laboratory tests on sand are recommended to give information about the following aspects

- Shear and volumetric strain accumulation for stress states near the CT-line
- Minimum volume reached by drained cyclic loading
- Permanent strain accumulation in the surcharacteristic domain

Static laboratory tests on sand are necessary to define better the dependency of elastic soil moduli, on soil properties and stress path characteristics.

Cyclic and static laboratory tests on clays and silts are recommended for the extension of the model presented in the thesis to cover clay materials. The objectives of this laboratory program should be:

- To establish a general behavioral pattern for the cyclic behavior of clays similar to that described in chapter 3 of the thesis
- To define an empirical relation between permanent volumetric strain and number of cycles, and also to define a similar relation for shear strain
- To relate elastic soil moduli with soil properties, stresses and stress path characteristics.

SOIL MODELLING

To improve the predictive capability of the model presented here modifications are necessary in order to

- include the effects of anisotropy on the cyclic behavior of sand
- obtain better predictions of the response of the sand due to static stress changes

The extension of the model to clays and silts will also require a major modelling effort because the cyclic response of clays and silts is, in some aspects, different than the response of sands [29,30,31].

NUMERICAL MODELLING

The Finite Element program FEAP-CYC can solve two dimensional problems only. Many practical problems, however, are three dimensional and cannot be realistically idealized as two dimensional ones. One such example is the displacement of laterally loaded piles. To solve similar problems FEAP-CYC has to be extended to cover three

dimensional stress and strain conditions.

The cyclic stresses for each element of the foundation are computed using a static analysis. When cyclic loading has high frequency, the cyclic stresses are generally different than those predicted by a static analysis, due to inertia effects. To account for such effects FEAP-CYC has to be extended to solve dynamic in addition to static problems.

The proposed analysis applies to cyclic loading under drained or fully undrained conditions. Partially undrained conditions, however, are also common in practice due to the long duration of some categories of cyclic loads (i.e. storms). Introduction of consolidation occurring in parallel with the cyclic loading would increase the practical value of the program.

Finally the analysis presented here treated the foundation with the underlying soil as a continuous medium. When the stiffness of the foundation is significantly different from the stiffness of the soil, slippage or "gap" may develop in the foundation soil interface. To account for the effects of such discontinuities on the prediction of permanent deformations, special contact elements must be added to the program.

LIST OF REFERENCESAbbreviations

<u>ASCE</u>	American Society of Civil Engineers
<u>ASTM</u>	American Society for Testing and Materials
<u>ICSMFE</u>	International Conference on Soil Mechanics and Foundation Engineering
<u>JEMD</u>	Journal of Engineering Mechanics Division
<u>JGED</u>	Journal of the Geotechnical Engineering Division
<u>JSMFD</u>	Journal of the Soil Mechanics and Foundation Division
<u>M.I.T</u>	Massachusetts Institute of Technology

1. Lambe T.W. (1977) : "Caisson Test-Neeltje Jans", Oosterschelde Storm Surge Barrier Project, Report prepared for Rijkwaterstaat Deltadienst, Carlisle, Massachusetts-U.S.A, August
2. Bea R.G., Audibert J.M.E. (1979): "Performance of Dynamically Loaded Pile Foundation", BOSS'79, Paper 68, Imperial College, London, England, 28-31 August
3. Van Weele A.F. (1979): "Pile Bearing Capacity under Cyclic Loading Compared with that under Static Loading", BOSS'79, Paper 36, Imperial College, London, England, 28-31 August
4. Lambe T.W., Boehmer J.W., Rosenbrand W.F. (1978): "Caisson Tests at Neeltje Jans, The Netherlands", Symposium on Foundation Aspects of Coastal Structures, Proceedings, Vol 2, Delft, the Netherlands, 9-12 October
5. Hedberg J. (1977): "Cyclic Stress-Strain Behavior of Sand in Offshore Environment", PhD Dissertation, M.I.T., Cambridge, MA
6. Urzua A. (1980): "Analysis of Permanent Displacements from Cyclic Loading of Foundations", PhD Dissertation, M.I.T., Cambridge, MA
7. Marr W.A., Christian J.T. (1981): "Permanent Deformations due to Cyclic Loading", JGED, ASCE, Vol 107, GT8, August, pp 1129-1149
8. Prevost J.H. (1978): "Anisotropic Stress-Strain Behavior of Clays", JGED, ASCE, Vol 104, G8, August

9. Prevost J.H. (1979): "Mathematical Modeling of Soil Stress-Strain Strength Behavior", International Conference on Numerical Methods in Geomechanics, Aachen, 2-6 April, pp. 347-361
10. Mroz Z., Norris V.A., Zienkiewicz O.C. (1978): "An Anisotropic Hardening Model for Soils and its Application to Cyclic Loading", Int. Journal for Numerical and Analytical Methods in Geomechanics, 2:203-221
11. Mroz Z., Norris V.A., Zienkiewicz O.C. (1979): "Application of an Anisotropic Hardening Model in the Analysis of Elastoplastic Deformations of Soils", Geotechnique, 29(1), pp. 1-34
12. Van Eekelen H.A.M. (1980): "Fatigue Models for Cyclic Degradation of Soils", Int. Symposium on Soils under Cyclic and Transient Loading, Swansea, pp. 447-450
13. Lee K.L. (1974): "Seismic Permanent Deformations in Earth Dams", UCLA-ENG7497, Report to the National Science Foundation, School of Engineering and Applied Science, University of California, LA
14. Serf N., Seed H.B., Makdisi F.I., Chang C.Y. (1976): "Earthquake Induced Deformation of Earth Dams", Report No. EERC 76-4, Earthquake Engineering Research Center, University of California, Berkeley
15. Dumas F., Lee K.L. (1980): "Cyclic Movement of Offshore Structures on Clays", JGED, ASCE, Vol 106, GT8, pp. 877-897
16. Poulos H.G. (1980): "Analysis of Cyclic Axial Response of a Single Pile", Research Report No. R362, School of Civil Engineering, the University of Sydney
17. Smits F.P., Andersen K.H., Gudehus G. (1978): "Pore Pressure Generation", Symposium on Foundation Aspects of Coastal Structures, Delft, the Netherlands, 9-12 October, Vol 1
18. Chang C.S. (1981): "Residual Pore Pressure and Deformation Behavior of Soil Samples Under Variable Cyclic Loading", Xth ICSMFE, Stockholm, June
19. Quelerij L., Broeze J.J. (1978): "Model Tests on Piers Scale 1:10", Symposium on Foundation Aspects of Coastal Structures, Delft, the Netherlands, 9-12 October
20. Rowe P.W., Craig W.H. (1978): "Prediction of Caisson and Pier Performance by Dynamically Loaded Centrifugal Models", Symposium on Foundation Aspects of Coastal Structures, Delft, the Netherlands, 9-12 October
21. Martin G.R., Finn W.D.L., Seed H.B. (1975): "Fundamentals of Liquefaction Under Cyclic Loading", JGED, ASCE, Vol 101, GT5, May, pp. 423-438
- 22a. Hodge W.E. (1978): "A Relationship between the Drained and Undrained Cyclic Behavior of Sand", S.M. Thesis, M.I.T.

- 22b. Hodge W.E., Marr W.A. (1979): "A Relationship between the Drained and Undrained Behavior of Sand", M.I.T., Research Report R79-23, June, Order NO. 645
23. Martin G.R., Finn W.D.L., Seed H.B. (1978): "Effects of System Compliance on Liquefaction Tests", JGED, ASCE, Vol 104, GT4, pp. 739-758
24. Zienkiewicz O.C. (1978): "The Finite Element Method", Mc Graw Hill, London
25. Luong M.P., Sidaner J.F. (1981): "Undrained Behaviour of Cohesionless Soils under Transient and Cyclic Loading", Inter. Conference on Recent Advances in Geotechnical Eng. and Soil Dynamics, St Louis, MO, April
26. Luong M.P., Sidaner J.F. (1981): "Comportment Cyclique et Transitoire des Sables", Xth ICSMFE, Stockholm, June
- 27a. Youd T.L. (1972): "Compaction of Sands by Repeated Shear Straining", JSMFD, ASCE, Vol 98, Sm7, pp. 709-725
- 27b. Youd T.L. (1971): "Maximum Density of Sands by Repeated Straining in Simple Shear", Highway Research Record No 374, pp. 1-6
28. Schofield A.N., Wroth C.P. (1968): "Critical State Soil Mechanics", New York, Mc Graw Hill Book Co.
29. Sangrey D.A., Henkel D.J., Esrig M.I. (1969): "The Effective Stress Response of a Saturated Clay Soil to Repeated Loading", Canadian Geotechnical Journal, Vol 6, No 3, Ottawa, Canada, August
30. France J.W., Sangrey D.A. (1977): "Effect of Drainage on Repeated Loading of Clays", JGED, ASCE, Vol 103, GT6, pp. 769-785
31. Sangrey D.A., Castro G., Poulos S.J., France J.W. (1978): "Cyclic Loading Sands, Silts and Clays", Earthquake Engineering Conference, Pasadena, California, June
32. Seed H.B., Lee K.L. (1966): "Liquefaction of Saturated Sands during Cyclic Loading", JSMFD, ASCE, Vol 92, SM6, pp. 105-134
33. Ishihara K., Tatsuoka F., Yasuda S. (1975): "Undrained Deformation and Liquefaction of Sand under Cyclic Stresses", Soils and Foundations Journal, Vol 15, No 1, March, pp. 29-44
34. Ishihara K., Okada S. (1978): "Effects of Stress History on Cyclic Behavior of Sand", Soils and Foundations Journal, Vol 18, No 4, December, pp. 31-45
35. Mroz Z., Norris V.A., Zienkiewicz O.C. (1979): "Application of an Anisotropic Hardening Model in the Analysis of Elastoplastic Deformations of Soils", Geotechnique 29, No 1, pp. 1-34

36. Kavvadas M. (1982): "Non-Linear Consolidation around Piles", PhD Dissertation, M. I. T., Cambridge, MA
37. Lade P.V., Duncan J.M. (1978): "Elastoplastic Stress-Strain Theory for Cohesionless Soil", JGED, ASCE, Vol 104, February, pp. 193
38. Prevost J.H. (1978): "Plasticity Theory for Soil Stress-Strain Behavior", JEMD, ASCE, EM5, October, pp. 1177-1193
39. Lambe T.W. and Associates (1977): "Static Triaxial Tests on Oosterschelde Sands", Document L-38, prepared for Rijkwaterstaat, Deltadienst, the Hague, the Netherlands, September
40. Lambe T.W. and Associates (1977): "Cyclic Triaxial Tests on Oosterschelde Sands", Document L-39, prepared for Rijkwaterstaat, Deltadienst, the Hague, the Netherlands, September
41. Ko H.Y., Scott R.F. (1967): "Deformation of Sand in Hydrostatic Compression", JSMFD, ASCE, Vol 93, No SM3, pp. 137-156
42. El-Sohby M.A., Andrawes K.Z. (1972): "Deformation Characteristics of Granular Materials under Hydrostatic Compression", Canadian Geotechnical Journal, Vol 9, pp. 338-350
43. Silver M.L., Seed H.B. (1971): "Volume Changes in Sands during Cyclic Loading", JSMFD, ASCE, Vol 97, No SM9, pp. 1171-1182
44. Hardin B.O. (1978): "The Nature of Stress-Strain Behavior for Soils", Proceedings, Earthquake Engineering Conference and Soil Dynamics, ASCE, Geotechnical Engineering Division, Vol I, pp. 3-90, 19-21 June
45. Hardin B.O., Drnevich V.P. (1972): "Shear Modulus and Damping in Soils: Design Equation and Curves", JSMFD, ASCE, Vol 98, No SM7, July, pp. 667-692
46. Hardin B.O. (1972): "Effects of Strain Amplitude on the Shear Modulus of Soils", Technical Report No. AWFL-TR-72-201, Air Force Weapons Laboratory, Kirtland Air Force Base, NM, November, 63 pages
47. Richart F.E., Jr (1977): "Dynamic Stress-Strain Relations for Soils, State of the Art Report", Proc, 9th ICSMFE, Tokyo, Vol 2, pp. 603-612
48. Kodner R.L. (1963): "Hyperbolic Stress-Strain Response: Cohesive Soils", JSMFD, ASCE, Vol 89, No SM1, February, pp. 115-143
49. Kodner R.L. (1963): "Void Ratio Effect on the Hyperbolic Stress-Strain Response of a Sand", Proceedings Second Pan-American Conference on Soil Mechanics and Foundation Engineering, Vol 1, pp. 289-333
50. Duncan J.M., Chang C.Y. (1970): "Nonlinear Analysis of Stress and Strain in Soils", JSMFD, ASCE, Vol 96, No SM5, September, pp. 1629-1653

51. Duncan J.M., Byrne P., Wong K.S., Mabry P. (1979): "Strength Stress-Strain and Bulk Modulus Parameters for Finite Element Analysis of Stresses and Movements in Soil Masses", Geotechnical Engineering Report, Univ. of California, Berkeley
52. Lee K.L., Chan C.K. (1972): "Number of Equivalent Significant Cycles in Strong Motion Earthquakes", Proceedings, International Conference on Microzonation, University of Washington, Seattle, Washington, Vol II, pp. 609-627
53. Annaki M., Lee K.L. (1976): "Equivalent Uniform Cycle Concept for Soil Dynamics", ASCE National Convention, Philadelphia, PA, Preprint 2752
54. Seed H.B., Idriss I.M., Makdissi F., Banerjee N. (1975): "Representation of Irregular Stress Time Histories by Equivalent Uniform Stress Series in Liquefaction Analysis", Research Report No. EERC 75-29, Univ. of California, Berkeley
55. Valanis K.C. (1971): "A Theory of Viscoplasticity without a Yield Surface", Archives of Mechanics, 23, 4, pp. 517-533, Warszawa
56. Ansal A.M., Bazant Z.P., Krizek R.J. (1979): "Viscoplasticity of Normally Consolidated Clays", JGED, ASCE, GT4, pp. 519-537
57. Martin G.R., Finn W.D.L., Seed H.B. (1978): "Effects of System Compliance on Liquefaction Tests", JGED, ASCE, GT4, pp. 463-479
58. Ko H.Y. (1980): "Data Reduction and Application for Analytical Modeling, State of the Art Paper", ASTM Symposium, Chicago, 25 June
59. Christian J.T., Marr W.A. (1976): "Finite Element Analysis of Hammen Section 25 Oosterschelde Closure", Report to the Rijkswaterstaat Deltadienst, the Hague, Netherlands
60. Wooten L. (1980): "An Experimental Evaluation of the Viscoelastic Model for Drained Cyclic Soil Behavior", S.M. Thesis, Civil Engineering Dpt., M.I.T., June
61. Finn W.D.L. (1981): "Liquefaction Potential : Developments Since 1976", Int. Conference on Recent Advances in Geot. Eng. and Soil Dynamics, 26/4 - 3/5, Vol. I, St Louis, MO
62. "Cyclic Triaxial Tests on Oosterschelde Sands", Department of Civil Engineering, M.I.T., R 79-24, Order No. 646, June 1979
63. Bathe K.J., Wilson E.L. (1976): "Numerical Methods in Finite Element Analysis", Prentice Hall Inc., Englewood Cliffs, New Jersey
64. Tong P., Rossettos J.N. (1977): "Finite Element Method : Basic Technique and Implementation", the M.I.T. Press, Cambridge, MA, and London, England
65. Zienkiewicz O.C. (1978): "The Finite Element Method in Engineering Science", Mc Graw Hill, London

66. Lambe T.W. (1961): "Soil Testing for Engineers", John Wiley and Sons Inc., New York
67. Tatsuoka F., Ishihara K. (1973): "Stress Path and Dilatancy Performance of Sand", Proceedings, 8th ICSMFE, Moscow, Vol 1, pp. 419-424
68. Tatsuoka F., Ishihara K. (1974a): "Yielding of Sand in Triaxial Compression", Soils and Foundations, Vol 14, No. 2, pp.63-76
69. Tatsuoka F., Ishihara K. (1974b): "Drained Deformation of Sand under Cyclic Stresses Reversing Direction", Soils and Foundations, Vol. 14, No. 3, pp. 51-65
70. Ishihara K., Tatsuoka F., Yasuda S. (1975): "Undrained Deformation and Liquefaction of Sand under Cyclic Stresses", Soils and Foundations, Vol 16, No. 1, pp. 1-16
71. Ishihara K., Lysmer J., Yasuda S., Hirao H. (1976): "Prediction of Liquefaction in Sand Deposits During Earthquakes", Soils and Foundations, Vol 16, pp. 1-16
72. Ishihara K., Okada S. (1978): "Yielding of Overconsolidated Sand and Liquefaction Model under Cyclic Stresses", Soils and Foundations, Vol 18, No. 1, pp. 57-72
73. Pender M.J. (1981): "Modeling Soil Behavior under Cyclic Loading", Xth ICSMFE, Stockholm June, pp. 57-72
74. Desai C.S., Christian J.T. (1977): "Numerical Methods in Geotechnical Engineering", Mc Graw Hill, New York
75. de Quelerij L., Broeze J.J. (1978): "Model Tests on Piers, scale 1:10", Symposium of Foundation Aspects of Coastal Structures, Proceedings Vol. 2, Delft the Netherlands, 9-12 October
76. Cristian J.T., Audibert J.M.E. (1976): "Analysis of Offshore Concrete Caisson Dikes under Cyclic Loading", Proceedings, Second International Conference in Geomechanics, Vol II, June, pp. 979-990
77. Simon R.M., Christian J.T., Ladd C.C. (1974): "Analysis of Undrained Behavior of Loads on Clays", Proceedings of ASCE Specialty Conference on Analysis and Design in Geotechnical Engineering, Austin, Texas, Vol 1, pp. 51-84
78. Castro G. (1975): "Liquefaction and Cyclic Mobility of Saturated Sands", JGED, ASCE, GT6, June
79. Castro G. (1969): "Liquefaction of Sands", Harvard Soil Mechanics series No. 81, Cambridge, MA, January
80. Fluge Wilhelm: "Viscoelasticity", 2nd Edition, Springer Verlag New York, Heidelberg, Berlin, 1975

APPENDIX ADESCRIPTION OF SAND A

The following description covers grain size distribution, mineralogy, relative density and specific gravity of Oosterschelde Sand A. The information were obtained from an M.I.T. Research Report of Cyclic Triaxial Testing on Oosterschelde Sand A [62].

Oosterschelde Sand A (previously called Oosterschelde Fine Sand) comes from samples taken at Neeltje Jans in the Oosterschelde Bay entrance, off the coast of southern Holland. Sand A has a uniform grain size as shown in Figure A.1 with a mean grain size, d_{50} , of 0.17 mm, and a d_{10} of 0.13 mm. The coefficient of uniformity ($u = d_{60}/d_{10}$) of 1.4 indicates a uniform sand. Sand A has less than 0.5% fines content (percent by weight passing #200 sieve). Sand A, was sieved through #10 sieve prior to testing and grain size analysis to remove large shell fragments and clay lumps. The removed material equaled about 1.5% of the sand by weight.

Observation of Sand A particles under magnification by an electron microscope shows the grains to be subrounded. X-ray diffraction of Sand A indicates 65% quartz, 5% calcite, and remainder dolomite, feldspars and argonite. The soil passing the 10 sieve contained no detectable clay. X-ray diffraction of the clay lumps not passing the #10

sieve indicates their composition as 30% calcite, 25% clay, 20% quartz and less abundant aragonite and feldspars. The clay itself is an illite-smectite with some chlorite and/or kaolinite. Limit determinations on the clay gave a plastic limit of 18.6%, a liquid limit of 45.4% and a plastic index of 26.8%.

The presence of numerous aggregates in the +#60 sieve material comprise a major feature of untested Sand A. These aggregates break down under cyclic loading. Detailed dispersive X-ray analysis shows the aggregates as quartz and feldspar grains cemented by calcium carbonate. The -#60 material contained between untested material and material subjected to cyclic testing in the finer sand fraction. Aggregates made up less than 2% of the total sand samples.

Relative density determination on Sand A adhered to ASTM D-2049-69 with three exceptions. Instead of oven drying prior to testing as specified in the standard, we air dried the sand. The cylinder on top of the 1/2 inch funnel was 3 inches in diameter and 30 inches high. The Soil Test vibratory table used for maximum density determination deviates slightly from ASTM requirements for velocity and acceleration. Table A.1 lists the results of the relative density tests.

Specific gravity determinations adhered to Lambe [66]. A determination performed on an unwashed sample, where salt present in the sand dissolved in the water thus increasing

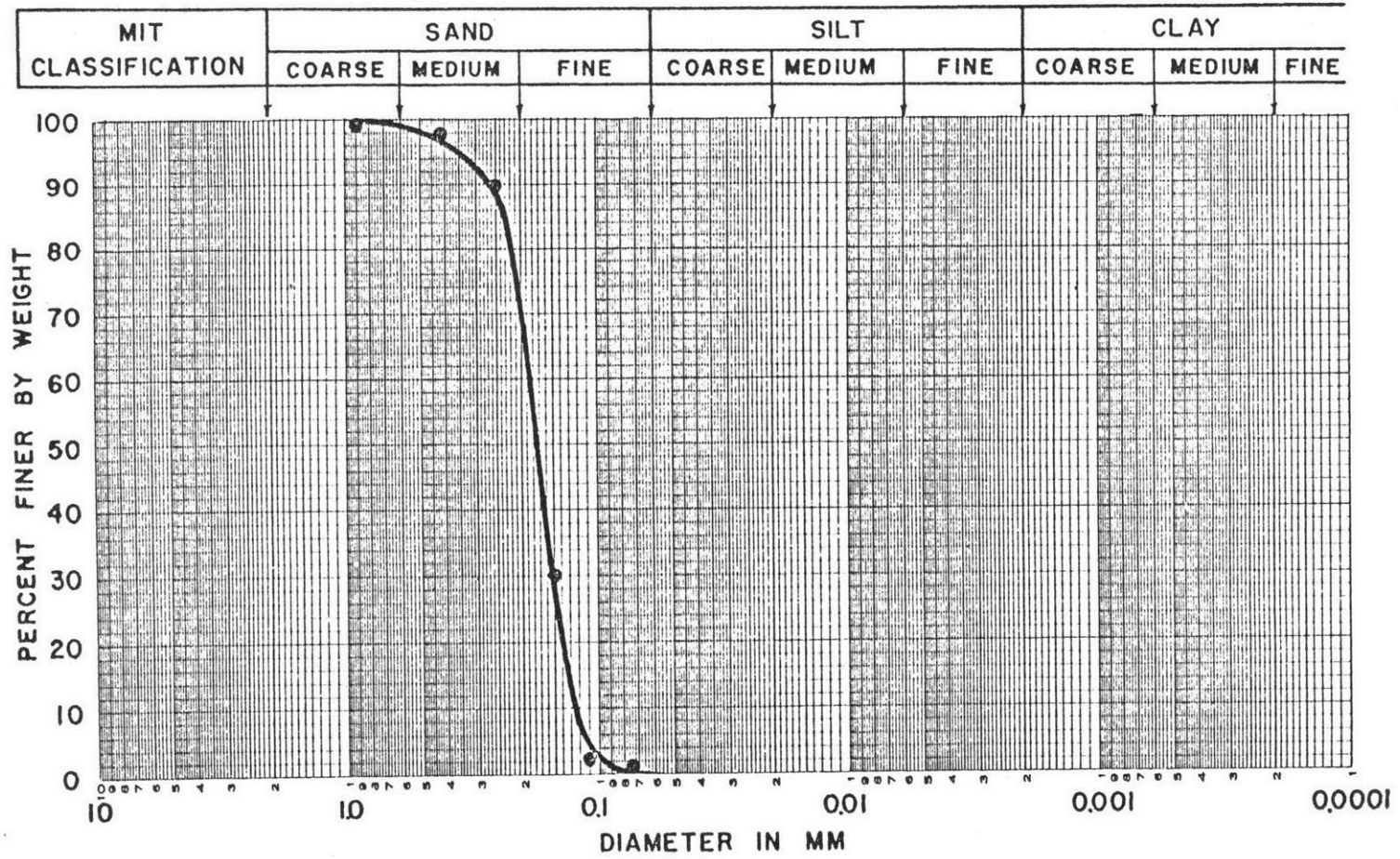
its unit weight, gave a specific gravity $G = 2.62$. Two other determinations, using sand carefully washed through filter paper to remove salt without loss of any sand fractions, gave $G = 2.646$ and $G = 2.643$ for an average specific gravity $G = 2.64$.

G_s	d_{10} (mm)	d_{50} (mm)	d_{90} (mm)	C_u	e_{min}	e_{max}	n_{min} (%)	n_{max} (%)
2,64	0.13	0.17	0,25	1.4	0.527	0.852	34.5*	46.0

* from modified ASTM procedure

TABLE A-1 ; Summary of Basic Characteristics of Sand A

FIGURE A.1 : GRAIN SIZE DISTRIBUTION



APPENDIX BSTRENGTH CHARACTERISTICS OF SAND A

In chapter three it was shown that knowledge of the ultimate strength of the material is necessary in order to be able to predict its response under cyclic loading. In this appendix the strength characteristics of Sand A will be estimated using data from static triaxial tests.

Hedberg [5] used data from drained static triaxial tests to determine the maximum friction angle (ϕ_{\max}) of Sand A; ϕ_{\max} is defined through the relationship:

$$\phi_{\max} = \sin^{-1} \frac{\sigma_v - \sigma_h}{\sigma_v + \sigma_h} \quad \text{maximum} \quad (\text{B.1})$$

Figure B.1 plots ϕ_{\max} versus the initial porosity of the sand as it was reported by Hedberg.

Estimation of the undrained strength of Sand A was done using undrained static triaxial tests. The initial conditions for the examined tests are summarized in table B.1; the test results are plotted in figure B.2 in terms of porosity and confining pressure. The results permit a rather crude estimation of the confining pressure at failure, as a function of porosity.

The undrained shear strength for Sand A can be computed from Figure B.2 through the equation

$$q_f = \sin \phi_{\max} P_f \quad (\text{B.2})$$

The resulting q_f as a function of porosity is plotted in Figure B.3.

Figures B.1 and B.3 define completely the strength of Sand A under both drained and undrained conditions.

TEST	TYPE	σ_{vo} (ksc)	σ_{ho} (ksc)	n %
66	CIU	1.99	2.00	44.7
67	CIU	1.99	2.00	45.1
74	CIU	1.00	1.02	41.4
77	CIU	2.00	2.00	46.6
80	CIU	1.00	1.00	41.3
90	CAU	2.50	2.50	41.1
93	CIU	2.00	2.00	46.3
100	CIU	2.00	2.00	45.9
101	CIU	2.00	2.00	45.6
103	CIU	2.00	2.00	46.2
104	CIU	5.00	5.00	45.2
105	CIU	1.00	1.00	46.2

TABLE B.1 : Summary of Undrained Triaxial Tests on Sand A

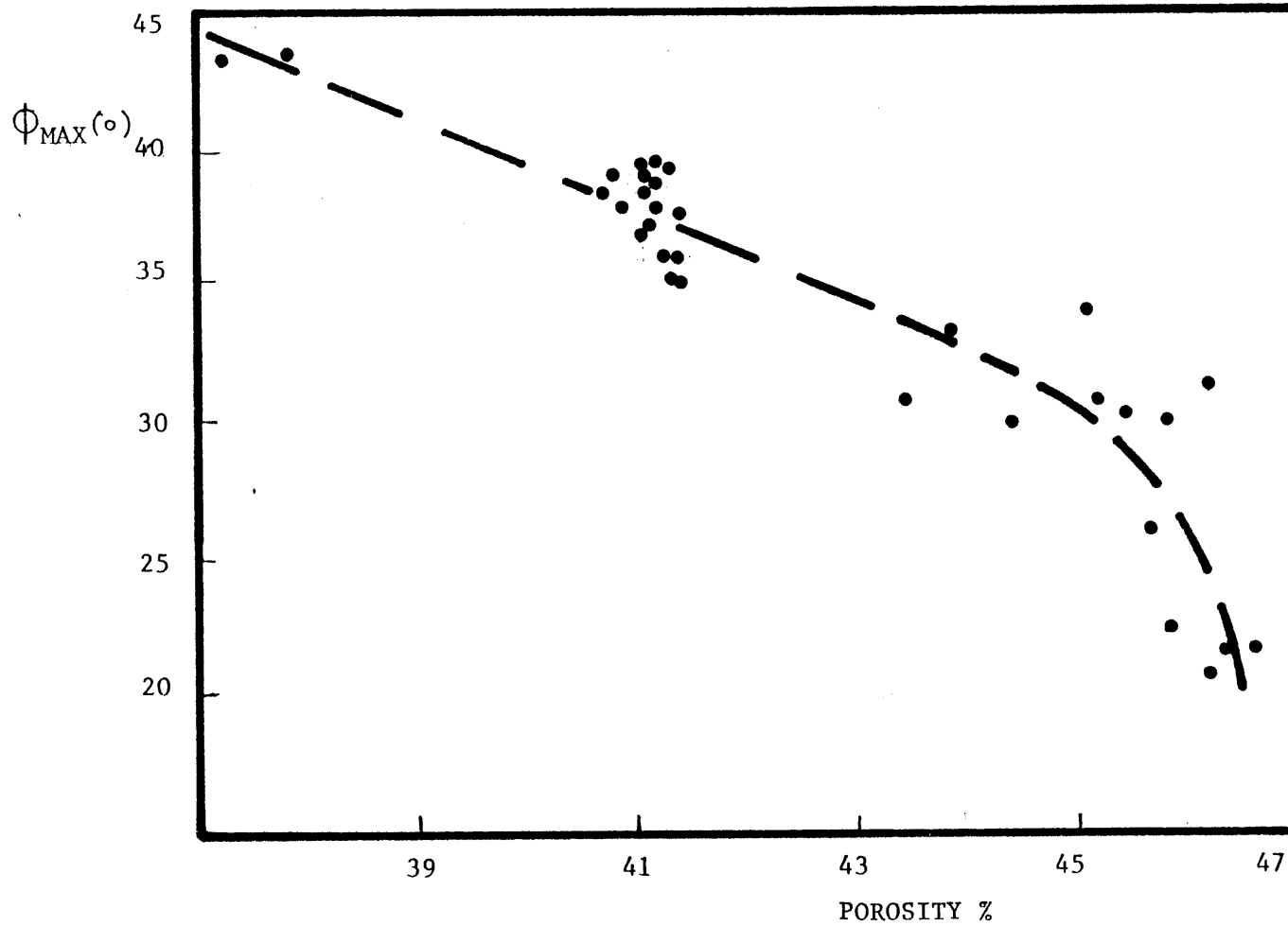


FIGURE B.1 ; Maximum Static Friction Angle versus Porosity - Sand A

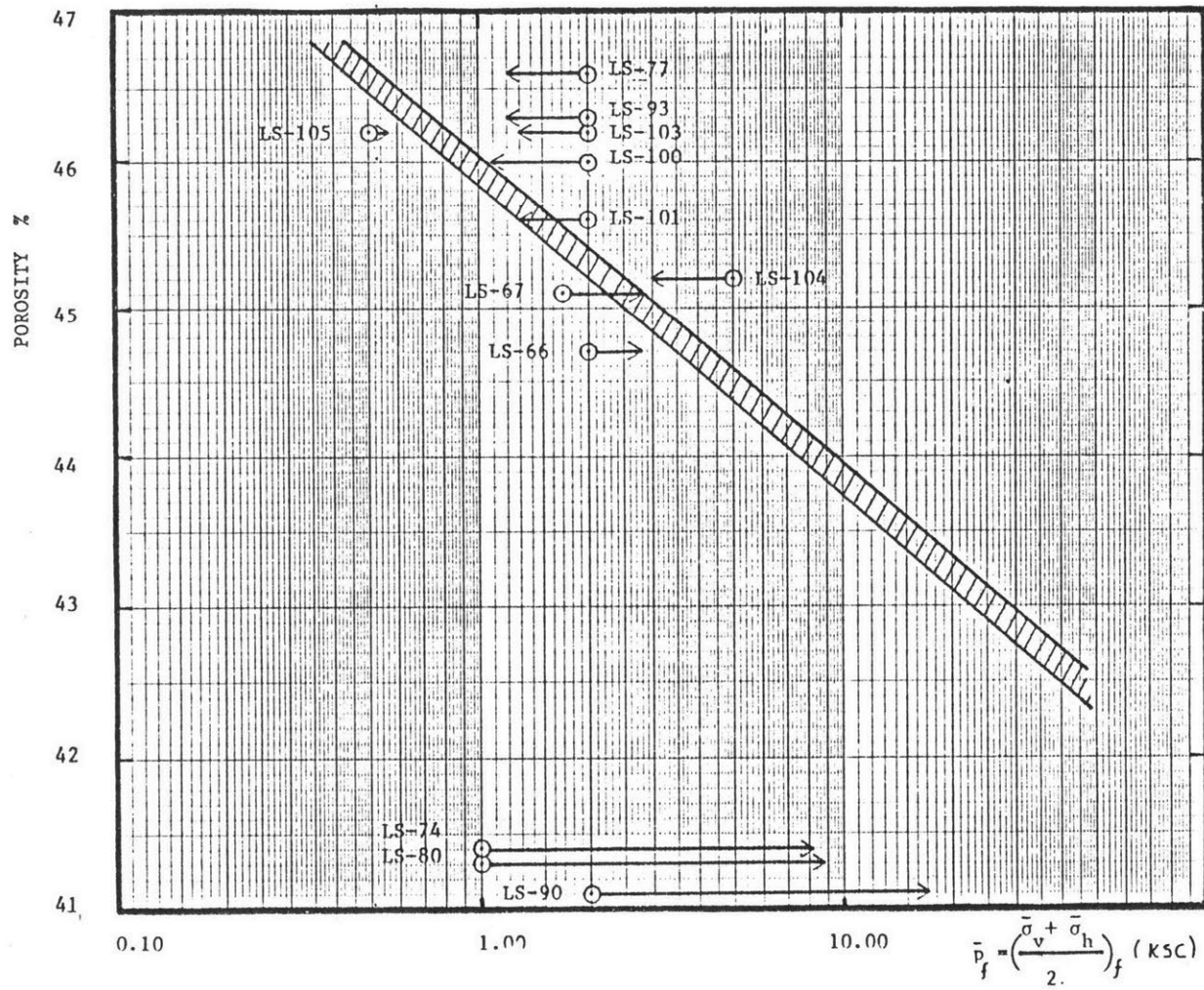


FIGURE B.2 : Mean Effective Stress at Failure versus Porosity - Sand A

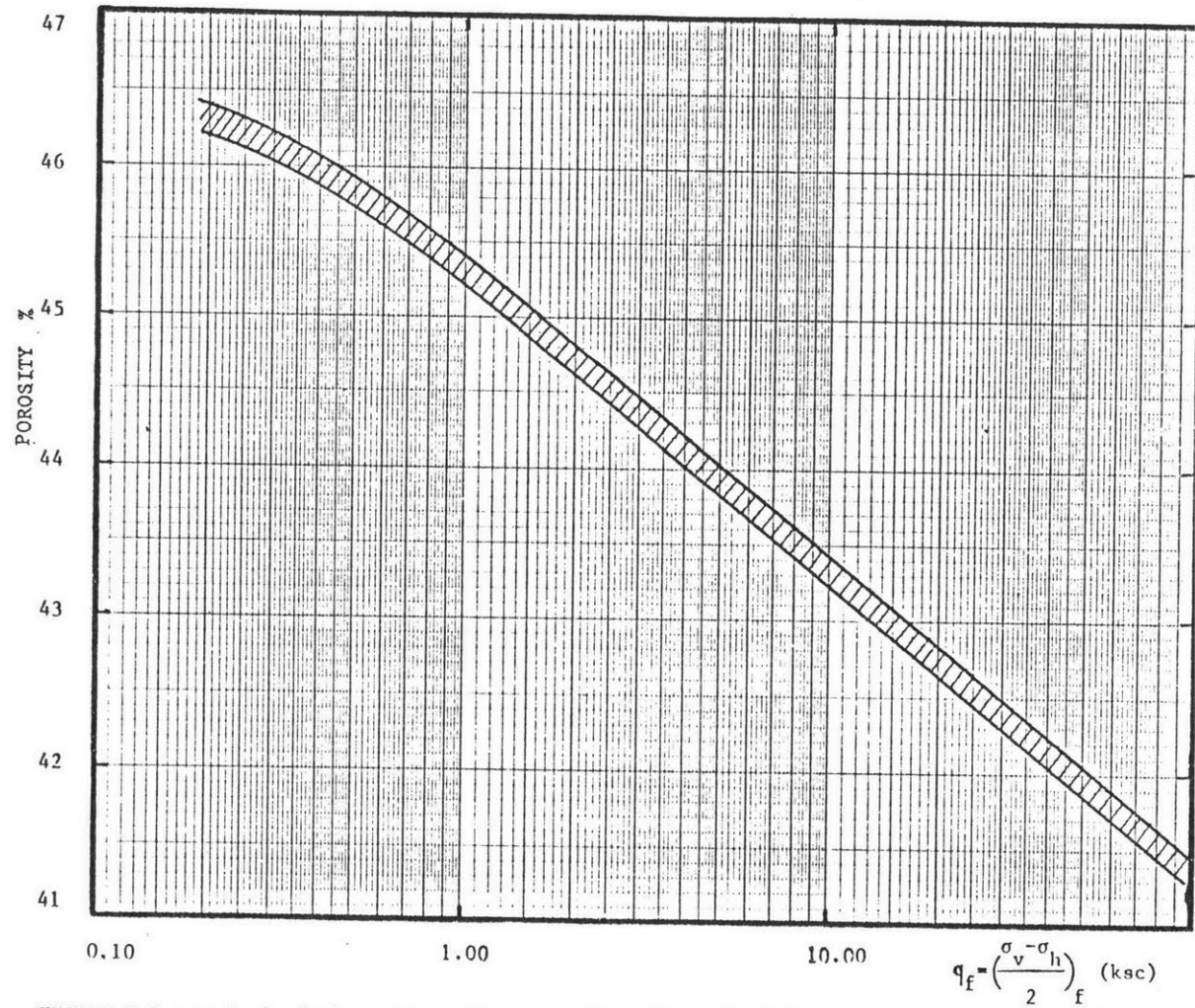


FIGURE B.3 : Undrained Shear Strength versus Porosity - Sand A

the general stress and strain vectors (section 6.1.1) are reduced as

$$\left. \begin{aligned} \underline{\underline{\epsilon}}^T &= \{\epsilon_{xx}, \epsilon_{yy}, \epsilon_{zz}, \epsilon_{xy}\} \\ \underline{\underline{\sigma}}^T &= \{\sigma_{xx}, \sigma_{yy}, \sigma_{zz}, \sigma_{xy}\} \end{aligned} \right\} \begin{array}{l} \text{plain strain} \\ \text{and} \\ \text{plane stress} \end{array}$$

$$\left. \begin{aligned} \underline{\underline{\epsilon}}^T &= \{\epsilon_{rr}, \epsilon_{\theta\theta}, \epsilon_{zz}, \epsilon_{rz}\} \\ \underline{\underline{\epsilon}}^T &= \{\epsilon_{rr}, \epsilon_{\theta\theta}, \epsilon_{zz}, \epsilon_{rz}\} \end{aligned} \right\} \text{axisymmetric}$$

The differential operator D is defined as:

$$\text{plane strain } \underline{\underline{D}} = \begin{bmatrix} \partial/\partial x & 0 \\ 0 & 0 \\ 0 & \partial/\partial y \\ \partial/\partial y & \partial/\partial x \end{bmatrix}$$

$$\text{plane stress } \underline{\underline{D}} = \begin{bmatrix} \partial/\partial x & 0 \\ -\frac{y}{1-\nu} \partial/\partial x & -\frac{y}{1-\nu} \partial/\partial y \\ 0 & \partial/\partial y \\ \partial/\partial y & \partial/\partial x \end{bmatrix}$$

$$\text{axisymmetric } \underline{\underline{D}} = \begin{bmatrix} \partial/\partial r & 0 \\ 1/r & 0 \\ 0 & \partial/\partial z \\ \partial/\partial z & \partial/\partial r \end{bmatrix}$$

The stress-strain stiffness matrix is:

$$\underline{C} = \frac{E}{(1+\nu)(1-2\nu)} \begin{bmatrix} 1-\nu & \nu & \nu & 0 \\ \nu & 1-\nu & \nu & 0 \\ \nu & \nu & 1-\nu & 0 \\ 0 & 0 & 0 & \frac{1-2\nu}{2} \end{bmatrix}$$

The Young's Modulus (E) and the Poisson's ratio (ν) are related to the Bulk (K) and Shear (G) moduli through the following relations:

$$E = \frac{9KG}{3K + G}$$

$$\nu = \frac{3K - 2G}{6K + 2G}$$

The unit matrix I is defined as

$$\underline{I}^T = [1 \quad 1 \quad 1 \quad 0]$$

The stiffness matrices K, H, G and the load vector R can be described from the previous Finite Element matrices; close form calculation of their elements, however, is too involved and for this reason all calculations are performed numerically.

APPENDIX DANALYTICAL SOLUTION FOR CYCLIC LOADING UNDERPLAIN STRAIN CONDITIONS

In this appendix the analytical solution for cyclic loading under plane strain conditions will be presented, for uniform applied stresses. The basic assumptions are as follows:

(i) No deformation is allowed in the y direction, implying that

$$\epsilon_{yy} = \epsilon_{xy} = \epsilon_{zy} = 0.$$

(ii) No shear stresses are applied ($\sigma_{xz} = 0.$)

(iii) The average total stresses in the x and z directions are kept constant during the cyclic loading ($\dot{\sigma}_{xx} = \dot{\sigma}_{zz} = 0.$)

The analytical solution depends on the drainage conditions, and thus, Drained and Undrained Cyclic loading will be considered separately.

DRAINED CYCLIC LOADING The strain rate in the y direction is written as:

$$\dot{\epsilon}_{yy} = \dot{\epsilon}_{yy} + \frac{1}{3} \dot{\epsilon}_{vol} \quad (D.1)$$

Combining equations D.1, 4.2 and assumption (i) yields

$$\frac{1}{3} \left(\frac{\dot{\bar{\sigma}}_{\text{oct}}}{K} + \frac{\bar{\sigma}_{\text{oct}}}{V} \right) + \frac{S_{yy}}{2G} + \frac{S_{yy}}{R} = 0. \quad (\text{D.2})$$

where

$$\bar{\sigma}_{\text{oct}} = (\bar{\sigma}_{xx} + \bar{\sigma}_{yy} + \bar{\sigma}_{zz}) / 3. \quad (\text{D.3})$$

and

$$S_{yy} = \frac{1}{3} (2\bar{\sigma}_{yy} - \bar{\sigma}_{xx} - \bar{\sigma}_{zz}) \quad (\text{D.4})$$

Due to the assumption (iii) the above equations in rate form are written as:

$$\dot{\bar{\sigma}}_{\text{oct}} = \frac{1}{3} \dot{\bar{\sigma}}_{yy} \quad (\text{D.5})$$

$$\dot{S}_{yy} = \frac{2}{3} \dot{\bar{\sigma}}_{yy} \quad (\text{D.6})$$

Substitution of the stress rates in equation (D.2) from equation (D.5) and (D.6), and solution of the resulting equation for $\dot{\bar{\sigma}}_{yy}$ gives:

$$\dot{\bar{\sigma}}_{yy} = - \left(\frac{\bar{\sigma}_{\text{oct}}}{3V} + \frac{S_{yy}}{R} \right) / \left(\frac{1}{3K} + \frac{1}{3G} \right) \quad (\text{D.7})$$

The strain rates in the directions x and z are expressed as:

$$\dot{\epsilon}_{xx} = \frac{1}{3} \left(\frac{\dot{\bar{\sigma}}_{oct}}{K} + \frac{\bar{\sigma}_{oct}}{V} \right) + \frac{\dot{S}_{xx}}{2G} + \frac{S_{xx}}{R} \quad (D.8)$$

$$\dot{\epsilon}_{zz} = \frac{1}{3} \left(\frac{\dot{\bar{\sigma}}_{oct}}{K} + \frac{\bar{\sigma}_{oct}}{V} \right) + \frac{\dot{S}_{zz}}{2G} + \frac{S_{zz}}{R} \quad (D.9)$$

where

$$S_{xx} = \frac{1}{3} (2\bar{\sigma}_{xx} - \bar{\sigma}_{yy} - \bar{\sigma}_{zz}) \quad (D.10)$$

$$S_{zz} = \frac{1}{3} (2\bar{\sigma}_{zz} - \bar{\sigma}_{xx} - \bar{\sigma}_{yy}) \quad (D.11)$$

The above equations yield the following deviatoric stress rates in x and z directions:

$$\dot{S}_{xx} = -\frac{1}{3} \dot{\bar{\sigma}}_{yy} \quad (D.12)$$

$$\dot{S}_{zz} = -\frac{1}{3} \dot{\bar{\sigma}}_{yy} \quad (D.13)$$

Back substitution into equations (D.8) and (D.9) result in expressions of the strain rates in the x and z directions in terms of the applied state of stress, and the stress rate in

the y direction:

$$\dot{\epsilon}_{xx} = \frac{\dot{\sigma}_{oct}}{3V} + \frac{S_{xx}}{R} + \left(\frac{1}{9K} - \frac{1}{6G}\right) \dot{\sigma}_{yy} \quad (D.14)$$

$$\dot{\epsilon}_{zz} = \frac{\dot{\sigma}_{oct}}{3V} + \frac{S_{zz}}{R} + \left(\frac{1}{9K} - \frac{1}{6G}\right) \dot{\sigma}_{yy} \quad (D.15)$$

Numerical integration of equations (D.7), (D.14), and (D.15) is necessary for the calculation of the corresponding quantities.

UNDRAINED CYCLIC LOADING

Under undrained conditions the volumetric component of strain is equal to zero, and consequently only deviatoric strains occur. The plane strain assumption combined with equation 4.2 is written as:

$$\dot{\epsilon}_{yy} = \frac{\dot{S}_{yy}}{2G_t} + \frac{S_{yy}}{R} = 0 \quad (D.16)$$

The stress deviator, S_{yy} , is expressed in terms of the total stresses as

$$S_{yy} = \frac{1}{3} (2\sigma_{yy} - \sigma_{xx} - \sigma_{zz}) \quad (D.17)$$

or after differentiation: $\dot{S}_{yy} = \frac{2}{3} \dot{\sigma}_{yy}$ (D.18)

Substitution of equation (D.18) into (D.16) leads to the expression for the total stress rate in the y direction

$$\dot{\sigma}_{yy} = -3G \frac{S_{yy}}{R} \quad (D.19)$$

According to equation (4.2) the volumetric strain rate is:

$$\dot{\epsilon}_{vol} = \frac{\dot{\bar{\sigma}}_{oct}}{K} + \frac{\bar{\sigma}_{oct}}{V} \quad (D.20)$$

The effective octahedral stress can be expressed in terms of total stresses and the pore pressure:

$$\bar{\sigma}_{oct} = \frac{\sigma_{xx} + \sigma_{yy} + \sigma_{zz}}{3} - u \quad (D.21)$$

Differentiation of equation D.22 yields

$$\dot{\bar{\sigma}}_{oct} = \dot{\sigma}_{yy}/3 - \dot{u} \quad (D.22)$$

Since the volumetric strain is zero, equations (D.22), (D.20) and (D.21) can be combined to give the rate of pore pressure accumulation:

$$\dot{u} = -G \frac{S_{yy}}{R} + K \frac{\bar{\sigma}_{oct}}{V} \quad (D.23)$$

The strain rates in the x and z coordinates is

$$\dot{\epsilon}_{xx} = \frac{\dot{S}_{xx}}{2G_t} + \frac{S_{xx}}{R} \quad (D.24)$$

$$\dot{\epsilon}_{zz} = \frac{\dot{S}_{zz}}{2G_t} + \frac{S_{zz}}{R} \quad (D.25)$$

and the corresponding stress deviators are

$$S_{xx} = \frac{1}{3} (2\sigma_{xx} - \sigma_{zz} - \sigma_{yy}) \quad (D.26)$$

$$S_{zz} = \frac{1}{3} (2\sigma_{zz} - \sigma_{xx} - \sigma_{yy}) \quad (D.27)$$

or after differentiation

$$\dot{S}_{xx} = -\frac{1}{3} \dot{\sigma}_{yy} \quad (D.28)$$

$$\dot{S}_{zz} = -\frac{1}{3} \dot{\sigma}_{yy} \quad (D.29)$$

Substitution of equations (D.28) and (D.29) into (D.24) and (D.25) respectively yields expressions for the strain rates in terms of the average state of stress, and the number of cycles:

$$\dot{\epsilon}_{xx} = \left(\frac{S_{yy}}{2} + S_{xx} \right) \frac{1}{R} \quad (D.30)$$

$$\dot{\epsilon}_{zz} = \left(\frac{S_{yy}}{2} + S_{zz} \right) \frac{1}{R} \quad (D.31)$$

Numerical integration of equations (D.19), (D.23), (D.30)

and (D.31) with respect to the number of cycles will give the variation of the corresponding quantities due to cyclic loading.

APPENDIX ELISTING OF FINITE ELEMENT PROGRAM FEAP-CYC

```

C.....MASTER MINIFEM
C.....SET PROGRAM CAPACITY * MAX MUST AGREE WITH DIMENSION OF M
      IMPLICIT DOUBLE PRECISION(A-H,O-Z)
      COMMON m(400000)
      COMMON/Psize/ MAX
      MAX=400000
      CALL PCONTR
      STOP
      END

      SUBROUTINE PCONTR
C
C.....FINITE ELEMENT ANALYSIS PROGRAM (FEAP) FOR SOLUTION OF GENERAL
C.....PROBLEM CLASSES USING THE FINITE ELEMENT METHOD. PROBLEM SIZE
C.....IS CONTROLLED BY THE DIMENSION OF BLANK COMMON AND VALUE OF MAX
C.....AS SET IN MAIN PROGRAM. ALL ARRAYS MUST RESIDE IN CENTRAL MEMORY.
C
C.....PROGRAMMED BY PROF. TAYLOR, DEPARTMENT OF CIVIL ENGINEERING
C.....UNIVERSITY OF CALIFORNIA, BERKELEY,CALIFORNIA 94720,U.S.A
C.....MODIFIED TO COMPUTE PERMANENT DEFORMATIONS OF FOUNDATIONS
C.....DUE TO CYCLIC LOADING BY G.BOUCKOVALAS, DEPARTMENT OF CIVIL
C.....ENGINEERING, M.I.T, CAMBRIDGE,MASSACHUSETTS, 02138,U.S.A
C
      IMPLICIT DOUBLE PRECISION(A-H,O-Z)
      LOGICAL PCOMP
      COMMON/CDATA/O,HEAD(20),NUMNP,NUMEL,NUMMAT,NEN,NEQ,IPR
      COMMON/LABEL/ PDIS(6),A(6),BC(2),DI(6),CD(3),TE(3),FD(3)
      COMMON M(1)
      DIMENSION TITL(20),WD(4)
      DATA WD/4HFEAP,4HMACR,4HSTOP,4HGO /
C.....READ A CARD AND COMPARE 4 FIRST COLUMNS WITH MACRO LIST
1     READ(5,1000) TITL
      IF(PCOMP(TITL(1),WD(1))) GO TO 100
      IF(PCOMP(TITL(1),WD(2))) GO TO 200
      IF(PCOMP(TITL(1),WD(3))) RETURN
      IF(PCOMP(TITL(1),WD(4))) GO TO 300
      GO TO 1
C.....READ AND PRINT CONTROL INFORMATION
100    DO 101 I=1,20
101    HEAD(I)=TITL(I)
      READ(5,1001) NUMNP,NUMEL,NUMMAT,NDM,NDF,NEN,NAD

```



```

WRITE(6,2000) HEAD,NUMNP,NUMEL,NUMMAT,NDM,NDF,NEN,NAD
C.....SET POINTERS FOR ALLOCATION OF DATA ARRAYS
PDIS(2)=A(NDM)
NEN1=NEN+1
NST=NEN*NDF+NAD
NSC=NDM*(NDM-1)/2+3
NO=1+NST*2*IPR
N1=NO+NEN*NDM*IPR
N2=N1+NEN*IPR
N3=N2+NST
N4=N3+NST*IPR
N5=N4+NST*NST*IPR
N6=N5+NUMMAT
N7=N6+35*NUMMAT*IPR
N8=N7+NDF*NUMNP
N9=N8+NDM*NUMNP*IPR
N10=N9+NEN1*NUMEL
N11=N10+NDF*NUMNP*IPR
N12=N11+NUMNP*IPR
N13=N12+NSC*NUMEL*IPR
N14=N13+NSC*NUMEL*IPR
N15=N14+NSC*NUMEL*IPR
N16=N15+NSC*NUMEL*IPR
N17=N16+NUMEL*IPR
N18=N17+NUMEL*IPR
N19=N18+NUMEL*IPR
N20=N19+NDF*NUMNP
C.....CHECK THAT SUFFICIENT MEMORY EXISTS
300 CALL SETMEM(N20)
CALL PZERO(M,N11)
C.....CALL MESH INPUT SUBROUTINE TO READ AND PRINT ALL MESH DATA
III=0
CALL PMESH(M,M(N2),M(N3),M(N4),M(N5),M(N6),M(N7),M(N8),M(N9),M(N10)
1 ),M(N11),NDF,NDM,NEN1,NST,III)
C.....ESTABLISH PROFILE OF RESULTING EQUATIONS FOR STIFFNESS, MASS, ETC
CALL PROFIL(M(N19),M(N7),M(N9),NDF,NEN1,NAD)
C.....SET POINTERS FOR SOLUTION ARRAYS* CHECK FOR SUFFICIENT MEMORY
N20=N19+NEQ
N21=N20+NEQ*IPR
N22=N21+NEQ*IPR
NE=N22+NUMNP*NDF*IPR
CALL SETMEM(NE)
GO TO 1
C.....CALL MACRO SOLUTION MODULE FOR ESTABLISHING SOLUTION ALGORITHM
200 CALL PMACR(M,M(N0),M(N1),M(N2),M(N3),M(N4),M(N5),M(N6),M(N7),M(N8)
1 ,M(N9),M(N10),M(N11),M(N19),M(N20),M(N22),M(N12),M(N13),M(N14),
2 M(N16),M(N17),M(N18),M(N15),M(N21),M(NE),NDF,NDM,NEN1,NSC,NST,
3 NE)
GO TO 1
C.....INPUT/OUTPUT FORMATS
1000 FORMAT(20A4)

```

```

1001  FORMAT(16I5)
2000  FORMAT(1H1,20A4//5X,30HNUMBER OF NODAL POINTS      =,I6/5X,30HNUM
      1BER OF ELEMENTS      =,I6/5X,30HNUMBER OF MATERIAL SETS      .
      2=,I6/5X,30HDIMENSION OF COORDINATE SPACE=,I6/5X,30HDEGREE OF FREED
      3OMS/NODE      =,I6/5X,30HNODES PER ELEMENT (MAXIMUM)      =,I6/5X,30HE
      4XTRA D.O.F. TO ELEMENT      =,I6)
      END

```

BLOCK DATA

```

IMPLICIT DOUBLE PRECISION(A-H,O-Z)
COMMON/CDATA/O,HEAD(20),NUMNP,NUMEL,NUMMAT,NEN,NEQ,IPR
COMMON/LABEL/PDIS(6),A(6),BC(2),DI(6),CD(3),TE(3),FD(3)
DATA A/2H,1,2H,2,2H,3,2H,4,2H,5,2H,6/,CD/4H COO,4HRDIN,4HATES/
DATA TE/4H TEM,4HPERA,4HTURE/,FD/4H FOR,4HCE/D,4HISPL/
DATA PDIS/4H(I10,2H, ,4HF13.,4H4, ,4H6E13,4H.4) /
DATA BC/4H B.C,2H. /,DI/4H DIS,2HPL,4H VEL,2HOC,4H ACC,2HEL/
DATA O/1H0/,IPR/2/
END
SUBROUTINE GENVEC(NDM,X,CD,PRT,ERR)

```

C

C.....GENERATE REAL DATA ARRAYS BY LINEAR INTERPOLATION

C

```

IMPLICIT DOUBLE PRECISION(A-H,O-Z)
LOGICAL PRT,ERR,PCOMP
COMMON /CDATA/ O,HEAD(20),NUMNP,NUMEL,NUMMAT,NEN,NEQ,IPR
DIMENSION X(NDM,1),XL(7),CD(2)
DATA BL/4HBLAN/
N=0
NG=0
102  L=N
      LG=NG
      READ(5,1000) N,NG,XL
      IF(N.LE.0.OR.N.GT.NUMNP) GO TO 108
      DO 103 I=1,NDM
103  X(I,N)=XL(I)
      IF(LG) 104,102,104
104  LG=ISIGN(LG,N-L)
      LI=(IABS(N-L+LG)-1)/IABS(LG)
      DO 105 I=1,NDM
105  XL(I)=(X(I,N)-X(I,L))/LI
106  L=L+LG
      IF((N-L)*LG.LE.0) GO TO 102
      IF(L.LE.0.OR.L.GT.NUMNP) GO TO 110
      DO 107 I=1,NDM
107  X(I,L)=X(I,L-LG)+XL(I)
      GO TO 106
110  WRITE(6,3000) L,(CD(I),I=1,3)
      ERR=.TRUE.
      GO TO 102
108  DO 109 I=1,NUMNP,50
      IF(PRT) WRITE(6,2000) O,HEAD,(CD(L),L=1,3),(L,CD(1),CD(2),L=1,NDM)

```

```

      N=MIN0(NUMNP,I+49)
      DO 109 J=1,N
      IF(PCOMP(X(1,J),BL).AND.PRT) WRITE(6,2008) N
109   IF(.NOT.PCOMP(X(1,J),BL).AND.PRT) WRITE(6,2009) J,(X(L,J),L=1,NDM)
      RETURN
1000  FORMAT(2I5,7F10.0)
2000  FORMAT(A1,20A4//5X, 5HNODAL,3A4//6X,4HNODE,9(I7,A4,A2))
2008  FORMAT(I10,32H HAS NOT BEEN INPUT OR GENERATED)
2009  FORMAT(I10,9F13.4)
3000  FORMAT(5X,43H**FATAL ERROR 02** ATTEMPT TO GENERATE NODE,I5,3H IN
      1  ,3A4)
      END
      SUBROUTINE PMESH(UL,IDL,P,S,IE,D,ID,X,IX,F,T,NDF,NDM,NEN1,NST,III)
C
C.....DATA INPUT ROUTINE FOR MESH DESCRIPTION
C
      IMPLICIT DOUBLE PRECISION(A-H,O-Z)
      LOGICAL PRT,ERR,PCOMP
      COMMON /CDATA/ O,HEAD(20),NUMNP,NUMEL,NUMMAT,NEN,NEQ,IPR
      COMMON /ELDATA/ DM,N,MA,MCT,IEL,NEL
      COMMON /LABEL/ PDIS(6),A(6),BC(2),DI(6),CD(3),TE(3),FD(3)
      DIMENSION IE(1),D(35,1),ID(NDF,1),X(NDM,1),IX(NEN1,1),XHED(17)
      1  ,UL(1),IDL(6),XL(3),F(NDF,1),FL(6),T(1),WD(10),VA(2),P(1),S(NST,
      2  1),ECS(6),CSI(6),CSTR(6),PECS(6)
      DATA WD/4HCOOR,4HELEM,4HMATE,4HBOUN,4HFORC,4HTEMP,4HEND ,4HPRIN,
      1  4HNOPR,4HPAGE/,BL/4HBLAN/,VA/4H VAL,2HUE/,LIST/10/,PRT/.TRUE./
C.....INITIALIZE ARRAYS
      ERR=.FALSE.
      IF(III.LT.0) GO TO 10
      DO 101 N=1,NUMNP
      DO 100 I=1,NDF
      ID(I,N)=0
100   F(I,N)=0.
101   T(N)=0.
      10   READ(5,1000)CC
      DO 20 I=1,LIST
      20   IF(PCOMP(CC,WD(I))) GO TO 30
      GO TO 10
      30   GO TO (1,2,3,4,5,6,7,8,9,11),I
C.....NODAL COORDINATE DATA INPUT
      1   DO 102 N=1,NUMNP
102   X(1,N)=BL
      CALL GENVEC(NDM,X,CD,PRT,ERR)
      GO TO 10
C.....ELEMENT DATA INPUT
      2   L=0
      DO 206 I=1,NUMEL,50
      IF(PRT) WRITE(6,2001) O,HEAD,(K,K=1,NEN)
      J=MIN0(NUMEL,I+49)
      DO 206 N=I,J
      IF(L-N) 200,202,203

```

```

200  READ(5,1001) L,LK,(IDL(K),K=1,NEN),LX
      IF(L.EQ.0) L=NUMEL+1
      IF(LX.EQ.0) LX=1
      IF(L-N) 201,202,203
201  WRITE(6,3001) L,N
      ERR=.TRUE.
      GO TO 206
202  NX=LX
      DO 207 K=1,NEN1
207  IX(K,L)=IDL(K)
      IX(NEN1,L)=LK
      GO TO 205
203  IX(NEN1,N)=IX(NEN1,N-1)
      DO 204 K=1,NEN
      IX(K,N)=IX(K,N-1)+NX
204  IF(IX(K,N-1).EQ.0) IX(K,N)=0
205  IF(PRT) WRITE(6,2002) N,IX(NEN1,N),(IX(K,N),K=1,NEN)
206  CONTINUE
      GO TO 10
C.....MATERIAL DATA INPUT
3    WRITE(6,2004) O,HEAD
      DO 300 N=1,NUMMAT
      READ(5,1002) MA,IEL,XHED
      WRITE(6,2003)MA,IEL,XHED
      IE(MA)=IEL
300  CALL ELMLIB(D(1,MA),UL,X,IX,T,S,P,ECS,CSI,CSTR,CVOL,CVI,S0,PECS,TIME,
1    DT,NDF,NDM,NST,1,IFLAG,0)
      GO TO 10
C.....READ IN THE RESTRAINT CONDITIONS FOR EACH NODE
4    IF(PRT) WRITE(6,2000) O,HEAD,(I,BC,I=1,NDF)
      III=1
      N=0
      NG=0
402  L=N
      LG=NG
      READ(5,1001) N,NG,IDL
      IF(N.LE.0.OR.N.GT.NUMNP) GO TO 60
      DO 51 I=1,NDF
      ID(I,N)=IDL(I)
51   IF(L.NE.0.AND.IDL(I).EQ.0.AND.ID(I,L).LT.0) ID(I,N)=-1
      LG=ISIGN(LG,N-L)
52   L=L+LG
      IF((N-L)*LG.LE.0) GO TO 402
      DO 53 I=1,NDF
53   IF(ID(I,L-LG).LT.0) ID(I,L)=-1
      GO TO 52
60   DO 58 N=1,NUMNP
      DO 56 I=1,NDF
56   IF(ID(I,N).NE.0) GO TO 57
      GO TO 58
57   IF(PRT) WRITE(6,2007) N,(ID(I,N),I=1,NDF)

```

```

58    CONTINUE
      GO TO 10
C.....FORCE/DISPLACEMENT DATA INPUT
5     CALL GENVEC(NDF,F,FD,PRT,ERR)
      GO TO 10
C.....TEMPERATURE DATA INPUT
6     CALL GENVEC(1,T,TE,PRT,ERR)
      GO TO 10
7     IF(ERR) STOP
      RETURN
8     PRT=.TRUE.
      GO TO 10
9     PRT=.FALSE.
      GO TO 10
11    READ(5,1000) O
      GO TO 10
1000  FORMAT(A4,75X,A1)
1001  FORMAT(16I5)
1002  FORMAT(I5,3X,I2,17A4)
2000  FORMAT(A1,20A4//5X,17HNODAL B.C.          //6X,4HNODE,9(I7,A4,A2)/1X)
2001  FORMAT(A1,20A4//5X,8HELEMENTS//3X,7HELEMENT,2X,8HMATERIAL,
1     14(I3,5H NODE)/(20X,14(I3,5H NODE)))
2002  FORMAT(2I10,14I8/(20X,14I8))
2003  FORMAT(/5X,12HMATERIAL SET,I3,17H FOR ELEMENT TYPE,I2,5X,17A4/1X)
2004  FORMAT(A1,20A4//5X,19HMATERIAL PROPERTIES)
2005  FORMAT(A1,20A4//5X,17HNODAL FORCE/DISPL//6X,4HNODE,9(I7,A4,A2))
2006  FORMAT(I10,9E13.3)
2007  FORMAT(I10,9I13)
3001  FORMAT(5X,20H**ERROR 03** ELEMENT,I5,22H APPEARS AFTER ELEMENT,I5)
      END

      SUBROUTINE SETMEM(J)

C
C.....MONITOR AVAILABLE MEMORY IN BLANK COMMON
C
      COMMON M(1)
      COMMON /PSIZE/ MAX
      K=J
      IF(K.LE.MAX) RETURN
      WRITE(6,1000) K,MAX
      STOP
1000  FORMAT(5X,49H**ERROR 01** INSUFFICIENT STORAGE IN BLANK COMMON/
1     17X,11HREQUIRED =,I8/17X,11HAVAILABLE =,I8/)
      END

      SUBROUTINE PMACR (UL,XL,TL,LD,P,S,IE,D,ID,X,IX,F,T,JDIAG,B,DR,
1     ECS,CSI,CSTR,CVOL,CVI,SO,PECS,DRS,CT,NDF,NDM,NEN1,NSC,NST,NEND)

C
C.....MACRO INSTRUCTION PROGRAM
C
C.....CONTROLS PROBLEM SOLUTION AND OUTPUT ALGORITHMS

```

C.....BY ORDER OF SPECIFYING MACRO COMMANDS IN ARRAY WD.

C

```

IMPLICIT DOUBLE PRECISION(A-H,O-Z)
LOGICAL AFR,BFR,CFR,AFL,BFL,CFL,DFL,EFL,FFL,GFL,PCOMP
COMMON M(1)
COMMON /CDATA/ O,HEAD(20),NUMNP,NUMEL,NUMMAT,NEN,NEQ,IPR
COMMON /LABEL/ PDIS(6),Z(6),BC(2),DI(6),CD(3),TE(3),FD(3)
COMMON /PRLD/ PROP
COMMON /TDATA/ TIME,DT,C1,C2,C3,C4,C5
DIMENSION WD(19),CT(4,1),CTL(4),LVS(9),LVE(9),JDIAG(1),
1  UL(1),XL(1),TL(1),LD(1),P(1),S(1),IE(1),D(1),ID(1),X(1),
2  IX(1),F(1),T(1),B(1),DR(1),ECS(1),CSI(1),CSTR(1),PECS(1),DRS(1)
3  ,CVOL(1),CVI(1),S0(1)
DATA WD/4HTOL ,4HDT ,4HSTRE,4HDISP,4HTANG,4HFORM,4HLOOP,4HNEXT,
1      4HDATA,4HTIME,4HCONV,4HSOLV,4HMESH,4HUTAN,4HREAC,4HCHEC,
2      4HSTRT,4HADD ,4HWEIG/
DATA NWD/19/,ENDM/4HEND /,NV,NC/1,1/

```

C.....SET INITIAL VALUES OF PARAMETERS

```

DT=0.
PROP=1.0
RNMAX=0.0
TIME=0.0
TOL=1.E-9
UN=0.0
AFL=.TRUE.
AFR=.FALSE.
BFL=.TRUE.
BFR=.FALSE.
CFL=.TRUE.
CFR=.FALSE.
DFL=.TRUE.
EFL=.TRUE.
FFL=.FALSE.
GFL=.TRUE.
NE=NEND
NNSC=NUMEL*NSC
NNEQ=NDF*NUMNP
NPLD=0
CALL PZERO(B,NEQ*IPR)
CALL PZERO(DR,NNEQ*IPR)
CALL PZERO(DRS,NEQ*IPR)
WRITE(6,2001) O,HEAD

```

C.....READ MACRO CARDS

```

LL=1
LMAX=16
CALL SETMEM(NE+LMAX*4*IPR)
CT(1,1)=WD(7)
CT(3,1)=1.0
100 LL=LL+1
IF(LL.LT.LMAX) GO TO 110
LMAX=LMAX+16

```

```

CALL SETMEM(NE+LMAX*4*IPR)
110 READ(5,1000) (CT(J,LL),J=1,4)
WRITE(6,2000) (CT(J,LL),J=1,4)
IF(.NOT.PCOMP(CT(1,LL),ENDM)) GO TO 100
200 CT(1,LL)=WD(8)
C.....SET LOOP MARKERS
NE=NE+LMAX*4*IPR
LX=LL-1
DO 230 L=1,LX
IF(.NOT.PCOMP(CT(1,L),WD(7))) GO TO 230
J=1
K=L+1
DO 210 I=K,LL
IF(PCOMP(CT(1,I),WD(7))) J=J+1
IF(J.GT.9) GO TO 401
IF(PCOMP(CT(1,I),WD(8))) J=J-1
210 IF(J.EQ.0) GO TO 220
GO TO 400
220 CT(4,I)=L
CT(4,L)=I
230 CONTINUE
J=0
DO 240 L=1,LL
IF(PCOMP(CT(1,L),WD(7))) J=J+1
240 IF(PCOMP(CT(1,L),WD(8))) J=J-1
IF(J.NE.0) GO TO 400
C.....EXECUTE MACRO INSTRUCTION PROGRAM
LV=0
L=1
299 DO 300 J=1,NWD
300 IF(PCOMP(CT(1,L),WD(J))) GO TO 310
GO TO 330
310 I=L-1
IF(L.NE.1.AND.L.NE.LL)
1WRITE(6,2010) I,(CT(K,L),K=1,4)
GO TO (1,2,3,4,5,6,7,8,9,10,11,12,13,14,15,16,17,18,19),J
C.....SET SOLUTION TOLERANCE
1 TOL=CT(3,L)
GO TO 330
C.....SET TIME INCREMENT
2 DT=(CT(3,L)**CT(4,L)+TIME**CT(4,L))**(1./CT(4,L))-TIME
GO TO 330
C.....PRINT STRESS VALUES
3 ISW=CT(4,L)
LX=LVE(LV)
IF(DMOD(CT(3,LX),DMAX1(CT(3,L),1.DO)).EQ.0.0)
1 CALL PFORM(UL,XL,TL,LD,P,S,IE,D,ID,X,IX,F,T,JDIAG,DR,DR,DR,
2 ECS,CSI,CSTR,CVOL,CVI,S0,PECS,TIME,DT,NDF,NDM,NEN1,NSC,NST,ISW
3 ,B,M(NV),.FALSE.,.FALSE.,.FALSE.,.FALSE.,IFLAG)
GO TO 330
C.....PRINT DISPLACEMENTS

```

```

4     LX=LVE(LV)
      IF(DMOD(CT(3,LX),DMAX1(CT(3,L),1.DO)).NE.0.0) GO TO 330
      WRITE(6,2003) 0,HEAD,TIME,PROP
      CALL PRTDIS(ID,D,X,B,F,NDM,NDF)
      GO TO 330
C.....FORM TANGENT STIFFNESS
14    IF(CFL) CALL PSETM(NC,NE,JDIAG(NEQ)*IPR,CFL)
      CALL PZERO(M(NC),JDIAG(NEQ)*IPR)
      CFR=.TRUE.
5     IF(J.EQ.5) CFR=.FALSE.
      IF(GFL) CALL PSETM(NA,NE,JDIAG(NEQ)*IPR,GFL)
      CALL PZERO(M(NA),JDIAG(NEQ)*IPR)
      CALL PFORM(UL,XL,TL,LD,P,S,IE,D,ID,X,IX,F,T,JDIAG,DR,M(NA),M(NC),
2     ECS,CSI,CSTR,CVOL,CVI,SO,PECS,TIME,DT,NDF,NDM,NEN1,NSC,NST,3
3     ,B,M(NV),.TRUE.,.FALSE.,CFR,.FALSE.,IFLAG)
      AFR=.TRUE.
      GO TO 330
C.....FORM OUT OF BALANCE FORCE FOR TIME STEP/ITERATION
6     CALL PLOAD(ID,F,DR,NNEQ,PROP)
      CALL PFORM(UL,XL,TL,LD,P,S,IE,D,ID,X,IX,F,T,JDIAG,DR,DR,DR,ECS,
2     CSI,CSTR,CVOL,CVI,SO,PECS,TIME,DT,NDF,NDM,NEN1,NSC,NST,6,B,
3     M(NV),.FALSE.,.TRUE.,.FALSE.,.FALSE.,IFLAG)
      BFR=.TRUE.
      GO TO 330
C.....SET LOOP START INDICATORS
7     LV=LV+1
      LX=CT(4,L)
      LVS(LV)=L
      LVE(LV)=LX
      CT(3,LX)=1.
      GO TO 330
C.....LOOP TERMINATOR CONTROL
8     N=CT(4,L)
      CT(3,L)=CT(3,L)+1.0
      IF(CT(3,L).GT.CT(3,N)) LV=LV-1
      IF(CT(3,L).LE.CT(3,N)) L=N
      GO TO 330
C.....READ COMMAND
9     READ(5,1000) (CTL(I),I=1,4)
      IF(.NOT.PCOMP(CT(2,L),CTL(1))) GO TO 402
      IF(PCOMP(CTL(1),WD(1))) TOL=CTL(3)
      IF(PCOMP(CTL(1),WD(2))) DT=CTL(3)
      GO TO 330
C.....INCREMENT TIME
10    TIME=TIME+DT
      RNMAX=0.0
      UN=0.0
      GO TO 330
C.....COMPUTE CONVERGENCE TEST
11    RN=0.0
      UN=0.0

```



```

DO 121 N=1,NEQ
UN=UN+DR(N)**2
121 RN=RN+(DR(N)-DRS(N))**2
UN=DMAX1(UN,RN)
CN=SQRT(UN)
RN=SQRT(RN)
WRITE(6,2002) TIME,CN,RN,TOL
LX=LVE(LV)
LO=LVS(LV)
IF(RN.LE.CN*TOL) CT(3,LX)=CT(3,LO)
IFLAG=1.
DO 122 N=1,NEQ
122 DRS(N)=DR(N)
CALL PZERO(DR,NNEQ*IPR)
GO TO 330
C.....SOLVE THE EQUATIONS
12 IF(CFR) GO TO 121
CALL ACTCOL(M(NA),DR,JDIAG,NEQ,AFR,BFR)
GO TO 132
131 CALL UACTCL(M(NA),M(NC),DR,JDIAG,NEQ,AFR,BFR)
132 AFR=.FALSE.
IF(.NOT.BFR) GO TO 330
BFR=.FALSE.
IF(CT(3,L).NE.0.) GO TO 330
DO 133 N=1,NEQ
133 B(N)=B(N)+DR(N)
GO TO 330
13 I=-1
CALL PMESH(u1,ld,P,S,IE,D,ID,X,IX,F,T,NDF,NDM,NEN1,NST,I)
IF(I.GT.0) GO TO 404
GO TO 330
C.....COMPUTE REACTIONS AND PRINT
15 CALL PZERO(DR,NNEQ*IPR)
CALL PFORM(UL,XL,TL,LD,P,S,IE,D,ID,X,IX,F,T,JDIAG,DR,DR,DR,ECS,
1 CSI,CSTR,CVOL,CVI,S0,PECS,TIME,DT,NDF,NDM,NEN1,NSC,NST,6,B,
2 M(NV),.FALSE.,.TRUE.,.FALSE.,.TRUE.,IFLAG)
CALL PRTREA(DR,NDF)
GO TO 330
16 CALL PFORM(UL,XL,TL,LD,P,S,IE,D,ID,X,IX,F,T,JDIAG,DR,DR,DR,ECS,
1 CSI,CSTR,CVOL,CVI,S0,PECS,TIME,DT,NDF,NDM,NEN1,NSC,NST,2,B,F,
2 .FALSE.,.FALSE.,.FALSE.,.FALSE.,IFLAG)
GO TO 330
C.....SET DISPLACEMENT INCREMENT TO ZERO,DEFINE PREDICTOR PROCEDURE
17 CALL PZERO(DR,NNEQ*IPR)
IFLAG=-1
GO TO 330
C.....ADD STRESS AND DISPLACEMENT INCREMENTS TO TOTAL VALUES
C.....ADD CYCLIC VOLUMETRIC STRAIN INCREMENT TO TOTAL VALUE
18 DO 500 N=1,NEQ
500 B(N)=B(N)+DRS(N)
CALL PZERO(DRS,NEQ*IPR)

```

```

DO 550 N=1,NNSC
STORE=ECS(N)
ECS(N)=PECS(N)
550 PECS(N)=STORE
DO 560 N=1,NUMEL
560 CVOL(N)=CVOL(N)+CVI(N)
GO TO 330
C.....COMPUTE GEOSTATIC STRESSES AND ADD THEM TO THE 'ECS' ARRAY
19 CALL PFORM(UL,XL,TL,LD,P,S,IE,D,ID,X,IX,F,T,JDIAG,DR,DR,DR,ECS,
1 CSI,CSTR,CVOL,CVI,S0,PECS,TIME,DT,NDF,NDM,NEN1,NSC,NST,5,B,F,
2 .FALSE.,.FALSE.,.FALSE.,.FALSE.,IFLAG)
330 L=L+1
IF(L.GT.LL) RETURN
GO TO 299
400 WRITE(6,4000)
RETURN
401 WRITE(6,4001)
RETURN
402 WRITE(6,4002)
RETURN
403 WRITE(6,4003)
404 WRITE(6,4004)
RETURN
1000 FORMAT(A4,1X,A4,1X,2F5.0)
2000 FORMAT(10X,A4,1X,A4,1X,2G15.5)
2001 FORMAT(A1,20A4//5X,18HMACRO INSTRUCTIONS//5X,15HMACRO STATEMENT,5X
1,10HVARIABLE 1,5X,10HVARIABLE 2)
2002 FORMAT(5X,29HDISPLACEMENT CONVERGENCE TEST,10X,14HCYCLE NUMBER =,F
1 10.2/10X,7HUNMAX =,G15.5,5X,7HUN =,G15.5,5X,7HTOL =,G15.5)
2003 FORMAT(A1,20A4,10X,4HTIME,G13.5//5X,17HPROPORTIONAL LOAD,G13.5)
2004 FORMAT(5X,4HCN =,G12.5,5X,4HDN =,G12.5,5X,4HUN =,G12.5,5X,4HAG =
1 ,G12.5,5X,4HAC =,G12.5)
2005 FORMAT(5X,22HFORCE CONVERGENCE TEST/10X,7HRNMAX =,G15.5,5X,
1 7HRN =,G15.5,5X,7HTOL =,G15.5)
2010 FORMAT(2X,19H**MACRO INSTRUCTION,I4,13H EXECUTED** ,2(A4,2X), 6H.
1V1 = ,G13.4, 8H , V2 = ,G13.4)
4000 FORMAT(5X,46H**FATAL ERROR 10** UNBALANCED LOOP/NEXT MACROS )
4001 FORMAT(5X,45H**FATAL ERROR 11** LOOPS NESTED DEEPER THAN 8)
4002 FORMAT(5X,57H**FATAL ERROR 12** MACRO LABEL MISMATCH ON A READ COM
1MAND)
4003 FORMAT(5X,63H**FATAL ERROR 13** MACRO EXCD MUST BE PRECEDED BY LMA
1S AND FORM)
4004 FORMAT(5X,84H**FATAL ERROR 14** ATTEMPT TO CHANGE BOUNDARY RESTRAI
1NT CODES DURING MACRO EXECUTION )
END
SUBROUTINE PFORM(UL,XL,TL,LD,P,S,IE,D,ID,X,IX,F,T,JDIAG,B,A,C,
1ECS,CSI,CSTR,CVOL,CVI,S0,PECS,TIME,DT,NDF,NDM,NEN1,NSC,NST,ISW,U,
2UD,AFL,BFL,CFL,DFL,IFLAG)
C
C.....COMPUTE ELEMENT ARRAYS AND ASSEMBLE GLOBAL ARRAYS
C

```

```

IMPLICIT DOUBLE PRECISION(A-H,O-Z)
LOGICAL AFL,BFL,CFL,DFL
COMMON /CDATA/ O,HEAD(20),NUMNP,NUMEL,NUMMAT,NEN,NEQ,IPR
COMMON /ELDATA/ DM,N,MA,MCT,IEL,NEL
COMMON/PRLOD/ PROP
DIMENSION XL(NDM,1),LD(NDF,1),P(1),S(NST,1),IE(1),D(35,1),ID(NDF,1
1),X(NDM,1),IX(NEN1,1),F(NDF,1),JDIAG(1),B(1),A(1),C(1),UL(NDF,1)
2  ,TL(1),T(1),U(1),UD(NDF,1),ECS(NSC,1),CSI(NSC,1),CSTR(NSC,1)
3  ,PECS(NSC,1),CVOL(1),CVI(1),SO(1)
C.....LOOP ON ELEMENTS
  IEL=0
  DO 110 N=1,NUMEL
C.....SET UP LOCAL ARRAYS
  DO 108 I=1,NEN
    II=IX(I,N)
    IF(II.NE.0) GO TO 105
    TL(I)=0.
  DO 103 J=1,NDM
103  XL(J,I)=0.
    DO 104 J=1,NDF
      UL(J,I)=0.
      UL(J,I+NEN)=0.
104  LD(J,I)=0
      GO TO 108
105  IID=II*NDF-NDF
      NEL=I
      TL(I)=T(II)
      DO 106 J=1,NDM
106  XL(J,I)=X(J,II)
        DO 107 J=1,NDF
          K=IABS(ID(J,II))
          UL(J,I)=F(J,II)*PROP
          UL(J,I+NEN)=UD(J,II)
          IF(K.GT.0) UL(J,I)=0.
          IF(K.GT.0.AND.ISW.NE.6) UL(J,I)=C(K)
          IF(DFL) K=IID+J
107  LD(J,I)=K
108  CONTINUE
C.....FORM ELEMENT ARRAY
  MA=IX(NEN1,N)
  IF(IE(MA).NE.IEL) MCT=0
  IEL=IE(MA)
  CALL ELMLIB(D(1,MA),UL,XL,IX(1,N),TL,S,P,ECS(1,N),CSI(1,N),CSTR(1,
1N),CVOL(N),CVI(N),SO(N),PECS(1,N),TIME,DT,NDF,NDM,NST,ISW,IFLAG,N)
C.....ADD TO TOTAL ARRAY
  IF(AFL.OR.BFL.OR.CFL) CALL ADDSTF(A,B,C,S,P,JDIAG,LD,NST,NEL*NDF,
1  AFL,BFL,CFL)
110 CONTINUE
  RETURN
  END

```

```

SUBROUTINE ELMLIB(D,U,X,IX,T,S,P,ECS,CSI,CSTR,CVOL,CVI,S0,PECS,
1 TIME,DT,I,J,K,ISW,IFLAG,LMNT)
C
C.....ELEMENT LIBRARY
C
      IMPLICIT DOUBLE PRECISION(A-H,O-Z)
      COMMON /ELDATA/ DM,N,MA,MCT,IEL,NEL
      DIMENSION P(K),S(K,K),D(1),U(1),X(1),IX(1),T(1)
      DIMENSION ECS(1),CSI(1),CSTR(1),PECS(1)
      IF(IEL.LT.-2.OR.IEL.GT.2) GO TO 400
      IF(ISW.LT.3) GO TO 30
      DO 20 L=1,K
      P(L)=0.0
      DO 20 M=1,K
20    S(L,M)=0.0
30    GO TO (1,2),IABS(IEL)
C.....ELMTO1-----> PLANE STRAIN CYCLIC ELEMENT
C.....ELMTO2-----> AXISYMMETRIC CYCLIC ELEMENT
1    CALL ELMTO1(D,U,X,IX,T,S,P,ECS,CSI,CSTR,CVOL,CVI,S0,PECS,TIME,DT,
1 I,J,K,ISW,IFLAG,LMNT)
      GO TO 10
2    CALL ELMTO2(D,U,X,IX,T,S,P,ECS,CSI,CSTR,CVOL,CVI,S0,PECS,TIME,DT,
1 I,J,K,ISW,IFLAG,LMNT)
10   RETURN
400  WRITE(6,4000) IEL
      STOP
4000 FORMAT(5X,39H**FATAL ERROR 04** ELEMENT CLASS NUMBER,I3,6H INPUT)
      END

SUBROUTINE MODEL(ECS,CSI,CSTR,CVOL,FI,S0,D,T,DT,I,LMNT,LINT)
C.....THIS SUBROUTINE 1)ESTIMATES THE TANGENT SHEAR AND BULK MODULUS
C.....OF THE SOIL AS FUNCTIONS OF THE EFFECTIVE STATE OF STRESS
C.....2) ESTIMATES THE CYCLIC STRAIN INCREMENT
      IMPLICIT DOUBLE PRECISION(A-H,O-Z)
      DIMENSION ECS(4),CSI(4),D(1),CSTR(4),P(4),S(3),EPS(3)
C.....INITIAL STATE OF STRESS
      DO 10 L=1,3
10   S(L)=ECS(L)
      CALL PSTRES(S,P(1),P(2),P(4))
      P(3)=ECS(4)
      SOCT=(P(1)+P(2)+P(3))/3.
      IF(SOCT.GE.0.) GO TO 400
      DO 20 L=1,3
20   S(L)=P(L)-SOCT
      TAU=1.224744871*SQRT(S(1)*S(1)+S(2)*S(2)+S(3)*S(3))
      TGM=-6.*SIN(D(11))/(3.-SIN(D(11)))
      IF(TGM.NE.0..AND.(TAU/SOCT).LT.TGM) SOCT=0.95*TAU/TGM
      IF(ECS(1).NE.ECS(3)) TAU=TAU*(ECS(1)-ECS(3))/ABS(ECS(1)-ECS(3))
      S0=DMAX1(-SOCT,S0)
      D(30)=DMAX1(D(30),D(14))
      TAUF=TGM*SOCT

```

```

      IF(D(13).GT.0.)  TAUFD=D(13)
      GO TO(30,50),I
C.....
C.....TANGENT SOIL MODULI.....
C.....
30    BULK=D(20)*D(16)*(-SOCT/D(16))**D(21)
      SHEAR=.23*D(17)*(D(18)-D(14))**2./(1.+D(14))*D(16)*(-SOCT/D(16))
      1    **D(19)
      IF(T.EQ.0..AND.LMNT.NE.0)
      1    WRITE(10,3000) LMNT,ECS,CSI,SOCT,TAU,TAUF
3000  FORMAT(' N',I5,' ECS',4F9.3,' CSI',4F9.3,' SOCT',F10.4,
      1' TAU',F10.4,' TAUF',F10.4)
      IF(ABS(TAU).GT.TAUF.AND.LMNT.NE.0) WRITE(6,2000) LMNT,SOCT,TAU,
      1  TAUF
2000  FORMAT('***LOCAL FAILURE***  ELEM=',I5,' SOCT=',F10.5,' TAU=',
      1F10.5,' TAUF=',F10.5)
      D(10)=(3.*BULK-2.*SHEAR)/(6.*BULK+2.*SHEAR)
      E=9.*BULK*SHEAR/(3.*BULK+SHEAR)
      D(1)=E*(1.+(1.-D(7))*D(10))/(1.+D(10))/(1.-D(7)*D(10))
      D(2)=D(10)*D(1)/(1.+(1.-D(7))*D(10))
      D(3)=E/2./(1.+D(10))
      RETURN
C.....
C.....CYCLIC STRAIN INCREMENT.....
C.....
50    IF(DT.EQ.0..OR.D(23).EQ.0.) GO TO 400
C.....
C.....STEP 1 :  CYCLIC SHEAR STRESS.....
      DSOCT=(CSI(1)+CSI(3)+CSI(4))/3.
      S(1)=CSI(1)-DSOCT
      S(2)=CSI(3)-DSOCT
      S(3)=CSI(4)-DSOCT
      DTAU=1.224744871*SQRT(S(1)*S(1)+S(2)*S(2)+S(3)*S(3)+CSI(2)*CSI(2))
      IF(S(1).NE.S(2))DTAU=DTAU*(S(1)-S(2))/ABS(S(1)-S(2))
      IF(DTAU.EQ.0.) GO TO 400
      IF(TAU.LT.0.) DTAU=-DTAU
      TAU=ABS(TAU)
      IF(DTAU.GT.0.) GO TO 40.
      DSOCT=-DSOCT
      DTAU=-DTAU
C.....
C.....STEP 2 :  CYCLIC STRESS PATH DIRECTION
40    TGL=-6.*SIN(D(12))/(3.-SIN(D(12)))
      IF(D(13).EQ.0.) GO TO 60
      TC=SOCT*TGL
      TE=-TC
      SOCTL=SOCT
      SOCTU=SOCT
      SOCTF=D(13)/TGM
      IF((TAU+DTAU).LE.TC) GO TO 65
      CALL INTERPOL(TC,SOCT,D(13),SOCTF,(TAU+DTAU),SOCTL)

```

```

IF(TAU.GT.TC) CALL INTERPOL(TAU,SOCT,D(13),SOCTF,(TAU+DTAU),SOCTL)
CALL INTERSECT(TAU,SOCT,(TAU+DTAU),SOCTL,-TGL,TE,SE)
CALL INTERPOL(TE,SE,-D(13),SOCTF,(TAU-DTAU),SOCTU)
IF((TAU-DTAU).GE.TE) CALL INTERPOL(TAU,SOCT,TE,SE,(TAU-DTAU)
1      ,SOCTU)
GO TO 65
60    SOCTL=SOCT+DSOCT
      SOCTU=SOCT-DSOCT
C.....
C.....STEP 3 :   CYCLIC SHEAR STRAIN.....
65    TAUL=SOCTL*TGM-TAU+DTAU
      TAUU=SOCTU*TGM+TAU+DTAU
      GO=D(17)*(D(18)-D(14))**2./(1.+D(14))*D(16)
      GO=GO*(-SOCT/D(16))**D(19)/100.
      HYP=DMAX1(.01D0,1.D0-2.D0*DTAU/TAUL)
      GPPL=DTAU/GO/HYP
      HYP=DMAX1(.01D0,1.D0-2.D0*DTAU/TAUU)
      GPPU=DTAU/GO/HYP
      GPP=GPPU
      IF(ECS(1).LT.ECS(3)) GPP=GPPL
      IF(GPP.LT.1.E-3) GO TO 400
C.....
C.....STEP 4 :   EFFECT OF CYCLIC LIMIT STATE.....
      DMAX=SO+TAU/TGL
      DELT=-SOCT+TAU/TGL
      IF(DELT.GE.DMAX) DELT=.9*DMAX
      SUN=DELT/(DMAX-DELT)
      DMAX=D(30)-D(15)
      DELT=D(14)-D(15)
      IF(DELT.GE.DMAX) DELT=.9*DMAX
      SDR=DELT/(DMAX-DELT)
      SS=DMIN1(SUN,SDR)
      EFCT=1.-EXP(-D(22)*SS)
      EFCT=DMAX1(EFCT,0.D0)
      IF(LINT.EQ.1) WRITE(10,4000)LMNT,SOCT,DSOCT,TAU,DTAU,TAUU,TAUL,
4000  1GPPL,GPPU,GPP,EFCT
      FORMAT(' N',I3,' S',F9.3,' DS',F9.3,' T',F9.3,' DT',F9.3,
1' TU',F9.3,' TL',F9.3,' GPL',F10.5,' GPU',F10.5,' GP',F10.5,
2' ECT',F8.5)
C.....
C.....STEP 5 :   CYCLIC STRAIN INCREMENT IN PRINCIPAL DIRECTIONS.....
      TS=(-CVOL/(D(23)*GPP**D(25)))*(1./D(24))
      FI=-D(23)*GPP**D(25)*((TS+DT)**D(24)-TS**D(24))
      F=FI*EFCT
      IF(TAU.EQ.0..OR.FI.EQ.0.) GO TO 90
      R=-D(26)*(TAU/2.)*(D(27)-1.)/(-SOCT)**D(27)*FI
      R=1.3333333333333333/R
      DO 70 L=1,3
      S(L)=P(L)-SOCT
70    EPS(L)=S(L)/R+F/3.
      GO TO 80

```

```

90   DO 95 L=1,3
95   EPS(L)=F/3.
C.....
C.....STEP 6 : CYCLIC STRAIN INCREMENT IN NATURAL COORDINATES
80   THETA=P(4)
      CO=COS(THETA*.0174532925)
      SI=SIN(THETA*.0174532925)
      CSTR(1)=EPS(1)*CO*CO+EPS(2)*SI*SI
      CSTR(3)=EPS(1)*SI*SI+EPS(2)*CO*CO
      CSTR(2)=CO*SI*(EPS(1)-EPS(2))
      CSTR(4)=EPS(3)
      RETURN
400  DO 450 L=1,4
450  CSTR(L)=0.
      FI=0.
      RETURN
      END
      SUBROUTINE ELMT01(D,UL,XL,IX,TL,S,P,ECS,CSI,CSTR,CVOL,CVI,SO,
1    PECS,TIME,DT,NDF,NDM,NST,ISW,IFLAG,LMNT)
C
C.....PLANE NON-LINEAR CYCLIC ELEMENT ROUTINE
C
      IMPLICIT DOUBLE PRECISION(A-H,O-Z)
      COMMON /CDATA/ O,HEAD(20),NUMNP,NUMEL,NUMMAT,NEN,NEQ,IPR
      COMMON /ELDATA/ DM,N,MA,MCT,IEL,NEL
      DIMENSION D(1),UL(NDF,1),XL(NDM,1),IX(1),TL(1),S(NST,1),P(1)
1    ,SHP(3,9),SHPP(3,9),SG(9),TG(9),WG(9),SIG(7),EPS(4),WD(2)
      DIMENSION ECS(1),CSI(1),CSTR(1),PECS(1),EECS(4)
      DATA WD/4HRESS,4HRAIN/
C.....GO TO CORRECT ARRAY PROCESSOR
      GO TO(1,2,3,4,5,4,4,4,4), ISW
C.....INPUT MATERIAL PROPERTIES
1    READ(5,1000) E,XNU,D(4),L,K,I,D(8)
      IF(I.NE.0) I=1
      IF(I.EQ.0) I=2
      D(1)=E*(1.+(1-I)*XNU)/(1.+XNU)/(1.-I*XNU)
      D(2)=XNU*D(1)/(1.+(1-I)*XNU)
      D(3)=E/2./(1.+XNU)
      L=MIN0(3,MAX0(1,L))
      D(5)=L
      K=MIN0(3,MAX0(1,K))
      D(6)=K
      D(7)=I
      LINT=0
      WRITE(6,2000) WD(I),E,XNU,D(4),L,K,D(8)
      D(9)=1.
      D(10)=XNU
      READ(5,1600) (D(NI),NI=11,27)
      PHI1=D(11)*57.29577951
      PHI2=D(12)*57.29577951
      WRITE(6,2003) PHI1,PHI2,(D(NI),NI=13,27)

```

```

      RETURN
2     RETURN
3     L=D(5)
      IF(L*L.NE.LINT) CALL PGAUSS(L,LINT,SG,TG,WG)
C.....FAST STIFFNESS COMPUTATION, COMPUTE INTEGRALS OF SHAPE FUNCTIONS
      NPP=NEL/2
      NPP1=NPP+1
      IF(IEL.LT.0) NPP1=1
      DO 325 L=1,LINT
        CALL SHAPE(SG(L),TG(L),XL,SHP,XSJ,NDM,NEL,IX,.FALSE.)
        XSJ=XSJ*WG(L)
C.....LOOP OVER ROWS
        J1=1
        DO 320 J=1,NEL
          W11=SHP(1,J)*XSJ
          W12=SHP(2,J)*XSJ
C.....LOOP OVER COLUMNS (SYMMETRY NOTED)
          K1=J1
          DO 310 K=J,NEL
            S(J1 ,K1 )=S(J1 ,K1 )+W11*SHP(1,K)
            S(J1 ,K1+1)=S(J1 ,K1+1)+W11*SHP(2,K)
            S(J1+1,K1 )=S(J1+1,K1 )+W12*SHP(1,K)
            S(J1+1,K1+1)=S(J1+1,K1+1)+W12*SHP(2,K)
310     K1=K1+NDF
320     J1=J1+NDF
          CALL SHAPE(SG(L),TG(L),XL,SHPP,XSJP,NDM,NPP,IX,.FALSE.)
          DO 322 J=NPP1,9
            DO 322 JJ=1,3
322     SHPP(JJ,J)=0.
            DO 325 J=1,NPP
              JB=J*NDF
              DO 325 K=1,NEL
                KB=K*NDF-2
                S(KB ,JB)=S(KB ,JB)+D(9)*SHPP(3,J)*SHP(1,K)*XSJ
                S(KB+1,JB)=S(KB+1,JB)+D(9)*SHPP(3,J)*SHP(2,K)*XSJ
                S(KB+2,JB)=S(KB+2,JB)+D(8)*SHPP(3,K)*SHPP(3,J)*XSJ
                S(JB,KB )=S(KB ,JB)
                S(JB,KB+1)=S(KB+1,JB)
325     S(JB,KB+2)=S(KB+2,JB)
C.....ASSEMBLE THE STIFFNESS MATRIX FROM INTEGRALS AND MATERIAL PROPS.
          NSL=NEL*NDF
          CALL EXTRA(ECS,PECS,EECS,IFLAG)
C          WRITE(6,1550) (ECS(J),J=1,4),(PECS(J),J=1,4),EECS,IFLAG
          IF(IEL.GE.0) CALL MODEL(EECS,CSI,CSTR,CVOL,CVI,SO,D,TIME,DT,1,
1 LMNT,1)
C          WRITE(6,1500) (ECS(J),J=1,4),(PECS(J),J=1,4),EECS,(CSTR(J),J=1,4)
          DO 330 J=1,NSL,NDF
            DO 330 K=J,NSL,NDF
              W11=S(J,K)
              W12=S(J,K+1)
              W21=S(J+1,K)

```



```

W22=S(J+1,K+1)
S(J ,K )=D(1)*W11+D(3)*W22
S(J ,K+1)=D(2)*W12+D(3)*W21
S(J+1,K )=D(2)*W21+D(3)*W12
S(J+1,K+1)=D(1)*W22+D(3)*W11
C.....FORM LOWER PART BY SYMMETRY
S(K,J)=S(J,K)
S(K,J+1)=S(J+1,K)
S(K+1,J)=S(J,K+1)
330 S(K+1,J+1)=S(J+1,K+1)
RETURN
4 L=D(6)
IF(ISW.EQ.6) L=D(5)
IF(L*L.NE.LINT) CALL PGAUSS(L,LINT,SG,TG,WG)
C.....COMPUTE ELEMENT STRESSES, STRAINS, AND FORCES
DO 600 L=1,LINT
C.....COMPUTE ELEMENT SHAPE FUNCTIONS
NPP=NEL/2
NPP1=NPP+1
IF(IEL.LT.0) NPP1=1
CALL SHAPE(SG(L),TG(L),XL,SHP,XSJ,NDM,NEL,IX,.FALSE.)
C.....COMPUTE STRAINS AND COORDINATES
DO 410 I=1,4
410 EPS(I)=0.0
XX=0.0
YY=0.0
DO 420 J=1,NEL
XX=XX+SHP(3,J)*XL(1,J)
YY=YY+SHP(3,J)*XL(2,J)
EPS(1)=EPS(1)+SHP(1,J)*UL(1,J)
EPS(3)=EPS(3)+SHP(2,J)*UL(2,J)
420 EPS(2)=EPS(2)+SHP(1,J)*UL(2,J)+SHP(2,J)*UL(1,J)
IF(ISW.EQ.4) GO TO 427
CALL EXTRA(ECS,PECS,EECS,IFLAG)
IF(ISW.NE.6) GO TO 422
CALL MODEL(EECS,CSI,CSTR,CVOL,CVI,S0,D,TIME,DT,2,LMNT,L)
422 DO 425 I=1,4
425 EPS(I)=EPS(I)-CSTR(I)
C.....COMPUTE STRESSES
IF(IEL.GE.0.) CALL MODEL(EECS,CSI,CSTR,CVOL,CVI,S0,D,TIME,
1 DT,1,0,1)
SIG(1)=D(1)*EPS(1)+D(2)*EPS(3)+D(2)*EPS(4)
SIG(3)=D(2)*EPS(1)+D(1)*EPS(3)+D(2)*EPS(4)
SIG(2)=D(3)*EPS(2)
SIG(4)=D(2)*EPS(1)+D(2)*EPS(3)+D(1)*EPS(4)
IF(ISW.EQ.6) GO TO 620
IF(ISW.EQ.7) GO TO 630
IF(ISW.EQ.8) GO TO 640
IF(ISW.EQ.9) GO TO 650
427 DO 428 I=1,3
428 SIG(I)=ECS(I)

```

```

      CALL PSTRES(SIG,SIG(4),SIG(6),SIG(7))
      SIG(5)=ECS(4)
C.....OUTPUT STRESSES AND STRAINS
      MCT=MCT-2
      IF(MCT.GT.0) GO TO 430
      WRITE(6,2001) 0,HEAD
      MCT=50
430  WRITE(6,2002) N,MA,XX,YY,SIG
      GO TO 600
C.....COMPUTE AVERAGE CONSOLIDATION STRESS
630  DO 635 I=1,4
635  ECS(I)=ECS(I)+SIG(I)/LINT
      DO 636 I=1,4
636  PECS(I)=ECS(I)
      GO TO 600
C.....COMPUTE AVERAGE CYCLIC STRESS INCREMENT
640  DO 645 I=1,4
645  CSI(I)=CSI(I)+SIG(I)/LINT
      GO TO 600
650  DO 655 I=1,4
655  PECS(I)=ECS(I)+SIG(I)/LINT
1500 FORMAT(/' ECS :',4F10.3,' PECS :',4F10.3/' EECS:',4F10.3,' CSTR:
1',4E15.5/)
1550 FORMAT(/' ECS :',4F10.3,' PECS :',4F10.3/' EECS:',4F10.3,' IFLAG:'
1,I5/)
      GO TO 600
C.....COMPUTE INTERNAL FORCES
620  CALL SHAPE(SG(L),TG(L),XL,SHPP,XSJP,NDM,NPP,IX,.FALSE.)
      DO 618 I=NPP1,9
      DO 618 II=1,3
618  SHPP(II,I)=0.
      DV=XSJ*WG(L)
      PPLD=0.
      DO 615 J=1,NPP
615  PPLD=PPLD+SHPP(3,J)*UL(3,J)*D(9)
      PWF=0.
      DO 611 J=1,NEL
611  PWF=PWF+(SHP(1,J)*UL(1,J)+SHP(2,J)*UL(2,J))*D(9)+SHPP(3,J)*UL(3,J)
1 *D(8)
      J1=1
      DO 610 J=1,NEL
      P(J1)=P(J1)-(SHP(1,J)*SIG(1)+SHP(2,J)*SIG(2))*DV-SHP(1,J)*PPLD*DV
      P(J1+1)=P(J1+1)-(SHP(1,J)*SIG(2)+SHP(2,J)*SIG(3))*DV-SHP(2,J)*PPLD
1 *DV
      P(J1+2)=P(J1+2)-SHPP(3,J)*PWF*DV
610  J1=J1+NDF
      GO TO 600
C.....COMPUTE GEOSTATIC CONSOLIDATION STRESS
5  CALL SHAPE(0.,0.,XL,SHP,XSJ,NDM,NEL,IX,.FALSE.)
      CKO=D(10)/(1.-D(10))
      YY=0.

```

```

DO 700 I=1,NEL
700  YY=YY+SHP(3,I)*XL(2,I)
    DECS=YY*D(4)
    DECS=-ABS(DECS)
    ECS(1)=ECS(1)+DECS*CKO
    ECS(3)=ECS(3)+DECS
    ECS(4)=ECS(4)+DECS*CKO
    DO 710 I=1,4
710  PECS(I)=ECS(I)
600  CONTINUE
    RETURN
C.....FORMATS FOR INPUT-OUTPUT
1000 FORMAT(3F10.0,3I5,F10.0)
1600 FORMAT(6F10.5)
2000 FORMAT(/5X,8HPLANE ST,A4,26H NON LINEAR CYCLIC ELEMENT//
110X,12HYOUNG'S MOD.,E15.5,10H (CONST.)/10X,13HPOISSON RATIO,F8.5/
210X,11HUNIT WEIGHT,E18.5/10X,13HGAUSS PTS/DIR,I3/10X,10HSTRESS PTS
3,I6/,10X,14HPENALTY CONST.,F7.5)
2001 FORMAT(A1,20A4//5X,16HELEMENT STRESSES//20H ELEMENT MATERIAL
1 ,4X,7H1-COORD,4X,7H2-COORD,3X,9H11-STRESS,3X,9H12-STRESS,3X,
2 9H22-STRESS,3X,8H1-STRESS,3X,8H2-STRESS,3X,8H3-STRESS,2X,5HANGL
3E)
2002 FORMAT(2I10,2F11.4,3E12.4,3E11.4,F7.2)
2003 FORMAT(10X,14HFRICION ANGLE,F8.2/10X,14HCYC. LMT STATE,F8.2/
110X,14HUNDR. STRENGTH,F8.2/10X,10HVOID RATIO,F10.3/10X,14HMIN VOID
2 RATIO,F10.3/10X,11HATM. PRESS.,F10.2/10X,13HSHEAR MODULUS,3F15.5/
310X,13HBULK MODULUS,2F15.5/10X,13HCYC. LMT EFCT,F13.5/10X,15HCYC.
4 VOL. STIF.,F12.5,2F15.5/10X,15HCYC. DEV. STIF.,F10.5,F15.5)
    END
    SUBROUTINE ACTCOL(A,B,JDIAG,NEQ,AFAC,BACK)
    IMPLICIT DOUBLE PRECISION(A-H,O-Z)
    LOGICAL AFAC,BACK
    COMMON/ENGYS/ AENGY
    DIMENSION A(1),B(1),JDIAG(1)
C
C.....ACTIVE COLUMN PROFILE SYMMETRIC EQUATION SOLVER
C
C.....FACTOR A TO UT*D*U, REDUCE B
    AENGY=0.0
    JR=0
    DO 600 J=1,NEQ
    JD=JDIAG(J)
    JH=JD-JR
    IS=J-JH+2
    IF(JH-2) 600,300,100
100  IF(.NOT.AFAC) GO TO 500
    IE=J-1
    K=JR+2
    ID=JDIAG(IS-1)
C.....REDUCE ALL EQUATIONS EXCEPT DIAGONAL
    DO 200 I=IS,IE

```

```

      IR=ID
      ID=JDIAG(I)
      IH=MIN0(ID-IR-1,I-IS+1)
      IF(IH.GT.0) A(K)=A(K)-DOT(A(K-IH),A(ID-IH),IH)
200   K=K+1
      C.....REDUCE DIAGONAL TERM
300   IF(.NOT.AFAC) GO TO 500
      IR=JR+1
      IE=JD-1
      K=J-JD
      DO 400 I=IR,IE
      ID=JDIAG(K+I)
      IF(A(ID).EQ.0.0) GO TO 400
      D=A(I)
      A(I)=A(I)/A(ID)
      A(JD)=A(JD)-D*A(I)
400   CONTINUE
      C.....REDUCE RHS
500   IF(BACK) B(J)=B(J)-DOT(A(JR+1),B(IS-1),JH-1)
600   JR=JD
      IF(.NOT.BACK) RETURN
      C.....DIVIDE BY DIAGONAL PIVOTS
      DO 700 I=1,NEQ
      ID=JDIAG(I)
      IF(A(ID).NE.0.0) B(I)=B(I)/A(ID)
700   AENGY=AENGY+B(I)*B(I)*A(ID)
      C.....BACKSUBSTITUTE
      J=NEQ
      JD=JDIAG(J)
800   D=B(J)
      J=J-1
      C   IF(J.LE.0) WRITE(6,5000) (B(I),I=1,NEQ)
      IF(J.LE.0) RETURN
      JR=JDIAG(J)
      IF(JD-JR.LE.1) GO TO 1000
      IS=J-JD+JR+2
      K=JR-IS+1
      DO 900 I=IS,J
900   B(I)=B(I)-A(I+K)*D
1000  JD=JR
      GO TO 800
C000  FORMAT(/,'  DISPLACEMENT' ,/,8F9.5)
      END

      SUBROUTINE ADDSTF(A,B,C,S,P,JDIAG,LD,NST,NEL,AFL,BFL,CFL)
      C
      C.....ASSEMBLE GLOBAL ARRAYS
      C
      IMPLICIT DOUBLE PRECISION(A-H,O-Z)
      LOGICAL AFL,BFL,CFL
      DIMENSION A(1),B(1),JDIAG(1),P(1),S(NST,1),LD(1),C(1)

```

```

DO 200 J=1,NEL
K=LD(J)
IF(K.EQ.0) GO TO 200
IF(BFL) B(K)=B(K)+P(J)
IF(.NOT.AFL.AND..NOT.CFL) GO TO 200
L=JDIAG(K)-K
DO 100 I=1,NEL
M=LD(I)
IF(M.GT.K.OR.M.EQ.0) GO TO 100 .
M=L+M
IF(AFL) A(M)=A(M)+S(I,J)
IF(CFL) C(M)=C(M)+S(J,I)
100 CONTINUE
200 CONTINUE
RETURN
END

```

```

FUNCTION DOT(A,B,N)
C
C.....VECTOR DOT PRODUCT
C
IMPLICIT DOUBLE PRECISION(A-H,O-Z)
DIMENSION A(1),B(1)
DOT=0.0
DO 100 I=1,N
100 DOT=DOT+A(I)*B(I)
RETURN
END

```

```

SUBROUTINE NORM(X,Y,N)
C
C.....NORMALIZE VECTOR Y TO UNIT VECTOR X
C
IMPLICIT DOUBLE PRECISION(A-H,O-Z)
DIMENSION X(1),Y(1)
SCALE=SQRT(DOT(Y,Y,N))
DO 100 I=1,N
100 X(I)=Y(I)/SCALE
RETURN
END

```

```

LOGICAL FUNCTION PCOMP(A,B)
PCOMP=.FALSE.
C.....IT MAY BE NECESSARY TO REPLACE THE FOLLOWING ALPHANUMERIC
C.....COMPARISON STATEMENT IF COMPUTER PRODUCES AN OVERFLOW
IF(A.EQ.B) PCOMP=.TRUE.
RETURN
END

```

```

SUBROUTINE PLOAD(ID,F,B,NN,P)
C

```

C.....FORM LOAD VECTOR IN COMPACT FORM

C

IMPLICIT DOUBLE PRECISION(A-H,O-Z)

DIMENSION ID(1),F(1),B(1)

DO 100 N=1,NN

J=ID(N)

100 IF(J.GT.0) B(J)=F(N)*P

RETURN

END

SUBROUTINE PROFIL (JDIAG, ID, IX, NDF, NEN1, NAD)

C

C.....COMPUTE PROFILE OF GLOBAL ARRAYS

C

IMPLICIT DOUBLE PRECISION(A-H,O-Z)

COMMON /CDATA/ O,HEAD(20),NUMNP,NUMEL,NUMMAT,NEN,NEQ,IPR

DIMENSION JDIAG(1),ID(NDF,1),IX(NEN1,1)

C.....SET UP THE EQUATION NUMBERS

NEQ=0

DO 50 N=1,NUMNP

DO 40 I=1,NDF

J=ID(I,N)

IF(J) 30,20,30

20 NEQ=NEQ+1

ID(I,N)=NEQ

JDIAG(NEQ)=0

GO TO 40

30 ID(I,N)=0

40 CONTINUE

50 CONTINUE

C.....COMPUTE COLUMN HEIGHTS

DO 500 N=1,NUMEL

DO 400 I=1,NEN

II=IX(I,N)

IF(II.EQ.0) GO TO 400

DO 300 K=1,NDF

KK=ID(K,II)

IF(KK.EQ.0) GO TO 300

DO 200 J=1,NEN

JJ=IX(J,N)

IF(JJ.EQ.0) GO TO 200

DO 100 L=1,NDF

LL=ID(L,JJ)

IF(LL.EQ.0) GO TO 100

M=MAXO(KK,LL)

JDIAG(M)=MAXO(JDIAG(M),IABS(KK-LL))

100 CONTINUE

200 CONTINUE

300 CONTINUE

400 CONTINUE

500 CONTINUE

C.....COMPUTE DIAGONAL POINTERS FOR ARRAYS

```

NAD=1
JDIAG(1)=1
IF(NEQ.EQ.1) RETURN
DO 600 N=2,NEQ
600 JDIAG(N)=JDIAG(N)+JDIAG(N-1)+1
NAD=JDIAG(NEQ)
RETURN
END

```

```

SUBROUTINE PROMUL(A,B,C,JDIAG,NEQ)
IMPLICIT DOUBLE PRECISION(A-H,O-Z)
DIMENSION A(1),B(1),C(1),JDIAG(1)

```

C

C.....ROUTINE TO FORM $C = C + A*B$ WHERE A IS A SYMMETRIC SQUARE MATRIX
C.....STORED IN PROFILE FORM,B,C ARE VECTORS,AND JDIAG LOCATES THE
C.....DIAGONALS IN A

C

```

JS=1
DO 200 J=1,NEQ
JD=JDIAG(J)
IF(JS.GT.JD) GO TO 200
BJ=B(J)
AB=A(JD)*BJ
IF(JS.EQ.JD) GO TO 150
JB=J-JD
JE=JD-1
DO 100 JJ=JS,JE
AB=AB+A(JJ)*B(JJ+JB)
100 C(JJ+JB)=C(JJ+JB)+A(JJ)*BJ
150 C(J)=C(J)+AB
200 JS=JD+1
RETURN
END

```

```

SUBROUTINE PRDIS(ID,D,X,B,F,NDM,PDF)

```

C

C.....OUTPUT NODAL VALUES

C

```

IMPLICIT DOUBLE PRECISION(A-H,O-Z)
LOGICAL PCOMP
COMMON/PRLD/ PROP
COMMON /CDATA/ O,HEAD(20),NUMNP,NUMEL,NUMMAT,NEN,NEQ,IPR
COMMON /LABEL/ PDIS(6),A(6),BC(2),DI(6),CD(3),TE(3),FD(3)
COMMON /TDATA/ TIME,DT,C1,C2,C3,C4,C5
DIMENSION X(NDM,1),B(1),UL(6),ID(PDF,1),F(PDF,1),D(1)
DATA BL/4HBLAN/
DO 102 II=1,NUMNP,50
WRITE(6,2000) O,HEAD,TIME,(I,CD(1),CD(2),I=1,NDM),(I,DI(1)
1 ,DI(2),I=1,PDF)

```

```

      JJ=MINO(NUMNP,II+49)
      DO 102 N=II,JJ
C     IF(ABS(X(1,N)).GT.90..OR.ABS(X(2,N)).GT.50.) GO TO 101
      IF(PCOMP(X(1,N),BL)) GO TO 101
      DO 100 I=1,NDF
      UL(I)=F(I,N)*PROP
      K=IABS(ID(I,N))
      IF(K.GT.0) UL(I)=B(K)
100    IF(I.EQ.3.AND.K.GT.0) UL(I)=B(K)*D(9)
      WRITE(6,PDIS) N,(X(I,N),I=1,NDM),(UL(I),I=1,NDF)
101    CONTINUE
102    CONTINUE
      RETURN
2000  FORMAT(A1,20A4//5X,19HNODAL DISPLACEMENTS,5X,4HTIME,E13.5//
1     6X,4HNODE,9(I7,A4,A2))
      END

```

```

      SUBROUTINE PRTREA(R,NDF)
C
C.....PRINT NODAL REACTIONS
C
      IMPLICIT DOUBLE PRECISION(A-H,O-Z)
      DIMENSION R(NDF,1),RSUM(6),ASUM(6)
      COMMON /CDATA/ O,HEAD(20),NUMNP,NUMEL,NUMMAT,NEN,NEQ,IPR
      DO 50 K=1,NDF
      RSUM(K)=0.
50    ASUM(K)=0.
      DO 100 N=1,NUMNP,50
      J=MINO(NUMNP,N+49)
      WRITE(6,2000) O,HEAD,(K,K=1,NDF)
      DO 100 I=N,J
      DO 75 K=1,NDF
      R(K,I)=-R(K,I)
      RSUM(K)=RSUM(K)+R(K,I)
75    ASUM(K)=ASUM(K)+ABS(R(K,I))
100   WRITE(6,2001) I,(R(K,I),K=1,NDF)
C.....PRINT STATICS TEST
      WRITE(6,2002) (RSUM(K),K=1,NDF)
      WRITE(6,2003) (ASUM(K),K=1,NDF)
      RETURN
2000  FORMAT(A1,20A4//5X,15HNODAL REACTIONS//6X,4HNODE,
1     6(I9,4H DOF))
2001  FORMAT(I10,6E13.4)
2002  FORMAT(/7X,3HSUM,6E13.4)
2003  FORMAT(/3X,7HABS SUM,6E13.4)
      END

```

```

      SUBROUTINE PSETM(NA,NE,NJ,AFL)
C
C.....SET POINTERS FOR ARRAYS
C

```



```

LOGICAL AFL
NA=NE
NE=NE+NJ
AFL=.FALSE.
CALL SETMEM(NE)
RETURN
END

SUBROUTINE PZERO(V,NN)
C
C.....ZERO REAL ARRAY
C
      DIMENSION V(NN)
      DO 100 N=1,NN
100    V(N)=0.0
      RETURN
      END

SUBROUTINE UACTCL(A,C,B,JDIAG,NEQ,AFAC,BACK)
IMPLICIT DOUBLE PRECISION(A-H,O-Z)
LOGICAL AFAC,BACK
DIMENSION A(1),B(1),JDIAG(1),C(1)
C
C.....UNSYMMETRIC, ACTIVE COLUMN PROFILE EQUATION SOLVER
C
C.....FACTOR A TO UT*D*U, REDUCE B TO Y
      JR=0
      DO 300 J=1,NEQ
      JD=JDIAG(J)
      JH=JD-JR
      IF(JH.LE.1) GO TO 300
      IS=J+1-JH
      IE=J-1
      IF(.NOT.AFAC) GO TO 250
      K=JR+1
      ID=0
C.....REDUCE ALL EQUATIONS EXCEPT DIAGONAL
      DO 200 I=IS,IE
      IR=ID
      ID=JDIAG(I)
      IH=MINO(ID-IR-1,I-IS)
      IF(IH.EQ.0) GO TO 150
      A(K)=A(K)-DOT(A(K-IH),C(ID-IH),IH)
      C(K)=C(K)-DOT(C(K-IH),A(ID-IH),IH)
150    IF(A(ID).NE.0.0) C(K)=C(K)/A(ID)
200    K=K+1
C.....REDUCE DIAGONAL TERM
      A(JD)=A(JD)-DOT(A(JR+1),C(JR+1),JH-1)
C.....FORWARD REDUCE THE R.H.S
250    IF(BACK) B(J)=B(J)-DOT(C(JR+1),B(IS),JH-1)
300    JR=JD

```

```

        IF(.NOT.BACK) RETURN
C.....BACKSUBSTITUTION
        J=NEQ
        JD=JDIAG(J)
500    IF(A(JD).NE.0.0) B(J)=B(J)/A(JD)
        D=B(J)
        J=J-1
        IF(J.LE.0) RETURN
        JR=JDIAG(J)
        IF(JD-JR.LE.1) GO TO 700
        IS=J-JD+JR+2
        K=JR-IS+1
        DO 600 I=IS,J
600    B(I)=B(I)-A(I+K)*D
700    JD=JR
        GO TO 500
        END

```

```

SUBROUTINE PGAUSS(L,LINT,R,Z,W)
IMPLICIT DOUBLE PRECISION(A-H,O-Z)

```

```

C
C.....GAUSS POINTS AND WEIGHTS FOR TWO DIMENSIONS
C
        DIMENSION LR(9),LZ(9),LW(9),R(1),Z(1),W(1)
        DATA LR/-1,1,1,-1,0,1,0,-1,0/,LZ/-1,-1,1,1,-1,0,1,0,0/
        DATA LW/4*25,4*40,64/
        LINT=L*L
        GO TO (1,2,3),L
C.....1X1 INTEGRATION
1        R(1)=0.
        Z(1)=0.
        W(1)=4.
        RETURN
C.....2X2 INTEGRATION
2        G=1./SQRT(3.)
        DO 21 I=1,4
        R(I)=G*LR(I)
        Z(I)=G*LZ(I)
21       W(I)=1.
        RETURN
C.....3X3 INTEGRATION
3        G=SQRT(0.6)
        H=1./81.
        DO 31 I=1,9
        R(I)=G*LR(I)
        Z(I)=G*LZ(I)
31       W(I)=H*LW(I)
        RETURN
        END

```

```

SUBROUTINE PSTRES(SIG,P1,P2,P3)

```



77 Massachusetts Avenue
Cambridge, MA 02139
<http://libraries.mit.edu/ask>

DISCLAIMER NOTICE

MISSING PAGE(S)

p.288

```

C
C.....COMPUTE PRINCIPAL STRESSES (2 DIMENSIONS)
C
      IMPLICIT DOUBLE PRECISION(A-H,O-Z)
      DIMENSION SIG(3)
C.....STRESSES MUST BE STORED IN ARRAY SIG(3) IN THE ORDER
C      TAU-XX,TAU-XY,TAU-YY
      XI1=(SIG(1)+SIG(3))/2.
      XI2=(SIG(1)-SIG(3))/2.
      RHO=SQRT(XI2*XI2+SIG(2)*SIG(2))
      P1=XI1+RHO
      P2=XI1-RHO
      P3=45.0
      IF(XI2.NE.0.0) P3=22.5*ATAN2(SIG(2),XI2)/ATAN(1.0)
      RETURN
      END

      SUBROUTINE SHAPE(SS,TT,X,SHP,XSJ,NDM,NEL,IX,FLG)
C
C.....SHAPE FUNCTION ROUTINE FOR TWO DIMENSIONAL ELEMENTS
C
      IMPLICIT DOUBLE PRECISION(A-H,O-Z)
      LOGICAL FLG
      DIMENSION SHP(3,1),X(NDM,1),S(4),T(4),XS(2,2),SX(2,2),IX(1)
      DATA S/-0.5,0.5,0.5,-0.5/,T/-0.5,-0.5,0.5,0.5/
C.....FORM 4-NODE QUADRILATERAL SHAPE FUNCTIONS
      DO 100 I=1,4
      SHP(3,I)=(0.5+S(I)*SS)*(0.5+T(I)*TT)
      SHP(1,I)=S(I)*(0.5+T(I)*TT)
100  SHP(2,I)=T(I)*(0.5+S(I)*SS)
      IF(NEL.GE.4) GO TO 120
C.....FORM TRIANGLE BY ADDING THIRD AND FOURTH TOGETHER
      DO 110 I=1,3
110  SHP(I,3)=SHP(I,3)+SHP(I,4)
C.....ADD QUADRATIC TERMS IF NECESSARY
120  IF(NEL.GT.4) CALL SHAP2(SS,TT,SHP,IX,NEL)
C.....CONSTRUCT JACOBIAN AND ITS INVERSE
      DO 130 I=1,NDM
      DO 130 J=1,2
      XS(I,J)=0.0
      DO 130 K=1,NEL
130  XS(I,J)=XS(I,J)+X(I,K)*SHP(J,K)
      XSJ=XS(1,1)*XS(2,2)-XS(1,2)*XS(2,1)
      IF(FLG) RETURN
      SX(1,1)=XS(2,2)/XSJ
      SX(2,2)=XS(1,1)/XSJ
      SX(1,2)=-XS(1,2)/XSJ
      SX(2,1)=-XS(2,1)/XSJ
C.....FORM GLOBAL DERIVATIVES
      DO 140 I=1,NEL
      TP      =SHP(1,I)*SX(1,1)+SHP(2,I)*SX(2,1)

```

```

      SHP(2,I) =SHP(1,I)*SX(1,2)+SHP(2,I)*SX(2,2)
140  SHP(1,I)=TP
      RETURN
      END

      SUBROUTINE SHAP2(S,T,SHP,IX,NEL)
C
C.....ADD QUADRATIC FUNCTIONS AS NECESSARY
C
      IMPLICIT DOUBLE PRECISION(A-H,O-Z)
      DIMENSION IX(1),SHP(3,1)
      S2=(1.-S*S)/2.
      T2=(1.-T*T)/2.
      DO 100 I=5,NEL
      DO 100 J=1,3
100  SHP(J,I)=0.0
C.....MIDSIDE NODES (SERENDIPITY)
      IF(IX(5).EQ.0) GO TO 101
      SHP(1,5)=-S*(1.-T)
      SHP(2,5)=-S2
      SHP(3,5)=S2*(1.-T)
101  IF(NEL.LT.6) GO TO 107
      IF(IX(6).EQ.0) GO TO 102
      SHP(1,6)=T2
      SHP(2,6)=-T*(1.+S)
      SHP(3,6)=T2*(1.+S)
102  IF(NEL.LT.7) GO TO 107
      IF(IX(7).EQ.0) GO TO 103
      SHP(1,7)=-S*(1.+T)
      SHP(2,7)= S2
      SHP(3,7)=S2*(1.+T)
103  IF(NEL.LT.8) GO TO 107
      IF(IX(8).EQ.0) GO TO 104
      SHP(1,8)=-T2
      SHP(2,8)=-T*(1.-S)
      SHP(3,8)=T2*(1.-S)
C.....INTERIOR NODE (LAGRANGIAN)
104  IF(NEL.LT.9) GO TO 107
      IF(IX(9).EQ.0) GO TO 107
      SHP(1,9)=-S*T2
      SHP(2,9)=-T*S2
      SHP(3,9)=4.*S2*T2
C.....CORRECT EDGE NODES FOR INTERIOR NODE (LAGRANGIAN)
      DO 106 J=1,3
      DO 105 I=1,4
105  SHP(J,I)=SHP(J,I)-0.25*SHP(J,9)
      DO 106 I=5,8
106  IF(IX(I).NE.0) SHP(J,I)=SHP(J,I)-.5*SHP(J,9)
C.....CORRECT CORNER NODES FOR PRESENCE OF MIDSIDE NODES
107  K=8
      DO 109 I=1,4

```

```

      L=I+4
      DO 108 J=1,3
108   SHP(J,I)=SHP(J,I)-.5*(SHP(J,K)+SHP(J,L))
109   K=L
      RETURN
      END

      SUBROUTINE ELMTO2(D,UL,XL,IX,TL,S,P,ECS,CSI,CSTR,CVOL,CVI,SO,
1      PECS,TIME,DT,NDF,NDM,NST,ISW,IFLAG,LMNT)
C
C.....AXISYMMETRIC NON-LINEAR CYCLIC ELEMENT ROUTINE
C
      IMPLICIT DOUBLE PRECISION(A-H,O-Z)
      COMMON/CDATA/O,HEAD(20),NUMNP,NUMEL,NUMMAT,NEN,NEQ,IPR
      COMMON/ELDATA/DM,N,MA,MCT,IEL,NEL
      DIMENSION D(1),UL(NDF,1),XL(NDM,1),IX(1),TL(1),S(NST,1),P(1),
1      SHP(3,9),SHPP(3,9),SG(9),TG(9),WG(9),SIG(7),EPS(4)
      DIMENSION ECS(1),CSI(1),CSTR(1),PECS(1),EECS(4)
C.....GO TO CORRECT ARRAY PROCESSOR
      GO TO(1,2,3,4,5,4,4,4,4),ISW
C.....INPUT MATERIAL PROPERTIES
1      READ(5,1000) E,XNU,D(4),L,K,I,D(8)
      D(1)=E*(1.-XNU)/(1.+XNU)/(1.-2.*XNU)
      D(2)=D(1)*XNU/(1.-XNU)
      D(3)=E/2./(1.+XNU)
      L=MINO(3,MAXO(1,L))
      D(5)=L
      K=MINO(3,MAXO(1,K))
      D(6)=K
      D(7)=2
      LINT=0
      WRITE(6,2000) E,XNU,D(4),L,K,D(8)
      D(9)=1.
      D(10)=XNU
      READ(5,1600) (D(NI),NI=11,27)
      PHI1=D(11)*57.29577951
      PHI2=D(12)*57.29577951
      WRITE(6,2003) PHI1,PHI2,(D(NI),NI=13,27)
      RETURN
2      RETURN
3      L=D(5)
      IF(L*L.NE.LINT) CALL PGAUSS(L,LINT,SG,TG,WG)
C.....FAST STIFFNESS COMPUTATION
      CALL EXTRA(ECS,PECS,EECS,IFLAG)
      IF(IEL.GE.0) CALL MODEL(EECS,CSI,CSTR,CVOL,CVI,SO,D,TIME,DT
1      ,1,LMNT,1)
C      WRITE(6,1500) (ECS(I),I=1,4),(PECS(I),I=1,4),EECS
      NPP=NEL/2
      NPP1=NPP+1
      IF(IEL.LT.0) NPP1=1
      DO 325 L=1,LINT

```

```

CALL SHAPE(SG(L),TG(L),XL,SHP,XSJ,NDM,NEL,IX,.FALSE.)
XX=0.
DO 330 J=1,NEL
330 XX=XX+SHP(3,J)*XL(1,J)
   XSJ=6.2831852*XX*WG(L)*XSJ
C.....LOOP OVER ROWS
   J1=1
   DO 320 J=1,NEL
C.....LOOP OVER COLUMNS (SYMMETRY NOTED)
   K1=J1
   DO 310 K=J,NEL
   S(J1 ,K1 )=S(J1 ,K1 )+D(1)*(SHP(1,J)*SHP(1,K)+SHP(3,J)*SHP(3,K
1 )/XX/XX)*XSJ+D(2)*(SHP(3,J)*SHP(1,K)+SHP(1,J)*SHP(3,K))*XSJ/XX+
2 D(3)*SHP(2,J)*SHP(2,K)*XSJ
   S(J1 ,K1+1)=S(J1 ,K1+1)+D(2)*(SHP(1,J)+SHP(3,J)/XX)*SHP(2,K)*XSJ
1 +D(3)*SHP(2,J)*SHP(1,K)*XSJ
   S(J1+1,K1 )=S(J1+1,K1 )+D(2)*(SHP(1,K)+SHP(3,K)/XX)*SHP(2,J)*XSJ
1 +D(3)*SHP(1,J)*SHP(2,K)*XSJ
   S(J1+1,K1+1)=S(J1+1,K1+1)+D(1)*SHP(2,J)*SHP(2,K)*XSJ+D(3)*SHP(1,J)
1 *SHP(1,K)*XSJ
310 K1=K1+NDF
320 J1=J1+NDF
CALL SHAPE(SG(L),TG(L),XL,SHPP,XSJP,NDM,NPP,IX,.FALSE.)
DO 322 J=NPP1,9
DO 322 JJ=1,3
322 SHPP(JJ,J)=0.
   DO 325 J=1,NPP
   JB=J*NDF
   DO 325 K=1,NEL
   KB=K*NDF-2
   S(KB ,JB)=S(KB ,JB)+D(9)*SHPP(3,J)*(SHP(1,K)+SHP(3,K)/XX)*XSJ
   S(KB+1,JB)=S(KB+1,JB)+D(9)*SHPP(3,J)*SHP(2,K)*XSJ
   S(KB+2,JB)=S(KB+2,JB)+D(8)*SHPP(3,K)*SHPP(3,J)*XSJ
   S(JB,KB )=S(KB ,JB)
   S(JB,KB+1)=S(KB+1,JB)
325 S(JB,KB+2)=S(KB+2,JB)
C.....FORM LOWER PART BY SYMMETRY
   NSL=NEL*NDF
   DO 340 J=1,NSL,NDF
   DO 340 K=J,NSL,NDF
   DO 340 JJ=1,2
   KK=JJ-1
   S(K+KK,J)=S(J,K+KK)
340 S(K+KK,J+1)=S(J+1,K+KK)
   RETURN
4 L=D(6)
CALL EXTRA(ECS,PECS,EECS,IFLAG)
IF(ISW.NE.6) GO TO 405
L=D(5)
CALL MODEL(EECS,CSI,CSTR,CVOL,CVI,S0,D,TIME,DT,2,LMNT,L)
405 IF(L*L.NE.LINT) CALL PGAUSS(L,LINT,SG,TG,WG)

```

```

C.....COMPUTE ELEMENT STRESSES AND FORCES
      DO 600 L=1,LINT
C.....COMPUTE ELEMENT SHAPE FUNCTIONS
      NPP=NEL/2
      NPP1=NPP+1
      IF(IEL.LT.0) NPP1=1
      CALL SHAPE(SG(L),TG(L),XL,SHP,XSJ,NDM,NEL,IX,.FALSE.)
C.....COMPUTE STRAINS AND COORDINATES
      DO 410 I=1,4
410   EPS(I)=0.0
      XX=0.0
      YY=0.0
      DO 415 J=1,NEL
      XX=XX+SHP(3,J)*XL(1,J)
415   YY=YY+SHP(3,J)*XL(2,J)
      IF(ISW.EQ.4) GO TO 427
      DO 420 J=1,NEL
      EPS(1)=EPS(1)+SHP(1,J)*UL(1,J)
      EPS(3)=EPS(3)+SHP(2,J)*UL(2,J)
      EPS(4)=EPS(4)+SHP(3,J)*UL(1,J)/XX
420   EPS(2)=EPS(2)+SHP(1,J)*UL(2,J)+SHP(2,J)*UL(1,J)
      DO 425 I=1,4
425   EPS(I)=EPS(I)-CSTR(I)
C.....COMPUTE (EFFECTIVE) STRESSES
      IF(IEL.GE.0) CALL MODEL(EPCS,CSI,CSTR,CVOL,CVI,S0,D,TIME,DT,1,
1      0,1)
      SIG(1)=D(1)*EPS(1)+D(2)*EPS(3)+D(2)*EPS(4)
      SIG(3)=D(2)*EPS(1)+D(1)*EPS(3)+D(2)*EPS(4)
      SIG(4)=D(2)*EPS(1)+D(2)*EPS(3)+D(1)*EPS(4)
      SIG(2)=D(3)*EPS(2)
      GO TO(620,630,640,650),(ISW-5)
427   DO 428 I=1,3
428   SIG(I)=ECS(I)
      CALL PSTRES(SIG,SIG(4),SIG(6),SIG(7))
      SIG(5)=ECS(4)
C.....OUTPUT STRESSES
      MCT=MCT-2
      IF(MCT.GT.0) GO TO 430
      WRITE(6,2001) 0,HEAD
      MCT=50
430   WRITE(6,2002) N,MA,XX,YY,SIG
      GO TO 600
C.....COMPUTE AVERAGE EFFECTIVE INITIAL STRESSES
630   DO 635 I=1,4
      ECS(I)=ECS(I)+SIG(I)/LINT
635   PECS(I)=ECS(I)
      GO TO 600
C.....COMPUTE AVERAGE CYCLIC STRESS INCREMENT
640   DO 645 I=1,4
645   CSI(I)=CSI(I)+SIG(I)/LINT
      GO TO 600

```



```

C.....COMPUTE AVERAGE EFFECTIVE STRESSES AT TIME 'T + DT'
650 DO 655 I=1,4
655 PECS(I)=ECS(I)+SIG(I)/LINT
GO TO 600
C.....COMPUTE INTERNAL FORCES
620 CALL SHAPE(SG(L),TG(L),XL,SHPP,XSJP,NDM,NPP,IX,.FALSE.)
C.....COMPUTE PORE PRESSURE
DO 618 I=NPP1,9
DO 618 II=1,3
618 SHPP(II,I)=0.
PPLD=0.
DV=6.2831852*XX*WG(L)*XSJ
DO 615 J=1,NPP
615 PPLD=PPLD+SHPP(3,J)*UL(3,J)*D(9)
PWF=0.
DO 611 J=1,NEL
611 PWF=PWF+((SHP(1,J)+SHP(3,J)/XX)*UL(1,J)+SHP(2,J)*UL(2,J))*D(9)
1 +SHPP(3,J)*UL(3,J)*D(8)
C.....COMPUTE TOTAL STRESSES
SIG(1)=SIG(1)+PPLD
SIG(3)=SIG(3)+PPLD
SIG(4)=SIG(4)+PPLD
C.....COMPUTE INTERNAL FORCES
J1=1
DO 610 J=1,NEL
P(J1 )=P(J1 )-(SHP(1,J)*SIG(1)+SHP(3,J)/XX*SIG(4)+SHP(2,J)*SIG(2)
1 )*DV
P(J1+1)=P(J1+1)-(SHP(2,J)*SIG(3)+SHP(1,J)*SIG(2))*DV
P(J1+2)=P(J1+2)-SHPP(3,J)*PWF*DV
610 J1=J1+NDF
600 CONTINUE
RETURN
C.....COMPUTE GEOSTATIC STRESSES
5 CALL SHAPE(0.,0.,XL,SHP,XSJ,NDM,NEL,IX,.FALSE.)
CKO=D(10)/(1.-D(10))
YY=0.
DO 700 I=1,NEL
700 YY=YY+SHP(3,I)*XL(2,I)
DECS=YY*D(4)
DECS=-ABS(DECS)
ECS(1)=ECS(1)+DECS*CKO
ECS(3)=ECS(3)+DECS
ECS(4)=ECS(4)+DECS*CKO
DO 710 I=1,4
710 PECS(I)=ECS(I)
RETURN
C.....FORMATS FOR INPUT-OUTPUT
1000 FORMAT(3F10.0,3I5,F10.0)
1500 FORMAT('/' ECS=',4F10.3,' PECS=',4F10.3/' EECS=',4F10.3,' CSTR=',
1 4E15.5/)
1600 FORMAT(6F10.5)

```

```

2000  FORMAT(/5X,12HAXISYMMETRIC,26H NON LINEAR CYCLIC ELEMENT//
1 10X,12HYOUNG'S MOD.,E15.5,10H (CONST.)/10X,13HPOISSON RATIO,F8.5
1/10X,11HUNIT WEIGHT,E18.5/10X,13HGAUSS PTS/DIR,I3/10X,10HSTRESS PT
2S,I6/10X,14HPENALTY CONST.,E15.5)
2001  FORMAT(A1,20A4//5X,16HELEMENT STRESSES//20H ELEMENT MATERIAL,4X
1,7H1-COORD,4X,7H2-COORD,3X,9H11-STRESS,3X,9H12-STRESS,3X,
29H22-STRESS,3X,8H1-STRESS,3X,8H2-STRESS,3X,8H3-STRESS,2X,5HANGLE)
2002  FORMAT(2I10,2F11.4,3E12.4,3E11.4,F7.2)
2003  FORMAT(10X,14HFRICITION ANGLE,F8.2/10X,14HCYC. LMT STATE,F8.2/10X,
114HUNDR. STRENGTH,F8.2/10X,10HVOID RATIO,F10.3/10X,14HMIN VOID RAT
2IO,F10.3/10X,11HATM. PRESS.,F10.2/10X,13HSHEAR MODULUS,3F15.5/10X,
313HBULK MODULUS,2F15.5/10X,13HCYC. LMT EFCT,F13.5/10X,15HCYC. VOL
4. STIF.,F12.5,2F15.5/10X,15HCYC. DEV. STIF,F10.5,F15.5)
END

```

```

SUBROUTINE EXTRA(A1,A2,A0,I)
IMPLICIT DOUBLE PRECISION(A-H,O-Z)
DIMENSION A1(1),A2(1),A0(1)
THETA=0.0
THETA=THETA*I
DO 100 N=1,4
100  A0(N)=A1(N)*(1.-THETA)+A2(N)*THETA
RETURN
END

```

```

SUBROUTINE INTERPOL(Q1,S1,Q2,S2,Q,S)
IMPLICIT DOUBLE PRECISION(A-H,O-Z)
SLOPE=(Q1-Q2)/(S1-S2)
S=S2+(Q-Q2)/SLOPE
RETURN
END

```

```

SUBROUTINE INTERSECT(Q1,S1,Q2,S2,SLOPE,Q,S)
IMPLICIT DOUBLE PRECISION(A-H,O-Z)
SLOPS=(Q1-Q2)/(S1-S2)
S=(Q1-SLOPS*S1)/(SLOPE-SLOPS)
Q=SLOPE*S
RETURN
END

```